**University of Southampton**
Faculty of Physical and Applied Science
School of Electronics and Computer Science
Southampton S017 1BJ

# Hybrid Automatic-Repeat-reQuest Systems for Cooperative Wireless Communications

by

*Hoang Anh Ngo*
*B.Eng, M.Sc*

A doctoral thesis submitted in partial fulfilment of the
requirements for the award of Doctor of Philosophy
at the University of Southampton

January 2012

SUPERVISOR: *Professor Lajos Hanzo*
Dipl. Ing, M.Sc, Ph.D, D.Sc, FREng, FIEEE, FIET
Chair of Telecommunications
School of Electronics and Computer Science
University of Southampton
Southampton SO17 1BJ
United Kingdom

.

**D**edicated to

my beloved parents

for their tremendous patience and care

with all my love and respect $\cdots$

.

UNIVERSITY OF SOUTHAMPTON

ABSTRACT

FACULTY OF PHYSICAL AND APPLIED SCIENCE
SCHOOL OF ELECTRONICS AND COMPUTER SCIENCE

Doctor of Philosophy

**Hybrid Automatic-Repeat-reQuest Systems for Cooperative Wireless Communications**

by Hoang Anh Ngo

As a benefit of achieving a diversity gain and/or a multiplexing gain, MIMO techniques are capable of significantly increasing the achievable throughput and/or the network coverage without additional bandwidth or transmit power. For the sake of striking an attractive trade-off between the attainable diversity gain and/or multiplexing gain, in this thesis the novel Space-Time-Frequency Shift Keying (STFSK) concept is proposed for the family of MIMO systems. More specifically, in order to generate space-time-frequency domain codewords, the STFSK encoding schemes activate one out of $Q$ dispersion matrices, and the associated address bits are then combined with a classic time-domain and frequency-domain modulation scheme. The resultant arrangements impose no inter-symbol interference and are capable of eliminating the inter-antenna interference, hence offering a range of benefits over other classic MIMO arrangements. Additionally, a soft-output STFSK demodulator is designed for iterative detection and the complexity of both the hard- as well as soft-decision demodulators is quantified. Furthermore, the STFSK performance is studied in both the single-user and the multiple-user multi-cell environment in order to investigate the effects of these techniques on the performance of the holistically optimized systems.

Furthermore, we studied the H-ARQ systems advocated in the context of cooperation-aided wireless networks, where the MIMO elements are constituted by the individual elements of separate network nodes. Both perfect and imperfect coherent detection as well as non-coherent detection aided cooperative H-ARQ schemes are considered. In the perfect coherent detection based pilot symbol assisted scheme, a novel relay-switching aided H-ARQ scheme is proposed for mitigating the effects of correlation in fading wireless channels, followed by a H-ARQ scheme employing systematic Luby transform codes. In contrast to the unrealistic perfect coherent detection, realistic imperfect coherent schemes are studied, where the channel impulse responses are imperfectly estimated. Furthermore, non-coherent differential detection aided cooperative H-ARQ schemes are proposed and compared to their coherent detection assisted counterparts. Finally, a novel cooperative H-ARQ arrangement based on distributed space-time codes is proposed for the sake of improving the attainable system throughput, while reducing the system's complexity.

.

## DECLARATION OF AUTHORSHIP

I, **Hoang Anh Ngo**, declare that the thesis entitled "**Hybrid Automatic-Repeat-reQuest Systems for Cooperative Wireless Communications**" and the work presented in this thesis are both my own, and have been generated by me as the result of my own original research. I confirm that:

- this work was done wholly or mainly while in candidate for a research degree at this University;
- where any part of this thesis has previously been submitted for a degree or any other qualification at this University or any other institution, this has been clearly stated;
- where I have consulted the publish work of others, this is always clearly attributed;
- where I have quoted from the work of others, the source is always given. With the exception of such equations, this thesis is entirely my own work;
- I have acknowledged all main sources of help;
- where the thesis is based on work done by myself jointly with others, I have made clear exactly what was done by others and what I have contributed myself;
- parts of this work have been published as [1–8].

**Signed**: .....

**Date**:.....

.

# Acknowledgements

I would like to express my sincere gratitude to Professor Lajos Hanzo for his outstanding supervision and support throughout my research. His guidance, inspiration and encouragement have greatly benefited me not only in work but also in life. Most importantly, I would like to thank him for his invaluable friendship.

Many thanks also to my colleagues and the staff of the Communications Group, both past and present, for their support, help and discussions throughout my research. I would like to thank Dr. Robert Maunder, Dr. Soon Xin Ng, Dr. Dang Thanh Nguyen, Viet Hung Nguyen, Chao Xu, Tim Stevens and all other colleagues and staff, too numerous to mention here explicitly. Special thanks are also due to Denise Harvey for her help in administrative matters.

The financial support of the Engineering and Physical Sciences Research Council (EPRSC), United Kingdom, is also gratefully acknowledged.

I would also like to express my warmest gratitude to my father, Kim Sach Ngo, and my mother, Thi The Hoang, as well as to my sister, Minh Tam Ngo, and her family for their love, support and faith. Thanks are also due to Canon Gary Philbrick for his encouragement and support during my life in Southampton. Special thanks also to my friends in Southampton for their friendship. Finally, to a special one, without her inspiration, I would not have been able to finish this research.

# List of Publications

## Journal

1. **H. A. Ngo, L. Hanzo**, "Area Spectral Efficiency of Soft-Decision Space-Time-Frequency Shift Keying Aided Slow Frequency Hopping Multiple Access", IEEE Transactions on Vehicular Technology, 2012 (In print).

2. **H. A. Ngo, S. Ahmed, L.-L. Yang, L. Hanzo**, "Non-Coherent Cooperative Communications Dispensing with Channel Estimation Relying on Erasure Insertion Aided Reed-Solomon Coded SFH M-ary FSK Subjected to Partial-Band Interference and Rayleigh Fading", IEEE Transactions on Communications, 2012 (In print).

3. **H. A. Ngo, T. D. Nguyen, L. Hanzo**, "Amplify-Forward and Decode-Forward Aided HARQ Using Systematic LT Coding", IET Communications, vol. 5, pp. 1096-1106, May 2011, ISSN 1751-8628.

4. **H. A. Ngo, C. Xu, S. Sugiura, L. Hanzo**, "Space-Time-Frequency Shift Keying for Dispersive Channels", IEEE Signal Processing Letters, vol. 18, pp. 177-180, March 2011, ISSN 1070-9908.

## Conference

1. **H. A. Ngo, S. Sugiura, L. Hanzo**, "Iterative Soft-Detection of Space-Time-Frequency Shift Keying", Proceedings of the IEEE International Conference on Communications (ICC), 2012 (In print).

2. **H. A. Ngo, L. Hanzo**, "Area Spectral Efficiency of Soft-Decision Space-Time-Frequency Shift Keying Aided Slow Frequency Hopping Multiple Access", Proceedings of IEEE Vehicular Technology Conference (VTC) Spring, 2012 (In print).

3. **H. A. Ngo, S. Ahmed, L.-L. Yang, L. Hanzo**, "Erasure Insertion in Reed-Solomon Coded SFH M-ary FSK with Partial-Band Interference and Rayleigh Fading for Non-Coherent Cooperative Communications", Proceedings of IEEE Vehicular Technology Conference (VTC) Fall, 5-8 September 2011, San Francisco, United States of America.

4. **H. A. Ngo, R. Maunder, L. Hanzo**, "Relay Switching Aided Turbo Coded Hybrid-ARQ for Correlated Fading Channel", Proceedings of IEEE Wireless Communications and Networking Conference (WCNC), 28-31 March 2011, Cancun, Mexico.

5. **H. A. Ngo, T. D. Nguyen, L. Hanzo**, "HARQ Aided Systematic LT Coding for Amplify-Forward and Decode-Forward Cooperation", Proceedings of IEEE Vehicular Technology Conference (VTC) Fall, 6-9 September 2010, Ottawa, Canada.

6. **H. A. Ngo, L. Hanzo**, "Impact of Imperfect Channel State Information on RS Coding Aided Hybrid-ARQ in Rayleigh Fading Channels", Proceedings of IEEE International Conference on Communications (ICC), 23-27 May 2010, Cape Town, South Africa.

7. **H. A. Ngo, L. Hanzo**, "Amplify-and-Forward Relaying Aided Reed-Solomon Coded Hybrid-ARQ Relying on Realistic Channel Estimation", Proceedings of IEEE Vehicular Technology Conference (VTC) Spring, 16-19 May 2010, Taipei, Taiwan.

8. **H. A. Ngo, T. Stevens, R. G. Maunder, L. Hanzo**, "A Systematic LT Coded Arrangement for Transmission Over Correlated Shadow Fading Channels in 802.11 Ad-hoc Wireless Networks", Proceedings of IEEE Vehicular Technology Conference (VTC) Spring, 16-19 May 2010, Taipei, Taiwan.

# List of Symbols

## General notation

- The superscript $^*$ is used to indicate complex conjugation. Therefore, $a^*$ represents the complex conjugate of the variable $a$.
- The superscript $^T$ is used to indicate matrix transpose operation. Therefore, $\mathbf{a}^T$ represents the transpose of the matrix $\mathbf{a}$.
- The superscript $^H$ is used to indicate complex conjugate transpose operation. Therefore, $\mathbf{a}^H$ represents the complex conjugate transpose of the matrix $\mathbf{a}$.
- The notation $*$ denotes the convolutional process. Therefore, $a * b$ represents the convolution between variables $a$ and $b$.
- The notation $\hat{x}$ represents the estimate of $x$.

## Special symbols

$\beta$: The amplifying factor at the relay.

$\chi$: The dispersion matrix.

$\eta$: The throughput/spectral efficiency.

$\eta_g$: The goodput.

$\pi$: Interleaver.

$\pi^{-1}$: Deinterleaver.

$\sigma$: The variance.

$a_{cell}$: The traffic load.

$B_D$: The maximum Doppler spread.

$C$: The capacity.

$C^+$: The number of additions.

$C^x$: The number of multiplications.

$C_c$: The full reuse cluster size.

$d$: The normalized distance.

$E_T$: The total transmit energy.

$E_b$: The bit energy.

$E_p$: The pilot symbol energy.

$E_s$: The data symbol energy.

$F_D$: The normalized Doppler frequency.

$f_D$: The (maximum) Doppler frequency.

$f_s$: The channel spacing.

$G$: The path-loss-related power gain.

$\boldsymbol{H}$: The channel state information matrix.

$I_a$: The $a-priori$ information.

$I_e$: The $extrinsic$ information.

$L_{pl}$: The path-loss.

$L_a$: The $a-priori$ log-likelihood ratio.

$L_e$: The *extrinsic* log-likelihood ratio.

$L_p$: The *posteriori* log-likelihood ratio.

$M_c$: The number of sub-clusters.

$K$: The number of uncoded data/information bits/symbols.

$N$: The number of coded bits/symbols.

$N_0$: The power spectral density of white noise.

$N_I$: The power spectral density of interference.

$N_c$: The number of frequencies assigned to each cell.

$N_p$: The number of pilot symbols.

$n_T$: The number of transmit antennas.

$n_R$: The number of receive antennas.

$n_{call}$: The number of calls per time-slot.

$n_t$: The number of time-slots per TDM frame.

$P_E$: The accepted packet error ratio.

$P_R$: The transmit power of a relay.

$P_S$: The transmit power of a source.

$P_{cd}$: The probability of correct decoding.

$P_{de}$: The probability of an detected packet error.

$P_e$: The probability of an packet error.

$P_p$: The transmit power of a pilot symbol.

$P_s$: The transmit power of a data/information symbol.

$P_{ue}$: The probability of an undetected packet error.

$p_e$: The bit error probability.

$p_s$: The symbol error probability.

$q_c$: The probability of correct reception of a hop.

$R$: The code rate.

$r_a$: The voice active ratio.

$\boldsymbol{S}$: The transmitted signal matrix.

$T$: The space-time block length in time-slot.

$T_c$: The channel's coherent time.

$T_s$: The signal's coherent time.

$U$: The channel utilization.

$\boldsymbol{V}$: The complex-valued AWGN signal matrix.

$W$: The allocated bandwidth.

$w_i$: The weighting factor.

$\boldsymbol{Y}$: The received signal matrix.

.

# Contents

.

# Chapter 1

# Overview of Wireless Communications

## 1.1 Wireless Communications

The era of wireless communications began with Marconi's pioneering discoveries in radio communications. Since then it has played an important role in society, wealth-creation as well as in the telecommunication sector in particular. Wireless communications encompasses diverse types of fixed, mobile, and portable two-way radios, cellular telephones, personal digital assistants, and wireless networking. The International Telecommunication Union (ITU) estimated that the penetration of telephone subscribers will have reached 67 per 100 inhabitants across the globe by the end of 2010 [9]. The TeleGeography's GlobalComms Database showed a record increase of 196 million mobile subscribers globally in the fourth quarter of 2010, surpassing the record of nearly 190 million new subscribers set at the same time of 2007. The total number of mobile subscribers stood at over 5.3 billions in 2010, an increase of almost 690 million compared to the year before [9, 10]. Other types of wireless communications, such as WiFi, WiMAX, bluetooth, etc., have also developed intensively during the past two decades.

A mobile communication system consists of radio transmitters and receivers communicating over the wireless channel. In the transmitter, the source information, including analogue signals such as voice, or digital signals, such as binary data, is first encoded by the source encoder, which typically uses fewer digital bits to represent the original signal. Then, the channel encoder attaches redundant bits to the source encoded sequence for the sake of correcting errors imposed by the propagation environments. Then the modulator turns the encoded sequences into a suitable intermediate passband waveform for transmission. In order to transmit the signal to a distant destination, the intermediate passband waveform is further converted to the radio frequency, before being passed to the transmit antenna. When travelling through the wireless channel, the signal will be corrupted by the channel's fading, noise and interference. The radio frequency signal received at the receiver is converted and demodulated to the baseband signal. After error detection and/or correction, the signal is passed to the source decoder to recover the original signal, such as the voice, video signal or binary data. The block diagram of a typical wireless communication system is portrayed in Fig. 1.2.

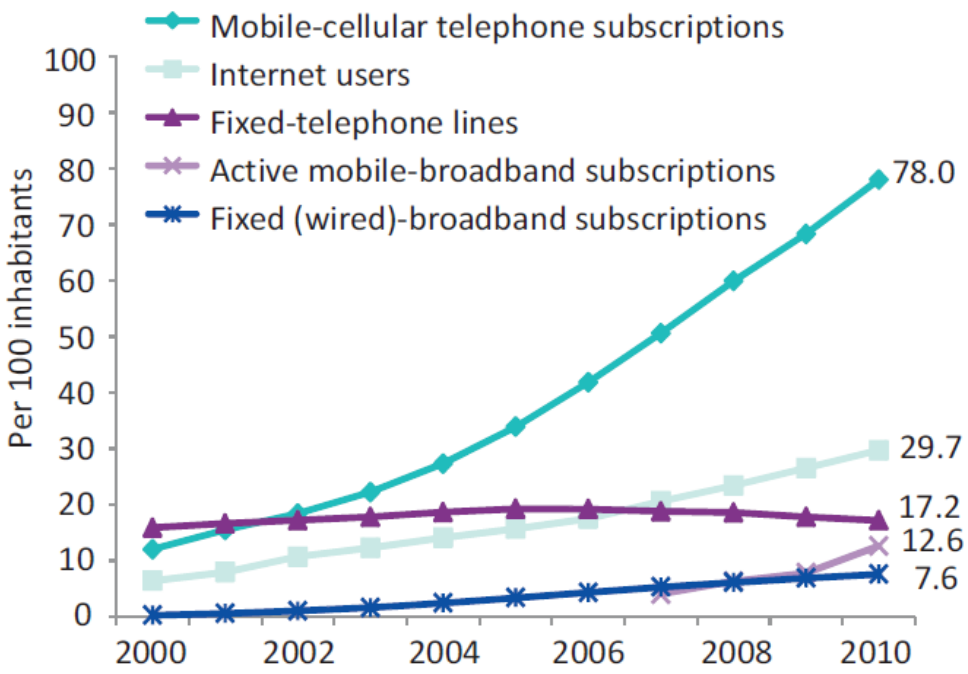


Figure 1.1: The penetration of the global ICT developments during the period 2000-2010 (©ITU World Telecommunication/ICT Indicators database [9], p.1).

### 1.1.1 Wireless Channel

The communications channels play an important role in predetermining the attainable performance of every communication system. Understanding the channel characteristics facilitates the design of efficient communication systems. Therefore, in this section we will study the characteristics of various channel models as well as standardized channels, which are extensively employed by the research and industrial communities.

When simulating a communication link, a model of the channel's behaviour is required, which typically consist of three components: the path-induced attenuation, the log-normal shadow fading and the multipath fading. If the transmit signal is $x(t)$, then the received signal $y(t)$ may be modelled

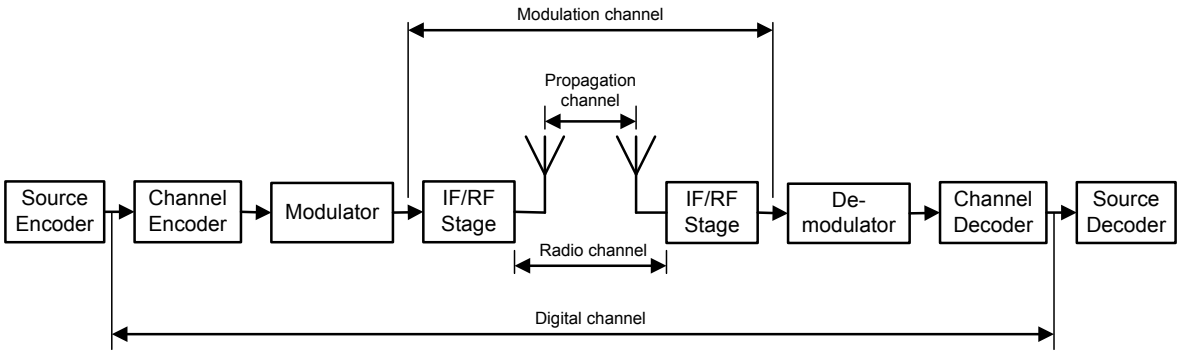


Figure 1.2: Wireless Communication System.

as

$$y(t) = h(t) * x(t), \tag{1.1}$$

where $h(t)$ represents the Channel Impulse Response (CIR), with each tap obeying a specific distribution and $*$ denotes the convolution.

#### 1.1.1.1 Gaussian Channel

The ubiquitous Additive White Gaussian Noise (AWGN) represents the simplest type of Light-of-Sight (LOS) radio channels. The noise imposed by the channel is assumed to have a constant power spectral density over the channel bandwidth and a Gaussian amplitude distribution given by [11]

$$f(x) = \frac{1}{\sigma\sqrt{2\pi}} e^{-(x-\mu)^2/(2\sigma^2)}, \tag{1.2}$$

where $\mu$ represents the mean value, while $\sigma^2$ denotes the variance of the variable $x$.

The Gaussian channel is a typical model for many satellite and deep space communication links. It is not a generally suitable model for terrestrial radio links imposing multipath propagation, fading, interference, etc. However, again in micro-cells having a LOS with no multipath propagation, the AWGN channel model may be applicable. Even when multipath propagation exists but the Mobile Station (MS) is stationary and there is no other moving objects, the mobile channel may still be considered to be Gaussian with a path loss representing the effects of fading.

#### 1.1.1.2 Fading Channel

1. **Rayleigh Fading Channels**: The Rayleigh fading channel is often used to model dense scattering environments, such as built-up urban areas where the radio signals reach the receiver via multiple paths. If each multipath component is received independently at the receiver, the Probability Distribution Function (PDF) of its envelope will follow the Rayleigh distribution given by [11]

$$f(x) = \begin{cases} \frac{x}{\sigma^2} exp\Big(-\frac{x^2}{2\sigma^2}\Big) & : \quad 0 \leq x < \infty \\ 0 & : \quad x < 0 \end{cases}, \tag{1.3}$$

   where $\sigma$ is the root mean square of the received signal before envelope detection and $\sigma^2$ is the time-averaged power of the received signal before envelope detection.

2. **Ricean Fading Channel**: When a strong LoS-path is dominant among the multiple paths arriving at the receiver, the Ricean fading channel may be more suitable than the Rayleigh channel, which has a PDF given by [12]

$$f(x) = \begin{cases} \frac{x}{\sigma^2} exp\Big(-\frac{x^2+\nu^2}{2\sigma^2}\Big) I_0\Big(\frac{x\nu}{\sigma^2}\Big) & : \quad 0 \leq x < \infty \\ 0 & : \quad x < 0 \end{cases}, \tag{1.4}$$

   where $\nu$ denotes the peak amplitude of the dominant LOS signal and $I_0(\cdot)$ represents the modified zero-order Bessel function of the first kind.

The Ricean PDF is often described in terms of the parameter $K$, which is the ratio between the power in the direct LoS path and the other scattered paths, yielding $K = \nu^2/\sigma^2$. Note that when $K = 0$, the channel becomes Rayleigh, whereas if $K = \infty$, the channel is Gaussian.

3. **Flat-Fading and Frequency-Selective-Fading Channels**:

   - Due to the effects of multipath propagation caused by the reflections of radio signals from the surrounding objects, the frequency components of a wideband received signal experience different attenuations and/or phase changes. This effect is typically termed as *'frequency-selective fading'*.
   - When the transmitters and/or receivers roam around in the network, the radio channel imposes time-varying attenuations on the individual multipath components, i.e. on the CIR taps. This effect is generally termed as *'time-selective fading'*.
   - For a simple scenario, where all individual frequency components are attenuated by the same amount, the channel is referred to as *'flat fading'*.

4. **Slow- and Fast-Fading Channels**: Each fading channel may be characterized by the so-called coherence time, which characterises the time-varying nature of the channel's frequency dispersion in the time domain. More simply, it is defined as the minimum time-domain, over which the fading envelope remains fairly correlated, or - synonymously - time required for the magnitude change between the two consecutive instants of the channel to become uncorrelated.

   The mobility of a user roaming in the network imposes a Doppler-induced frequency change on the signal, resulting in a frequency shift, generally known as the Doppler shift. The signal components travelling in different paths may have different Doppler shifts. The difference between the Doppler shifts is defined as the Doppler spread. In general, the coherence time is defined as the reciprocal of the maximum Doppler spread, approximately expressed as

$$T_c \sim \frac{1}{B_D}, \tag{1.5}$$

   where $T_c$ is the coherence time and $B_D$ is the maximum Doppler spread. Depending on the relationship between the channel's coherence time $T_c$ and the signal's coherence time $T_s$, the channel may be categorized as '*slow-fading*' or '*fast-fading*'.

   - *Slow-fading*: occurs when the symbol-durations is equivalently lower than the channel's coherence time, or $T_s << T_c$.
   - *Fast-fading*: occurs when the channel's envelope fluctuates rapidly during a single complex envelope symbol period, i.e. we have $T_s > T_c$. In case of extremely rapid fading the channel's consecutive samples become uncorrelated, hence this channel may be referred to as an uncorrelated fading channel.

   To reflect the rate of change in the channel, the so-called (maximum) Doppler frequency $f_D$ is specified based on the velocity $v$ of the MS and the carrier frequency $f_c$ as

$$f_D = \frac{v}{\lambda} = \frac{v f_c}{c}, \tag{1.6}$$

   where $\lambda$ denotes the wavelength, while $c$ represents the speed of light.

In order to evaluate the effects of fading imposed on different systems under fair conditions, where the systems might have different symbol-durations, the normalized Doppler frequency $F_D$ may be employed, which is expressed as

$$F_D = f_D \cdot T_s. \tag{1.7}$$

#### 1.1.1.3 Standardized Wireless Channel Models

In order to simulate practical wireless channels, a number of channels were standardized, such as for example,

1. **ITU Channel Model**: The ITU-Recommendation M.1225 channel specifies a model [13], which is a measurement based channel model proposed for the 3GPP WCDMA system. The recommendation specifies three different test environments: Indoor office, outdoor-to-indoor or pedestrian and vehicular - high antenna scenarios. Since the delay spread may vary significantly, the recommendation specifies two different delay spreads for each test environment: low delay spread (A), and medium delay spread (B), resulting in six channels models. Each of the models has a multipath tap delay profile, which is specified in Tables 1.1-1.3 of Appendix I.1.

2. **COST-207 Channel Model**: The COST-207 [13] models are capable of characterising diverse typical propagation environments, which may be classified into rural area (Rural Area - RA), areas typical for cities and suburbs (Typical Urban - TU), densely built-up urban areas imposing hostile propagation conditions (Bad Urban - BU), and for hilly terrains (Hilly Terrain - HT). For example, a number of COST-207 channel models are shown in Table 1.4 of Appendix I.2.

3. **COST-259 Channel Model**: The COST-259 models [14,15] were proposed in order to replace the older models such as ITU-R and COST-207, which were characteristic of narrowband systems or the power delay profiles of the second-generation digital wideband systems. The COST-259 recommendations set out to develop channel models, which allowed researchers to generate simulation results that were in good agreement with measurements, while exhibiting consistency, simplicity as well as completeness. The COST-259 models were categorized for macro-cells, micro-cells and pico-cells, each of which includes further sub-categories. For example, a number of COST-259 channel models are shown in Table 1.5 of Appendix I.3.

### 1.1.2 Wireless Communications Systems

#### 1.1.2.1 Cellular Mobile Technologies

The first-generation mobile communications network (1G) used analogue frequency modulation and was limited to voice only services. One of the first 1G networks was launched in 1979 by the Nippon Telegraph and Telephone (NTT) corporation in Japan. It was followed by a number of other systems, such as the Nordic Mobile Telephone (NMT) system in the Northern European countries, the Advanced Mobile Phone System (AMPS) used in North America and Australia, and so on.

The second-generation mobile communications network (2G), marked by the launch of the Global System for Mobile (GSM) communications [16], employed digital technology instead of its analogue

1G counterpart, resulting in a higher capacity and better voice quality. Owing to the employment of digital technology, the 2G systems are also capable of supporting data services, such as the Short Message Service (SMS) and Electronic Mail Service (Email), as well as enhancing their information security. The 2G systems are widely deployed. The GSM system [11] employs Time Division Multiple Access (TDMA) to separate users, while the Code Division Multiple Access (CDMA) distinguishes users by employing direct-sequence CDMA in combination with Phase Shift Keying (PSK) modulation and channel coding.

The 2G systems also include several evolutionary successors. For example, the employment of High-Speed Circuit-Switched Data provides higher data rates for circuit-switched services by reserving several time slots in each TDMA frame. The Generic Packet Radio Service (GPRS) [17] increases the peak data rate up to 140 kbps, when users occupy all time slots. Furthermore, the system known as the Enhanced Data rate for GSM Evolution (EDGE) system [18] offers a peak data rate of up to 384 kbps owing to employing high-level adaptive modulation and coding.

The 2G systems were succeded by the third-generation systems (3G) in early 2000s [19]. Along with the voice and data services of the 2G systems, the 3G systems additionally support mobile Internet access, video calls as well as mobile TV. The first 3G standard, which was the direct succesor of the GSM system, was referred to as Universal Mobile Telecommunications System (UMTS) [20] by the 3GPP in 2001, where the air interfaces options include Wideband CDMA (WCDMA) using a 5 MHz bandwidth, Time Division CDMA (TD-CDMA) and Time Division Synchronous CDMA (TD-SCDMA) [20]. The cdma-2000 system [21] using a 1.25 MHz bandwidth represents a further evolution of the classic CDMA principle.

The cdma-2000 system further evolved into the cdma-2000 1xEV-DO [22] arrangement by introducing the high rate packet data mode, which is capable of enabling a high data rate beyond 2 Mbps and relies on packet-switched techniques. The WCDMA concept evolved further by the introduction of the High-Speed Downlink Packet Access (HSDPA) in 2001 and then the High-Speed Uplink Packet Access (HSUPA) in 2005, that provided higher data speed rates up to 13 Mbps. The combination of HSDPA and HSUPA is known as HSPA at the time of writing [19]. By employing Multiple-Input-Multiple-Output (MIMO) techniques [23] combined with high-order modulation such as 16-QAM, HSPA further evolved into HSPA+ [23], that is capable of supporting peak data rates up to 84 Mbps in the downlink and 22 Mbps in the uplink per 5 MHz carrier.

More recently, the Long Term Evolution (LTE) standard [24] was ratified and is being rolled out at the time of writing. LTE is an all-IP based network architecture, utilizing cutting-edge hardware and digital signal processing techniques, such as MIMO, Orthogonal Frequency Division Multiple (OFDM) and so on. LTE is capable of supporting multiple bandwidths ranging from 1.4 MHz to 20 MHz, with a downlink peak data rate of at least 100 Mbps and uplink peak rates of at least 50 Mbps. The LTE system is often referred to the 3.9G arrangement.

The 2G and 3G systems may be expected to be replaced by the fourth-generation (4G) system, which is expected to provide a comprehensive and secure all-IP based mobile broadband solution to laptop computer based wireless modems, smart-phones and other mobile devices. The target of the 4G systems is to provide a peak data rate of up to 100 Mbps for high-mobility communication (such as from trains and cars) and up to 1 Gbps for low-mobility communication (such as pedestrians and

stationary users).

#### 1.1.2.2 Other Broadband Wireless Technologies

The so-called Wireless Fidelity (WiFi) system [25] provides another solution for broadband wireless access. The popular WiFi standards are based on the IEEE 802.11 family of standards [26, 27], employed primarily for Wireless Local Area Networking (WLAN). The 802.11a/b/g WiFi system operates in the unlicensed carrier bands of 2.4GHz and 5 GHz, supporting a peak data rate of 54 Mbps for both indoor and outdoor coverage over a range of a few hundred meters. Therefore, they can create a wireless communication infrastructure for small coverage areas such as an enterprise, an airport or hotel networks. Due to employing a simple so-called Carrier Sense Multiple Access scheme and operating in unlicensed carrier bands, the performance of WiFi is limited to small areas and low-speed mobility.

In order to overcome the constraints of the WiFi network, the Worldwide Interoperability for Microwave Access (WiMAX) system specified by the IEEE 802.16 standard [28] was developed for Wireless Metropolitan Area Networks (WMAN). WiMAX employs advanced communication techniques, such as Adaptive Modulation and Coding (AMC), Hybrid Automatic Repeat reQuest (H-ARQ), fast packet scheduling and bandwidth efficient handovers. Therefore, it is capable of offering peak data rates of up to 1 Gbps. Mobile WiMAX, an evolution of WiMAX based on the IEEE 802.16e standard [29], is capable of supporting both fixed and mobile applications, while improving the users' integrity, throughput and mobility.

The evolution of wireless standards is illustrated in Fig. 1.8.

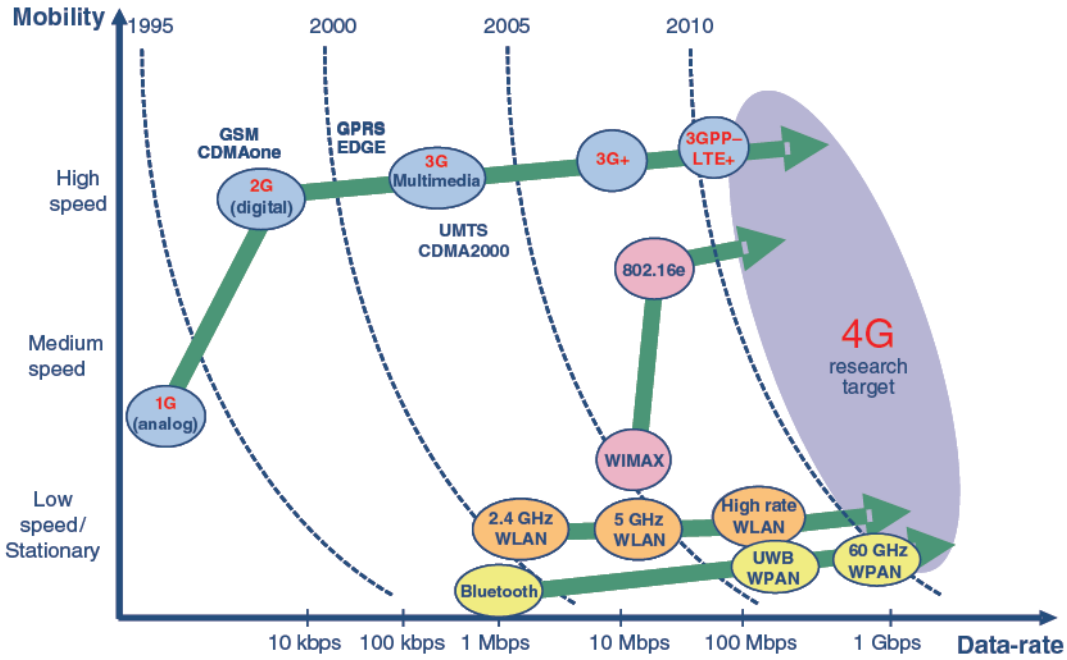


Figure 1.3: The evolution of wireless standards (©Ali-Yahiya [30], p.3).

## 1.1.3 Co-located and Cooperative MIMO Systems

### 1.1.3.1 Co-located MIMO Systems

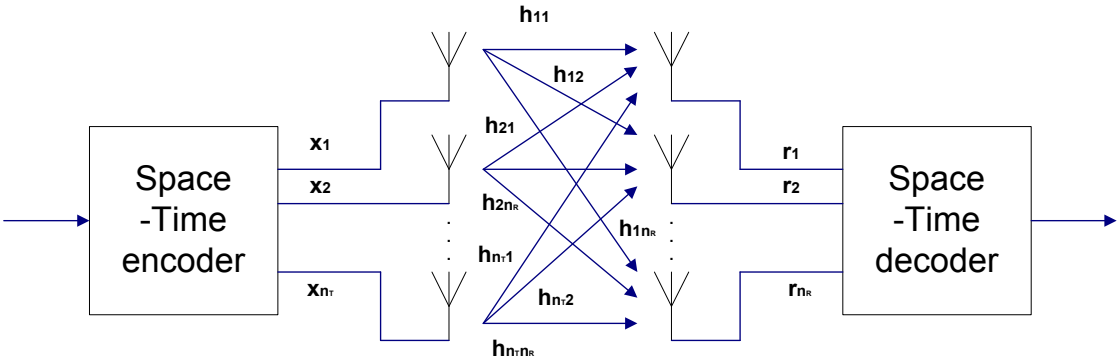


Figure 1.4: A typical MIMO communication.

In radio frequency communications, the term 'Multiple-Input-Multiple-Output' (MIMO) indicates the employment of multiple antennas at both the transmitter and receiver for the sake of improving the attainable performance. In a MIMO system, as seen in Fig. 1.4, the transmit signals are preprocessed and then sent simultaneously using several transmit antennas, before being separated at the receiver with the aid of advanced algorithms. The principle of MIMO communications offers the following advantages:

- Increasing the data throughput (more bits per second per Hertz of bandwidth) since multiple symbols are transmitted at the same time.
- Providing an improved transmission quality, since the fading effects are reduced by the diversity gain attained.
- Extending the network's coverage as a benefit of higher-signal-quality reception.
- Improving the user position estimation with the aid of the reference arriving from various paths at an improved signal quality.

Despite its advantages, MIMO systems also have their disadvantages, namely:

- Increasing the system's complexity, since more components as well as advanced processing algorithms are required for separating the desired signals.
- Increasing the physical dimension of mobile devices, because a significant distance has to be maintained between the antenna elements, in order to guarantee the independent fading of the transmitted signals of each antenna.

MIMOs may be divided into three main categories, as follows:

- Beamforming: In wireless transmissions the transmitted signals propagate via several paths and hence arrive at the receiver from different directions. If the directions of the propagation paths

are known at the transmitter or receiver, beamforming techniques may be employed in order to form a directional beam pattern towards a specified antenna. In other words, the signal is emitted from each of the transmit antennas with appropriate phase (and sometimes gain) weighting, so that the transmitted signal power is maximized in the direction of the receiver, while less power is wasted in other directions. Hence, significant SNR gains, which are also termed as 'array gains', can be achieved in comparison to a single-antenna aided system. Additionally, beamforming is capable of reducing the co-channel interference or multi-user interference, since the transmitted signal's beam is directed towards the desired receiver, rather than interfering with others.

- Spatial multiplexing: In spatial multiplexing the source bit sequence is split into $N_t$ sequences, which are processed and transmitted simultaneously from $N_t$ antennas using the same frequency. At the receiver, interference cancelation is employed for separating the transmitted sequences. Spatial multiplexing is a powerful technique of increasing the attainable channel capacity at higher SNRs, which may be employed both with and without the knowledge of the channel of each antenna element.

- Diversity-oriented MIMOs: In transmit diversity arrangements the transmitted signal is processed by space-time coding and then transmitted from multiple antennas. An SNR gain, also known as diversity gain, may be achieved by exploiting the independent fading of the multiple antenna links.

Owing to these properties, MIMOs constitute an important part of wireless communication standards, such as IEEE 802.11n (WiFi), 3GPP LTE, WiMAX as well as the forthcoming 4G scheme. In this thesis the classic MIMO systems are employed, where multiple transmit and/or receive antennas are invoked at a specific transmitter and/or receiver. These arrangements may be referred to as MIMOs having co-located elements, in order to distinguish them from the family of distributed MIMOs, also known as 'cooperative' MIMOs. The scenario of cooperating distributed antenna elements will be detailed in Section 1.1.3.2, where the transmit and/or receive antennas may belong to different transmitters and/or receivers.

#### 1.1.3.2 Cooperative MIMO Systems

As mentioned in Section 1.1.3.1, MIMO techniques require a substantial spacing amongst the antennas to achieve the maximum attainable diversity gains. This requirement makes the employment of MIMOs in compact mobile handsets impractical. Cooperative MIMO communications, which allow single-antenna aided mobiles to reap some of the benefits of MIMO systems, emerges as a solution. The basic idea is that single-antenna aided mobiles operating in a multi-user scenario can "share" their antennas in a manner that creates a virtual MIMO system. The cooperative arrangements allow the system to approach the maximum attainable diversity gain as well as the multiplexing gain of co-located MIMOs. However, to achieve the potential benefits of co-located MIMOs, the cooperative MIMOs have to address a range of challenges, such as the throughput loss of the cooperating mobiles, the increased interference in the network, cooperating partner assignment and hand-overs, fairness of the system, etc.

The technical description and historic evolution of both co-located and cooperative MIMOs will

be detailed in Chapter 2.

## 1.2 Hybrid Automatic-Repeat-reQuest Protocol

### 1.2.1 ARQ Protocol

The Automatic-Repeat-reQuest (ARQ) protocol [31] constitutes a beneficial error-control method conceived for data communication over hostile channels. Its operation relies on both packet acknowledgement and time-out mechanisms. More particularly, if an acknowledgement from the receiver does not reach the transmitter before the elapse of its time-out period, the packet will be retransmitted until an acknowledgement is received or the predefined number of retransmissions has been exhausted.

There are three main types of the ARQ protocol, including:

- Stop-and-wait ARQ: In this type, the transmitter sends one packet at a time and waits for the acknowledgement. If the acknowledgement is received, a new packet will be transmitted. Otherwise, a retransmission is activated.
- Go-Back-N ARQ: The transmitter continuously sends a number of packets specified by a window size of $N$. The receiver will observe the packet index. If a packet's index is not as expected, a negative acknowledgement will be returned to the transmitter, which contains this index and all the following packets will be ignored. The transmitter will retransmit the packets, commencing from the most recent positively acknowledged packet. If the acknowledgement is missing, all the packets belonging to the specific window size will be retransmitted.
- Selective Repeat ARQ: Unlike the Go-Back-N ARQ, this type will continue to process the packets after the expected packet index, which was missing. As a result, only the specific packets, which are missing or corrupted, are retransmitted.

### 1.2.2 H-ARQ Protocol

In order to improve the achievable ARQ efficiency in wireless channels, the ARQ protocol is usually combined with Forward Error Correcting (FEC) and detection codes. This combination is known as the Hybrid-ARQ (H-ARQ) protocol. This technique was introduced in the 1960s by Wozencraft and Horstein [31, 32], for both error detection and error correction combined with retransmission requests. If the channel quality is sufficiently good and all transmission errors are correctable, the receiver will request a new packet's transmission. On the other hand, if not all transmission errors may be corrected at the receiver, the received coded data block is rejected and a retransmission is requested by the receiver, similar to basic ARQ philosophy [33]. This system is now known as the Type-I H-ARQ.

An improved version of this system, known as the Type-II H-ARQ, was invented by Lin and Yu [34], which was then modified in [35]. In the Type-II H-ARQ system, the transmitter sends additional parity bits to the receiver instead of simply retransmitting the original packet, when a retransmission request is issued. If packet still cannot be correctly decoded, the consecutive transmissions may provide further parity information [33].

Naturally, the combination of FEC codes and the classic ARQ protocol is capable of improving the achievable throughput and of reducing the number of retransmissions, hence the delay. Type-I H-ARQ typically suffers from a throughput loss due to rejecting erroneous packets, which may be partially recoverable. By contrast, Type-II H-ARQ does not, because only additional parity bits are transmitted and combined with subsequent transmissions attempts in order to improve the probability of error-free detection. Under favourable propagation conditions, Type-II H-ARQ performs as well as standard ARQ in terms of its throughput. By contrast, in poor signal conditions, Type-II H-ARQ performs as well as standard FEC dispensing with retransmissions.

Diverse FEC schemes may be employed in H-ARQ systems. In the early stages of development, simple channel codes, such as Golay codes or the Reed-Solomon (ReS) codes were combined with ARQ. The development of further advanced codes such as Turbo Codes [36] or Low Density Parity Check (LDPC) [37] rendered H-ARQ schemes more attractive in terms of improving the system's efficiency. More recently, the family of rateless codes, which are powerful erasure-filling codes, including Luby Transform (LT) codes [38] and Raptor codes [39] were also employed in H-ARQ systems for transmission over wireless networks. The H-ARQ principle is widely employed in contemporary communication systems, such as the UMTS and the 3GPP LTE standards [19] or in the IEEE 802.16 mobile WiMAX systems [29].

## 1.3 Outline of the Thesis and Novel Contributions

### 1.3.1 Outline of the Thesis

In this thesis, the performance of H-ARQ systems will be investigated in the context of cooperative wireless communications networks. First, the family of MIMO techniques is reviewed briefly in Chapter 2 in order to understand their advantages as well as disadvantages when employed in practical systems. A range of recent cooperative communication techniques will also be detailed and categorized in this chapter. In Chapter 3, systems utilizing coherent detection will be studied in order to evaluate the potential performance benefits of an H-ARQ system in cooperative environments. We will demonstrate that apart from their beneficial diversity gain, cooperative schemes are also capable of improving both the achievable throughput and power efficiency. Chapter 4 analyses the impact of channel estimation (CE) accuracy on coherent detection aided H-ARQ schemes, using FEC coding for transmission over both the conventional direct transmission aided and cooperative communication networks, since naturally, perfect CE is not possible in practical systems. Furthermore, in order to avoid the detrimental effects of channel estimation errors in coherent detection aided schemes, non-coherent detection schemes combined with H-ARQ are also investigated in Chapter 5. Our comparisons between the coherent and non-coherent detection arrangements are also included in Chapter 5. Finally, our conclusions and future research suggestions are offered in Chapter 6. The organization of the thesis is summarized in Fig. 1.5 and detailed as follows:

- **Chapter 2: Multiple-Input-Multiple-Output Systems Using Co-located and Distributed Antenna Elements**
  - In this chapter the well-known transmit and receive diversity based MIMO techniques will

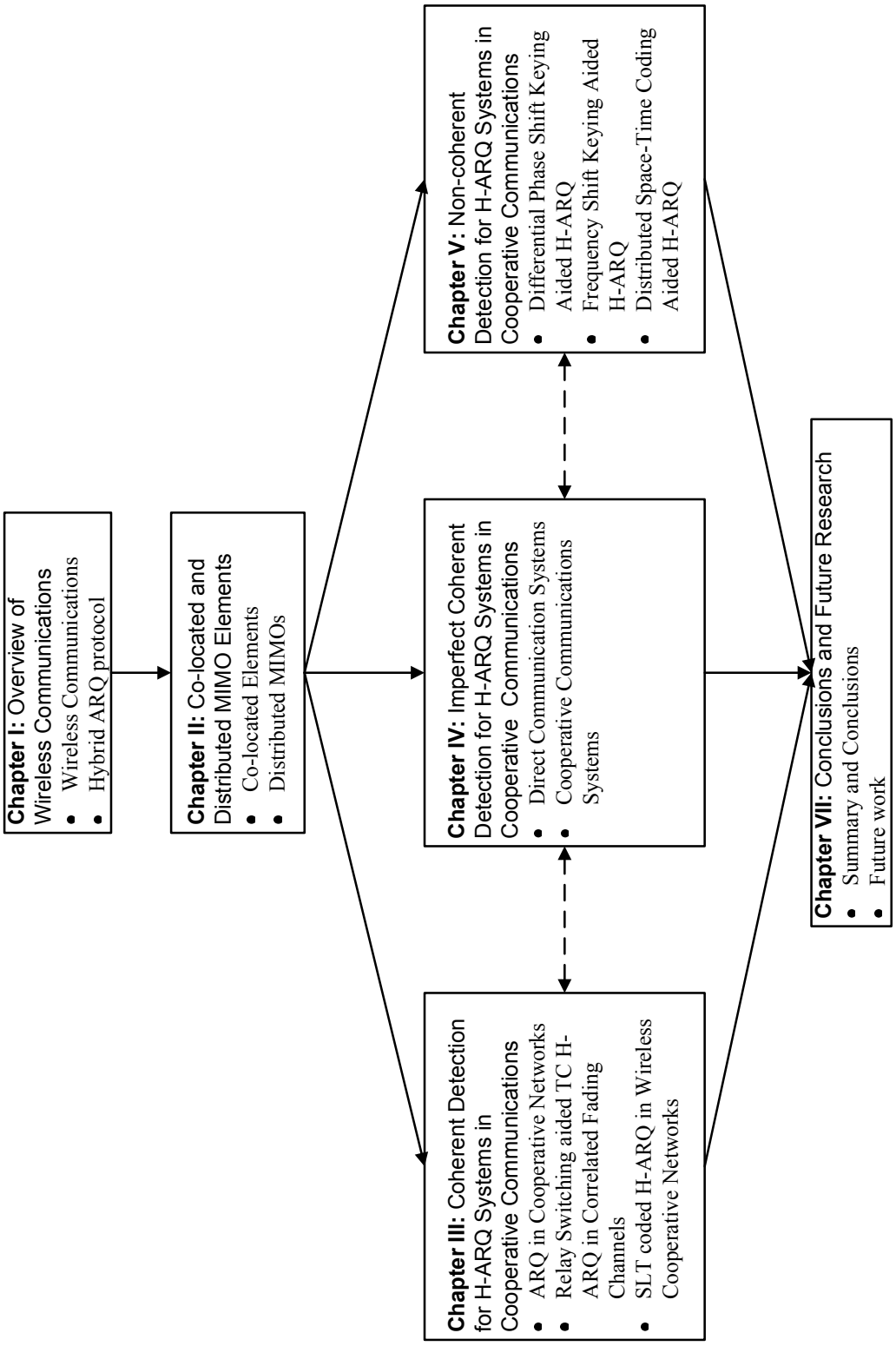


Figure 1.5: Thesis organization

be reviewed in Sections 2.2.1-2.2.3. They are followed by the introduction of the novel Space-Time-Frequency Shift Keying (STFSK) concept, where a beneficial diversity gain may be gleaned from three different domains, namely the Space-, Time- and Frequency-Domain (SD, TD, FD) in Section 2.2.4. In Section 2.2.4.4 we propose the soft-output STFSK demapper concept, which is a crucial element conceived for supporting iterative detection, while the decoding complexity of both soft- and hard-detections is considered in Section 2.2.4.7. Furthermore, the performance of the proposed STFSK scheme is detailed in Section 2.2.4.9. More particularly, STFSK is first investigated in single-user interference-limited environments. Then the philosophy of STFSK is developed into a multi-user, multi-cell Slow Frequency Hopping Multiple Access (SFHMA) system in order to investigate the effects of these techniques on the performance of the holistically optimized system. The proposed system's area spectral efficiency is investigated in various cellular frequency reuse structures. Additionally, it is compared to both classic Gaussian Minimum Shift Keying (GMSK) aided SFHMA as well as to GMSK assisted Time Division/ Frequency Division Multiple Access (TD/FDMA). The more sophisticated third-generation WCDMA and the LTE systems are also included in our comparisons.

– Apart from co-located MIMO elements, we also introduced the concept of cooperative communications in Section 2.3. The most popular cooperation techniques are described in Section 2.3.2, while the class of cooperative protocols will be detailed in Section 2.3.3. In Section 2.3.4 a number of performance results are provided, where both uncoded and distributed space-time coded systems are considered. We will demonstrate in Section 2.3.4 that the employment of MIMO techniques in cooperative wireless networks achieves diversity and/or multiplexing gains, as in the traditional co-located MIMO systems, but these benefits are offset by the throughput-reduction imposed by invoking some of the time/frequency slots for cooperation.

- **Chapter 3: Coherent Detection for H-ARQ Aided Cooperative Wireless Communications**

  – In this chapter we combine the advantages of cooperative wireless networks with those of H-ARQ systems employing coherent detection, where perfect CSI is assumed to be available at the receivers. We commence in Section 3.2 by investigating the attainable performance of cooperative ARQ solutions in both uncorrelated and correlated fading channels, where a novel relay-switching regime is proposed for mitigating the detrimental effects of correlated fading without unduly increasing the system's complexity and delay. In Section 3.2.5 we demonstrate that the proposed relay-switching scheme not only improves the system's BER and FER performance, but additionally reduces the number of retransmission. Hence, this proposal may reduce the transmit power, delay as well as interference imposed, despite increasing the achievable throughput. Furthermore, in Section 3.3 a novel relay-switching regime is proposed and intrinsically amalgamated with turbo coded H-ARQ schemes for achieving further improvements. In this relay-switching turbo coded H-ARQ regime the so-called Selective-Segment-Repeat (SSR) [23] technique is employed for transmission over fading channels.

  – We continue in Section 3.4 by studying H-ARQ systems employing Systematic Luby Trans-

form codes (SLT) [38, 40], which constitute a family of rateless codes in the context of cooperative wireless networks. First, in Section 3.4.1 we conceive a novel system based on the concatenation of SLT codes and 16-QAM, where the decoder and the demodulator iteratively exchange *extrinsic* information. We will demonstrate in Section 3.4.4 that the arrangement advocated is capable of providing a significant coding gain for transmission over Rayleigh fading channels compared to the system, where the SLT coding scheme and the demodulator operate independently. Moreover, a sophisticated H-ARQ aided SLT coded 16-QAM scheme using iterative detection is introduced in a relay-aided wireless network. The proposed scheme provides an increased spatial diversity gain for the signals received at the destination. As a result, the achievable Bit Error Ratio (BER) performance is enhanced. Additionally, in Section 3.4.4 we investigate the best transmit power sharing between the source and the relay stations and determine the best location for both AF and DF relaying schemes. Furthermore, we introduce an 'actively-cooperative' SLT coded 16-QAM aided H-ARQ scheme in Section 3.4.2 in order to reduce the number of incremental redundancy transmissions required. This arrangement may reduce the system's total transmit power as well as may increase the attainable throughput, as detailed in Section 3.4.4. Analytical expressions are provided in Section 3.4.3 for characterizing the system.

- **Chapter 4: Imperfect Coherent Detection for H-ARQ Aided Cooperative Wireless Communications**
  - *Direct Communications Systems:* In Section 4.2 the associated goodput equation is derived based on the achievable throughput and the accepted packet error ratio (APER). Owing to the dependence of both the throughput and the APER on the CE, we demonstrate in Section 4.2.3.1 that the goodput also varies in accordance with the CE. Thus, the accuracy of the CE has an important role in determining the achievable goodput. The Mean Square Error (MSE) of the channel estimates is utilized as a quality metric. Moreover, it is plausible that the channel estimates' accuracy depends on the energy of pilot symbols. Thus, a power sharing between the uncoded pilot and coded data bits will be proposed in Section 4.2.3.2 in order to maximize the system's goodput. The results of Section 4.2.4 will quantify the impact of CE accuracy on the ReS/H-ARQ systems' performance.
  - *Cooperative Communications Systems:* The investigations cast in the context of direct communications systems in Section 4.2 will be further developed to cooperative communication networks in Section 4.3. The proposed system will then be studied in the context of both AF and DF relaying networks, where the benefits of multiple cooperative stations will also be quantified. Similar to direct communication systems, the corresponding bit error probability and goodput will be characterized in Section 4.3.2 in order to theoretically evaluate the entire system's performance. The effects of several components on the CE accuracy will also be considered. Furthermore, the results of Section 4.3.3 will be employed to find optimal solutions both for minimizing the BEP and for maximizing the system's attainable goodput. Finally, both relay-position selection and source-relay power allocation arrangements will be suggested, based on the procedures of Section 4.3.3, in order to maximize the overall achievable performance.
- **Chapter 5: Non-coherent Detection for H-ARQ Aided Cooperative Wireless Com-**

**munications**

- In order to avoid channel estimation, non-coherent detection schemes will be proposed for H-ARQ systems in this chapter. The first non-coherent detection technique studied in Section 5.2 is based on classic Differential Phase Shift Keying (DBPSK), where both the single-symbol and multiple-symbol differential detection are compared. These investigations are followed by the comparison of both perfect and imperfect channel estimation aided, as well as of non-coherent detection assisted schemes in Section 5.2.3.
- Furthermore, non-coherent FSK aided H-ARQ arrangements are proposed in Section 5.3. In this section, we propose and characterize a ReS coded SFH M-FSK system, which is subjected to both partial-band interference and Rayleigh fading in the context of a cooperative wireless network. An Erasure Insertion (EI) scheme conceived for error-and-erasure ReS decoding based on the joint Maximum Output - Ratio Threshold Test (MO-RTT) technique will be invoked. In Section 5.3.1.3 the related decision statistics will be analysed and the corresponding analytical expressions of the ReS codeword error probability as well as of the bit error ratio (BER) of error-and-erasure decoding will be derived. The performance of our relay-aided ReS coded SFH M-FSK system using EI techniques will be characterized in Section 5.3.1.4. Moreover, we compare the attainable performance of the proposed ReS coded system to that of convolutional codes and LDPC codes [37], both of which support efficient iterative detection at the cost of relying on sophisticated transceiver designs. As a further study, in Section 5.3.2 non-coherent FSK is combined with convolutional coding in order to carry out iterative detection in the context of cooperative wireless communications.
- Finally, in order to mitigate the throughput loss imposed by the cooperative phase of relaying networks, in Section 5.4 we propose a novel system design based on differential space-time-block codes [41] and cooperative H-ARQ. The system design and its analysis are detailed in Section 5.4.1.2, while its performance is characterized in Section 5.4.1.3.

- **Chapter 6: Conclusions and Future Research**
  The last chapter includes summaries and conclusions on the main findings of this thesis. They are followed by a number of suggestions for my future research.

### 1.3.2 Novel Contributions

The thesis is based on 8 publications and 4 submitted papers, which [1–8, 42–45] cover the following novel aspects.

- In Section 2.2.4 the novel STFSK concept [5] is proposed, where a beneficial diversity gain may be gleaned from three different domains, namely the SD, the TD, and the FD. This scheme is capable of striking a flexible diversity versus multiplexing tradeoff, while reducing the effects of both inter-channel interference as well as of inter-symbol interference. The design also includes the soft-output STFSK demodulator conceived for iterative detection in Section 2.2.4.4. Furthermore, the decoding complexity of both the hard- and soft-decision aided STFSK demodulator is derived in Section 2.2.4.7, followed by its detailed performance characterization in Section 2.2.4.9 [44].

- In Section 2.2.4.9 the STFSK concept is further developed into a multi-user, multi-cell SFHMA system in order to investigate the effects of these techniques on the performance of the holistically optimized system. The resultant system is compared to standardized wireless communication systems, such as the GSM, the WCDMA and the LTE systems [43, 45].

- In order to mitigate the detrimental effects of correlated fading without unduly increasing the system's complexity and delay, in Section 3.3 a novel relay-switching regime is proposed and intrinsically amalgamated with turbo coded H-ARQ schemes for the sake of achieving additional improvements. Furthermore, this turbo coded relay-switching H-ARQ scheme is combined with the SSR [23] technique for the sake of exploiting the block-error characteristics of turbo codes, when communicating over fading channels. This arrangement improves both the attainable BER as well as FER performance, while reducing the number of retransmissions. Hence, the overall system throughput is improved [7].

- In Section 3.4 we conceive a novel system based on the concatenation of SLT codes and 16-QAM [2,4,6], where the decoder and the demodulator iteratively exchange *extrinsic* information, as detailed in Section 3.4.1. As demonstrated in Section 3.4.4, the arrangement is capable of providing a significant coding gain for transmission over Rayleigh fading channels over the system, where the SLT coding scheme and the demodulator operate independently. Moreover, a sophisticated H-ARQ aided SLT coded 16-QAM scheme using iterative detection is introduced in our relay-aided wireless network, where the best transmit power sharing regime between the source and the relay stations as well as the best location of both AF and DF relays is identified as part of a novel resource allocation regime. Furthermore, we proposed an 'actively-cooperative' SLT coded 16-QAM aided H-ARQ scheme in Section 3.4.2 in order to reduce the system's total transmit power, while increasing the attainable throughput.

- In Section 4.2 we conceived a frame work for analysing the impact of imperfect CSI on a H-ARQ scheme. In particular, both the goodput and the APER are derived in Section 4.2.3.1 based on the MSE of channel estimation. Moreover, a power-sharing regime between the uncoded pilots and the coded data bits will be proposed in Section 4.2.3.2 in order to maximize the system's goodput [1].

- Based on the process proposed for the conventional direct communication based systems, the impact of imperfect CSI on a relay-aided H-ARQ scheme [7] is investigated in Section 4.3. The proposed system is considered in the context of both AF and DF relaying networks, where the effects of multiple cooperating stations are also studied. Similarly, the goodput and the APER are characterized in Section 4.3.2 based on the MSE of channel estimation. These investigations recommend optimal solutions both for minimizing the BEP and for maximizing the system's attainable goodput. Additionally, both relay-position selection and source-relay power allocation arrangements are found in Section 4.3.3, in order to maximize the achievable performance.

- In Section 5.3.1, we propose and characterize a ReS coded SFH M-FSK system, which is subjected to both partial-band interference/jamming and to Rayleigh fading in the context of our cooperative network [8, 42]. An EI scheme conceived for error-and-erasure ReS decoding based on the joint MO-RTT technique is invoked. The related decision statistics are analysed and

the corresponding analytical expressions of the ReS codeword error probability as well as of the BER is derived in Section 5.3.1.3.

- We propose a novel system design based on differential space-time-block codes [41] and cooperative H-ARQ in Section 5.4. This arrangement only invokes retransmissions during the cooperation phase, instead of splitting the original single timeslot into two phases, as in traditional cooperation. Moreover, the initial transmission is also exploited as one of the components of the STBC. As a result, the proposed scheme may significantly improve the system's overall performance in terms of the BER and FER performance as well as the throughput.

## 1.4 Chapter Summary

In this chapter we provided an overview of wireless communications systems. Initially, simple wireless channels, including both theoretical models and standardized channels, were introduced in Section 1.1.1 in order to review their characteristics, which have significant effects on the attainable performance of wireless systems. Then the well-known wireless standards and their historic evolution was reviewed in Section 1.1.2. Section 1.1.3 briefly discussed both co-located and distributed MIMO elements and their benefits. Furthermore, the ARQ and H-ARQ protocols were introduced in Section 1.2. Finally, Section 1.3 provided the outline of the thesis and its novel contributions.

# Appendix I.

## I.1. ITU Channel Models

Table 1.1: ITU channel model for indoor office

| Tap | Channel A | | Channel B | |
|---|---|---|---|---|
| | Relative Delay (ns) | Average Power (dB) | Relative Delay (ns) | Average Power (dB) |
| 1 | 0 | 0 | 0 | 0 |
| 2 | 50 | -3.0 | 100 | -3.6 |
| 3 | 110 | -10.0 | 200 | -7.2 |
| 4 | 170 | -18.0 | 300 | -10.8 |
| 5 | 290 | -26.0 | 500 | -18.0 |
| 6 | 310 | -32.0 | 700 | -25.2 |

Table 1.2: ITU channel model for outdoor to indoor and pedestrian test environment

| Tap | Channel A | | Channel B | |
|---|---|---|---|---|
| | Relative Delay (ns) | Average Power (dB) | Relative Delay (ns) | Average Power (dB) |
| 1 | 0 | 0 | 0 | 0 |
| 2 | 110 | -9.7 | 200 | -0.9 |
| 3 | 190 | -19.2 | 800 | -4.9 |
| 4 | 410 | -22.8 | 1200 | -8.0 |
| 5 | - | - | 2300 | -7.8 |
| 6 | - | - | 3700 | -23.9 |

Table 1.3: ITU channel model for vehicular test environment

| Tap | Channel A | | Channel B | |
|---|---|---|---|---|
| | Relative Delay (ns) | Average Power (dB) | Relative Delay (ns) | Average Power (dB) |
| 1 | 0 | 0.0 | 0 | -2.5 |
| 2 | 310 | -1.0 | 300 | 0.0 |
| 3 | 710 | -9.0 | 8900 | -12.8 |
| 4 | 1090 | -10.0 | 12900 | -10.0 |
| 5 | 1730 | -15.0 | 17100 | -25.2 |
| 6 | 2510 | -20.0 | 20000 | -16.0 |

## I.2. COST-207 Channel Models

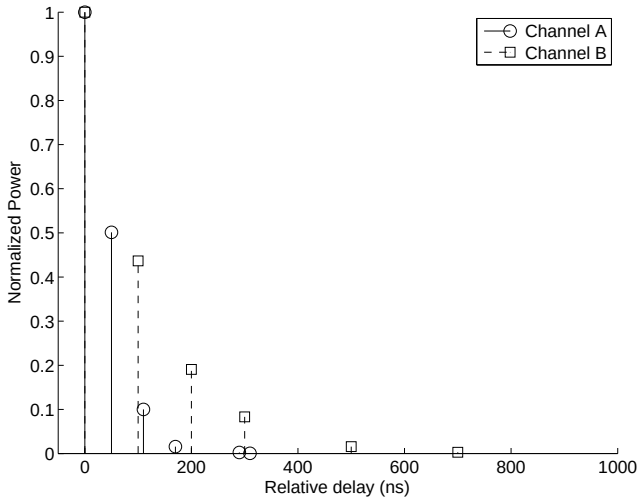


Figure 1.6: The channel impulse response of the ITU channel model for the indoor of office of Table 1.1.

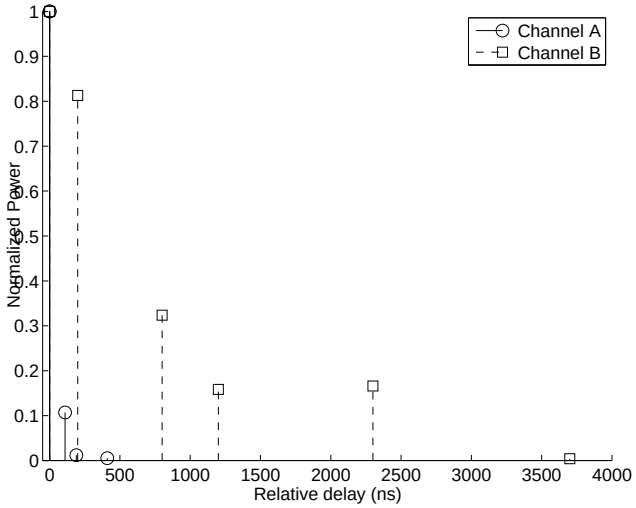


Figure 1.7: The channel impulse response of the ITU channel model for the outdoor to indoor and pedestrian test environment of Table 1.2.

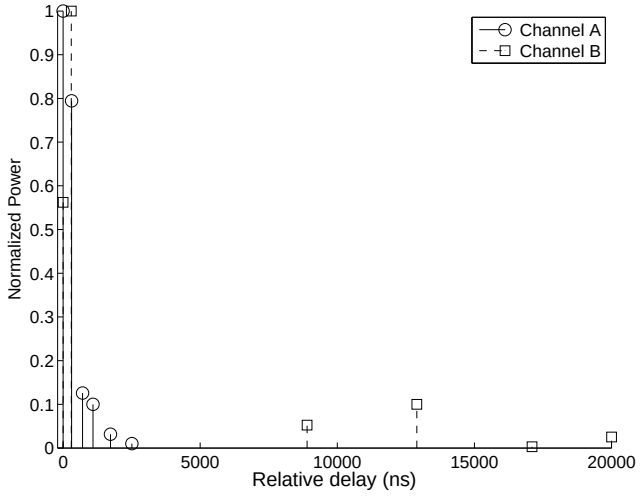


Figure 1.8: The channel impulse response of the ITU channel model for the vehicular test environment of Table 1.3.

Table 1.4: COST-207 channel models for Rural Area (RA), Typical Urban (TU), Bad Urban (BU) and Hilly Terrain (TU) environments.

| Tap | COST-207-RA | | | COST-207-TU | | | COST-207-BU | | | COST-207-HT | | |
|---|---|---|---|---|---|---|---|---|---|---|---|---|
| | Relative delay (ns) | Average power (dB) | Doppler spectrum | Relative delay (ns) | Average dower (dB) | Doppler spectrum | Relative delay (ns) | Average power (dB) | Doppler spectrum | Relative delay (ns) | Average power (dB) | Doppler spectrum |
| 1 | 0 | 0 | Jakes | 0 | -3 | Jakes | 0 | -3 | Jakes | 0 | 0 | Jakes |
| 2 | 100 | -4 | Jakes | 200 | 0 | Jakes | 400 | 0 | Jakes | 200 | -2 | Jakes |
| 3 | 200 | -8 | Jakes | 600 | -2 | GaussI | 1000 | -3 | GaussI | 400 | -4 | Jakes |
| 4 | 300 | -12 | Jakes | 1600 | -6 | GaussI | 1600 | -5 | GaussI | 600 | -7 | Jakes |
| 5 | 400 | -16 | Jakes | 2400 | -8 | GaussII | 5000 | -2 | GaussII | 15000 | -6 | GaussII |
| 6 | 500 | -20 | Jakes | 5000 | -10 | GaussII | 6600 | -4 | GaussII | 17200 | -12 | GaussII |
| 1 | | | | 0 | -4 | Jakes | 0 | -7 | Jakes | 0 | -10 | Jakes |
| 2 | | | | 200 | -3 | Jakes | 200 | -3 | Jakes | 200 | -8 | Jakes |
| 3 | | | | 400 | 0 | Jakes | 400 | -1 | Jakes | 400 | -6 | Jakes |
| 4 | | | | 600 | -2 | GaussI | 800 | 0 | GaussI | 600 | -4 | GaussI |
| 5 | | | | 800 | -3 | GaussI | 1600 | -2 | GaussI | 800 | 0 | GaussI |
| 6 | | | | 1200 | -5 | GaussI | 2200 | -6 | GaussII | 2000 | 0 | GaussI |
| 7 | | | | 1400 | -7 | GaussI | 3200 | -7 | GaussII | 2400 | -4 | GaussII |
| 8 | | | | 1800 | -5 | GaussI | 5000 | -1 | GaussII | 15000 | -8 | GaussII |
| 9 | | | | 2400 | -6 | GaussII | 6000 | -2 | GaussII | 15200 | -9 | GaussII |
| 10 | | | | 3000 | -9 | GaussII | 7200 | -7 | GaussII | 15800 | -10 | GaussII |
| 11 | | | | 3200 | -11 | GaussII | 8200 | -10 | GaussII | 17200 | -12 | GaussII |
| 9 | | | | 2400 | -6 | GaussII | 6000 | -2 | GaussII | 15200 | -9 | GaussII |
| 10 | | | | 3000 | -9 | GaussII | 7200 | -7 | GaussII | 15800 | -10 | GaussII |
| 11 | | | | 3200 | -11 | GaussII | 8200 | -10 | GaussII | 17200 | -12 | GaussII |
| 12 | | | | 5000 | -10 | GaussII | 10000 | -15 | GaussII | 20000 | -14 | GaussII |

## I.3. COST-259 Channel Models

Table 1.5: COST-259 channel models for Rural Area (RA), Typical Urban (TU) and Hilly Terrain (TU) environments.

| Tap | COST-259-TUx | | COST-259-RAx | | COST-259-HTx | |
|---|---|---|---|---|---|---|
| | Relative Delay (ns) | Average Power (dB) | Relative Delay (ns) | Average Power (dB) | Relative Delay (ns) | Average Power (dB) |
| 1 | 0 | -5.7 | 0 | -5 | 0 | -13 |
| 2 | 217 | -7.6 | 42 | -6.4 | 356 | -8.9 |
| 3 | 512 | -10.1 | 101 | -8.4 | 441 | -10.2 |
| 4 | 514 | -10.2 | 129 | -9.3 | 528 | -11.5 |
| 5 | 517 | -10.2 | 149 | -10.0 | 546 | -11.8 |
| 6 | 674 | -11.5 | 245 | -13.1 | 609 | -12.7 |
| 7 | 882 | -13.4 | 312 | -15.3 | 625 | -13.0 |
| 8 | 1230 | -16.3 | 410 | -28.5 | 842 | -16.2 |
| 9 | 1287 | -16.9 | 469 | -20.4 | 916 | -17.3 |
| 10 | 1311 | -17.1 | 528 | -22.4 | 941 | -17.7 |
| 11 | 1349 | -17.4 | | | 15000 | -17.6 |
| 12 | 1533 | -19.0 | | | 16172 | -22.7 |
| 13 | 1535 | -19.0 | | | 16492 | -24.1 |
| 14 | 1622 | -19.8 | | | 16876 | -25.8 |
| 15 | 1818 | -21.5 | | | 16882 | -25.8 |
| 16 | 1836 | -21.6 | | | 16978 | -26.2 |
| 17 | 1884 | -22.1 | | | 17615 | -29.0 |
| 18 | 1943 | -22.6 | | | 17827 | -29.9 |
| 19 | 2048 | -23.5 | | | 17849 | -30.0 |
| 20 | 2140 | -24.3 | | | 18015 | -30.7 |

# Chapter 2

# Multiple-Input-Multiple-Output Systems Using Co-located and Distributed Antenna Elements

## 2.1 Introduction

The family of multiple-input-multiple-output (MIMO) arrangements designed for wireless communications has attracted substantial research attention owing to its potential to increase the attainable capacity without requiring additional bandwidth. The class of spatial division multiplexing, such as the family of BLAST schemes [46], is capable of increasing the transmission rate, i.e the multiplexing gain, at the cost of significantly increasing the decoding complexity. By contrast, the low complexity Space-Time-Block-Codes (STBC) [47, 48] are capable of maximizing the attainable diversity order, but fail to attain a multiplexing gain. A tradeoff between the two schemes can be achieved by employing the Linear Dispersion Codes (LDC) proposed in [49]. Furthermore, Haas and his team [50, 51] proposed the Spatial Modulation (SM), while the team of Ghrayaeb and Szczecinski [52] introduced the Space Shift Keying (SSK) concept into MIMO communications. The philosophy of these schemes is to activate only a single transmit antenna at any instant in order to maintain a low complexity, whilst avoiding any inter-antenna interference and inter-antenna synchronization. Motivated by the above concepts, the authors of [53] conceived Space-Time Shift Keying (STSK), which strikes an improved diversity versus multiplexing tradeoff. Additionally, it results in a reduced-complexity system operating at a higher capacity than the SM/SSK and BLAST schemes. All of the well-known MIMO techniques are summarized in Table 2.1 and briefly reviewed in this chapter.

Against this backcloth, Section 2.2.4 of this chapter describes the novel Space-Frequency Shift Keying (SFSK) concept, where the transmit signal is spread across both the space and frequency domains, as well as the further evolved Space-Time-Frequency Shift Keying (STFSK) concept, where a beneficial diversity gain may be gleaned from three different domains, namely the Space-, Time- and Frequency-Domain (SD, TD, FD). In addition to the advantages provided by STSK modulation, the STFSK scheme also avoids the Inter-Symbol Interference (ISI) imposed by frequency-selective fading channels. In Section 2.2.4.4 we propose the soft-output STFSK demapper concept, which is a crucial

Table 2.1: Major MIMO techniques

| Year | Author(s) | Contribution |
|---|---|---|
| 1959 | Brennan [54] | Provided analyses of three types of diversity combining systems, namely Selection Combining (SC), Maximal-Ratio Combining (MRC), and Equal-Gain Combing (EGC). |
| 1991 | Wittneben [55] | Proposed a base station modulation diversity scheme which employs multiple BSs transmitting the same signals in order to gain a bandwidth efficiency. |
| 1993 | Wittneben [56] | Proposed and analysed a system employing several transmit antennas, which have different modulation parameters, to achieve diversity at the benefit of no bandwidth expansion. |
| 1994 | Winters [57] | Demonstrated that the number of transmit antennas may provide the same diversity benefit as the scheme proposed in [55]. |
| 1996 | Foschini [46] | Invented the diagonal BLAST providing the MIMO multiplexing gain. |
| 1998 | Wolniansky [58] | Proposed the V-BLAST architecture, which reduces the complexity of the diagonal ones. |
| | Alamouti [47] | Introduced a two-transmit antenna diversity scheme with simple linear detection. |
| | Tarokh *et al.* [48] | Studied the design criteria to achieve maximum diversity and coding gains, along with proposing the STTCs. |
| 1999 | Tarokh *et al.* [59–61] | Generalized Alamouti's scheme [47] for a system equipped with more than two transmit antennas, constituting STBCs. |
| | Guey *et al.* [62] | Proposed design criteria to achieve maximum transmit diversity gain. |
| 2001 | Hochwald *et al.* [63] | Presented the Space-Time-Spreading scheme. |
| | Jafarkhani [64] | Developed the quasi-orthogonal STBC, which achieves rate-one coding and partial diversity gain. |
| 2002 | Hassibi and Hochwald [49] | Proposed and analysed the LDCs, which offer a flexible trade-off between the diversity gain and multiplexing gain. |
| 2008 | Mesleh *et al.* [51] | Developed the SM, which provides a low-complexity implementation, whilst avoiding any inter-antenna interference and inter-antenna synchronization. |
| 2010 | Sugiura *et al.* [53, 65] | Conceived the STSK, which strikes an improved diversity versus multiplexing trade-off, while offering a higher-capacity than the SM and BLAST schemes. |

element conceived for supporting iterative detection, while the decoding complexity of both soft- and hard-detections is considered in Section 2.2.4.7.

Furthermore, in Section 2.2.4.9 the philosophy of STFSK is developed into a multi-user, multi-cell Slow Frequency Hopping Multiple Access (SFHMA) system in order to investigate the effects of these techniques on the performance of the holistically optimized system. More particularly, the proposed system's area spectral efficiency is investigated in various cellular frequency reuse structures. Additionally, it is compared to both classic Gaussian Minimum Shift Keying (GMSK) aided SFHMA as well as to GMSK assisted Time Division/ Frequency Division Multiple Access (TD/FDMA). The more sophisticated third-generation WCDMA and the LTE systems are also included in our comparisons.

In Section 2.3 we will introduce cooperative communications and some of its relevant aspects, such as the types of cooperation and the class of cooperative protocols. In Section 2.3.4 a number of performance results are provided where both the uncoded systems and distributed space-time coded systems are considered. We will demonstrate in Section 2.3.4 that the employment of MIMO techniques in wireless cooperative networks may reduce the network resources consumed, while retaining the diversity and/or multiplexing gains of the traditional co-located MIMO systems.

## 2.2 Co-located MIMO Elements

### 2.2.1 Spatial Diversity

#### 2.2.1.1 Receive Antenna Diversity

Receive antenna diversity is a classic low-complexity diversity technique, where multiple antennas are employed at the receiver. The independent signal paths received at the receive antenna are combined before recovering the transmit signal. In order to allow the received multiple-antenna-signal to be independent, the separation among the receive antennas must be sufficiently high. This condition makes the receive diversity techniques suitable for the Uplink (UL) where the base station is capable of accommodating multiple receive antennas.

Another factor affecting the system's performance is the choice of diversity combining techniques, each of which treats the treatment of the combined signals' phase and amplitude differently at the receiver. The receive diversity combining techniques are often divided into four main categories [66,67], as follows

- **Selection Combining (SC)**: The block diagram of the SC scheme [54], where $n_R$ antennas are employed at the receiver, is shown in Fig. 2.1, where the signal having the highest instantaneous SNR out of $n_R$ received signals is selected at every symbol interval as the output, implying the detection of the best incoming signal. In reality, the signal with the highest power at the receiver is often selected, since it is hard to estimate the SNR. Naturally, this combining scheme does not perform well in the low SNR region, because it is likely to select the signal contaminated by the highest noise power. This technique does not require CSI. Hence, it can be employed in both coherent and non-coherent modulation schemes.
- **Switched Combining (SwC)**: In the switched combining scheme [68], the receiver scans all

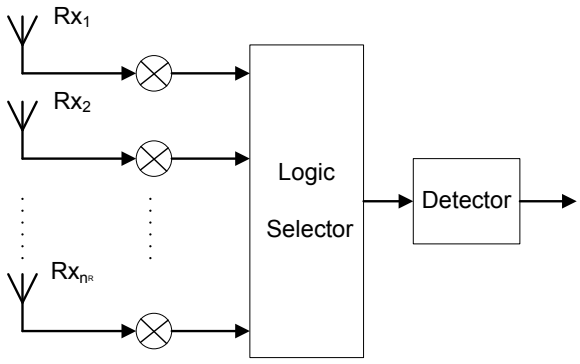


Figure 2.1: Selection combining.

signal paths received at the $n_R$ antennas and chooses a particular path, which has an SNR higher than a predefined SNR threshold. The chosen path is detected and remained, until its signal's SNR becomes lower than the threshold. In this case, the receiver will scan the received multipath signal again and will switch to another path, where the signal power is higher than the threshold value. In contrast to the SC scheme, which scans all received signal paths continuously and selects the path with the highest SNR value, the SwC scheme only detected the selected path upon its SNR still higher than the SNR threshold. Thus, it can reduce the system's complexity at the cost of an inferior performance, since the signal associated with the highest SNR might be ignored. Similar to the SC, the switched combining scheme can be employed in conjunction with both coherent and non-coherent modulation schemes.

- **Equal Gain Combining (EGC)**: The EGC technique [54] does not require the knowledge of the fading amplitude at the receiver. Thus, the weighting factor $w_i$ is simplified to [66]

$$w_i = e^{-j\phi_i}, \tag{2.1}$$

where $\phi_i$ is the phase of the channel coefficients. Compared to MRC, the EGC's performance is only slightly inferior, but its complexity is significantly reduced, since the knowledge of the fading amplitudes is not required. This technique is known as suboptimal. For coherent detection, the EGC can only be applied in conjunction with modulation schemes having identical symbol energies. If coherent detection is unavailable, the EGC must rely on non-coherent detection techniques such as Frequency Shift Keying (FSK) or DPSK modulation.

- **Maximum Ratio Combining (MRC)**: When accurate CSI is available at the receiver, the most potent MRC linear combining method [54] may be employed. As shown in Fig. 2.2, the signals received from $n_R$ antennas are individually weighted, before being phase-coherently combined. The weighting factor $w_i$ $(i = 1, 2, ..., n_R)$ may be chosen as [66]

$$w_i = \frac{h_i^*}{\sum_{i=1}^{n_R} h_i^* \cdot h_i}, \tag{2.2}$$

where $h_i$ is the channel coefficient at branch $i$. This combining technique is capable of maximizing the output SNR [66]. Thus it is known as the optimum receive diversity combining method. Due to the requirement of accurate CSI, the technique is only applicable to systems employing coherent detections.

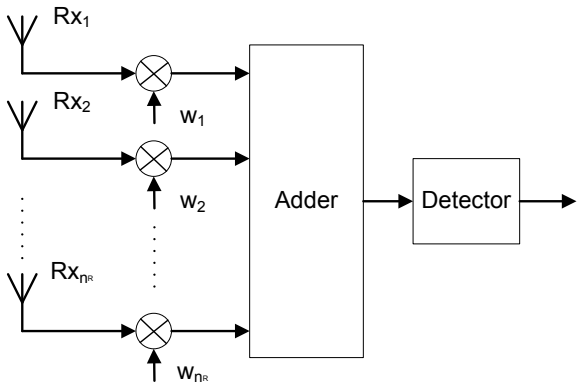


Figure 2.2: Maximum ratio combining, where the weighting factors are inserted before the adder, which replaces the logic selector in Fig. 2.1.

#### 2.2.1.2 Transmit Antenna Diversity

Exploiting multiple transmit antennas is another diversity technique, which requires the signals to be preprocessed or precoded before being allocated to the transmit antennas for transmission. Due to its substantial space requirements and signal preprocessing, the arrangement is more suitable for Downlink (DL) scenarios.

Consider a MIMO system equipped with $n_T$ transmit and $n_R$ receive antennas. Assuming that the data stream is encoded into a ST codeword of size $(n_T \times T)$, where $T$ is the ST block length, the signal vector received in time-slot $t$ $(t = 1, 2, ..., T)$ is given by

$$\boldsymbol{y}[t] = \boldsymbol{H}\boldsymbol{s}[t] + \boldsymbol{n}[t], \tag{2.3}$$

where $\boldsymbol{H}$ represents the $(n_R \times n_T)$-element channel matrix, while $\boldsymbol{n}$ is the AWGN vector associated with a covariance matrix of $N_0 I_{n_R}$. All the $T$ vectors may be stacked together, yielding

$$\boldsymbol{Y} = \boldsymbol{H}\boldsymbol{S} + \boldsymbol{N}, \tag{2.4}$$

where $\boldsymbol{Y} = [\boldsymbol{y}[1]\ \boldsymbol{y}[2] \cdots \boldsymbol{y}[T]]$ and $\boldsymbol{N} = [\boldsymbol{n}[1]\ \boldsymbol{n}[2] \cdots \boldsymbol{n}[T]]$ are matrices of size $(n_R \times T)$.

When the CSI is available and the ML detector is employed at the receiver, the estimated codeword may be obtained as

$$\hat{\boldsymbol{S}} = arg \min_{\boldsymbol{S}} ||\boldsymbol{Y} - \boldsymbol{H}\boldsymbol{S}||^2 = arg \min_{\boldsymbol{S}} \sum_{t=1}^{T} ||\boldsymbol{y}[t] - \boldsymbol{H}\boldsymbol{s}[t]||^2. \tag{2.5}$$

If the receiver detects a codeword other than a transmitted codeword, an error will occur.

**a. Space-Time Block Codes**

One of the renowned transmit diversity schemes is constituting by STBC, which was conceived by Alamouti [47] for a two-transmit antenna aided system. This scheme was then further developed by Tarokh *et al.* [48] for multiple transmit antennas.

An STBC may be represented by an $(n_T \times T)$-element encoding matrix, where each column represents a time slot and each row represents a specific antenna's transmission time slot. For example,

Alamouti's coding matrix for a two-transmit antenna aided system may be formulated as

$$\boldsymbol{S} = \begin{vmatrix} s_1 & -s_2^* \\ s_2 & s_1^* \end{vmatrix},$$

where $^*$ denotes the complex conjugate. In the first transmission time slot, the symbols $s_1$ and $s_2$ are transmitted by antenna 1 and antenna 2, respectively. In the next slot, the signal -$s_2^*$ is sent from antenna 1, while the signal $s_1^*$ is from antenna 2.

In order to achieve the maximum attainable diversity gain, the STBC has to satisfy the so-called orthogonal design criterion, which was derived by Tarokh *et al.* in [48]. Briefly, the encoding matrices have to satisfy the orthogonal property, which may be mathematically represented as

$$S.S^H = c(|s_1|^2 + |s_2|^2 + \cdots + |s_{n_T}|^2)I_{n_T}, \tag{2.6}$$

where $c$ is a constant, while $I_{n_T}$ represents an $(n_T \times n_T)$ identity matrix.

Each STBC is also represented by a code rate of

$$R = \frac{k}{T}, \tag{2.7}$$

where $k$ is the number of symbols in each encoding block while $T$ is the number of time slots used. The studies of [59,69,70] showed that only Alamouti's orthogonal STBC design is capable of achieving the maximum attainable rate of unity, which is also often termed as having full-rate. By contrast, other space-time codes have to sacrifice some proportion of their data rate for the sake of maximizing the diversity gain.

In contrast to the family of orthogonal STBC codes, which suffers throughput loss, the class of quasi-orthogonal STBCs and their design criteria was proposed by Jafarkhani [64]. The design allows a higher achievable code rate at the cost of imposing Inter-Symbol Interference (ISI) owing to the non-orthogonal transmissions from the different antennas/time-slots, which degrades the BER performance.

**b. Space-Time Trellis Codes**

STTCs were first proposed by Tarokh *et al.* [48, 60], which constitute further development of the conventional trellis codes [71] for multiple antenna aided systems. These codes are designed to achieve both a diversity gain and a coding gain. The design criteria conceived for PSK modulation are detailed in [72], while the general design criteria are described in [73]. Similar to classic trellis codes, each STTC is described by a trellis, where the number of nodes in the trellis diagram corresponds to the number of encoder states. Each node has a specific number of groups of symbols, which is known as the constellation size while each group consists of $n_T$ entries corresponding to the symbols transmitted from $n_T$ transmit antennas.

For instance, the trellis diagram of a 4-QAM scheme associated with a four-state trellis code and two-transmit antennas is illustrated in Fig. 2.3. The trellis has four nodes corresponding to four states. Each node has four legitimate entries constituted by two symbols, which are the outputs assigned to the two transmit antennas. The outputs $\{0, 1, 2, 3\}$ are mapped to the 4-QAM modulated symbols $\{1, j, -1, -j\}$. More particularly, observe in Fig. 2.3 that assuming the current symbols are 03 and the current state is 0, the output of 3 and 0 are assigned to antenna 1 and antenna 2, respectively,

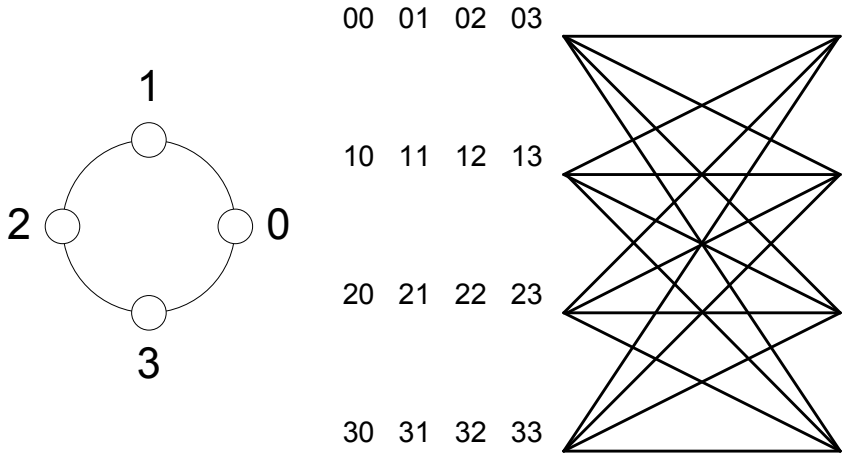


Figure 2.3: Trellis diagram for a 4-QAM, four-state trellis code

which are mapped to the modulated symbols of $-1$ and 1. If the incoming symbols are 23, the trellis state will change to state 3.

At the receiver, ML sequence estimation using the Viterbi algorithm [74] may be employed for decoding the received signal. The studies of [48, 73] showed that increasing the number of states is capable of increasing the coding gain, while increasing the number of receive antennas may increase both the coding gain and the diversity gain.

### 2.2.2 Spatial Multiplexing

The family of space-time codes offers an improved BER performance for MIMO systems owing to possessing a diversity gain. However, they are unable to approach a tight lower bound on the MIMO channel capacity. Foschini [46] proposed a Layered Space-Time (LST) architecture, also known as a spatial multiplexing, which exploits the MIMO channels for the sake of improving the transmission rate rather than the BER. The throughput performance improvement due to employing spatial multiplexing is often referred to as having a multiplexing gain. In practice, there is a trade-off between the diversity gain and the multiplexing gain, when designing MIMO systems.

#### 2.2.2.1 Layered Space-Time Transmitters

**Horizontal Layered Space-Time Coding**

The schematic of the Horizontal Layer Space-Time (HLST) coding scheme is shown in Fig. 2.4. In HLSTs, the bit stream is first demultiplexed into $n_T$ separate streams by a serial-parallel converter. Subsequently, each stream is independently encoded, interleaved and modulated before being transmitted from a specific antenna, hence, the spatial throughput becomes $r_s = n_T$. When the receiver employs $n_R$ receive antennas, the HLST may achieve a diversity order of $n_R$, since each symbol is only transmitted from a single antenna and received by $n_R$ antennas. Therefore, the simple HLST constitutes a sup-optimal architecture. In order to increase the attainable diversity order as close to the expected value of $(n_T \times n_R)$, two modified arrangements, namely the Diagonal LST (DLST) [46]

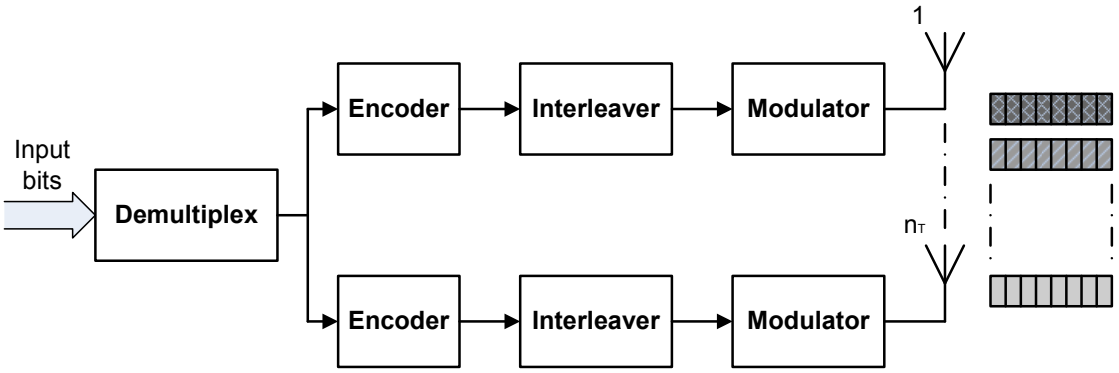


Figure 2.4: The HLST architecture using separate channel codes in each layer.

and the threaded LST (TLST) [75] arrangements, were proposed.

- **DLST**: The DLST scheme, which is often known as D-BLAST, was proposed by Foschini [46]. Observe by comparing Figs. 2.4 and 2.5 that the initial signal processing in this scheme is similar to that of HLST. However, the demultiplexed streams of Fig 2.4 are passed through a 'stream rotator', which rotates the frame in a round-robin fashion before passing it to the transmit antenna. The codewords have to be of appropriate length to ensure that they are mapped to and transmitted over all $n_T$ transmit antennas. Again, the D-BLAST encoding scheme is illustrated in Fig. 2.5. According to the figure, there is an unexploited space-time area in the concept of D-BLAST, which is beneficial from a different perspective, since it facilitates optimal decoding at the receiver, as demonstrated in Chapter 11 of [73].

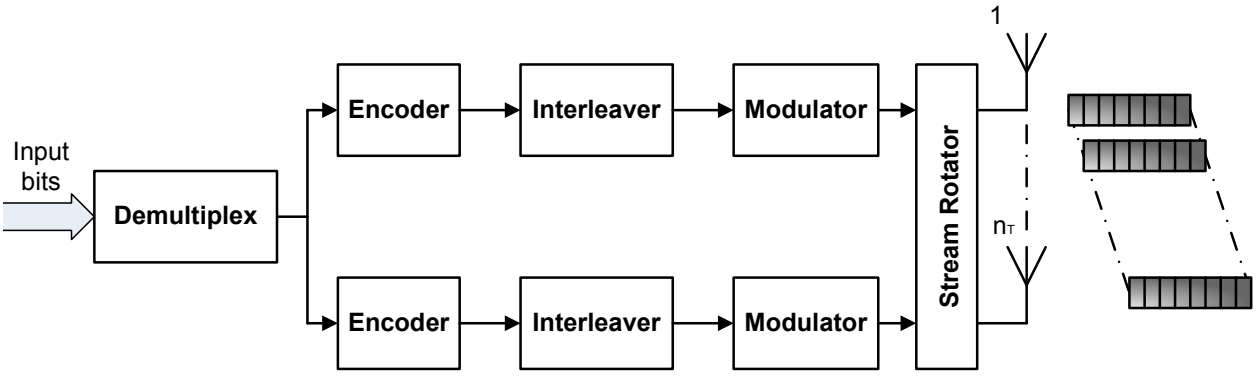


Figure 2.5: The DLST architecture using separate channel codes in each layer. In contrast to Fig. 2.4, a stream rotator is inserted between the modulators and transmit antennas.

- **TLST**: The TLST scheme of Fig. 2.6 constitutes another version of HLST, where a spatial interleaver is inserted after the modulators. Owing to the spatial interleaver, the resultant codeword extends beyond the diagonal of the space-time stripe and wraps around, whilst creating multiple stripes, as shown in Fig. 2.6. This LST type offers an improved temporal diversity. However, the joint decoding of multiple threads is required, resulting in a higher implementation complexity than both the general HLST scheme of Fig 2.4 and the D-BLAST scheme of Fig. 2.5.

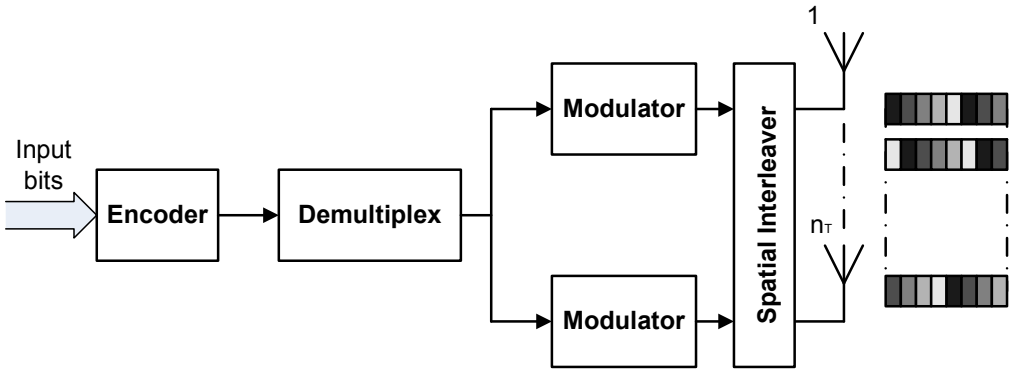


Figure 2.6: The TLST architecture using a single joint channel code for multiple layers. In contrast to the DLST architecture of Fig. 2.5, in TLST the encoder is incorporated in front of the demultiplexer, while the spatial-domain interleaver replaces the stream rotator.

### Vertical Layered Space-Time Coding

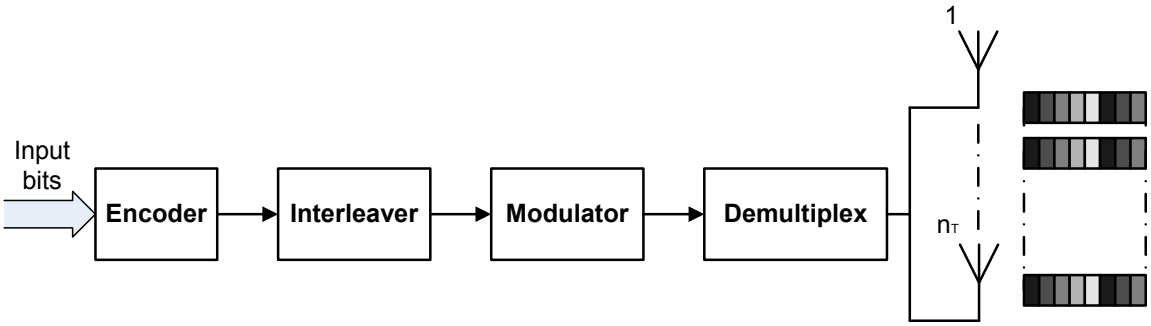


Figure 2.7: The VLST architecture using a single joint channel code for multiple layers, where a time-domain interleaver is arranged between the encoder and the modulator, instead of having a spatial-domain interleaver between the modulators and transmit antennas, as in Fig. 2.6.

The Vertical Layered Space-Time (VLST) philosophy, also known as V-BLAST, was proposed by Wolniansky *et al.* [58]. In the VLST architecture shown in Fig. 2.7 the bit stream is channel encoded along the temporal domain, interleaved and modulated before being demultiplexed into $n_T$ sub-streams. This type of LST has the benefit of spreading its information bits across all antennas. However, the VLST's joint decoding of the bit streams significantly increases the receiver's complexity.

Again, the scheme is capable of achieving a spatial rate of $r_s = n_T$ and a diversity order higher than $n_R$, since the information symbols are spread over more than one antenna. The attainable coding gain depends on the choice of the temporal-domain channel codes employed and an array gain of $n_R$ is achievable.

#### 2.2.2.2 Layered Space-Time Receivers

The spatial multiplexing imposes spatial interference on the receive antennas at the receiver side. The interference-contaminated signal at the receiver may be represented by the following matrix operation

$$\boldsymbol{y} = \boldsymbol{H}\boldsymbol{s} + \boldsymbol{n}, \tag{2.8}$$

where $\mathbf{y}$ represents the received $(n_R \times 1)$-element vector, $\mathbf{H}$ is the channel matrix of size $(n_R \times n_T)$, $\mathbf{s}$ denotes the $(n_T \times 1)$-element transmit vector and $\mathbf{n}$ is the AWGN. Numerous decoding algorithms may be used at the receiver, which are briefly described below.

**Maximum Likelihood Receiver**

In the Maximum Likelihood (ML) receiver, the estimated symbol vector $\hat{\boldsymbol{s}}$ is decided by solving the following problem:

$$\hat{\boldsymbol{s}} = arg\ min||\boldsymbol{y} - \boldsymbol{H}\boldsymbol{s}||^2. \tag{2.9}$$

The ML receiver searches for the entire space of legitimate transmit vectors. Therefore, the search complexity is proportional to $M^{n_T}$, where $M$ is the number of the modulation levels. This type of receiver is referred to as the optimal ML receiver. In order to reduce its decoding complexity, the sphere decoding technique detailed in [76, 77] may be employed.

**Zero-Forcing Receiver**

The Zero-Forcing (ZF) receiver may be viewed as a linear filter, which separates the signal streams and decodes each stream independently, hence it is referred to as a linear receiver. The estimated symbol vector $\hat{\boldsymbol{s}}$ may be obtained as [46]

$$\hat{\boldsymbol{s}} = (\boldsymbol{H}^H\boldsymbol{H})^{-1}\boldsymbol{y} = (\boldsymbol{H}^H\boldsymbol{H})^{-1}(\boldsymbol{H}\boldsymbol{s} + \boldsymbol{n}) = \boldsymbol{H}^{\ddagger}\boldsymbol{s} + (\boldsymbol{H}^H\boldsymbol{H})^{-1}\boldsymbol{n}, \tag{2.10}$$

where $^H$ denotes the complex conjugate transpose and $^{\ddagger}$ indicates the pseudoinverse of a matrix [78]. As shown in [73], this scheme attains a diversity order of $(n_R - n_T + 1)$ for each stream and hence it is suboptimal.

**Minimum-Mean-Square-Error Receiver**

The Minimum-Mean-Square-Error (MMSE) receiver concept is based on minimizing the square of the estimation error caused by fading, noise and interference amongst cochannel signals. The estimated symbol vector $\hat{\boldsymbol{s}}$ is formulated as [79]

$$\hat{\boldsymbol{s}} = \left(\frac{1}{\gamma}\boldsymbol{I}_{n_R} + \boldsymbol{H}^H\boldsymbol{H}\right)^{-1}\boldsymbol{H}^H\boldsymbol{y}, \tag{2.11}$$

where $\gamma$ is the SNR.

**Successive-Cancellation Receiver**

Instead of jointly decoding the stream, the Successive-Cancellation (SuC) algorithm generally detects signals on a row-by-row basis. The effect of each detected and remodulated row is cancelled from the received signal, in order to reduce the interference. If the information of each layer is detected correctly, there is no error propagation. However, when the weakest stream's signal is detected first, the errors might be propagated to the other stream during the decoding process, resulting in a degraded

performance. To avoid this problem, the signal associated with the highest SNR is detected first, based on a signal-strength-aided ordering, as proposed in [80]. The SuC algorithm is often combined with the ZF or MMSE algorithms in the V-BLAST receivers.

### 2.2.3 Tradeoff between Spatial Coding and Spatial Multiplexing

As a benefit of the channel-coding redundancy imposed by the associated trellis codes, STTC is capable of providing both fading- and noise-resistance at the cost of an increased detection complexity, while the family of STBCs imposes a lower complexity at the cost of a reduced BER performance. At high data rates, which is typically achieved with the aid of a high number of antennas, these STBCs generally exhibit a degraded performance due to the interference between the data streams. By contrast, the class of SM schemes, such as V-BLAST schemes, offers both an attractive performance as well as simple encoding and decoding at a throughput as high as dozens of bits/sec/Hz. However, their performance significantly degrades, when the number of receive antennas is less than the number of transmit antennas. Hence, the employment of SM is more beneficial for UL communication, where the BS may employ a sufficiently high number of antennas. Furthermore, the SM schemes often suffer from deep fades because their data streams are transmitted independently without invoking spatial spreading and/or coding. Therefore, there is a tradeoff between the achievable BER performance and effective throughput in the context of MIMO system designs, which is often referred to as the diversity/multiplexing gain trade-off. In order to resolve this design-dilemma, Hassibi *et al.* [49,81,82] conceived the Linear Dispersion Coding (LDC) concept in order to handle any arbitrary configuration of transmit and receive antennas, while achieving the required effective throughput and diversity gains despite its decoding simplicity.

**Linear Dispersion Codes**

The concept of the Linear Dispersion Codes (LDC) is to invoke a matrix-based linear modulation framework, where the transmitted space-time spreading matrix $\boldsymbol{S}$ is generated by linearly combining $Q$ dispersion matrices, each of which is weighted by one of $Q$ symbols acting as weighting factors. More particularly, let $\boldsymbol{K} = [s_1, s_2, ..., s_Q]^T$ (superscript $^T$ indicates matrix transpose) be a set of scalar symbols from an arbitrary complex-valued modulation constellation that are to be transmitted and $\boldsymbol{A}_q$ be a specific dispersion matrix from the set of $\zeta^{n_T \times T}$. Then the transmitted space-time matrix $\boldsymbol{S}$ is attained by superposition of weighted dispersion matrices weighted by the scalar symbols, yielding

$$\boldsymbol{S} = \sum_{q=1}^{Q} \boldsymbol{A}_q s_q. \tag{2.12}$$

Fig. 2.8 shows the space-time codeword $\boldsymbol{S}$, which should satisfy the power constraint given by

$$tr\left[\sum_{q=1}^{Q} \boldsymbol{A}_q^H \boldsymbol{A}_q\right] = T, \tag{2.13}$$

where $tr$ indicates the matrix trace operation.

Subsequently, the signal $\overline{\boldsymbol{Y}}$ received at the destination may be presented in scalar form as

$$\overline{\boldsymbol{Y}} = \overline{\boldsymbol{H}} \chi \boldsymbol{K} + \overline{\boldsymbol{V}}, \tag{2.14}$$

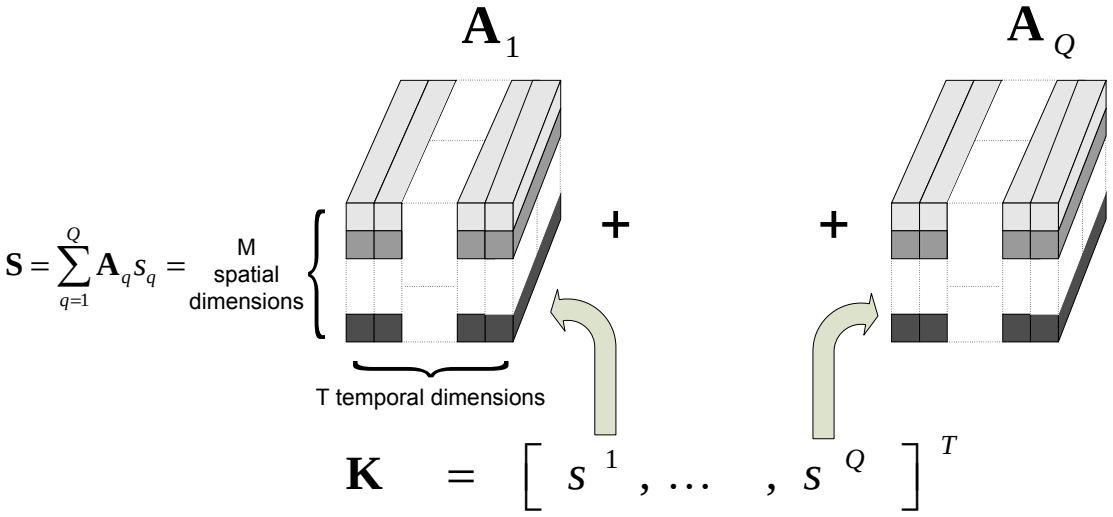


Figure 2.8: The space-time codeword $\boldsymbol{S}$ employing the linear dispersion structure, based on Eq. (2.12). The set of dispersion matrices $\boldsymbol{A}_q$ is known to both the transmitter and the receiver.

where $\overline{\boldsymbol{H}}$ represents the channel coefficient matrix and $\overline{\boldsymbol{V}}$ represents the AWGN noise, while $\chi$ is referred to as the decoding matrix. More explicitly, the terms may be further extracted as

$$\overline{\boldsymbol{Y}}(i) = vec(\boldsymbol{Y}(i)) \quad \in \mathcal{C}^{n_R T \times 1}, \tag{2.15}$$

$$\overline{\boldsymbol{H}}(i) = \boldsymbol{I} \otimes \boldsymbol{H}(i) \quad \in \mathcal{C}^{n_R T \times n_T T}, \tag{2.16}$$

$$\overline{\boldsymbol{V}}(i) = vec(\boldsymbol{V}(i)) \quad \in \mathcal{C}^{n_R T \times 1}, \tag{2.17}$$

$$\chi = [vec(\boldsymbol{A}_1) \cdots vec(\boldsymbol{A}_Q)] \quad \in \mathcal{C}^{n_T T \times Q}, \tag{2.18}$$

where $\boldsymbol{I}$ is the $(T \times T)$-element identity matrix and $\otimes$ is the Kronecker product.

The ML estimation of the transmitted signal vector $\boldsymbol{K}$ may be formulated as

$$\hat{\boldsymbol{K}} = arg\ min\big(||\overline{\boldsymbol{Y}} - \overline{\boldsymbol{H}}\chi\boldsymbol{K}_f||^2\big), \tag{2.19}$$

where $\overline{\boldsymbol{K}}_f$ denotes all the possible combinations of the $Q$ transmitted symbols. Note that the set of dispersion matrices $\boldsymbol{A}_q$ is known to both the transmitter and the receiver.

As shown in Fig. 2.8 and Eq. (2.12), the transmitted space-time matrix $\boldsymbol{S}$ is constituted by the superposition of $Q$ symbols, resembling a SM scheme. The summation in Eq. (2.12) also implies that each symbol is spread to all the antennas in the spatial-domain and to all the time-slots in the time domain. Moreover, the value of $Q$ is unrestricted and determined by the system designer, implying that LDC codes are capable of supporting an arbitrary number of layers.

On the other hand, if each individual dispersion matrix $\boldsymbol{A}_q$ is constituted by orthogonal patterns as well as the set of $Q$ dispersion matrices are orthogonal to each other, the resultant transmitted codeword matrix $\boldsymbol{S}$ is also constituted by orthogonal patterns, hence it is capable of achieving the maximum attainable diversity gain, which is often termed as having 'full' diversity. However, the $Q$ LDC matrices do not have to be orthogonal to each other. Indeed, the specific degree of orthogonality may be adjusted by appropriately choosing the set of dispersion matrices. Hence, LDC schemes offer an increased system design flexibility as detailed in [23].

In summary, LDCs offer the following advantages:

- LDCs subsume both the family of SM schemes and STBCs, while striking an arbitrary trade-off between the achievable diversity and multiplexing gain.
- LDCs are capable of supporting an arbitrary number of transmit and receive antennas as well as modulation types, hence facilitating a high degree of system design flexibility.
- As demonstrated in [83], LDCs are capable of attaining a maximum diversity order of $n_R \times min(n_T, T)$, which implies that the diversity order cannot be increased upon increasing the number of time slots $T$ beyond the number of transmit antennas $n_T$. By contrast, the diversity order will be decreased, if the number of time slots $T$ is less than $n_T$.

### 2.2.4 Space-Time-Frequency Diversity

All of the MIMO techniques mentioned above spread the transmitted signal across the SD and the TD. By contrast, a novel concept, which spread the signal in three domains, namely the SD, TD and FD, is proposed in this section.

Again, consider an $(n_T \times n_R)$-element MIMO system, where the transmitter and receiver employ $n_T$ and $n_R$ antennas, respectively. The channel is assumed to impose frequency-selective Rayleigh fading. Generally, a transmission block-based system model may be described as:

$$\boldsymbol{Y}(i) = \sum_{j=0}^{J-1} \boldsymbol{H}(i-j, j)\boldsymbol{S}(i-j) + \boldsymbol{V}(i), \tag{2.20}$$

where $i$ indicates the block index and $j$ represents the tap index of the tapped-delay-line channel model, which consists of $J$ taps. Naturally, flat fading is encountered for $J = 1$. Furthermore, $\boldsymbol{Y} \in \mathcal{C}^{n_R \times T}$ represents the signals received by the $n_R$ antennas and $\boldsymbol{S} \in \mathcal{C}^{M \times T}$ denotes the signal transmitted from the $n_T$ antennas in $T$ time slots. Furthermore, $\boldsymbol{H}(i, j) \in \mathcal{C}^{n_R \times n_T}$ characterizes the coefficients of the $i^{th}$ symbol at the $j^{th}$ channel tap, each obeying correlated frequency-selective Rayleigh fading. Finally, $\boldsymbol{V}$ denotes the complex-valued zero-mean Gaussian distribution of $\mathcal{CN}(0, N_0)$, where $N_0$ is the noise variance. It is also assumed that both the fading and noise coefficients remain constant during each time slot.

Let us now briefly review the STSK modulation concept proposed in [53]. Moreover, we introduce two novel modulation schemes, namely the SFSK as well as the STFSK regimes, where the signal is spread across the Space-Time-Frequency (STF) domain.

#### 2.2.4.1 Space-Time Shift Keying

Fig. 2.9 illustrates the transmitter of the STSK scheme, where the information bits are divided into two parallel bits streams. The first bit stream is mapped by $Q$ pre-defined dispersion matrices $\boldsymbol{A}_q \in \mathcal{C}^{n_T \times T}$ $(q = 1, 2, ..., Q)$, while the second is mapped to $s_l(i)$ symbols $(l = 1, 2, ..., L)$ by a conventional modulation scheme, such as $L$-PSK or $L$-QAM. Then, the resultant streams are multiplied together in order to create the space-time block $\boldsymbol{S}(i) \in \mathcal{C}^{n_T \times T}$, which consists of a total of $log_2(Q \cdot L)$ source bits, yielding

$$\boldsymbol{S}(i) = s(i)\boldsymbol{A}(i). \tag{2.21}$$

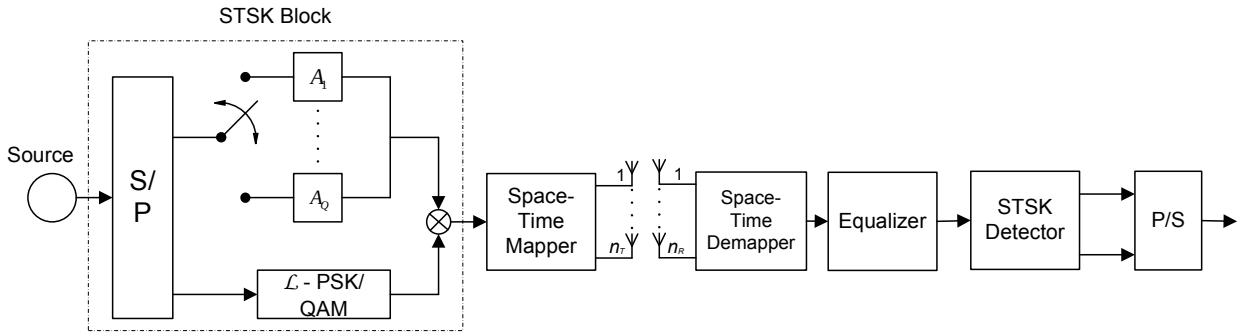


Figure 2.9: Transceiver block diagram of the STSK scheme.

It is noted that each symbol $s(i)$ is a function of time during the period $T_s$ of each time slot.

As in [53], the signal received at the destination may be presented in scalar form as

$$\overline{\boldsymbol{Y}}(i) = \overline{\boldsymbol{H}}(i)\chi\boldsymbol{K}(i) + \overline{\boldsymbol{V}}(i), \tag{2.22}$$

with the variables formulated as

$$\overline{\boldsymbol{Y}}(i) = \quad vec(\boldsymbol{Y}(i)) \quad \in \mathcal{C}^{n_R T \times 1}, \tag{2.23}$$

$$\overline{\boldsymbol{H}}(i) = \quad \boldsymbol{I} \otimes \boldsymbol{H}(i) \quad \in \mathcal{C}^{n_R T \times n_T T}, \tag{2.24}$$

$$\overline{\boldsymbol{V}}(i) = \quad vec(\boldsymbol{V}(i)) \quad \in \mathcal{C}^{n_R T \times 1}, \tag{2.25}$$

$$\chi = \quad [vec(\boldsymbol{A}_1) \cdots vec(\boldsymbol{A}_Q)] \quad \in \mathcal{C}^{n_T T \times Q}, \tag{2.26}$$

where $\boldsymbol{I}$ is the $(T \times T)$-element identity matrix and $\otimes$ is the Kronecker product. Furthermore, $\boldsymbol{K}(i) \in \mathcal{C}^{Q \times 1}$ is the equivalent transmitted signal vector, which may be expressed as

$$\boldsymbol{K}(i) = [\underbrace{0, \cdots, 0}_{q-1}, s(i), \underbrace{0, \cdots, 0}_{Q-q}]^T, \tag{2.27}$$

where $^T$ indicates the matrix transpose operation.

When the coherent maximum likelihood detector [84] is employed, the STSK modulated signal may be recovered by searching for an appropriate pair of the $l^{th}$ $(l = 1, \cdots, L)$ PSK/QAM symbol and the $q^{th}$ $(q = 1, \cdots, Q)$ dispersion matrix. More particularly, the estimate $(\hat{q}, \hat{l})$ is given by minimizing the following metric

$$(\hat{q}, \hat{l}) = arg \min_{q,l} \left|\left| \overline{\boldsymbol{Y}}(i) - \overline{\boldsymbol{H}}(i)\chi\boldsymbol{K}_{q,l}(i) - \sum_{j=1}^{J-1} \overline{\boldsymbol{H}}(i-j, j)\chi\boldsymbol{K}(i-j) \right|\right|^2 \tag{2.28}$$

$$= arg \min_{q,l} \left|\left| \overline{\boldsymbol{Y}}(i) - s_l(i)\big(\overline{\boldsymbol{H}}(i)\chi\big)_q - \sum_{j=1}^{J-1} \overline{\boldsymbol{H}}(i-j, j)\chi\boldsymbol{K}(i-j) \right|\right|^2, \tag{2.29}$$

where $s_l(i)$ is the $l^{th}$ symbol in the $L$-point constellation at the $i^{th}$ block index and the signal vector $\boldsymbol{K}_{q,l}$ $(1 \leq q \leq Q, 1 \leq l \leq L)$ is presented by

$$\boldsymbol{K}_{q,l}(i) = [\underbrace{0, \cdots, 0}_{q-1}, s_l(i), \underbrace{0, \cdots, 0}_{Q-q}]^T. \tag{2.30}$$

Furthermore, $\sum_{j=1}^{J-1} \overline{\boldsymbol{H}}(i-j,j)\chi \boldsymbol{K}(i-j)$ represents the delayed paths of the dispersive channel, which is omitted in flat-fading environment, while $\left(\overline{\boldsymbol{H}}(i)\chi\right)_q$ denotes the $q^{th}$ column of the matrix $\overline{\boldsymbol{H}}(i)\chi$.

It is noted that $n_T$ should be less than or equal to $T$ ($n_T \leq T$), since no further capacity gain may be achieved for $n_T > T$, as shown in [85, 86]. Additionally, in order to maintain a unity transmission power for a STSK symbol duration, each of the $Q$ dispersion matrices has to obey the power constraint of [53]

$$tr[\boldsymbol{A}_q^{\dagger}\boldsymbol{A}_q] = T \qquad (q = 1, \cdots, Q), \tag{2.31}$$

where $tr[\cdot]$ indicates the matrix trace operation, while the superscript † denotes the complex conjugate transpose operation.

#### 2.2.4.2 Space-Frequency Shift Keying

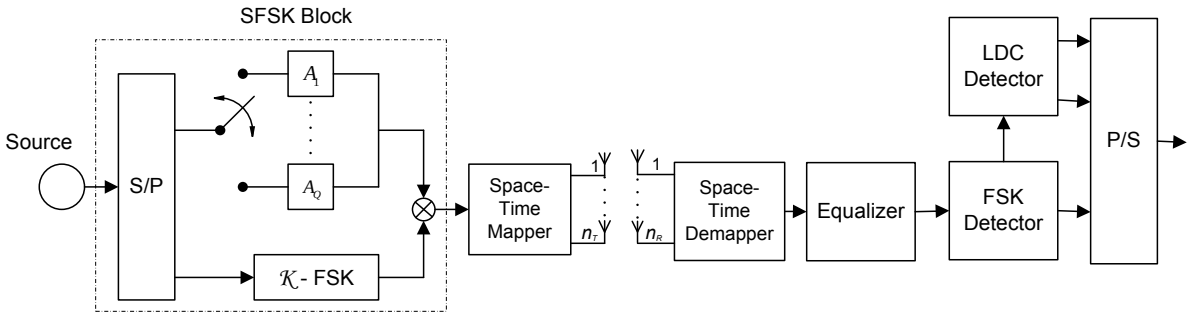


Figure 2.10: Transceiver block diagram of the SFSK scheme, where the FSK block replaces the PSK block in the STSK scheme of Fig. 2.9.

The transmitter of the SFSK modulation scheme is shown in Fig. 2.10, where the PSK/QAM modulator is replaced by the FSK modulator. Due to this modification, the transmitted block $\boldsymbol{S}(i) \in \mathcal{C}^{n_T \times T}$ is modified as

$$\boldsymbol{S}(i) = r(i)\boldsymbol{A}(i), \tag{2.32}$$

where the $log_2(K)$ source bits are mapped to the FSK symbol $r(i)$, which is represented by $r(i) = cos(2\pi f_i t + \varphi_i)$, where $f_i$ is the frequency associated with the $i^{th}$ transmitted FSK symbol and $\varphi_i$ is the random phase during the $i^{th}$ symbol interval.

At the receiver, we employ a demodulator consisting of a bank of $K$ parallel square-law detectors [66] in order to detect the activated frequencies of the SFSK symbols. Then the ML detector is employed to identify the transmitted dispersion matrix by substituting the following vector into Eq. (2.28):

$$\boldsymbol{K}_q(i) = [\underbrace{0, \cdots, 0}_{q-1}, r(i), \underbrace{0, \cdots, 0}_{Q-q}]^{Tr}. \tag{2.33}$$

In order to maintain orthogonality, the frequency between the adjacent signalling tones of the FSK modulator has to be separated by at least $1/T_s$ Hz, where $T_s$ is the duration of a time slot [87].

#### 2.2.4.3 Space-Time-Frequency Shift Keying

Based on the STSK and SFSK modulation schemes of Sections 2.2.4.1 and 2.2.4.2, the architecture of the STFSK scheme is portrayed in Fig. 2.11, where three symbol sub-streams are combined before

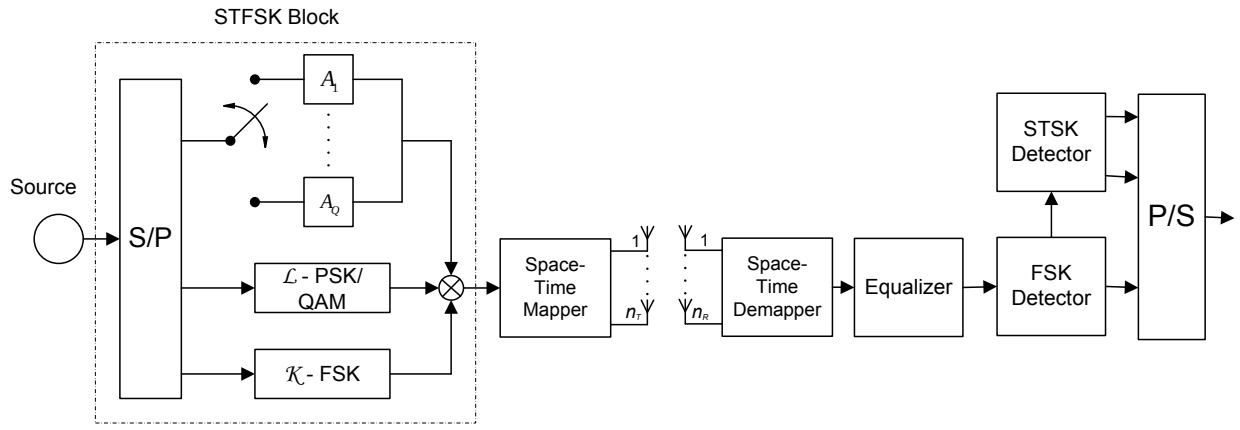


Figure 2.11: Transceiver block diagram of the STFSK scheme, where both the PSK/QAM block and the FSK block are employed, instead of using either only the PSK/QAM block in the STSK scheme of Fig. 2.9 or the FSK block in the SFSK scheme of Fig. 2.10.

being mapped to the transmit antennas. As a result, the transmitted signal may be expressed as

$$\boldsymbol{S}(i) = r(i)s(i)\boldsymbol{A}(i). \tag{2.34}$$

An example of various STFSK mapping schemes is shown in Table 2.2, where a space-time-frequency block of $B = log_2(K \times Q \times L) = 3\ bits$ is employed. According to the table, if the information bits "011" are input to our STFSK encoder using BPSK modulation ($L = 2$) and BFSK modulation ($K = 2$) associated with ($Q = 2$), then the modulated space-time-frequency signal of $\boldsymbol{S} = e^{j\pi}\boldsymbol{A}_2 cos(2\pi f_1 t + \varphi_1)$ will be transmitted.

Consequently, the signal received at the STFSK receiver may be formulated as

$$\overline{\overline{\boldsymbol{Y}}}(i) = \left\{\overline{\boldsymbol{Y}}_1(i), \overline{\boldsymbol{Y}}_2(i), ..., \overline{\boldsymbol{Y}}_k(i), ..., \overline{\boldsymbol{Y}}_K(i)\right\}, \tag{2.35}$$

where we have

$$\overline{\boldsymbol{Y}}_k(i) = \begin{cases} \overline{\boldsymbol{H}}(i)\chi\boldsymbol{K}(i) + \overline{\boldsymbol{V}}(i) & : \ at\ the\ transmitted\ frequency \\ \overline{\boldsymbol{V}}(i) & : \ otherwise. \end{cases} \tag{2.36}$$

Again, a low-complexity square-law detector is employed first to detect the activated frequencies, i.e the FSK symbols. Then, the PSK/QAM symbols and the dispersion matrices are detected by substituting the following vector into Eq. (2.28)

$$\boldsymbol{K}_{q,l,k}(i) = [\underbrace{0, \cdots, 0}_{q-1}, r(i)s_l(i), \underbrace{0, \cdots, 0}_{Q-q}]^T. \tag{2.37}$$

It may be observed that the STSK and the SFSK schemes constitute special cases of STFSK, when we have $K = 1$ and $L = 1$, respectively. In order to reduce the impact of the ISI imposed by frequency-selective fading, the signal may be equalized before carrying out detection.

#### 2.2.4.4 Soft STFSK Demodulator

The iterative turbo-like detection concept [23,36] was shown to provide a significant improvement of the attainable system performance. Therefore, in this section we proposed the soft STFSK demodulator concept, which plays an important role in the iterative decoding architecture.

Table 2.2: Example of STFSK modulation scheme, mapping 3 bits per Space-Time-Frequency block

| Options | | 000 | 001 | 010 | 011 | 100 | 101 | 110 | 111 |
|---|---|---|---|---|---|---|---|---|---|
| $K=1$ | $f_k$ | $f_1$ | $f_1$ | $f_1$ | $f_1$ | $f_1$ | $f_1$ | $f_1$ | $f_1$ |
| $L=1$ | $s_l$ | $s_1=1$ | $s_1=1$ | $s_1=1$ | $s_1=1$ | $s_1=1$ | $s_1=1$ | $s_1=1$ | $s_1=1$ |
| $Q=8$ | $\mathbf{A}_q$ | $\mathbf{A}_1$ | $\mathbf{A}_2$ | $\mathbf{A}_3$ | $\mathbf{A}_4$ | $\mathbf{A}_5$ | $\mathbf{A}_6$ | $\mathbf{A}_7$ | $\mathbf{A}_8$ |
| $K=1$ | $f_k$ | $f_1$ | $f_1$ | $f_1$ | $f_1$ | $f_1$ | $f_1$ | $f_1$ | $f_1$ |
| $L=2$ | $s_l$ | $s_1=1$ | $s_2=e^{j\pi}$ | $s_1=1$ | $s_2=e^{j\pi}$ | $s_1=1$ | $s_2=e^{j\pi}$ | $s_1=1$ | $s_2=e^{j\pi}$ |
| $Q=4$ | $\mathbf{A}_q$ | $\mathbf{A}_1$ | $\mathbf{A}_1$ | $\mathbf{A}_2$ | $\mathbf{A}_2$ | $\mathbf{A}_3$ | $\mathbf{A}_3$ | $\mathbf{A}_4$ | $\mathbf{A}_4$ |
| $K=1$ | $f_k$ | $f_1$ | $f_1$ | $f_1$ | $f_1$ | $f_1$ | $f_1$ | $f_1$ | $f_1$ |
| $L=4$ | $s_l$ | $s_1=1$ | $s_2=e^{j\frac{2\pi}{2}}$ | $s_3=e^{j\frac{2\pi}{2}}$ | $s_4=e^{j\frac{3\pi}{2}}$ | $s_1=1$ | $s_2=e^{j\frac{2\pi}{2}}$ | $s_3=e^{j\frac{2\pi}{2}}$ | $s_4=e^{j\frac{3\pi}{2}}$ |
| $Q=2$ | $\mathbf{A}_q$ | $\mathbf{A}_1$ | $\mathbf{A}_1$ | $\mathbf{A}_1$ | $\mathbf{A}_1$ | $\mathbf{A}_2$ | $\mathbf{A}_2$ | $\mathbf{A}_2$ | $\mathbf{A}_2$ |
| $K=1$ | $f_k$ | $f_1$ | $f_1$ | $f_1$ | $f_1$ | $f_1$ | $f_1$ | $f_1$ | $f_1$ |
| $L=8$ | $s_l$ | $s_1=1$ | $s_2=e^{j\frac{2\pi}{4}}$ | $s_3=e^{j\frac{2\pi}{4}}$ | $s_4=e^{j\frac{3\pi}{4}}$ | $s_5=e^{j\frac{4\pi}{4}}$ | $s_6=e^{j\frac{5\pi}{4}}$ | $s_7=e^{j\frac{6\pi}{4}}$ | $s_8=e^{j\frac{7\pi}{4}}$ |
| $Q=1$ | $\mathbf{A}_q$ | $\mathbf{A}_1$ | $\mathbf{A}_1$ | $\mathbf{A}_1$ | $\mathbf{A}_1$ | $\mathbf{A}_1$ | $\mathbf{A}_1$ | $\mathbf{A}_1$ | $\mathbf{A}_1$ |
| $K=2$ | $f_k$ | $f_1$ | $f_1$ | $f_1$ | $f_1$ | $f_2$ | $f_2$ | $f_2$ | $f_2$ |
| $L=1$ | $s_l$ | $s_1=1$ | $s_1=1$ | $s_1=1$ | $s_1=1$ | $s_1=1$ | $s_1=1$ | $s_1=1$ | $s_1=1$ |
| $Q=4$ | $\mathbf{A}_q$ | $\mathbf{A}_1$ | $\mathbf{A}_2$ | $\mathbf{A}_3$ | $\mathbf{A}_4$ | $\mathbf{A}_1$ | $\mathbf{A}_2$ | $\mathbf{A}_3$ | $\mathbf{A}_4$ |
| $K=2$ | $f_k$ | $f_1$ | $f_1$ | $f_1$ | $f_1$ | $f_2$ | $f_2$ | $f_2$ | $f_2$ |
| $L=2$ | $s_l$ | $s_1=1$ | $s_2=e^{j\pi}$ | $s_1=1$ | $s_2=e^{j\pi}$ | $s_1=1$ | $s_2=e^{j\pi}$ | $s_1=1$ | $s_2=e^{j\pi}$ |
| $Q=2$ | $\mathbf{A}_q$ | $\mathbf{A}_1$ | $\mathbf{A}_1$ | $\mathbf{A}_2$ | $\mathbf{A}_2$ | $\mathbf{A}_1$ | $\mathbf{A}_1$ | $\mathbf{A}_2$ | $\mathbf{A}_2$ |
| $K=2$ | $f_k$ | $f_1$ | $f_1$ | $f_1$ | $f_1$ | $f_2$ | $f_2$ | $f_2$ | $f_2$ |
| $L=4$ | $s_l$ | $s_1=1$ | $s_2=e^{j\frac{2\pi}{2}}$ | $s_3=e^{j\frac{2\pi}{2}}$ | $s_4=e^{j\frac{3\pi}{2}}$ | $s_1=1$ | $s_2=e^{j\frac{2\pi}{2}}$ | $s_3=e^{j\frac{2\pi}{2}}$ | $s_4=e^{j\frac{3\pi}{2}}$ |
| $Q=1$ | $\mathbf{A}_q$ | $\mathbf{A}_1$ | $\mathbf{A}_1$ | $\mathbf{A}_1$ | $\mathbf{A}_1$ | $\mathbf{A}_1$ | $\mathbf{A}_1$ | $\mathbf{A}_1$ | $\mathbf{A}_1$ |
| $K=4$ | $f_k$ | $f_1$ | $f_2$ | $f_3$ | $f_4$ | $f_1$ | $f_2$ | $f_3$ | $f_4$ |
| $L=1$ | $s_l$ | $s_1=1$ | $s_1=1$ | $s_1=1$ | $s_1=1$ | $s_1=1$ | $s_1=1$ | $s_1=1$ | $s_1=1$ |
| $Q=2$ | $\mathbf{A}_q$ | $\mathbf{A}_1$ | $\mathbf{A}_1$ | $\mathbf{A}_1$ | $\mathbf{A}_1$ | $\mathbf{A}_2$ | $\mathbf{A}_2$ | $\mathbf{A}_2$ | $\mathbf{A}_2$ |
| $K=4$ | $f_k$ | $f_1$ | $f_2$ | $f_3$ | $f_4$ | $f_1$ | $f_2$ | $f_3$ | $f_4$ |
| $L=2$ | $s_l$ | $s_1=1$ | $s_1=1$ | $s_1=1$ | $s_1=1$ | $s_2=e^{j\pi}$ | $s_2=e^{j\pi}$ | $s_2=e^{j\pi}$ | $s_2=e^{j\pi}$ |
| $Q=1$ | $\mathbf{A}_q$ | $\mathbf{A}_1$ | $\mathbf{A}_1$ | $\mathbf{A}_1$ | $\mathbf{A}_1$ | $\mathbf{A}_1$ | $\mathbf{A}_1$ | $\mathbf{A}_1$ | $\mathbf{A}_1$ |
| $K=8$ | $f_k$ | $f_1$ | $f_2$ | $f_3$ | $f_4$ | $f_5$ | $f_6$ | $f_7$ | $f_8$ |
| $L=1$ | $s_l$ | $s_1=1$ | $s_1=1$ | $s_1=1$ | $s_1=1$ | $s_1=1$ | $s_1=1$ | $s_1=1$ | $s_1=1$ |
| $Q=1$ | $\mathbf{A}_q$ | $\mathbf{A}_1$ | $\mathbf{A}_1$ | $\mathbf{A}_1$ | $\mathbf{A}_1$ | $\mathbf{A}_1$ | $\mathbf{A}_1$ | $\mathbf{A}_1$ | $\mathbf{A}_1$ |

As shown in Fig. 2.12, the input of a soft STFSK demodulator relies on the channel's output information gleaned by the receiver and on the *a-priori* information $L_a$ fed back from the inner detector, constituted for example by the channel decoder. The soft STFSK demodulator outputs the *a-posteriori* information $L_p$, which is converted into the *extrinsic* information $L_e$ by subtracting the *a-priori* information $L_a$. All of these information types are typically represented in terms of the so-called Log Likelihood Ratio (LLR) [88]. In a binary system, the LLR of a data bit $b_k$ is defined as:

$$L(b_k) \triangleq ln\left[\frac{p(b_k=+1)}{p(b_k=-1)}\right], \tag{2.38}$$

where $p$ represents the probability that the data bit assumes the value +1 or -1. Note that the polarity of the LLR determines the sign of the data bit $b_k$, while its amplitude quantifies the probability of a correct decision.

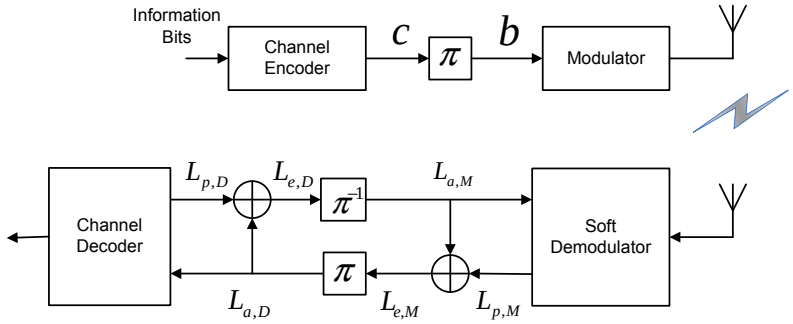


Figure 2.12: Bit-based turbo detection architecture.

For a soft STFSK demodulator, the LLR of the output *extrinsic* information depends on both the feedback *a-priori* information $L_a$ and on the channel information, where the conditional probability $p(\overline{\boldsymbol{Y}}|\boldsymbol{K}_{q,l,k})$ given a signal vector $\boldsymbol{K}_{q,l,k}$ transmitted over a fading channel is determined by the PDF of the noise, which is formulated as [23]:

$$p(\overline{\boldsymbol{Y}}|\boldsymbol{K}_{q,l,k}) = \frac{1}{(\pi N_0)^{NT}} \exp\left(-\frac{||\overline{\boldsymbol{Y}}_k - \overline{\boldsymbol{H}}\boldsymbol{\chi}\boldsymbol{K}_{q,l,k}||^2}{N_0}\right). \tag{2.39}$$

Note that the equivalent received signals $\overline{\boldsymbol{Y}}$ carry $B = log_2(KLQ)$ channel-coded binary bits $\boldsymbol{b} = [b_1, b_2, \cdots, b_B]$. Therefore, the resultant extrinsic LLR value of bit $b_k$ for $k = 1, \cdots, B$ may be rewritten as [89]

$$\begin{aligned} L_{\mathrm{e}}(b_k) &= \ln \frac{\sum\limits_{\boldsymbol{K}_{q,l,k}\in\boldsymbol{Z}_1^k} p(\overline{\boldsymbol{Y}}|\boldsymbol{K}_{q,l,k}) \cdot e^{\left[\sum\limits_{j\neq k} b_j L_a(b_j)\right]}}{\sum\limits_{\boldsymbol{K}_{q,l\in\boldsymbol{Z}_0^k}} p(\overline{\boldsymbol{Y}}|\boldsymbol{K}_{q,l,k}) \cdot e^{\left[\sum\limits_{j\neq k} b_j L_a(b_j)\right]}} \\ &= \ln \frac{\sum\limits_{\boldsymbol{K}_{q,l,k}\in\boldsymbol{Z}_1^k} e^{\left[\frac{-\left|\left|\overline{\boldsymbol{Y}}_k - \overline{\boldsymbol{H}}\boldsymbol{\chi}\boldsymbol{K}_{q,l}\right|\right|^2}{N_0} + \sum\limits_{j\neq k} b_j L_a(b_j)\right]}}{\sum\limits_{\boldsymbol{K}_{q,l,k}\in\boldsymbol{Z}_0^k} e^{\left[\frac{-\left|\left|\overline{\boldsymbol{Y}}_k - \overline{\boldsymbol{H}}\boldsymbol{\chi}\boldsymbol{K}_{q,l}\right|\right|^2}{N_0} + \sum\limits_{j\neq k} b_j L_a(b_j)\right]}}, \end{aligned} \tag{2.40}$$

where $\boldsymbol{Z}_1^k$ and $\boldsymbol{Z}_0^k$ represent the sub-space of the legitimate equivalent signals $\boldsymbol{Z}$, satisfying $\boldsymbol{Z}_1^k \equiv \{\boldsymbol{K}_{q,l,k} \in \boldsymbol{Z} : b_k = 1\}$ and $\boldsymbol{Z}_0^k \equiv \{\boldsymbol{K}_{q,l,k} \in \boldsymbol{Z} : b_k = 0\}$, respectively, while $L_a(\cdot)$ represents the *a priori* information expressed in terms of the LLRs of the corresponding bits.

In order to dramatically reduce the computational complexity of the demodulator, the max-log approximation was proposed [90], which transfers the recursions into the logarithmic domain and invokes an approximation, which is formulated as:

$$ln\left(\sum_i e^{x_i}\right) = \max_i(x_i). \tag{2.41}$$

When employing Eq. (2.41), Eq. (2.40) may be simplified to

$$\begin{aligned} L_{\mathrm{e}}(b_k) &= \max_{\boldsymbol{K}_{q,l,k} \in \boldsymbol{Z}_1^k} \left[ -\frac{||\overline{\boldsymbol{Y}}_k - \overline{\boldsymbol{H}}\boldsymbol{\chi}\boldsymbol{K}_{q,l,k}||^2}{N_0} + \sum_{j \neq k} b_j L_a(b_j) \right] \\ &- \max_{\boldsymbol{K}_{q,l,k} \in \boldsymbol{Z}_0^k} \left[ -\frac{||\overline{\boldsymbol{Y}}_k - \overline{\boldsymbol{H}}\boldsymbol{\chi}\boldsymbol{K}_{q,l,k}||^2}{N_0} + \sum_{j \neq k} b_j L_a(b_j) \right]. \end{aligned} \tag{2.42}$$

#### 2.2.4.5 Binary EXIT Chart Analysis

EXtrinsic Information Transfer (EXIT) charts were proposed by S. ten Brink [89,91], which constitute powerful tools designed for the analysis of iterative decoding schemes. This tool allows designers to graphically visualize the characteristics of a demodulator/decoder based on the soft-input soft-output decisions, which are exchanged between the decoder components. More explicitly, the EXIT chart describes the dependence of the *extrinsic* information on the *a-priori* information, which is typically quantified in terms of the mutual information expressed in the form of the LLRs. For the EXIT chart analysis, we assume that [23]:

- The *a-priori* LLRs are fairly uncorrelated, which may be achieved by employing long interleavers,
- The *a-priori* LLRs obey a Gaussian PDF.

**a. EXIT Characteristics of the Demodulator**

According to Fig. 2.12, the demodulator's input consists of the *a-priori* information $L_{a,M}$ fed back from the outer channel decoder and of the contaminated channel-output information, while its output is the *a-posteriori* information $L_{p.M}$. Observe from Fig. 2.12 that the *a-priori* information $L_{a,M}$ is subtracted from $L_{p,M}$ to generate the *extrinsic* information $L_{e,M}$. Based on the above assumptions, the *a-priori* information $L_{a,M}$ may be modelled using the independent zero-mean Gaussian random variable $n_A$ having a variance of $\sigma_A^2$ [92]. For the outer channel coded and interleaved bits $b \in \{0, 1\}$ of Fig. 2.13, or equivalently for $x \in \{-1, +1\}$, the *a-priori* information $L_{a,M}$ may be written as [89]

$$L_{a,M} = \frac{\sigma_A^2}{2} \cdot x + n_A, \tag{2.43}$$

while its conditional PDF is given as

$$p_A(\zeta | X = x) = \frac{1}{\sqrt{2\pi}\sigma_A} exp\left[ -\frac{(\zeta - (\sigma_A^2/2) \cdot x)^2}{2\sigma_A^2} \right], \tag{2.44}$$

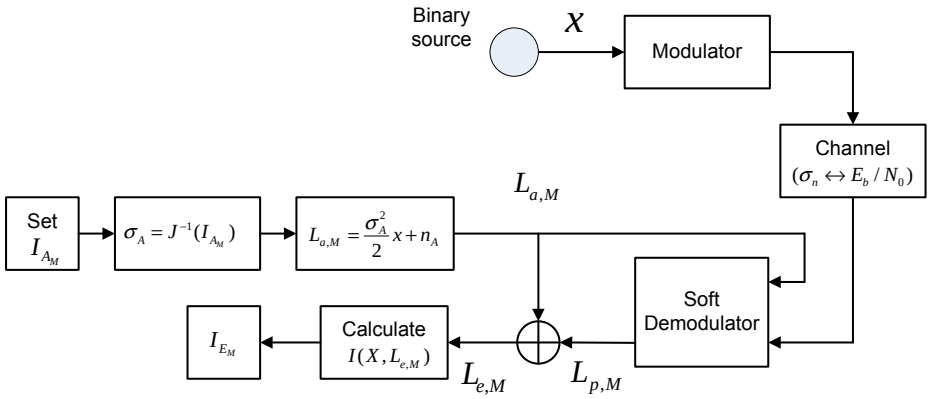


Figure 2.13: Evaluation of the demodulator EXIT characteristic, where the turbo detection architecture is shown in Fig. 2.12.

where $\zeta$ represents the channel output received at the receiver.

The information content of the *a-priori* information may be quantified in terms of the mutual information $I_{A_M} = I(X; L_{a,M})$ between x and $L_{a,M}$, which is given by [93]

$$I_{A_M} = \frac{1}{2} \sum_{x=\pm 1} \int_{-\infty}^{+\infty} p_A(\zeta|X=x) \cdot log_2 \frac{2p_A(\zeta|X=x)}{p_A(\zeta|X=-1) + p_A(\zeta|X=+1)} d\zeta. \tag{2.45}$$

Using Eq. (2.44), Eq. (2.45) may be rewritten as

$$I_{A_M}(\sigma_A) = 1 - \frac{1}{\sqrt{2\pi}\sigma_A} \int_{-\infty}^{+\infty} exp\left[ - \frac{(\zeta - (\sigma_A^2/2) \cdot x)^2}{2\sigma_A^2} \right] \cdot log_2(1 + e^{-\zeta}) d\zeta. \tag{2.46}$$

Similarly, the information content of the *extrinsic* information $L_{e,M}$ may be quantified in terms of the mutual information $I_{A_M} = I(X; L_{a,M})$, which is computed as in Eq. (2.44) using the PDF $p_E$ of the extrinsic output, yielding

$$I_{E_M} = \frac{1}{2} \sum_{x=\pm 1} \int_{-\infty}^{+\infty} p_E(\zeta|X=x) \cdot log_2 \frac{2p_E(\zeta|X=x)}{p_E(\zeta|X=-1) + p_E(\zeta|X=+1)} d\zeta. \tag{2.47}$$

Since the demodulator's *extrinsic* output depends on both the *a-priori* information and on the received signal, $I_{E_M}$ may be considered as a function of both $I_{A_M}$ and of the $E_b/N_0$ value encountered at the receiver. Therefore, the demodulator's EXIT characteristic may be written as [89, 91]

$$I_{E_M} = T_M(I_{A_M}, E_b/N_0). \tag{2.48}$$

The EXIT functions of the various STFSK schemes characterized in Table 2.3 are shown in Fig. 2.14, which lead to the following observations:

- Increasing the number of frequencies, $K$, may increase the *extrinsic* information at the cost of extending the bandwidth used. This fact may be inferred by comparing Schemes 1,2,3 and 4, where we have $K$=16, 8, 4 and 2, respectively.
- Increasing the number of dispersion matrices, $Q$, reduces the *extrinsic* information, when the same number of frequencies, $K$, is employed, which may be observed by comparing Schemes 3, 6 and 8 of Table 2.3.

Table 2.3: Parameters of modulation schemes.

| Scheme Identifier | $n_T n_R TQ$ | $L$-PSK | $K$-FSK | $bits/block$ | $bits/slot$ | $\eta$ |
|---|---|---|---|---|---|---|
| 1 | 4/1/4/2 | 2 | 16 | 6 | 1.5 | 0.19 |
| 2 | 4/1/4/2 | 4 | 8 | 6 | 1.5 | 0.38 |
| 3 | 4/1/4/2 | 8 | 4 | 6 | 1.5 | 0.75 |
| 4 | 4/1/4/2 | 16 | 2 | 6 | 1.5 | 1.50 |
| 5 | 4/1/4/4 | 2 | 8 | 6 | 1.5 | 0.38 |
| 6 | 4/1/4/4 | 4 | 4 | 6 | 1.5 | 0.75 |
| 7 | 4/1/4/4 | 8 | 2 | 6 | 1.5 | 1.50 |
| 8 | 4/1/4/8 | 2 | 4 | 6 | 1.5 | 0.75 |
| 9 | 4/1/4/8 | 4 | 2 | 6 | 1.5 | 1.50 |
| 10 | 4/1/4/16 | 2 | 2 | 6 | 1.5 | 1.50 |

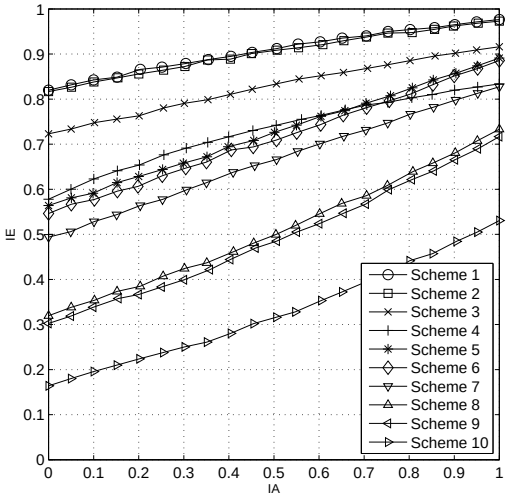


Figure 2.14: The EXIT functions of various STFSK schemes of Table 2.3 using soft-demodulation ($B = log_2(K \times Q \times L) = 3$ bits/block). The corresponding BER curves are shown in Fig. 2.22 of Section 2.2.4.9.

### b. Extrinsic Information Transfer Charts

The EXIT chart [89, 91] visualizes the *extrinsic* information exchanged between two decoding components, such as the soft demodulator and the outer channel decoder by portraying the EXIT characteristics of both the components in a joint diagram. The outer channel decoder's *extrinsic* output $I_{E_D}$, which is independent of the $E_b/N_0$ value ($I_{E_D} = T_M(I_{A_D})$ presented on the x-axis becomes the demodulator's *a-priori* input $I_{A_M}$. Similarly, the demodulator's *extrinsic* output $I_{E_M}$ scaled on the y-axis becomes the outer channel decoder's *a-priori* input $I_{A_D}$. However, in order to be consistent with the original EXIT chart concept, the horizontal and vertical axes of the outer channel decoder are swapped in the joint diagram in comparison to the inner component, so that the *extrinsic* information is scaled on the horizontal axis, while the *a-priori* information is represented on the vertical axis, as shown in Fig. 2.15.

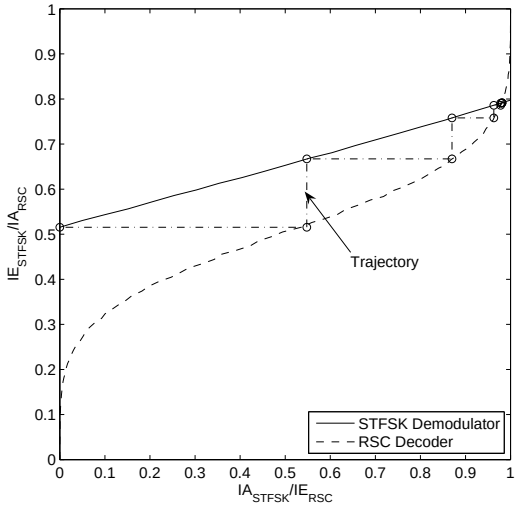


Figure 2.15: EXIT chart of the RSC coded STFSK scheme of Fig. 2.12 using iterative decoding and recorded at $E_b/N_0 = -1\ dB$, where the system parameters are provided in Table 2.7. The corresponding BER performance is shown in Fig. 2.20.

For example, Fig. 2.15 shows the EXIT chart of turbo-detection exchanging *extrinsic* information between the STFSK soft demodulator and the RSC channel decoder, when communicating over a frequency-flat Rayleigh fading channel. Ideally, the EXIT curves of the STFSK soft demodulator and of the RSC channel decoder should not intersect before reaching the (1,1) point of the EXIT chart at the $E_b/N_0$ value considered, which results in an open 'convergence tunnel' [89, 91] between the two decoding components' EXIT curves. The narrower the EXIT-tunnel, the more iteration are required to reach the point of perfect decoding convergence at (1,1), which again increases the iterative decoding complexity. If the two curves intersect at a point close to the (1,1) point, a low BER may still be achieved. Based on the EXIT chart, other properties are also achieved [94]

- The area under the demodulator's EXIT curse is given by the code-rate.
- The area in the open EXIT tunnel is proportional to discrepancy between the system's capacity and the specific $E_b/N_0$ value, where the BER suddenly drops to a vanishingly low value.
- If an intercept point exists between the EXIT curves and hence there is no open tunnel leading to the (1,1) point, then a residual BER floor is expected.

#### 2.2.4.6 Achievable Throughput

**STFSK**

For an STFSK system activating $K$ orthogonal frequencies, each STFSK block consists of $log_2(KLQ)$ bits, which are transmitted during $T$ symbol periods. Hence, the normalized throughput of STFSK may be expressed as

$$\eta_{STFSK} = \frac{2log_2(KLQ)}{KT} \quad (bits/T_s/frequency). \tag{2.49}$$

**STSK**

An STSK system may be considered as a simplified STFSK arrangement having a single transmit

frequency ($K = 1$). Therefore, the normalized throughput of STSK may be expressed as

$$\eta_{STSK} = \frac{log_2(LQ)}{T} \quad (bits/T_s/frequency). \tag{2.50}$$

It is noted that Eq. (2.50) is identical to Eq. (3) of [53].

**SFSK**

Similarly, an SFSK scheme may be considered as a simplified STFSK system employing $K$ transmit frequencies and a single-symbol PSK/QAM modulation scheme ($L = 1$). Therefore, the normalized throughput of SFSK may be calculated as

$$\eta_{SFSK} = \frac{2log_2(KQ)}{KT} \quad (bits/T_s/frequency). \tag{2.51}$$

For instance, the normalized throughput of some schemes are shown in Table 2.4.

Table 2.4: Parameters of LDC, STSK, SFSK and STFSK schemes.

| Parameters | $n_T n_R TQ$ | $L$ | $K$ | $bits/block$ | $bits/slot$ | Throughput |
|---|---|---|---|---|---|---|
| **LDC** | 4/1/4/16 | N/A | N/A | 4 | 1 | |
| **STSK** | 4/1/4/4 | 4 | N/A | 4 | 1 | |
| **SFSK** | 4/1/4/8 | N/A | 2 | 4 | 1 | 1 $bit/T_s/freq$ |
| **STFSK** | 4/1/4/2 | 4 | 2 | 4 | 1 | |
| **LDC** | 4/1/2/16 | N/A | N/A | 4 | 2 | |
| **STSK** | 4/1/2/4 | 4 | N/A | 4 | 2 | |
| **SFSK** | 4/1/2/8 | N/A | 2 | 4 | 2 | 2 $bit/T_s/freq$ |
| **STFSK** | 4/1/2/4 | 2 | 2 | 4 | 2 | |
| **STSK** | 4/1/2/64 | N/A | N/A | 6 | 3 | |
| **STSK** | 4/1/2/8 | 8 | N/A | 6 | 3 | |
| **SFSK** | 4/1/2/32 | N/A | 2 | 6 | 3 | 3 $bit/T_s/freq$ |
| **STFSK** | 4/1/2/8 | 4 | 2 | 6 | 3 | |
| **LDC** | 4/1/1/16 | N/A | N/A | 4 | 4 | |
| **STSK** | 4/1/1/4 | 4 | N/A | 4 | 4 | |
| **SFSK** | 4/1/1/8 | N/A | 2 | 4 | 4 | 4 $bit/T_s/freq$ |
| **STFSK** | 4/1/1/4 | 2 | 2 | 4 | 4 | |

#### 2.2.4.7 Detection Complexity

Let us quantify the computational complexity imposed by both the ML hard-detection and the soft-detection of STFSK schemes, which is given by the number of real-valued multiplications and real-valued additions. We make the following assumptions:

- Each complex-valued addition is equivalent to two real-valued additions.
- Each complex-valued multiplication is equivalent to four real-valued multiplications plus two real-valued addition.

- Each square of absolute value calculation carried out for a complex number is equivalent to two real-valued multiplication and one real-valued addition.

### a. Hard Demodulator

**a.1. STFSK**: First, we consider the complexity of the FSK detector. If the square-law FSK detector is employed as mentioned in Sec. 2.2.4.3, then the number of multiplications, $C^{\times}$, and the number of additions, $C^{+}$, may be obtained as

$$C^{\times} = 2K, \tag{2.52}$$
$$C^{+} = K. \tag{2.53}$$

In order to evaluate the complexity of the STSK detector, Eq. (2.28) can be utilized, where the product of $\chi \boldsymbol{K}$ involves the multiplication of two matrices, where one has a dimension of $(n_T \times Q)$, while the other has a dimension of $(Q \times 1)$. However, the vector $\boldsymbol{K}$ has only a single non-zero element. Therefore, instead of carrying out the matrix multiplication, the encoder may select the elements of $\chi$ at the specific positions corresponding to the non-zero element in $\boldsymbol{K}$. This reduces the decoding complexity imposed. As a result, the number of multiplications and the number of additions required for evaluating the decision matrix is equal to

$$C^{\times} = (4n_T T + 4n_T T n_R T + 2n_R T)QL, \tag{2.54}$$
$$C^{+} = [2n_T T + 2(2n_T T - 1)n_R T + 2Jn_R T + 2n_R T - 1]QL. \tag{2.55}$$

Note that $J$ denotes the number of taps describing our fading model, where the decoder has to eliminate the interfering signals dispersed from the previous symbol intervals. For a flat-fading channel, we have $J = 1$.

Since the vector $\boldsymbol{K}$ host both the FSK symbols and the PSK/QAM symbols, the encoder requires additional multiplications and addition, which are quantified as

$$C^{\times} = 4QL, \tag{2.56}$$
$$C^{+} = 2QL. \tag{2.57}$$

Each STFSK block consists of $log_2(K \cdot Q \cdot L)$ bits. Hence, by employing Eqs. (2.52-2.57), the average number of multiplications, $\bar{C}^{\times}$, and the average number of additions, $\bar{C}^{+}$, required for each bit of a STFSK scheme is given by

$$\bar{C}^{\times} = \frac{2K + (4n_T T + 4n_T T n_R T + 2n_R T)QL + 4QL}{log_2(KQL)}, \tag{2.58}$$
$$\bar{C}^{+} = \frac{K + [2n_T T + 2(2n_T T - 1)n_R T + 2Jn_R T + 2n_R T - 1]QL + 2QL}{log_2(KQL)}. \tag{2.59}$$

**a.2. STSK**: STSK is a special case of STFSK, where $K = 1$, no FSK detector is necessary. Furthermore, the vector $\boldsymbol{K}$ now only contains PSK/QAM symbols. Hence, the average number of multiplications and additions for each bit of a STSK scheme may be reduced to

$$\bar{C}^{\times} = \frac{(4n_T T + 4n_T T n_R T + 2n_R T)QL}{log_2(QL)}, \tag{2.60}$$
$$\bar{C}^{+} = \frac{[2n_T T + 2(2n_T T - 1)n_R T + 2Jn_R T + 2n_R T - 1]QL}{log_2(QL)}. \tag{2.61}$$

**a.3. SFSK**: Similarly, SFSK is another special case of STFSK, where we have $L = 1$ and the vector $\boldsymbol{K}$ now only hosts FSK symbols. Therefore, the average number of multiplications and additions for each bit of a SFSK scheme may be reduced to

$$\bar{C}^{\times} = \frac{2K + (4n_T T + 4n_T T n_R T + 2n_R T)Q}{log_2(KQ)}, \tag{2.62}$$

$$\bar{C}^{+} = \frac{K + [2n_T T + 2(2n_T T - 1)n_R T + 2Jn_R T + 2n_R T - 1]Q}{log_2(KQ)}. \tag{2.63}$$

**a.4. LDC**: LDC is a special case of STSK, where we have $L = 1$. Thus, the vector $\boldsymbol{K}$ is redundant in the decision metric of Eq. (2.28). Hence, the average number of multiplications and additions for each bit of a LDC scheme may be simplified to

$$\bar{C}^{\times} = \frac{(4n_T T n_R T + 2n_R T)QL}{log_2(QL)}, \tag{2.64}$$

$$\bar{C}^{+} = \frac{[2(2n_T T - 1)n_R T + 2Jn_R T + 2n_R T - 1]QL}{log_2(QL)}. \tag{2.65}$$

**b. Soft Demodulator**

**b.1. STFSK**: In a soft STFSK demodulator each computation of Eq. (2.42) consists of two evaluations of Eq. (2.28) plus $log_2(QLK)$ multiplications and $log_2(QLK)$ additions required for adding the *a-priori* information. However, the search-space may be halved. Therefore, the average number of multiplications and additions becomes equivalent to

$$\bar{C}^{\times} = \frac{[4n_T T + 4n_T T n_R T + 2n_R T + 4 + log_2(QLK)]QLK}{log_2(QLK)}, \tag{2.66}$$

$$\bar{C}^{+} = \frac{[2n_T T + 2(2n_T T - 1)n_R T + 2Jn_R T + 2n_R T + log_2(QLK)]}{log_2(QLK)}. \tag{2.67}$$

**b.2. STSK**: Similar to the hard-decision STSK demodulator, the soft-decision STSK demodulator only has to process PSK/QAM symbols, where $K = 1$. Hence, the average number of multiplications and additions for each bit of a STSK scheme may be reduced to

$$\bar{C}^{\times} = \frac{[4n_T T + 4n_T T n_R T + 2n_R T + log_2(QL)]QL}{log_2(QL)}, \tag{2.68}$$

$$\bar{C}^{+} = \frac{[2n_T T + 2(2n_T T - 1)n_R T - 2 + 2Jn_R T + 2n_R T + log_2(QL)]}{log_2(QL)}. \tag{2.69}$$

**b.3. SFSK**: Similarly, the average number of multiplications and additions required for each bit of a soft-decision SFSK scheme, where we have $L = 1$, may be reduced to

$$\bar{C}^{\times} = \frac{[4n_T T + 4n_T T n_R T + 2n_R T + log_2(QK)]QK}{log_2(QK)}, \tag{2.70}$$

$$\bar{C}^{+} = \frac{[2n_T T + 2(2n_T T - 1)n_R T - 2 + 2Jn_R T + 2n_R T + log_2(QK)]}{log_2(QK)}. \tag{2.71}$$

**b.4. LDC**: Finally, the average number of multiplications and additions associated with each bit of a soft-decision LDC scheme becomes

$$\bar{C}^{\times} = \frac{[4n_T T n_R T + 2n_R T + log_2(Q)]Q}{log_2(Q)}, \tag{2.72}$$

$$\bar{C}^{+} = \frac{[2(2n_T T - 1)n_R T - 2 + 2Jn_R T + 2n_R T + log_2(Q)]}{log_2(Q)}. \tag{2.73}$$

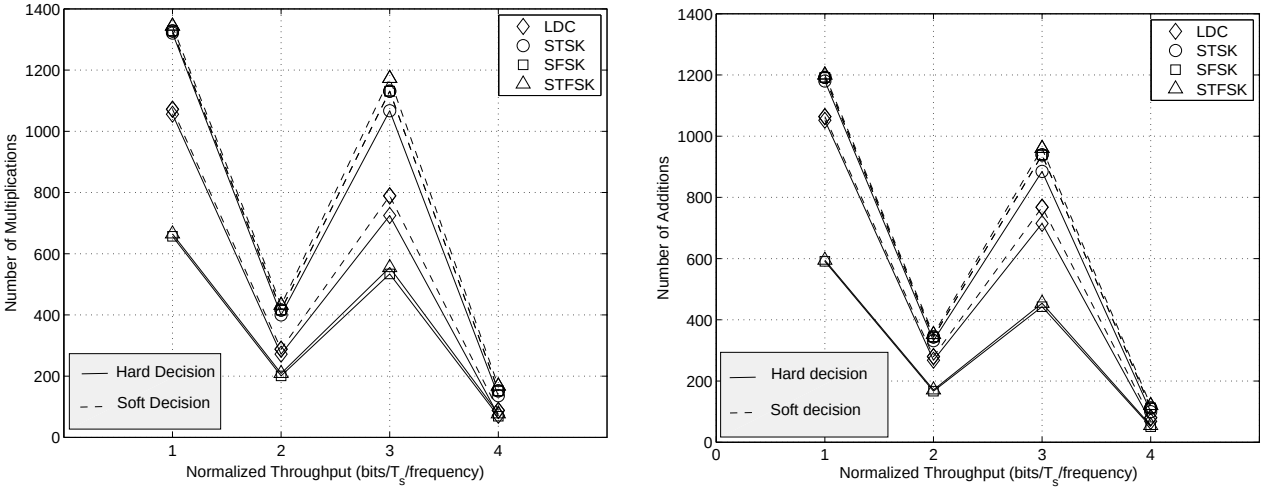


(a) Number of multiplications required

(b) Number of additions required

Figure 2.16: Complexity versus the normalized throughput of the LDC, STSK, SFSK and STFSK schemes, where the system parameters are provided in Table 2.4.

Table 2.5: Complexity of STFSK schemes.

| Scheme Identifier | $n_T n_R TQ$ | $L$-PSK | $K$-FSK | $\eta$ | Hard-decision | | Soft-decision | |
|---|---|---|---|---|---|---|---|---|
| | | | | | $\bar{C}^{\times}$ | $\bar{C}^{+}$ | $\bar{C}^{\times}$ | $\bar{C}^{+}$ |
| 1 | 4/1/4/2 | 2 | 16 | 0.1875 | 227 | 201 | 3605 | 3221 |
| 2 | 4/1/4/2 | 4 | 8 | 0.375 | 445 | 397 | 3605 | 3221 |
| 3 | 4/1/4/2 | 8 | 4 | 0.75 | 887 | 793 | 3605 | 3221 |
| 4 | 4/1/4/2 | 16 | 2 | 1.5 | 1771 | 1584 | 3605 | 3221 |
| 5 | 4/1/4/4 | 2 | 8 | 0.375 | 455 | 397 | 3605 | 3221 |
| 6 | 4/1/4/4 | 4 | 4 | 0.75 | 887 | 793 | 3605 | 3221 |
| 7 | 4/1/4/4 | 8 | 2 | 1.5 | 1771 | 1584 | 3605 | 3221 |
| 8 | 4/1/4/8 | 2 | 4 | 0.75 | 887 | 793 | 3605 | 3221 |
| 9 | 4/1/4/8 | 4 | 2 | 1.5 | 1771 | 1584 | 3605 | 3221 |
| 10 | 4/1/4/16 | 2 | 2 | 1.5 | 1771 | 1584 | 3605 | 3221 |

The complexity results of the STFSK, STSK and SFSK schemes summarized in Table 2.4 are shown in Fig. 2.16, where the continuous and the dashed lines portray the detection complexity of the hard- and soft- demapper, respectively. As seen in Fig. 2.16, the complexity of the hard-decision STFSK schemes is comparable to that of the SFSK schemes in term of the number of multiplications and additions. By contrast, the hard-decision STSK schemes have doubled the complexity of the hard-decision STFSK and SFSK arrangements, when considering the same normalized throughput, while the number of multiplications and additions required by the hard-decision LDC demappers is 50% higher than those of the hard-decision STFSK schemes. Observe furthermore from Fig. 2.16 that the complexity of the soft-decision STSK, SFSK and STFSK demappers is comparable, while they are slightly more complex than the soft-decision LDC demapper. Furthermore, we found that in case of the SFSK and STFSK schemes the soft demappers doubled the complexity of the hard demappers, whilst in case of the STSK and LDC schemes the complexity of the soft- and hard-demappers remain comparable.

Furthermore, the complexity of the hard- and the soft-decision STFSK schemes of Table 2.3 is summarized in Table 2.5, where the block size of 6 bits per symbol is employed. The following observations may be made:

- For the hard-decision, the complexity of decoder is reduced, when the number of frequencies, $K$, is increased.
- For a given value of $K$ and for a given value of the product $QL$, all possible combinations of $Q$ and $L$ exhibit the same decoding complexity when hard-decision is employed.
- In case of hard-decision, the complexity of a STFSK scheme increases upon increasing the normalized throughput.
- The complexity of a soft-decision STFSK demodulator depends only on the product of $Q \times L \times K$, rather than on all possible combinations of $Q$, $L$ and $K$.

#### 2.2.4.8 Parameter Selection

The STFSK is a sophisticated scheme, which beneficially transforms the binary bits in the STF-domain signal. Therefore, appropriately configuring the system parameters is important.

For a system having a relatively narrow bandwidth and operating in a flat-fading channel, STSK, which represents STFSK associated with $K = 1$, constitutes a suitable selection. This is because FSK only exhibits substantial advantages in frequency-selective fading channels, where transmission during prolonged fades are avoided by hopping to an independently faded tone outside the coherence bandwidth. Moreover, a tight bandwidth constraint does not allow a sufficiently high number of frequencies to be selected. The parameter configuration process conceived for the STSK scheme was detailed in [53].

By contrast, when a sufficiently high bandwidth is available, the STFSK concept ($K \geq 2$) may significantly improve the attainable system performance, as a benefit of spreading the signal over the STF domain. Moreover, it can also offer a high system configuration flexibility. Let us briefly exemplify the mapping rules of our STFSK scheme, where a fixed number of $B = log_2(KLQ) = 3$

bits per STF block $S$ is transmitted. As demonstrated in Table 2.2, we can use one of the following combinations:

$$B = log_2(KLQ) = 3bits \Leftrightarrow \begin{cases} K = 1, (L, Q) = (1, 8; 2, 4; 4, 2; 8, 1) \\ K = 2, (L, Q) = (1, 4; 2, 2; 4, 1) \\ K = 4, (L, Q) = (1, 2; 2, 1) \\ K = 8, (L, Q) = (1, 1). \end{cases} \quad (2.74)$$

Clearly, for a fixed number of 3 bits per transmitted block, the STFSK scheme may offer ten different system configuration choices, compared to the four STSK options of [53].

According to Eq. (2.49), as the value of $K$ or $T$ increases, the throughput of the system linearly decreases. At the same time, the throughput is increased relatively slowly, namely as a function of $log_2(K \cdot L \cdot Q)$ with the product $(K \cdot L \cdot Q)$. Again, the classic tradeoff between the achievable diversity and multiplexing gain has to be considered here. Moreover, increasing $K$ also leads to an increased complexity at the demodulator, since more matched filters are required. As shown in [66,87], the incremental BER improvement slows down for high values of $K$, namely for $K > 4$. Therefore, the values of $K = \{2, 4\}$ constitute reasonable choices in order to mitigate the effects of frequency-selective fading, while maintaining a high throughput. Finally, the number of transmit antennas employed should obey $n_T \leq T$, as mentioned above.

#### 2.2.4.9 Performance of Space-Time-Frequency Shift Keying

**a. Performance in Interference-Limited Environments**

In this section, the BER performance of the STSK, SFSK and STFSK modulation schemes will be investigated and compared. The modulation parameters of the three schemes are provided in Table 2.6, where the normalized throughput of 1 $bit/T_s/frequency$ is applied to all schemes in order to make a fair comparison. At the receiver, the square-law detector [66] is employed to detect the FSK symbols, while the maximum likelihood STSK detector is utilized to detect both the PSK/QAM symbols and the LDC matrices.

Table 2.6: Parameters of LDC, STSK, SFSK and STFSK schemes, employing 1 $bit/T_s/freq$.

| Parameters | $n_T n_R TQ$ | $L$ | $K$ | Throughput |
|---|---|---|---|---|
| **LDC** | 4/1/4/16 | N/A | N/A | 1 $bit/T_s/freq$ |
| **STSK** | 4/1/4/4 | 4 | N/A | 1 $bit/T_s/freq$ |
| **SFSK** | 4/1/4/8 | N/A | 2 | 1 $bit/T_s/freq$ |
| **STFSK** | 4/1/4/2 | 4 | 2 | 1 $bit/T_s/freq$ |

Fig. 2.17 shows the BER performance of the four schemes of Table 2.6, when the channels are assumed to be uncorrelated and frequency-flat Rayleigh faded, where STSK achieves a power gain of about 3 dB over SFSK across the $E_b/N_0$ range considered. This may be explained by the fact that STSK is not affected by the frequency-flat fading. As an additional benefit, it may glean a diversity gain from the time domain, which SFSK fails to achieve. Hence, STSK may outperform SFSK. At

the same throughput, the STSKs performance also dominates that of the conventional LDC. More particularly, as shown in Fig. 2.17, the LDC achieved a BER of $3.10^4$ at the $E_b/N_0$ of 20 dB, while the STSK further reduced the BER to $4.10^6$ at the same $E_b/N_0$ value. However, its BER performance is still worse than that of STFSK. More particularly, STFSK offers a power gain of 3 dB over STSK. This may be explained by observing that STFSK transmits $Q = 2$ symbols in $T = 4\ T_s$, compared to the $Q = 4$ symbols transmitted in $T = 4\ T_s$ by the STSK scheme. Therefore, STFSK is capable of gleaning a higher diversity gain from the TD.

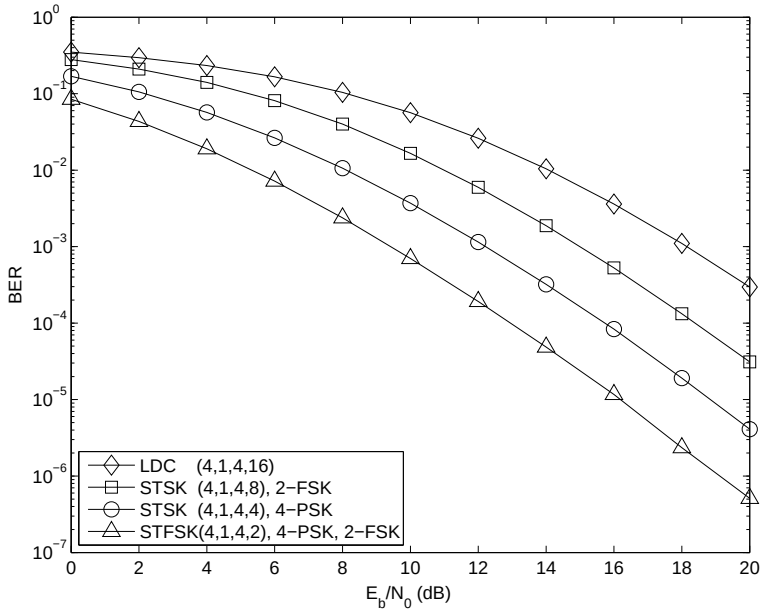


Figure 2.17: The performance of the hard-decision LDC, STSK, SFSK and STFSK modulation schemes for uncorrelated frequency-flat Rayleigh fading channels, where the system parameters are provided in Table 2.6.

The performance of the three schemes in the frequency-selective fading environment considered is characterized in Fig. 2.18. The 4-tap ITU-A channel model [13] having a normalized Doppler frequency of 0.001 is employed here. As shown in the figure, STFSK outperforms the STSK and SFSK schemes. It is also observed that the performance of the STFSK and the SFSK systems remains more-or-less unaffected in the face of the frequency-selective fading channels considered, while the STSK's performance degrades by 1 dB, since the STSK scheme attains no diversity gain in the FD. Therefore, the STSK signal is contaminated by the ISI imposed by the frequency-selective fading.

Additionally, we investigate the scenario, when the ISI imposes a more grave impact on the attainable system performance by introducing the 6-tap COST207 rural area channel model [13], which is detailed in Section 1.1.1.3. According to Fig. 2.18, the performance of the STFSK and the STSK schemes recorded for the 6-tap COST207 channel becomes more degraded in the low $E_b/N_0$ region, namely below 10 dB, than for the 4-tap ITU-A channel but in the rest of the $E_b/N_0$ region, they perform comparably well. By contrast, the STSK's performance continues to degrade. More particularly, the gap between the BER curves of the STSK and the SFSK schemes is reduced by 2 dB, compared to the uncorrelated frequency-flat fading scenario, resulting in a power gain of 1 dB.

Furthermore, we evaluated the attainable BER performance of the three schemes seen in Table 2.6, when the Channel State Information (CSI) is imperfect at the receiver. The 6-tap COST207 rural area

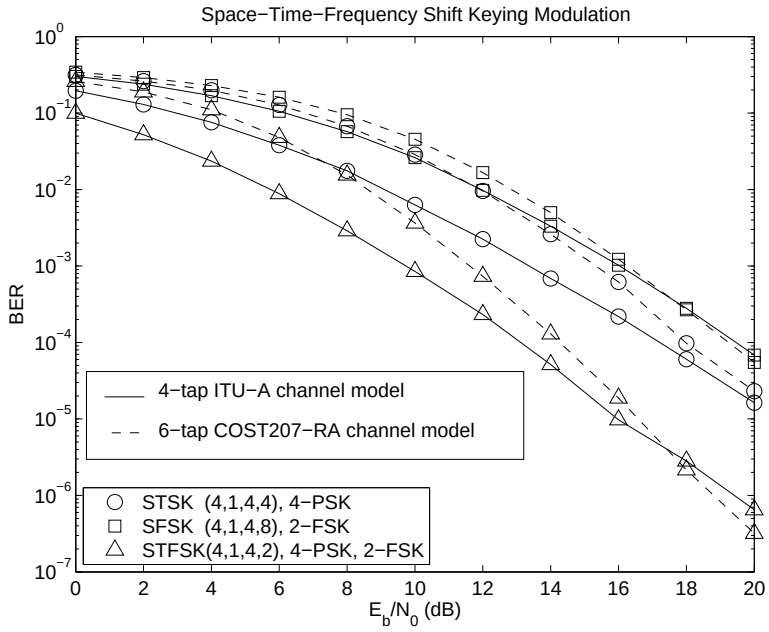


Figure 2.18: The performance of the hard-decision STSK, SFSK and STFSK modulation schemes for frequency-selective Rayleigh fading channel with the normalized Doppler frequency of $10^{-1}$, where the system parameters are provided in Table 2.6. The corresponding performance over frequency-flat Rayleigh fading is shown in Fig. 2.17.

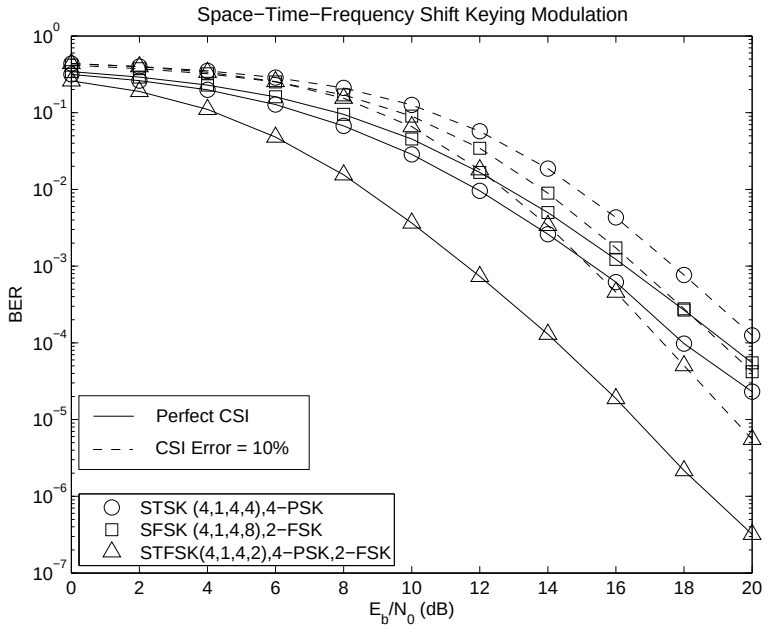


Figure 2.19: The performance of the hard-decision STSK, SFSK and STFSK modulation schemes under the 6-tap COST207 rural area channel model with the normalized Doppler frequency of $10^{-1}$ when the CSI is imperfect at the receiver, where the system parameters are provided in Table 2.6. The coressponding performance under the perfect CSI is shown in Fig. 2.18.

channel model is continued to be used, while a Gaussian CSI estimation error of 10% is assumed here. The BER performance of the scenario is shown in Fig. 2.19. In contrast to the results of Fig. 2.18, at the CSI error of 10% the STSK scheme performs worse than SFSK, since the BER performance of the latter was only slightly degraded. As seen in Fig. 2.19, the BER performance of STFSK is also significantly degraded, requiring an approximately 3 dB higher channel SNR for maintaining a specific BER, when a realistic CSI error is imposed.

In the following, we consider the achievable iterative detection aided performance, when the soft STFSK demapper iteratively exchanges *extrinsic* information with the Recursive-Systematic-Convolutional (RSC) decoder. The RSC codec employs a half-rate, constraint-length-3 code having the generator polynomial of $\frac{1+Z^{-2}}{1+Z^{-1}+Z^{-2}}$. The STFSK scheme's parameters are provided in Table 2.7. Observe from Fig. 2.20 that the achievable performance is significantly improved, when the number of iterations between the soft demapper and the RSC decoder was increased. Quantitatively, an $E_b/N_0$ improvement of 3 dB was achieved at the BER of $10^{-4}$, when the number of iterations was increased from one to five.

Table 2.7: Parameters of the RSC coded STFSK schemes.

| Parameter | Value |
|---|---|
| Information/Encode bits | 600/1200 |
| Channel code | RSC(5,7) |
| STFSK modulation | 4/1/4/2-4-2 |
| Demodulator type | Soft-decision |
| Decoding type | Iterative-detection |
| Number of iterations | $I = 1...5$ |
| Channel type | flay-Rayleigh fading |

The results of Fig. 2.20 are further supplemented by the EXIT charts of Fig. 2.21. As seen in Fig. 2.21(a), at the $E_b/N_0$ value of -3 dB the intersection of the two EXIT curves is at the point of (0.75,0.55) and up to this point a gradually narrowing tunnel exists between the two EXIT curves. Hence, at this value of $E_b/N_0$, only an insignificant improvement is obtained upon increasing the number of decoding iterations between the STFSK demodulator and the RSC decoder. By contrast, the tunnel is more widely open in case of $E_b/N_0 = -1$ dB in Fig. 2.21(b) and the *extrinsic* information gleaned increases significantly, when the number of iterations increases from one to three. This explains why the attainable BER performance improves rapidly for the first three iterations, while the BER improvement significantly reduces for the fourth and fifth iteration.

Fig. 2.22 characterizes the attainable performance of all the ten STFSK schemes of Table 2.3, where all other system parameters are provided in Table 2.7. The performance confirms the EXIT-chart based performance predictions of Fig. 2.14. More particularly, based on the results, the ten schemes may be divided into four groups. The first group, including Schemes {1,2,3}, exhibits the best performance, achieving a $BER$ of $10^{-4}$ at an $E_b/N_0$ value around 0 dB. The EXIT functions of the demappers in these three schemes are shown at the top of Fig. 2.14, where a significant advantage is shown in comparison to the remaining schemes. The second group consisting Schemes {4,5,6,7} achieved the same $BER$, namely $10^{-4}$, at the $E_b/N_0$ of about 2.5 dB. The EXIT functions of these

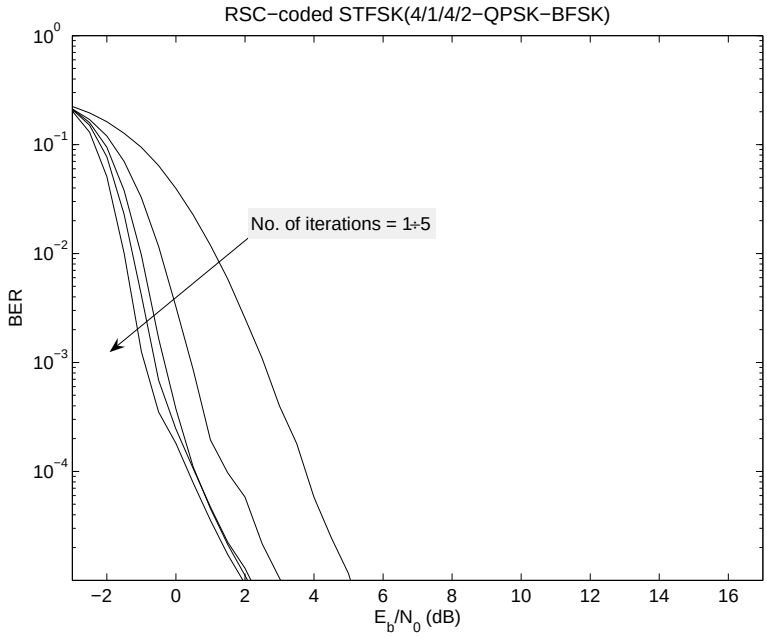


Figure 2.20: The performance of the soft-decision RSC-coded STFSK(4/1/4/2) with the aid of QPSK and BFSK modulations, where the system parameters are provided in Table 2.7 and the corresponding EXIT charts are shown in Fig. 2.21.

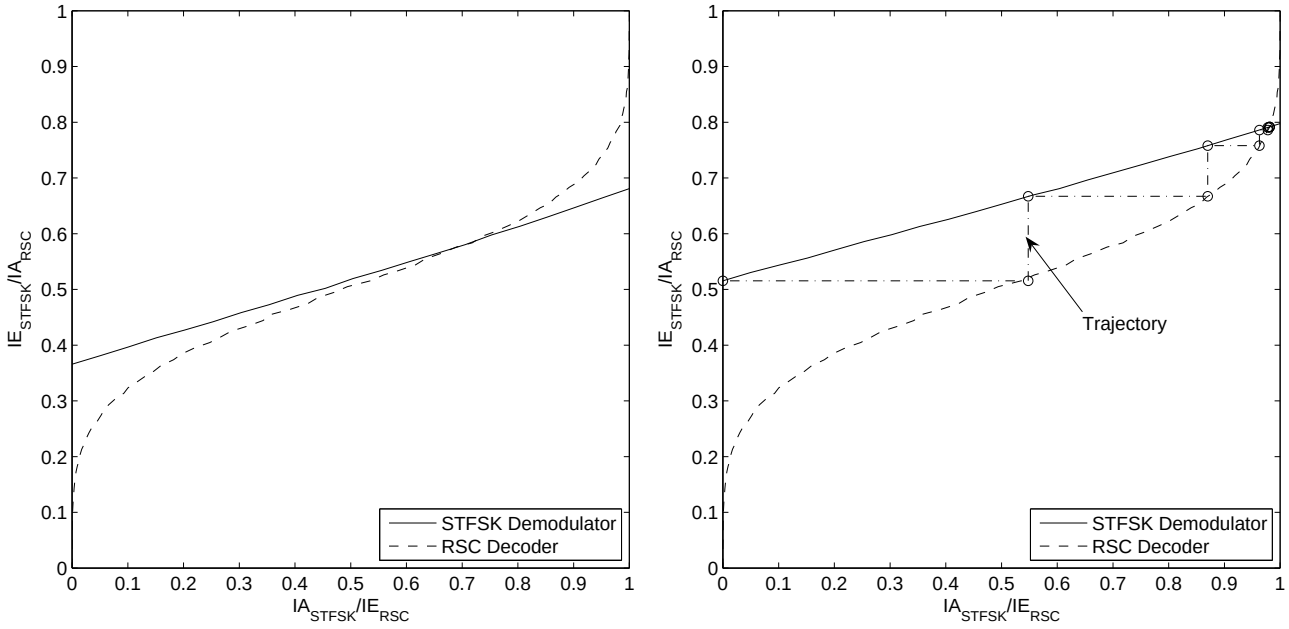


(a) $E_b/N_0 = -3\ dB$ (b) $E_b/N_0 = -1\ dB$

Figure 2.21: EXIT charts of the RSC coded STFSK using iterative decoding, where the system parameters are provided in Table 2.7 and the associated BER performance is shown in Fig. 2.20.

schemes remained significantly below those of the first group. The third group contained Scheme 8 and Scheme 9, whose EXIT functions remained further below those of Schemes {4,5,6,7} in Fig. 2.14. They achieved the $BER$ of $10^{-4}$ around the $E_b/N_0$ value of 5.5 dB. Finally, Scheme 10, which has the demapper EXIT function at the bottom of Fig. 2.14, acquired the same $BER$ around the $E_b/N_0$ value of 9.5 dB.

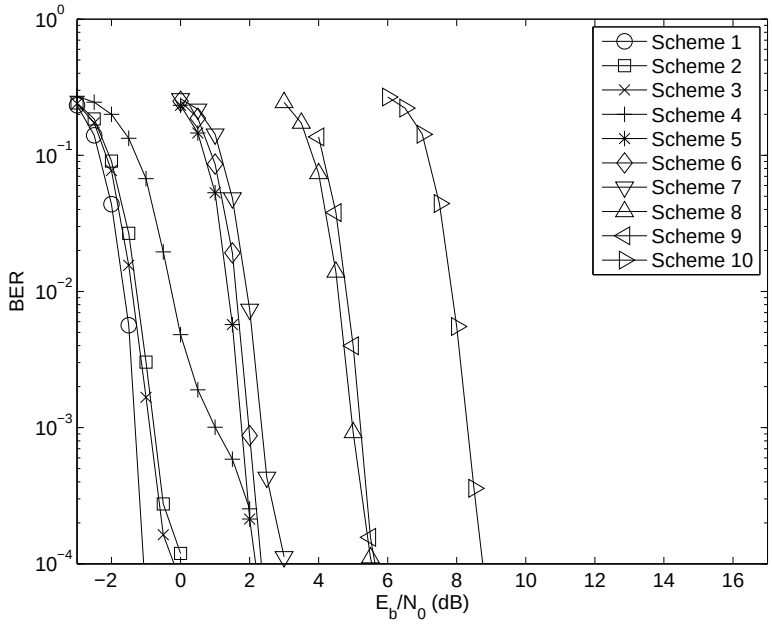


Figure 2.22: The performance of the soft-decision aided RSC-coded STFSK schemes of Table 2.3, where the other system parameters are provided in Table 2.7, while the EXIT functions of the STFSK demodulators recorded at $E_b/N_0 = 0$ dB are shown in Fig. 2.14.

### b. Performance in Multi-user and Multi-cell Environments

One of the disadvantage of the STFSK scheme is the vulnerability of its FSK component to the co-channel interference. By contrast, the co-channel interference may be diminished by employing Slow Frequency Hopping Multiple Access (SFHMA) [95], which not only provides inherent frequency diversity but also advantageously randomises the effects of cochannel interference. Furthermore, SFHMA is capable of avoiding the problem of prolonged fades typically experienced by stationary or slow moving Mobile Stations (MS) because hopping to another independently faded frequency might curtail fading. The classic SFH900 mobile system [96, 97] which was based on "mixed" Slow Frequency Hopping (SFH) combined with time division demonstrated the benefits of SFHMA.

Motivated by its substantial benefits, in this section we develop the single-link STFSK philosophy into a multi-user, multi-cell SFHMA system in order to investigate the inter-play of these techniques and their impact on the performance of the holistically optimized system. The novelty and rationale of our proposed scheme is summarized as follows:

1. *First, we intrinsically amalgamate the STFSK with SFHMA and then investigate the achievable Area Spectral Efficiency (ASE) of a realistic multi-user, multi-cell wireless environment under different cellular frequency reuse structures.*

2. *The study in Chapter 7 of [11] showed that the SFHMA system is superior in comparison to the Time Division/ Frequency Division Multiple Access (TD/FDMA) benchmarker for a low-*

*complexity 16 kbit/s subband speech codec combined with Reed-Solomon coding. By contrast, in this section we demonstrate that the SFHMA system becomes inferior to the TD/FDMA system when state-of-the-art components, such as the Advanced Multi-rate (AMR) speech codec and the convolutional coding are employed.*

3. *Finally, we demonstrate that by intrinsically amalgamating low-complexity STFSK and SFHMA, we attained an improved ASE, compared to those of TD/FDMA and WCDMA. However, this ASE remains lower than that of the more complex LTE system, when the same convolutional channel code and the same system bandwidth are employed.*

### b.1. Slow Frequency Hopping Multiple Access

*Slow Frequency Hopping Multiple Access Protocols*

The Slow Frequency Hopping Multiple Access (SFHMA) technique employs SFH relying on unique, user-specific pseudo-random hopping sequences for supporting multiple users. The SFH family may be divided into three categories, as follows:

- **Orthogonal**: a set of orthogonal sequences of length $N_c$ are allocated to each cell to permit access to $N_c$ frequencies. In any hop, each active user within a cell is assigned one of these sequences, which allows the user to transmit on a particular frequency. In adjacent cells orthogonal transmissions are ensured by allocating distinct sets of frequencies. As in any cellular network, frequency reuse can be employed by assigning the same set of frequencies to the cells, whose geographic separation is not lower than the affordable reuse distance.

- **Random**: each active user is assigned a unique frequency-hopping sequence, which is uncorrelated with all other sequences. This arrangement allows the generation of a significantly higher number of sequences, hence potentially allowing more users to join the network. As a price, due to the eroded orthogonality between the hopping sequences, cochannel interference will appear even in non-dispersive propagation scenarios. However, in each hop a different subset of active users will generate the interference, which randomizes its effects. In other words, it spreads the interference over all the frequencies, hence reducing its power-spectral density and therefore it can make the employment of frequency reuse based cellular planning unnecessary.

- **Mixed**: Based on the above two arrangements, a mixed protocol is proposed, in which a pair of uncorrelated sequences of length $N_c$ facilitate hopping to the same frequency in only one of the $N_c$ hops. This arrangement reduces the effects of cochannel interference and hence becomes capable of supporting a high number of users. As a benefit of providing an increased freedom in system design and of its improved spectral efficiency [96, 97], the above-mentioned mixed protocol will be considered in the following sections.

*Cellular Reuse Structure*

The basic form of the reuse structure, which has three basic frequency-sets, also often referred to as 'colours' is illustrated in Fig. 2.23 for the SFHMA system detailed in [96, 97]. Each colour is represented by one of the letters A, B, C and each contains a set of $N_c$ frequencies. For a given reference cell associated with colour A, all other cells marked A are full-reuse cells, relying on the

same set of frequencies. For the full-reuse structure, an active user in the reference cell will experience interference from an active user in the reuse cell, during one of each sequence of $N_c$ hops, when they happen to use the same frequency. Each additional active user from the same or other reuse cell will impose the same frequency collision probability, but at a different frequency in the reference user's sequence. Therefore, the so-called 'frequency collision rate' is defined as the proportion of the hopping sequence, when a 'hit' by an identical-frequency active user is encountered. For a full reuse cluster size $C_c$, the frequency collision rate equals to $C_c/3N_c$.

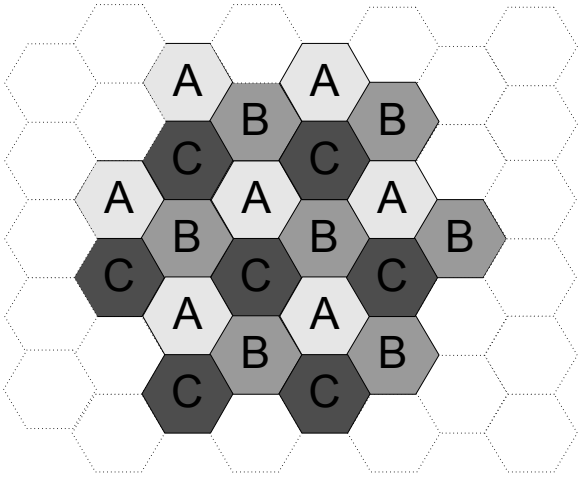


Figure 2.23: Three-colour cellular frequency reuse structure.

By constrast, in a fractional reuse structure, each colour is divided into $M_c$ overlapping sub-sets of $L_c$ groups of frequencies, which are referred as 'shades' of that colour, or 'pseduo-colour' [96]. Hence, the frequency-reuse cluster contains $3M_c$ cells divided into $M_c$ sub-clusters of size 3, each using a different shade of 3 colours. This is known as a $3M_c/L_c$ fractional structure [96], where $L_c/M_c$ is the fraction of the $N_c$ frequencies making up a colour, which is constituted by the set of shades. Fig 2.24 shows an example of a 21/3 reuse structure, where we have $M_c = 7$ and $L_c = 3$. A shade allocation for colour A is given in Table 2.8, which indicates the fractional overlap of hopping frequencies of 1/3. The characteristics of other classic fractional reuse structures are summarized in Table 2.9. Finally, the frequency collision rate is expressed as

$$y = \frac{M_c k}{L_c N_c}, \tag{2.75}$$

where $k$ is the fractional overlap factor. Note that we have $k = 0$ for cells of different colours, while $k = 1$ for cells of the same colour and shade. Other values of $k$ may be found in Table 2.9.

### b.2. Spectral Efficiency of STFSK Aided SFHMA

*Spectral Efficiency of the SFHMA system*

In this section, the method proposed in [11, 97] will be employed for evaluating the ASE of the proposed STFSK aided SFHMA system. Furthermore, the spectral efficiency of the STFSK aided SFHMA, the GMSK aided SFHMA and the conventional GMSK aided TD/FDMA systems will be compared. In this study we focus our attention on the base-to-mobile DownLink (DL).

In order to calculate the ASE of the entire system, we first consider the probability of correct reception of a hop, $q_c$, ensured by the FEC coding and by the audio/video codec of a multimedia

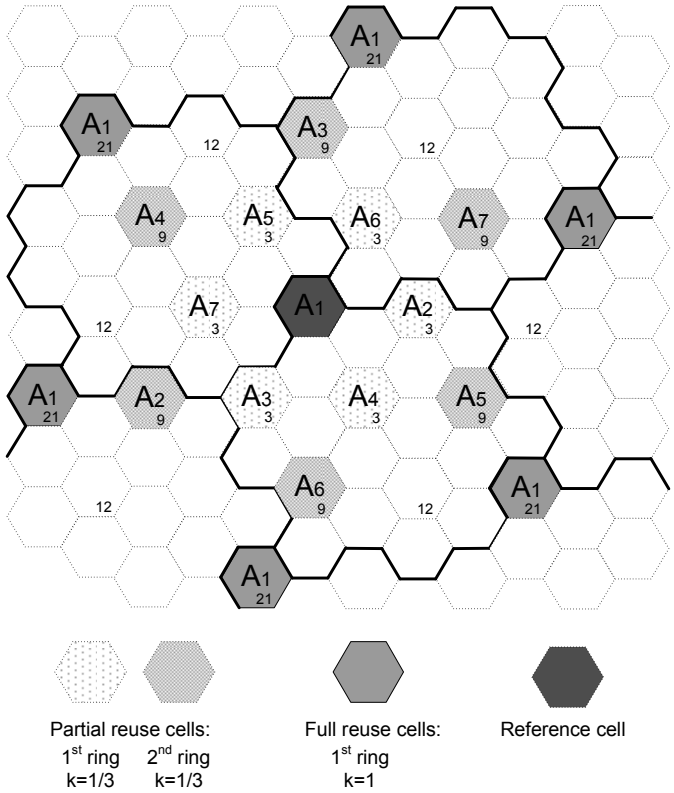


Figure 2.24: Frequency reuse cells of a 21/3 fractional reuse structure. The 'A' cells associated with the same colours and shades are full-reuse cells, while those with the same colours but different shades are fractional reuse cells. In contrast to Fig. 2.23, all 'A' cells have the same colours and shades, resulting in only full reuse cells.

Table 2.8: Shade allocation for a 21/3 frequency reuse structure

| Frequency | Shade | | | | | | |
|---|---|---|---|---|---|---|---|
| group | A1 | A2 | A3 | A4 | A5 | A6 | A7 |
| f1 | * | * | * | | | | |
| f2 | * | | | * | * | | |
| f3 | * | | | | | * | * |
| f4 | | * | | * | | * | |
| f5 | | * | | | * | | * |
| f6 | | | * | * | | | * |
| f7 | | | * | | * | * | |

Table 2.9: Fractional reuse structure characteristics

| Cluster | $M_c$ | $L_c$ | $k$ | $y$ | |
|---|---|---|---|---|---|
| size | | | | fractional | full |
| 9/2 | 3 | 2 | 1/2 | $9/4N_c$ | $3/2N_c$ |
| 12/2 | 4 | 2 | 1/2 | $1/N_c$ | $2/N_c$ |
| 12/3 | 4 | 3 | 2/3 | $8/9N_c$ | $4/3N_c$ |
| 21/3 | 7 | 3 | 1/3 | $7/9N_c$ | $7/3N_c$ |
| 21/4 | 7 | 4 | 1/2 | $7/8N_c$ | $7/4N_c$ |

session for the sake of guaranteeing an acceptable service quality. This probability may be achieved, when the signal's Carrier-to-Interference Ratio (CIR) at the receiver is lower than an $E_b/N_0$ value, which corresponds to a specific $BER$ threshold. According to [97], a $q_c$ value of 0.7 is capable of guaranteeing an acceptable speech quality for a system utilizing the Reed-Solomon (RS) (8,4) channel code and a 16 kbit/s sub-band codec, resulting in an ReS-decoded BER of approximately $3\times10^{-3}$. It is worth nothing that the state-of-the-art Advanced Multi-Rate (AMR) speech codec [98] provides a good speech quality even at $BER = 10^{-2}$. However, in order to facilitate reliable system synchronization, the target $BER$ of $10^{-3}$ is chosen in this study. The probability $q_c$ of correct reception of a hop may be formulated as [97]:

$$q_c \quad = \quad \boldsymbol{Prob}\{\lambda \geq \gamma\}, \tag{2.76}$$

where $\gamma$ presents the $E_b/N_0$ value corresponding to the $BER$ threshold and $\lambda$ is the CIR at the receiver considered, where the interference is imposed by all the adjacent cells. Note that the CIR depends on the received power, on the shadowing and fast-fading parameters, as well as on the interference imposed by other cells in the network. More particularly, if a reference cell is interfered by $M_I$ adjacent cells, then the probability $q_c$ of correct reception will be the product of $M_I$ probabilities, each of which is the probability of correct reception conditioned on the CIR $\Lambda_i$ corresponding to the $i^{th}$ cell. Hence, Eq. (2.76) may be further expressed as [11]

$$q_c = \prod_{i=1}^{M_I} \left(1 - \frac{p_i\gamma}{\Lambda_i + \gamma}\right), \tag{2.77}$$

where $p_i$ presents the frequency-collision probability.

In line with [11], we assume that the locations of MSs are random in the reference cell. Therefore, $q_c$ may be calculated for various values of the tele-traffic load, $X$, which is also known as the average number of users actively engaged in calls per MHz per cell. In the analysis of [11], the '90% worst case value', $q_{90}$, defined as the specific value of $q_c$, which is exceeded with a probability of 90%, is utilized. The study of [97] suggested that the specific operating point where we have $q_{90} = 0.7$ in the graph of $q_{90}$ versus $X$ should be selected in order to ensure an acceptable reception quality. However, the analysis of [11] indicated that $q_{90} = 0.8$ might be a better choice for the minimum $q$ to determine the ASE. Hence, the value of $q_{90} = 0.8$ is considered in our following analysis.

The ASE calculation may then be simplified to:

$$\eta = a_{cell}/W = X, \tag{2.78}$$

where $a_{cell}$ is the traffic load and W is the total allocated bandwidth. Furthermore, the frequency-collision probability may be expressed as

$$p_i = \frac{y_i r_a W X}{n_t n_{call}}, \tag{2.79}$$

where $n_t$ is the number of slots per TDM frame and $n_{call}$ is the number of calls per timeslot, while $r_a$ is the Voice Activity Ratio (VAR), typically assumed to be 0.5 for the downlink [97]. For a full-reuse cell cluster of size $C_c$, the frequency-collision rate $y_i$ becomes $C_c/3N_c$. By contrast, we have $y_i = k_i M_c/L_c N_c$ for the $3M/L$ fractional reuse structure. As regards to the channel spacing $f_s$, the number of hopping frequencies assigned to each of the three basic colours is given by

$$N = \frac{W}{3f_s}. \tag{2.80}$$

Hence, Eq. (2.79) may be simplified to

$$p_i = \frac{CXr_a f_s}{n_t n_{call}}, \tag{2.81}$$

for the full-reuse cells and

$$p_i = \frac{3k_i MXr_a f_s}{Ln_t n_{call}}, \tag{2.82}$$

for fractional reuse.

In reality, most cellular systems employ fixed beam-forming-based angular sectorization, at least near the cell-edge. Thus, in the scenario of $120^o$ sectorization only 3 of 6 neighbour cells impose interference on the reference cell. However, there are only two cells, which contribute the full interference. Moreover, the authors of [97] demonstrated that the probability of the event, when the worst-case value $q_{90}$ occurs is comparable to the probability of $\Lambda_{90}$, which is defined as the '90% worst-case value' CIR, in other words, $\boldsymbol{Prob}(q_c > q_{90}) = \boldsymbol{Prob}(\Lambda > \Lambda_{90}) = 90\%$. Hence, $q_{90}$ may be expressed as

$$q_{90} = \prod_{i=1}^{K_I} \left(1 - \frac{p_i \gamma}{2\Lambda_i + \gamma}\right)^2, \tag{2.83}$$

where $K_I$ is the number of cellular rings using a different frequency set around the reference cell.

Fig. 2.25 shows the BER performance of both GMSK and STFSK(4/1/4/2-4-2), where we employ $M/N/T/Q = 4/1/4/2$, 4-PSK and 2-FSK modulation for transmission over the COST-207 rural area channel model [13], when assuming a maximum multipath delay of 20 $\mu s$, corresponding to an Inter-Symbol Interference (ISI) of 6 symbols at a bit rate of about 300 kbits/s. The half-rate channel codes ReS(8,4) [11] and the recursive systematic convolutional code RSC(23,33) using the octally represented generator polynomials of 23 and 33 [99] are considered. For RSC-coded system, soft-decision were used at the receiver. The system parameters are summarized in Table 2.10. According to Fig. 2.25, the target BER of $10^{-3}$ was achieved at the $E_b/N_0$ value of $\gamma$ =26.0 dB, 19.0 dB and 8.5 dB for the uncoded, ReS coded and RSC coded GMSK schemes, respectively. For the same coding schemes invoked for the STFSK transceiver, the corresponding values are $\gamma$ =9.5 dB, 7.5 dB and 1.5 dB, respectively. All of these values will be used for computing the system's $q_{90}$ values as well as its ASE.

Table 2.10: Parameters of the SFHMA schemes.

| **Parameters** | **Values** |
|---|---|
| Channel codes | ReS(8,4)/RSC(23,33) |
| Code rate | 0.5 |
| Modulation type | GMSK/STFSK(4/1/4/2-4-2) |
| Channel model | 6-tap COST-207 - RA |

For a basic 3-cell structure using the above values of $\gamma$ as well as $\Lambda_{90}$ from Table 2.11 and assuming a frequency spacing of $f_s = 1/7$ MHz, the values of $q_{90}$ versus the average number of users, $X$, are presented in Fig. 2.26. The curves were plotted for the following conditions:

- Nearest reuse ring (cluster-size 3) only is marked by the circles.

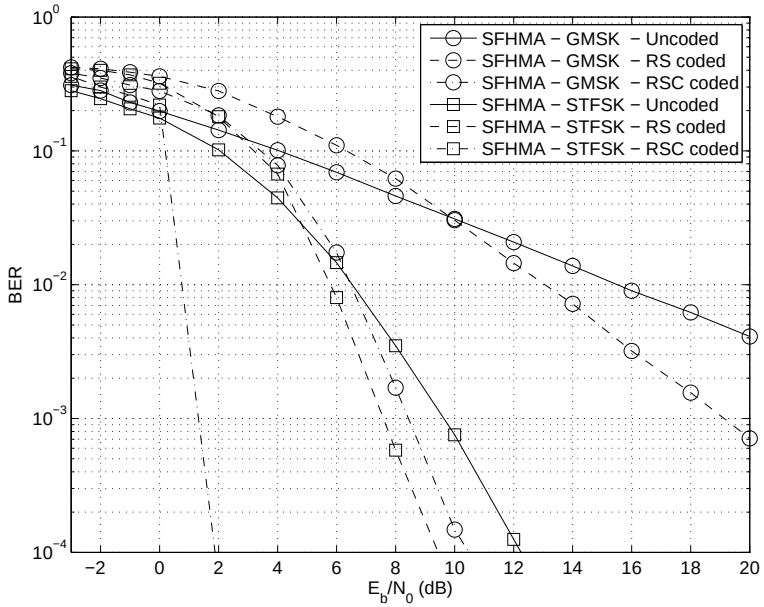


Figure 2.25: BER versus $E_b/N_0$ performance of the GMSK and the STFSK(4/1/4/2-4-2) schemes employing ReS and RSC channel codes for transmission over the 6-tap COST-207 rural area channel model subjected to Rayleigh fading and AWGN. The associated system parameters are summarized in Table 2.10.

Table 2.11: Values of $\Lambda_{90}$ versus reuse cluster size [11, 97]

| Size | 3 | 9 | 12 | 21 | 27 | 36 | 39 | 48 |
|---|---|---|---|---|---|---|---|---|
| $\Lambda_{90}$ (dB) | 5.2 | 13.0 | 14.5 | 18.2 | 20.6 | 22.9 | 23.5 | 25.1 |

- Nearest reuse ring plus two nearest rings of cells of the other colours which impose adjacent-channel interference, for which the values of $\Lambda_{90}$ taken from [97] are $R_{AC}+2$ dB and $R_{AC}+9$ dB, where $R_{AC} = 17$ dB is the adjacent-channel interference rejection for $f_s = 1/7$ MHz. This scenario is indicated by the down-facing triangles.
- The second reuse ring (size 9) only, as indicated by the upwards triangles.
- The first five reuse rings (size 3,9,12,21,27), as marked by the squares.

As seen in the figure, the tiny gaps between the circle-marked curves and the down-facing-marked curves indicate that the adjacent channel interference insignificantly affect the cell's performance. By contrast, due to the co-channel interference, the cell's tele-traffic load $X$ is reduced by approximately 1.5 $users/cell/MHz$ at $q_{90} = 0.8$ when the number of reuse rings increases from one to five.

Further values of $q_{90}$ recorded for the various reuse structures of the 27-cell network are provided in Fig. 2.27, when the uncoded, the ReS(8,4) coded and the soft-decision RSC(23,33) coded STFSK schemes are considered. Observe from the figure that the soft-decision RSC coded STFSK scheme significantly improved the cell's performance compared to the hard-decision-aided RS coding scheme. Based on the $q_{90}$ curves of Fig. 2.27, it is possible to find the system's ASE, $\eta_{sys}$, by spotting the $X$ value, where we have $q_{90} = 0.8$. Note that the ASE is quantified in terms of $Erlang/cell/MHz$, or as $Erl/cell/MHz$ for short.

Theoretically, the probability of frequency collision, $p_i$, depends on three factors, namely the

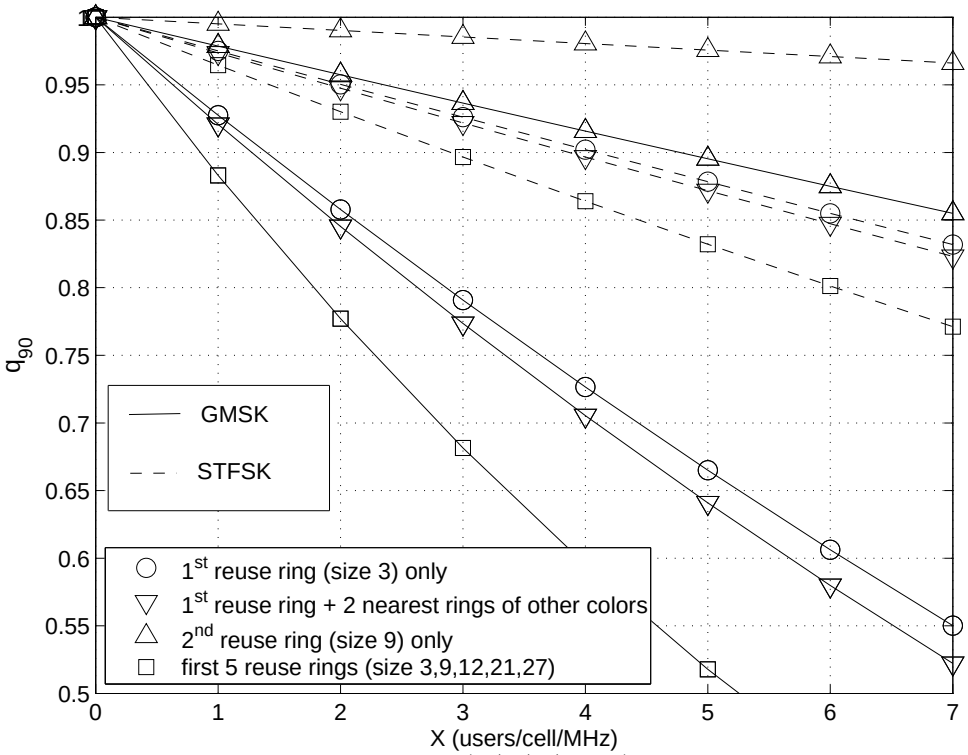


Figure 2.26: $q_{90}$ versus X for GMSK and STFSK(4/1/4/2-4-2) employing RSC channel code for the full-reuse cluster size of 3 and $r_a = 0.5$. The $E_b/N_0$ values $\gamma$ correspoding to the target $BER = 10^{-3}$ were extracted from Fig. 2.25. The associated system parameters are summarized in Table 2.10.

fractional overlap between the sets of frequencies in the reuse and reference cell, the VAR and the mean channel utilization, $U$. Thus, $p_i$ can be expressed as

$$p_i = k_i U r_a. \tag{2.84}$$

Note that $U = 1.0$, when all channels are occupied. Using the condition $U = 1.0$ and Eqs. (2.78-2.79), the maximum ASE may be obtained as

$$\eta_{max} = \frac{n_t}{C_c f_s} \tag{2.85}$$

for the full-reuse structure and as

$$\eta_{max} = \frac{L_c n_t}{3 M_c f_s} \tag{2.86}$$

for fractional reuse structure.

In practice, the achievable spectral efficiency, $\eta_{ach}$, of a system, which may be achieved with the aid of the Erlang B formula [100], depends additionally on the number of channels per cell, $n_{ch}$, and on the tolerable blocking probability, $P_B$. The achievable ASE may be obtained as

$$\eta_{ach} = U_{ach} \times \eta_{max}, \tag{2.87}$$

where $U_{ach}$ may be determined by the Erlang B equation, where we have the following relationship [100]

$$P_B = \frac{\frac{U_{ch}^{n_{ch}}}{n_{ch}!}}{\sum_{i=0}^{n_{ch}} \frac{U_{ch}^{i}}{i!}}. \tag{2.88}$$

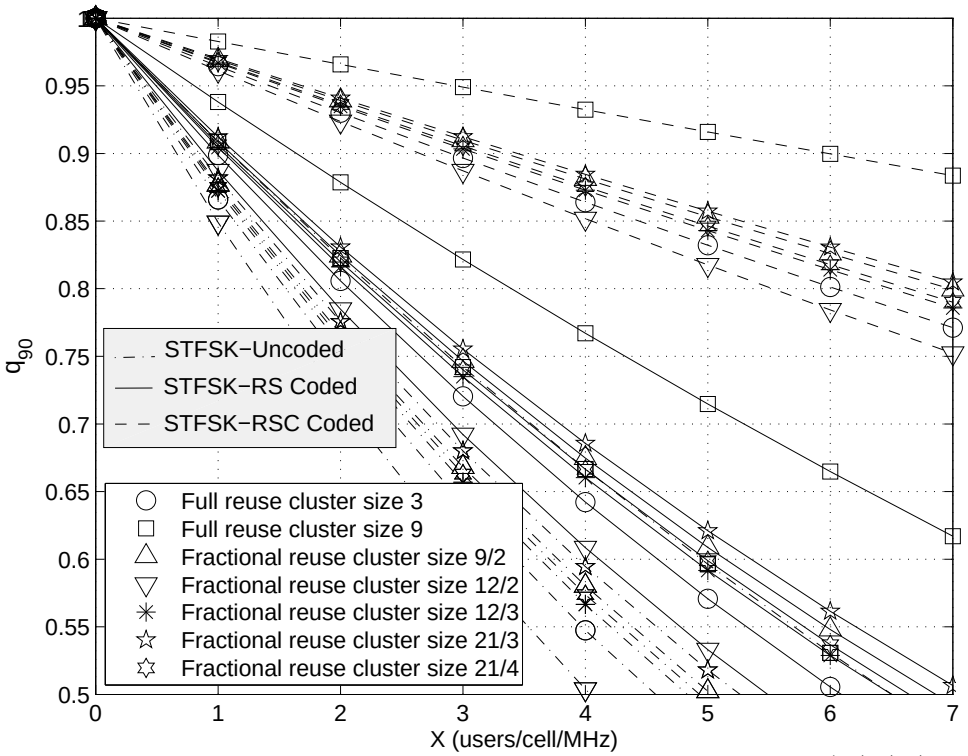


Figure 2.27: $q_{90}$ versus X for Uncoded, ReS coded and RSC coded STFSK(4/1/4/2-4-2) schemes under the assumption of the 27-cell network of Fig. 2.24.The $E_b/N_0$ values $\gamma$ correspoding to the target $BER = 10^{-3}$ were achieved from Fig. 2.25. The associated system parameters are summarized in Table 2.10.

Table 2.12 shows the maximum as well as the achievable spectral efficiency of various reuse structures, where we have $W = 24\ MHz$, $f_s = 1/7\ MHz$ and $P_B = 2\%$.

Consequently, the attainable ASE of a specific system is given by

$$\eta_{att} = min\{\eta_{sys}, \eta_{ach}\}. \tag{2.89}$$

The attainable ASE of various reuse structures is provided in Table 2.13. As seen in the table, the STFSK aided SFHMA system may triple the ASE compared to the one employing classic GMSK, when no channel coding is employed. When the hard-decision ReS(8,4) channel code was employed, the ASE of the STFSK system is still as twice as high as that of GMSK. Furthermore, with the aid of the soft-decision RSC(23,33) the STFSK may approach the maximum achievable ASE for all the reuse structures considered. By contrast, this was only possible for the full-reuse cluster size of 9 and for the fractional-reuse cluster size 21/3 in case of the RSC(23,33) coded GMSK.

*In summary, the attainable ASE can be estimated by the following steps:*

- ***Step 1****: Determine the $E_b/N_0$ threshold, $\gamma$, from Fig. 2.25 which offers the target BER.*
- ***Step 2****: Compute the frequency collision probability, $p_i$, from Eq. (2.81) or Eq. (2.82).*
- ***Step 3****: Calculate $q_{90}$ from Eq. (2.83).*
- ***Step 4****: Determine the system's ASE, $\eta_{sys}$ by looking for the operating point in Fig. 2.26, where we have the target $q_{90}$, i.e $q_{90} = 0.8$ in the graph of $q_{90}$ versus $X$.*

Table 2.12: Maximum values of channel utilization and spectral efficiency ($Erl/cell/MHz$): $P_B = 2\%$

| Cluster size | $\eta_{max}$ $(U = 1)$ | $n_{ch}$ | $U_{ach}$ | $\eta_{ach}$ |
|---|---|---|---|---|
| 3 | 7.00 | 168 | 0.901 | 6.31 |
| 9 | 2.33 | 56 | 0.803 | 1.87 |
| 9/2 | 4.67 | 112 | 0.872 | 4.07 |
| 12/2 | 3.50 | 84 | 0.846 | 2.96 |
| 12/3 | 5.25 | 126 | 0.881 | 4.63 |
| 21/3 | 3.00 | 71 | 0.831 | 2.49 |
| 21/4 | 4.00 | 96 | 0.859 | 3.44 |

- ***Step 5****: Calculate the achievable spectral efficiency, $\eta_{ach}$, from Eq. (2.87).*
- ***Step 6****: Determine the system's attainable ASE, $\eta_{att}$, which is the lower of the pair $\eta_{sys}$ and $\eta_{ach}$.*

*Comparison between the SFHMA and TD/FDMA systems*

Finally, we compare the attainable performance of STFSK aided SFHMA to that of conventional GMSK aided TD/FDMA, to that of the third-generation WCDMA system, as well as to the performance of the fourth-generation LTE system. The system parameters considered are provided in Table 2.14. In order to support a voice channel employing the AMR speech codec [98] operated for example at 12.2 kbps, in the 5 MHz-bandwidth WCDMA system a maximum of 98 users can be supported, when using a spreading factor of 128 [20]. For the same bandwidth of 5 MHz, the LTE system is capable of supporting up to 200 users [24]. Naturally, both the WCDMA and the LTE as well as the STFSK system are capable of supporting a significantly higher data rate than the 12.2 kbps speech rate. However, in this investigation we focussed our attention on the classic voice telephony service. Therefore, the voice data rate of 12.2 kbps is selected for all the systems considered. As a benefit of employing CDMA in WCDMA and OFDM in LTE, both systems are capable of operating at full frequency reuse in all the adjacent cells.

The performance of the three systems recorded at an $E_b/N_0$ of 30 dB is shown in Fig. 2.28 in terms of the BER versus the mean CIR. Based on Fig. 2.28, the threshold BER of $10^{-3}$ is achieved at the mean CIR of $\Lambda_{th}$=12 dB, 6.5 dB and -1.0 dB for GMSK-aided TD/FDMA, for GSMK-assisted SFHMA and TSFSK-aided SFHMA, respectively. These values will be used for determining the minimum reuse cluster size. More particularly, the selected reuse cluster size's $\Lambda_{90}$ must be higher than the threshold mean CIR $\Lambda_{th}$. In other words, the interference power imposed by frequency-reuse cells on the reference cell must be lower than the critical threshold interference level, which may be calculated from the threshold mean CIR $\Lambda_{th}$. For instance, in order to satisfy the condition of $\Lambda_{90} > (\Lambda_{th} = 10.0dB)$, the TD/FDMA's smallest reuse cluster size must be the full-reuse 9-cell cluster, where we have $\Lambda_{90} = 13.0\ dB$ based on Table 2.11. Similarly, observe from this table that the minimum cluster size is 3 for both the GMSK and the STFSK aided SFHMA system.

Table 2.13: Spectral efficiency ($Erl/cell/MHz$) for various reuse structures: $r_a = 0.5$; $P_B = 2\%$; $q_{90} = 0.8$; $n_{call} = 1$

| Cluster size | $\eta_{ach}$ | $\eta_{sys}$ | | $\eta_{att}$ | | $U\%$ | |
|---|---|---|---|---|---|---|---|
| | | Uncoded-GMSK | Uncoded-STFSK | Uncoded-GMSK | Uncoded-STFSK | Uncoded-GMSK | Uncoded-STFSK |
| 3 | 6.31 | 0.44 | 1.55 | **0.44** | **1.55** | 6 | 22 |
| 9 | 1.87 | 0.39 | 2.28 | **0.39** | **1.87** | 17 | 80 |
| 9/2 | 4.07 | 0.43 | 1.70 | **0.43** | **1.70** | 9 | 36 |
| 12/2 | 2.96 | 0.40 | 1.37 | **0.40** | **1.37** | 11 | 39 |
| 12/3 | 4.63 | 0.44 | 1.64 | **0.44** | **1.64** | 8 | 31 |
| 21/3 | 2.49 | 0.41 | 1.77 | **0.41** | **1.77** | 14 | 59 |
| 21/4 | 3.44 | 0.42 | 1.67 | **0.42** | **1.67** | 11 | 42 |
| | | ReS-GMSK | ReS-STFSK | ReS-GMSK | ReS-STFSK | ReS-GMSK | ReS-STFSK |
| 3 | 6.31 | 0.59 | 2.07 | **0.59** | **2.07** | 8 | 30 |
| 9 | 1.87 | 0.58 | 3.40 | **0.58** | **2.33** | 25 | 80 |
| 9/2 | 4.07 | 0.60 | 2.31 | **0.60** | **2.31** | 13 | 49 |
| 12/2 | 2.96 | 0.51 | 1.85 | **0.51** | **1.85** | 15 | 53 |
| 12/3 | 4.63 | 0.60 | 2.20 | **0.60** | **2.20** | 11 | 42 |
| 21/3 | 2.49 | 0.60 | 2.41 | **0.60** | **2.41** | 20 | 80 |
| 21/4 | 3.44 | 0.60 | 2.25 | **0.60** | **2.25** | 15 | 56 |
| | | RSC-GMSK | RSC-STFSK | RSC-GMSK | RSC-STFSK | RSC-GMSK | RSC-STFSK |
| 3 | 6.31 | 1.78 | 6.04 | **1.78** | **6.04** | 25 | 86 |
| 9 | 1.87 | 2.77 | $> 7.0$ | **1.87** | **1.87** | 80 | 80 |
| 9/2 | 4.07 | 1.97 | 6.98 | **1.97** | **4.07** | 42 | 87 |
| 12/2 | 2.96 | 1.59 | 5.53 | **1.59** | **2.96** | 45 | 85 |
| 12/3 | 4.63 | 1.88 | 6.50 | **1.88** | **4.63** | 36 | 88 |
| 21/3 | 2.49 | 2.05 | $> 7.0$ | **2.05** | **2.49** | 68 | 83 |
| 21/4 | 3.44 | 1.92 | 6.64 | **1.92** | **3.44** | 48 | 86 |

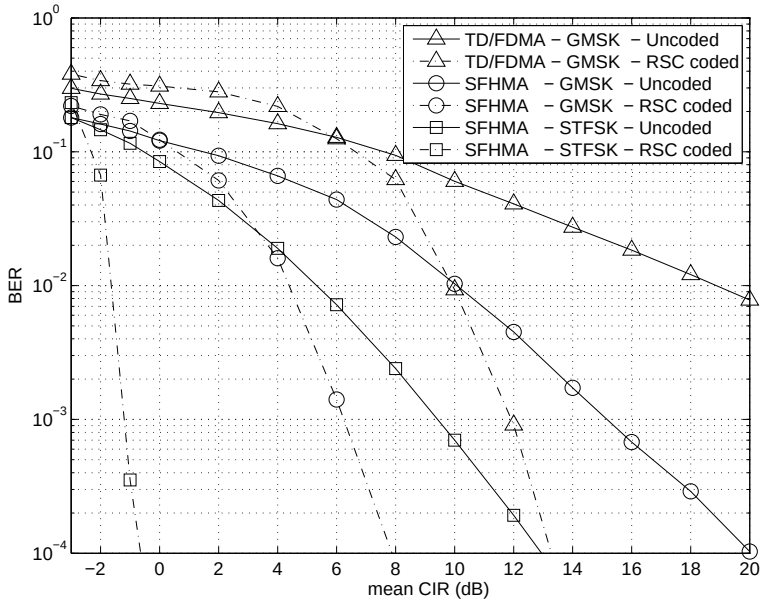


Figure 2.28: BER versus mean CIR for GMSK aided TD/FDMA, GMSK aided SFHMA and STFSK(4/1/4/2-4-2) aided SFHMA systems where RSC channel codes are employed in a Rayleigh fading AWGN channel at $E_b/N_0 = 30\ dB$. All other system parameters are summarized in Table 2.14.

Table 2.14: Spectral efficiency ($Erl/cell/MHz$) for various systems: $E_b/N_0 = 30dB$; $P_B = 2\%$. The $E_b/N_0$ values $\gamma$ correspoding to the target $BER = 10^{-3}$ were achieved from Fig. 2.28.

| System parameters | | TD-FDMA | SFHMA | | WCDMA | LTE |
|---|---|---|---|---|---|---|
| | | GMSK | GMSK | STFSK | | |
| Speech codec | | AMR (12.2kbps) | AMR (12.2kbps) | AMR (12.2kbps) | AMR (12.2kbps) | AMR (12.2kbps) |
| Channel code type | | RSC(23,33) | RSC(23,33) | RSC(23,33) | RSC(23,33) | RSC(23,33) |
| Modulation type | | GMSK | GMSK | STFSK (4142-4-2) | QPSK | QPSK |
| Antenna config. ($n_T/n_R$) | | 1/1 | 1/1 | 4/1 | 1/1 | 4/1 |
| System bandwidth (MHz) | $W$ | 5 | 5 | 5 | 5 | 5 |
| Cluster size | $C$ | 9 | 9 | 3 | 1 | 1 |
| No. of timeslots | $n_t$ | 8 | 3 | 3 | 1 | 1 |
| No. of call per timeslot | $n_{call}$ | 4 | 4 | 4 | 1 | 1 |
| Freq. spacing (MHz) | $f_s$ | 0.200 | 0.143 | 0.143 | 5 | 5 |
| No. of freq./system | $n_{f_s}$ | 25 | 35 | 168 | 1 | 1 |
| Spreading factor | | 1 | 1 | 1 | 128 | 512 |
| No. of channels/cell | $n_{ch}$ | 89 | 47 | 140 | 98 | 200 |
| Traffic/channel ($erl$) | $a_{ch}$ | 0.841 | 0.768 | 0.883 | 0.860 | 0.912 |
| Traffic/cell ($erl$) | $a_{cell}$ | 74.85 | 35.80 | 123.48 | 84.31 | 182.43 |
| Spectral efficiency ($Erl/cell/MHz$) | $\eta_{att}$ | 14.958 | 7.161 | 24.697 | 16.86 | 36.487 |

Applying the 6-step process outlined above, the various systems' ASEs are shown in the last line of Table 2.14. According to the table, the GMSK aided TD/FDMA system does not perform as well as the GMSK aided SFHMA arrangement in terms of the ASE, which is in contrast to the results of Chapter 7 in [11]. The reason for this fact is that when strong channel codes, such as the RSC or turbo codes, are employed, the reference BER value can be reduced, resulting in smaller reuse cluster sizes. The advantage of the small reuse cluster sizes in the SFHMA system becomes less dominant. Moreover, owing to the employment of SFH, the SFHMA system requires a longer time slot for each user. Hence, the GMSK aided SFHMA system performs less efficiently than GMSK aided TD/FDMA. However, the cell's performance may be significantly improved by employing STFSK. Quantitatively, STFSK aided SFHMA attained a spectral efficiency of 24.7 $Erl/cell/MHz$, outperforming the ASE of 15.0 $Erl/cell/MHz$ recorded for the GMSK aided TD/FDMA system. This ASE is also significantly higher than the WCDMA's ASE of 16.9 $Erl/cell/MHz$, which is only slightly better than that of the GMSK aided TD/FDMA system. Finally, the LTE system achieves an ASE of 36.5 $Erl/cell/MHz$, hence exhibiting a substantially better ASE than all the remaining systems considered.

## 2.3 Cooperative MIMOs

As mentioned in Section 2.2, space-time coding or spatial multiplexing schemes require sufficiently high antenna-separation for ensuring independent fading. This fact essentially limits the employment of multiple antennas to the BS. In order to overcome the limitation, the wireless cooperative network philosophy, which is also referred to as the distributed MIMO regime, was proposed, where single-antenna-sided mobiles cooperate to form a virtual MIMO.

The basic idea of cooperative communications can be traced back to the relay channel proposed by Van der Meulen [101] in 1971, which was further characterized by Cover and Gamal in [102]. In [103] Sendonaris *et al.* proposed the conventional relay model for multiple nodes, where the nodes transmit both their own signals as well as relay the others' signals. In [104] the authors developed an energy-efficiency cooperative diversity protocol based on the classic relay channel by exploiting the space-diversity gain of distributed antennas in order to improve the achievable data rate as well as to reduce the sensitivity of the system to channel variations. Hunter and Nosratinia [105] introduced channel coding methods into cooperative communications. At the same time, Dohler *et al.* [106] proposed concept of virtual antenna arrays by emulating the STBC codes for single-antenna-aided cooperating users. A range of other space-time codes and cooperative diversity protocols were proposed by Laneman and Warnell [107] for achieving an improved spectral efficiency. Furthermore, the analysis and comparison of various cooperative strategies were detailed in [108, 109]. More recently, the soft information relaying concept was proposed in [110, 111] for improving the reliability of the relay links. On the other hand, Xiao *et al.* [112] introduced the concept of network coding into cooperative communications, which was further developed in [113] for mitigating the throughput loss, while attaining the full diversity gain. In contrast to physical-layer cooperation, cooperation at the media access control layer was described in [114].

In principle, a typical cooperative network, as shown in Fig. 2.29 contains a Source Station (SS), a single- or multiple Relay Stations (RS) and a Destination Station (DS). In the first cooperative phase, the SS broadcasts its data to both the RSs and the DS. Then, depending on the relaying type

Table 2.15: Major cooperative MIMO techniques (Part 1).

| Year | Author(s) | Contribution |
|---|---|---|
| 1971 | Van der Meulen [101] | Investigated the three-node relay channel incorporating a transmitter, a relay and a receiver employing a time-sharing approach. |
| 1979 | Cover and Gamal [102] | Theoretically characterized the relay channel. |
| 1985 | Willems [115] | Proposed a partially cooperative communications scenario and derived the capacity region of the multiple access channel with partially cooperating. |
| 1998 | Sendonaris *et al.* [103] | Generalized the relay model to multiple nodes, where each node works as the transmitter as well as the relay for others. |
| 2001 | Laneman *et al.* [104] | Developed an energy-efficient cooperative diversity protocol built upon the classical relay channel and exploit space diversity at distributed antennas through coordinated transmission and processing by cooperating radios. |
| 2002 | Hunter and Nosratinia [105] | Proposed a user cooperation scheme employing channel coding for wireless cooperation. |
| | Dohler *et al.* [106] | Introduced the concept of virtual antenna arrays that emulate STBC for single-antenna-aided cooperating users. |
| 2003 | Sendonaris *at al.* [116, 117] | Proposed an user-cooperation methodology based on a DF signalling scheme using CDMA. |
| | Laneman and Warnell [107] | Presented space-time coded cooperative protocols for exploiting spatial diversity in a cooperation scenario. |
| 2004 | Laneman *et al.* [108] | Analysed and compared cooperative protocols, such as the AF, DF, selection relaying and incremental relaying. |
| | Nabar *et al.* [109] | Analysed the spatial diversity performance of various cooperative signalling protocols |
| | Stefanov and Erkip [118] | Analysed the performance of channel codes that are capable of achieving full diversity provided by user cooperation in the presence of inter-user interference. |
| 2005 | Azarian *at al.* [119] | Proposed the diversity-multiplexing trade-off amongst cooperative signalling protocols. |
| | Sneessens and Vandenporpe [110] | Proposed a soft DF signalling strategy. |
| | Hu and Li [120] | Proposed distributed source coding technologies based on Splepian-Wolf cooperation for wireless cooperative communications. |
| 2006 | Hunter *et al.* [121, 122] | Derived BER and FER bounds and the outage probability of coded cooperation. |
| | Hu and Li [123] | Presented Wyner-Ziv cooperation as a generalization of the Splepian-Wolf cooperation for a compress-and-forward strategy. |

Table 2.16: Major cooperative MIMO techniques (Part 2).

| Year | Author(s) | Contribution |
|---|---|---|
| 2007 | Bui and Yuan [111] | Proposed the soft information relaying where the relay's LLR values are quantified, encoded and superimposedly modulated before being forwarded to the destination. |
| | Khormuji and Larssin [124] | Improved the performance of the DF relaying by rearranging the constellation in the source and the relay. |
| | Bao and Li [125] | Presented the decode-amplify-forward, taking the benefits of both the AF and the DF relaying. |
| | Xiao *et al.* [112] | Proposed the concept of network coding in cooperative communications. |
| | Fan *et al.* [126] | Introduced successive relaying using repetition coding for reducing multiplexing loss. |
| 2008 | Yue *et al.* [127] | Compared the multiplexed coding and the superposition coding in the coded cooperation. |
| | Wang and Giannakis [113] | Presented the complex filed network coding that can mitigate the throughput loss in the conventional signalling schemes while retaining the full diversity gain. |
| 2009 | Shan *et al.* [114] | Investigated distributed cooperative medium access control protocol design for multihop wireless networks. |

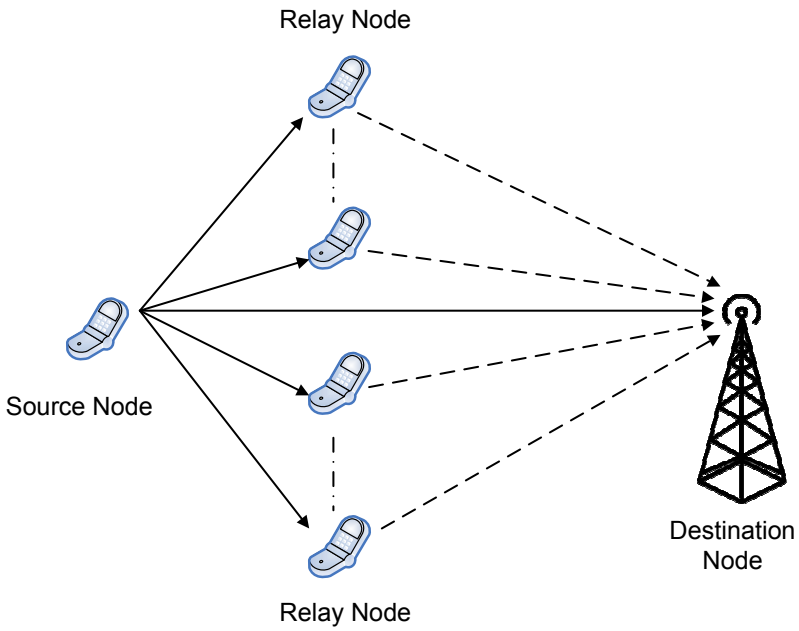


Figure 2.29: Relaying schematic

employed, the appropriate signal processing will be carried out at the RS and then the signal will be forwarded to the DS in the second cooperative phase. Finally, the multiple versions of signal received at the DS, which are spatially diverse, are combined and recovered. Owing to the assistance of relays, typically a better link quality is expected than in a direct single-link based communication system. Additionally, the RS may reduce the signal energy loss imposed by shadow-fading. Therefore, relay-aided systems are capable of increasing the attainable data rate, especially in the cell-edge region, where the MSs typically suffer both from low-power reception and from severe inter-cell interference.

### 2.3.1 Path-loss Related Power Gain

In a non-dispersive, single-user wireless channel, where both the multipath effects and multi-user interference are absent, there are four basic factors affecting the signal propagation, including the path-loss, shadowing and fast fading, as well as the AWGN. Since typically there is a significant distance among the source, the RS and the DS, their fading process and AWGN become independent, and so is their path-loss. The path-loss of the free-space propagation model is expressed in dB as [11]

$$L_{pl} = -10log_{10}\left(\frac{P_r}{P_t}\right) = -10log_{10}\left[G_T G_R \left(\frac{c}{4\pi df}\right)^2\right], \tag{2.90}$$

where $P_r$ and $P_t$ are the transmit and receive power, $G_T$ and $G_R$ are the transmit and receive antenna gains, $c$ is the speed of light, $f$ is the carrier frequency and $d$ is the distance from the transmitter to the receiver.

However, Eq. (2.90) only describes the unobstructed LOS path, while in reality the received signal is usually constituted by the sum of many reflected multipath components, possibly including the LOS component. Thus, the ground reflection model is often used in practice [11]

$$L_{pl} = -10log_{10}\left(\frac{P_r}{P_t}\right) = -10log_{10}\left[G_T G_R \left(\frac{h_{Tx}h_{Rx}}{d^2}\right)^2\right], \tag{2.91}$$

where $h_{Tx}$ and $h_{Rx}$ are the transmit and receive antenna height.

Clearly, the received power is proportional to $d^2$ and $d^4$ in the free-space and in the ground reflection propagation models of Eqs. (2.90) and (2.91), respectively. More accurate and practical path-loss models are based on Hata's models [11]. Briefly, the path-loss based on the geometrical distance may also be modelled by [128]:

$$L_{ab} = \frac{K}{d_{ab}^{\alpha}}, \tag{2.92}$$

where $K$ is a constant depending on the environment, $d_{ab}$ is the geometrical distance from node $a$ to node $b$ and $\alpha$ is the path-loss exponent. Again, we have $\alpha = 2$ for the free-space model of Eq. (2.90), while $\alpha = 4$ for the ground reflection model of Eq. (2.91). The relationship between the energy received at the RS, $E_{sr}$, and at the DS, $E_{sd}$, during the first time slot may be expressed as

$$E_{sr} = \frac{L_{sr}}{L_{sd}} E_{sd} = G_{sr} E_{sd}, \tag{2.93}$$

where $G_{sr}$ may be referred to as the path-loss-related power gain for the Source-to-Relay (SR) link. When taking into account Eq. (2.92), $G_{sr}$ is equal to

$$G_{sr} = \left(\frac{d_{sd}}{d_{sr}}\right)^2. \tag{2.94}$$

Similarly, the path-loss-related power gain for the Relay-to-Destination (RD) link is expressed as

$$G_{sr} = \left(\frac{d_{sd}}{d_{rd}}\right)^2. \tag{2.95}$$

### 2.3.2 Cooperation Types

In this section, we only consider a conventional single-relay-aided cooperative scenario, where two orthogonal phases are employed in order to avoid interference. These phases may be created by either in TDMA or FDMA.

- In phase 1, the SS broadcasts information to both the RS and the DS.
- In phase 2, the RS can assist the SS by forwarding or retransmitting the information to the DS.

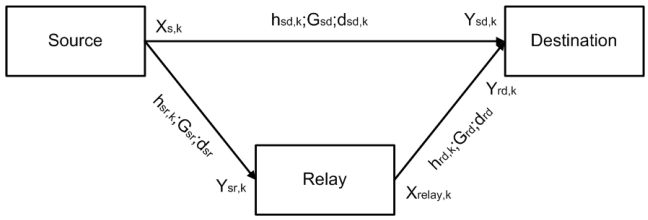


Figure 2.30: Conventional single-relay-aided network.

Fig. 2.30 depicts a general relay channel, where the source transmits at a power of $P_S$ and the relay transmits at a power of $P_R$. During the first phase, the source broadcasts its signal, $x$, to both the destination and to the relay. Hence, the signals $y_{SD}$ and $y_{SR}$ received at the destination and the relay, respectively, may be written as

$$y_{SR} = \sqrt{P_S} G_{SR} h_{SR} x + n_{SR}, \tag{2.96}$$

$$y_{SD} = \sqrt{P_S} G_{SD} h_{SD} x + n_{SD}, \tag{2.97}$$

where $G_{SD}$ and $G_{SR}$ are the path-loss-related-power gains detailed in Section 2.3.1, while $h_{SR}$ and $h_{SD}$ represent the coefficients of the SR and SD links' fading processes associated with a variance of $\sigma_f^2$, while $n_{SD}$ as well as $n_{SR}$ represent the AWGN noise associated with a zero mean and a variance of $\sigma_n^2$.

In phase 2, the relay forwards a processed version of the source's signal to the destination, which may be modelled as

$$y_{RD} = \sqrt{P_R} G_{RD} h_{RD} \Phi(y_{SD}) + n_{RD}, \tag{2.98}$$

where the function $\Phi(\cdot)$ defines the operation carried out at the relay. Again, $h_{RD}$ represents the coefficients of the RD link's fading process having a variance of $\sigma_f^2$, while $n_{RD}$ represents the AWGN noise having a zero mean and a variance of $\sigma_n^2$.

#### 2.3.2.1 Amplify-and-Forward

In AF relaying, the RS amplifies the signal received from the SS and forwards it to the DS, while aiming for eliminating the effects of the channel fades between the SS and the RS. This can be achieved

by simply scaling the received signal by a factor that is inversely proportional to the received power. When the channel coefficients are available at the RS, the associated $|h_{SD}|$-dependent gain may be expressed as [109]

$$\beta = \frac{1}{\sqrt{P_S G_{SR}|h_{SD}|^2 + \sigma_n^2}}. \tag{2.99}$$

By contrast, when only the variance of the fading process is known at the RS, the $|h_{SD}|$-independent gain may be expressed as [108]

$$\beta = \frac{1}{\sqrt{P_S G_{SR}\sigma_f^2 + \sigma_n^2}}. \tag{2.100}$$

Subsequently, the signal received at the DS during the second phase is given by

$$\begin{aligned} y_{RD} &= \beta\sqrt{P_R}G_{RD}h_{RD}y_{SR} + n_{RD} \\ &= \beta\sqrt{P_R}G_{RD}h_{RD}(\sqrt{P_S}G_{SR}h_{SR}x + n_{SR}) + n_{RD} \\ &= \beta\sqrt{P_R}G_{RD}h_{RD}\sqrt{P_S}G_{SR}h_{SR}x + n'_{RD}, \end{aligned} \tag{2.101}$$

where we have

$$n'_{RD} = \beta\sqrt{P_R}G_{RD}h_{RD}n_{SR} + n_{RD}. \tag{2.102}$$

If the noise terms $n_{SD}$ and $n_{RD}$ are independent, then the equivalent noise $n_{RD}$ is a zero-mean, complex-valued Gaussian random variable having a variance of

$$\sigma_n^{2\prime} = (\beta^2 P_R G_{RD}|h_{RD}|^2 + 1)\sigma_n^2 = \left(\frac{P_R G_{RD}|h_{RD}|^2}{P_S G_{SR}|h_{SR}|^2 + \sigma_n^2} + 1\right)\sigma_n^2. \tag{2.103}$$

As seen in Eq. (2.103), the unwanted noise is also amplified at the relay, imposing a degraded performance at the destination, when compared to the corresponding co-located MIMO. According to [23, 129], the relay should be close to the source in order to reduce the effects of noise amplification.

The destination receives two versions of the transmitted signal $x$ through the SD and RD links. As discussed in Section 2.2.1.1, various diversity combining techniques may be employed at the destination. If the channel knowledge is available at the destination, the optimal MRC technique may be employed for maximizing the overall signal-to-noise ratio. By contrast, the SC or EGC combining should be considered, when no channel information is available.

Given the knowledge of the channel coefficients $h_{SD}$ and $h_{RD}$, the output of the MRC detector at the destination may be expressed as

$$y = w_1 y_{SD} + w_2 y_{RD}, \tag{2.104}$$

where $w_1$ and $w_2$ represent the weighting factor of the MRC. As optimized in [130], the weighting factors $w_1$ and $w_2$ are given by

$$w_1 = \frac{\sqrt{P_S}h_{SD}^*}{\sigma_n^2} \qquad w_2 = \frac{\beta P_R P_S h_{SR}^* h_{RD}^*}{(\beta^2 P_R G_{RD}|h_{RD}|^2 + 1)\sigma_n^2}. \tag{2.105}$$

Therefore, the instantaneous SNR of the MRC's output is expressed as

$$\gamma = \gamma_1 + \gamma_2, \tag{2.106}$$

where we have

$$\gamma_1 = \frac{|w_1 P_S G_{SD} h_{SD}|^2}{|w_1|^2 \sigma_n^2} = \frac{P_S G_{SD} |h_{SD}|^2}{\sigma_n^2} \tag{2.107}$$

$$\gamma_2 = \frac{|w_2 \beta \sqrt{P_S} \sqrt{P_R} h_{SR} h_{RD}|^2}{|w_2|^2 \sigma_n^{2\prime}} = \frac{1}{\sigma_n^2} \frac{P_S P_R G_{SD} G_{RD} |h_{SR}|^2 |h_{RD}|^2}{P_S G_{SD} |h_{SR}|^2 + P_R G_{RD} |h_{RD}|^2 + \sigma_n^2}. \tag{2.108}$$

#### 2.3.2.2 Decode-and-Forward

In contrast to simply amplifying and forwarding data to the destination as in AF relaying, in DF relaying the relay fully decodes the received signal, before re-encoding and forwarding it to the destination. Assuming that $\hat{x}$ is the decoded signal at the relay, the signal received at the destination via the RD link may be expressed as

$$y_{RD} = \sqrt{P_R} G_{RD} h_{RD} \hat{x} + n_{RD}. \tag{2.109}$$

Consequently, given the knowledge of the channel coefficients $h_{SD}$ and $h_{RD}$, the output of the MRC detector at the destination may be expressed as

$$y = w_1 y_{SD} + w_2 y_{RD}, \tag{2.110}$$

where we have

$$w_1 = \frac{\sqrt{P_S} h_{SD}^*}{\sigma_n^2} \qquad w_2 = \frac{\sqrt{P_R} h_{RD}^*}{\sigma_n^2}. \tag{2.111}$$

The the instantaneous SNR at the MRC output is obtained as

$$\gamma = \gamma_1 + \gamma_2, \tag{2.112}$$

where we have

$$\gamma_1 = \frac{|w_1 P_S G_{SD} h_{SD}|^2}{|w_1|^2 \sigma_n^2} = \frac{P_S G_{SD} |h_{SD}|^2}{\sigma_n^2} \tag{2.113}$$

$$\gamma_2 = \frac{|w_2 P_R G_{RD} h_{RD}|^2}{|w_2|^2 \sigma_n^2} = \frac{P_R G_{RD} |h_{RD}|^2}{\sigma_n^2}. \tag{2.114}$$

As seen in Eq. (2.114), DF relaying has an advantage over AF relaying, since it is capable of reducing the effects of noise at the relay. However, if the relay incorrectly decodes and forwards the signal to the destination, then it imposes error propagation that may degrade the performance of the system. In this case, the DF scheme achieves a spatial diversity order of one, since the performance of the system is limited by the worst link in the set of the SR and SD links.

#### 2.3.2.3 Compress-and-Forward

In contrast to AF and DF relaying, in compress-and-forward relaying the relay transmits a quantized and compressed version of the received signal. Therefore, the DS will combine the message received from the SS and its quantized as well as compressed version received from the RS. The quantization and compression process invoked at the relay node is reminiscent of the process of source encoding.

At the DS, an estimate of the quantized and compressed message is obtained by decoding the received sequence of symbols. This decoding operation simply involves the mapping of the received symbols into a set of values that estimate the transmitted signal. This mapping process typically imposes distortion on the original transmitted signal that may be considered as a form of noise.

The nature of wireless networks is predetermined by the mobility of communicating nodes. In other words, the distances among the source, relay and destination nodes are time-variant. Therefore, an adaptive relaying scheme should be employed, instead of a fixed strategy at each relay. Such an adaptive scheme was proposed in [125, 131], while the condition of switching between the AF and DF was further investigated in [23, 129].

### 2.3.3 Relaying Protocols

#### 2.3.3.1 Traditional Relaying

As illustrated in Fig. 2.31, traditional relaying schemes require four communication phases: two for the UL and two for the DL. In the UL, the signal transmitted from the MS is broadcast to both the RS and the BS and then it is forwarded from the RS to the BS. The process is similar in the DL, but in the reverse-direction. The relaying protocol may be applied to all the above-mentioned relaying types.

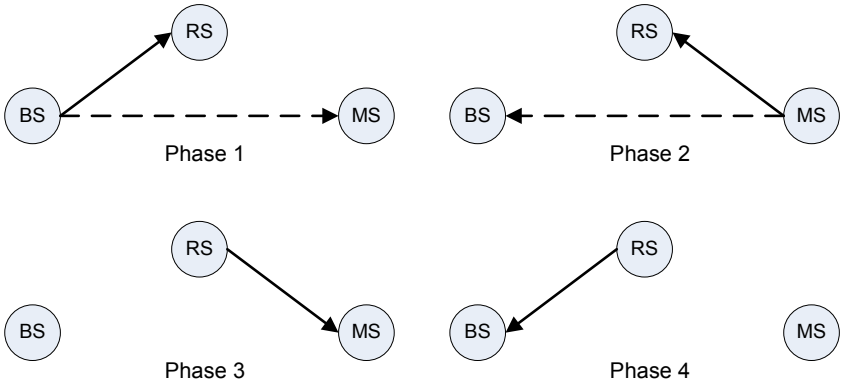


Figure 2.31: Traditional four-phase relaying

The four-phase relaying protocol provides a high diversity gain as well as an improved link quality at the cost of halving the effective throughput. However, the employment of relays is capable of offering an improved link quality owing to the presence of LOS paths. Consequently, an improved bandwidth efficiency may be achievable by exploiting higher-order, higher-throughput modulation and high-rate FEC codes.

#### 2.3.3.2 Successive Relaying

In order to reduce the number of slots required, the successive relaying technique [126, 132] was proposed, which relies on at least two relay stations. The DL communications of a two-relay aided network is illustrated in Fig. 2.32. According to the figure, in the first phase the BS broadcasts

message $m_1$ and $RS_1$ listens. In the second phase, $RS_1$ processes $m_1$ and then forwards it to the MS. Meanwhile, the BS broadcasts the next message $m_2$ while $RS_2$ listens. In the third phase, the BS broadcasts message $m_3$ and the $RS_1$ listens again, while $RS_2$ relays message $m_2$ to the MS. The process continues in a manner that the two relays alternatively listen and transmit.

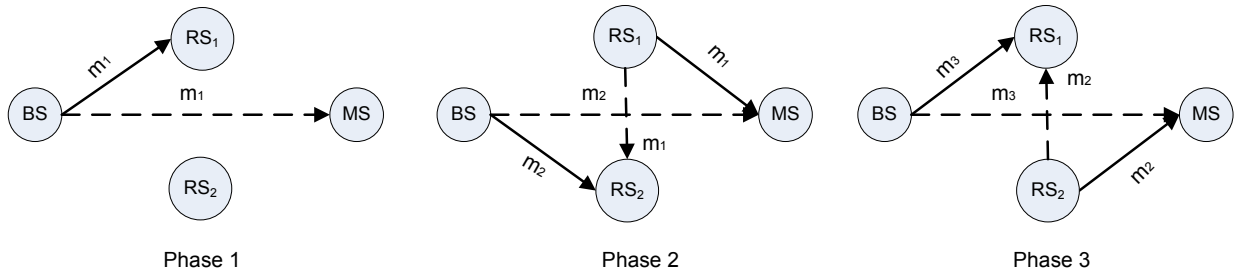


Figure 2.32: Three-phase successive relaying, which requires at least an extra relay compared to the traditional four-phases relaying of Fig. 2.31.

It may be readily realized that to transmit $N$ messages, $(N+1)$ slots are required. Therefore, the successive relaying philosophy may significantly reduce the throughput loss compared to the traditional four-phase relaying protocol, while the diversity order of two is still retained in case of two relays aided. Moreover, a specific drawback of this protocol is the presence of interference among messages. For instance, message $m_2$ is broadcast by the BS the same time as message $m_1$, which is relayed from $RS_1$. Consequently, the two messages interfere with each other, resulting in a degraded overall performance at the MS. Moreover, the extra relay required increases the overall infrastructure cost.

#### 2.3.3.3 Network Coding Aided Three-Phase Relaying

In order to avoid the requirement of an extra relay as in the successive relaying protocol, the Network Coding (NC) aided relaying protocol was designed in [133, 134]. As shown in Fig. 2.33, this protocol requires three communication slots. In the first two time slots, the MS and BS transmits the codeword $c_1$ and $c_2$ to the RS, respectively. The two corresponding signals $y_1$ and $y_2$ received at the RS are decoded and then combined into a single stream. More particularly, the bit-wise exclusive OR (XOR) operation of the two decoded codewords is executed at the RS to obtain the composite codeword $c_3 = c_1 \oplus c_2$. Thereafter, the codeword $c_3$ is sent to both the MS and the BS. Note that either zero padding or repetition coding has to be employed, when the lengths of $c_1$ and $c_2$ are different.

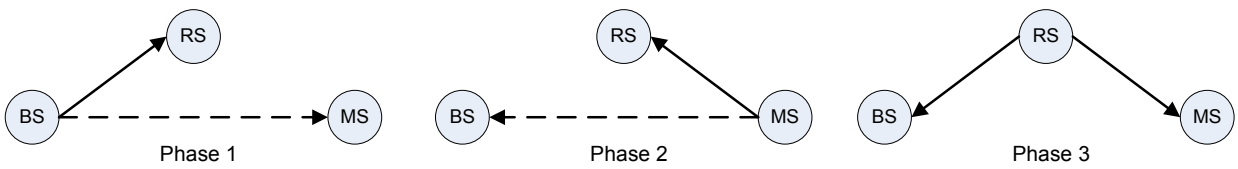


Figure 2.33: Network coded three-phase relaying, which avoids the requirement of an extra relay, as in the three-phase successive relaying of Fig. 2.32.

At the destinations, the signal received is the combination of the UL and DL packets. To recover

the desired packet, the a-priori knowledge of the transmit packet in the previous slot is employed at each destination node. For instance, the BS first computes the LLRs of the network-coded bits. To extract the soft information related to the UL packet, the sign of the network-coded bit LLR is flipped, when the corresponding DL bit was a logical 1 based on the XOR function, otherwise its magnitude is maintained. In order to achieve a diversity gain, the signal received during the third slot is often combined with the signal directly received from the source in the previous slots.

Due to requiring three time slots, the protocol obviously reduces the effective throughput by a third compared to the traditional direct communications. Similar to the four-phase relaying protocol, the high-order modulation and high-rate coding should be employed to improve the achievable throughput.

#### 2.3.3.4 Two-Phase Relaying

To further reduce the number of communication time slots required, the two-phase relaying protocols, which invoke the AF relaying, Denoise-and-Forward (DNF) [132, 135] or DF relaying, were proposed.

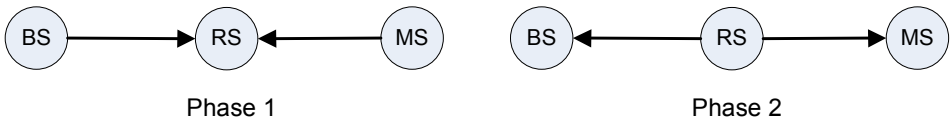


Figure 2.34: Network coded two-phase relaying, which eliminates one of the transmission phases compared to the network coded three-phase relaying regime of Fig. 2.33, albeit this is achieved at the cost of degrading the signal quality.

**Two-phase AF relaying**

In first phase, the MS and the BS simultaneously transmit their signal to the RS. At the relay, the superposition of the two signals is amplified and adjusted to conform with a power constraint before being forwarded to both the MS and the BS. Since the MS and the BS have their own knowledge about the previous transmitted signal, they can subtract the so-called back-propagation self-interference prior to decoding, provided that the Channel Impulse Response (CIR) of all links is available at the MS's and BS's receivers. In order to relay the composite signal, the RS has to increase the transmit power. Furthermore, the noise and interference amplification is unavoidable in this relaying protocol. Therefore, the overall BER performance of this protocol becomes significantly degraded compared to those of the above-mentioned protocols , which is the price paid for the reduction in the number of time slots employed.

**NC aided two-phase relaying**

Similar to the two-phase AF relaying, in the DNF relaying the BS and the MS simultaneously transmit their signal to the RS during the first phase of cooperating. Instead of amplifying the superposition based signal, the RS detects the modulated symbols received and generates a combined signal by employing the XOR-ed operation of the UL and the DL packet, which is the same as the corresponding operation of the NC aided three-phase relaying. This process of detecting the symbols is known as the denoising operation and hence the resultant relaying protocol is referred to as NC aided DNF relaying. As a benefit of the denoising process, the relaying protocol typically offers a

better BER performance than simple two-phase AF relaying.

In contrast to the NC aided two-phase DNF relaying, the NC aided two-phase DF relaying exploits the FEC code to further reduce the potential error propagation. More particularly, the signals are decoded and error correction is used after demodulation. Thereafter, they are combined, modulated and forwarded to both the MS and BS. Despite employing FEC decoding, the two-phase DF relaying protocol remains inferior to the three-phase DF relaying regime.

A summary of the relaying protocol is shown in Table 2.17.

Table 2.17: Comparison of relaying protocols

| **Relaying protocol** | **One-way relaying** | | | | **Two-way relaying** | | |
|---|---|---|---|---|---|---|---|
| | **4-AF** | **4-DF** | **Successive** | **3-DF** | **2-AF** | **2-DNF** | **2-DF** |
| Spectrum efficiency | Low | Low | High | Medium | High | High | High |
| Effective SINR | Low | High | Medium | High | Very low | Medium | High |
| System constraint | Low | Low | High | Medium | Low | Medium | Very high |
| Number of relays | 1 | 1 | 2 | 1 | 1 | 1 | 1 |
| Complexity | Low | High | High | High | Low | Medium | High |

## 2.3.4 Performance of Wireless Cooperative Networks

### 2.3.4.1 Uncoded Systems

First we study the performance of uncoded wireless cooperative networks. The performance of systems employing PSK/QAM schemes assisted by a single relay station, where the system parameters are summarized in Table 2.18, is shown in Fig. 2.35. Both the AF and DF relaying protocols are considered. According to the figure, all of the relaying schemes outperform the conventional direct communication scenario, since a diversity order of two was achieved by these relaying systems. As seen in the figure, the DF protocol is superior to the AF protocol in the high-$E_b/N_0$ region.

Furthermore, we vary the relay's position in order to observe its impact on the achievable system performance. Fig. 2.36 shows the performance of the system at $E_b/N_0 = 15\ dB$, when the ratio between the source-to-relay distance and the source-to-destination distance varies from 0.1 to 0.9. The results indicate that the relay using the DF protocol should be close to the source while it should

Table 2.18: Parameters of the uncoded PSK/QAM aided cooperative communications.

| **Parameters** | **Value** |
|---|---|
| Modulation type | {2,4,8,16}-PSK/{4,16,64}-QAM |
| Relay type | fixed AF/DF |
| N$^o$ of relays | L=1 |
| Normalized $d_{SR_l}/d_{R_lD}$ | 0.5/0.5 |
| Source's transmit power | $E_S = \frac{E_b}{G_{rd}+1}$ |
| Relays' transmit power | $E_{R_l} = \frac{G_{rd}E_b}{G_{rd}+1}$ |
| Channel model | frequency-flat Rayleigh fading |

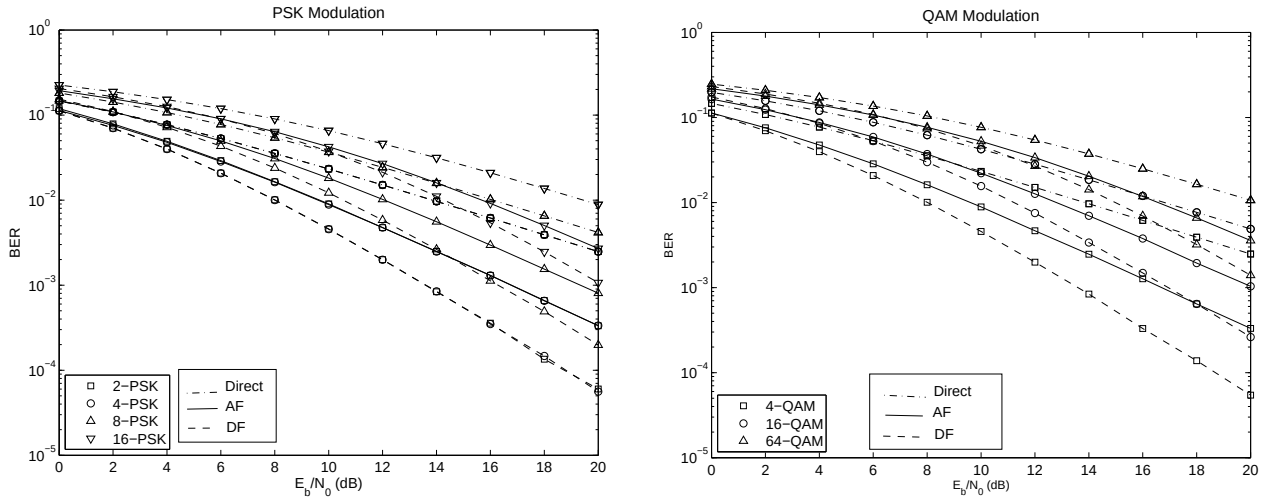


(a) PSK Modulation (b) QAM Modulation

Figure 2.35: Performance of cooperative communication using PSK/QAM modulation transmitted over frequency-flat Rayleigh fading channels, where the relays are at the half-way position. The other system parameters are summarized in Table 2.18. The effects of relay position and source-relay power allocation are shown in Figs. 2.36 and 2.37, respectively.

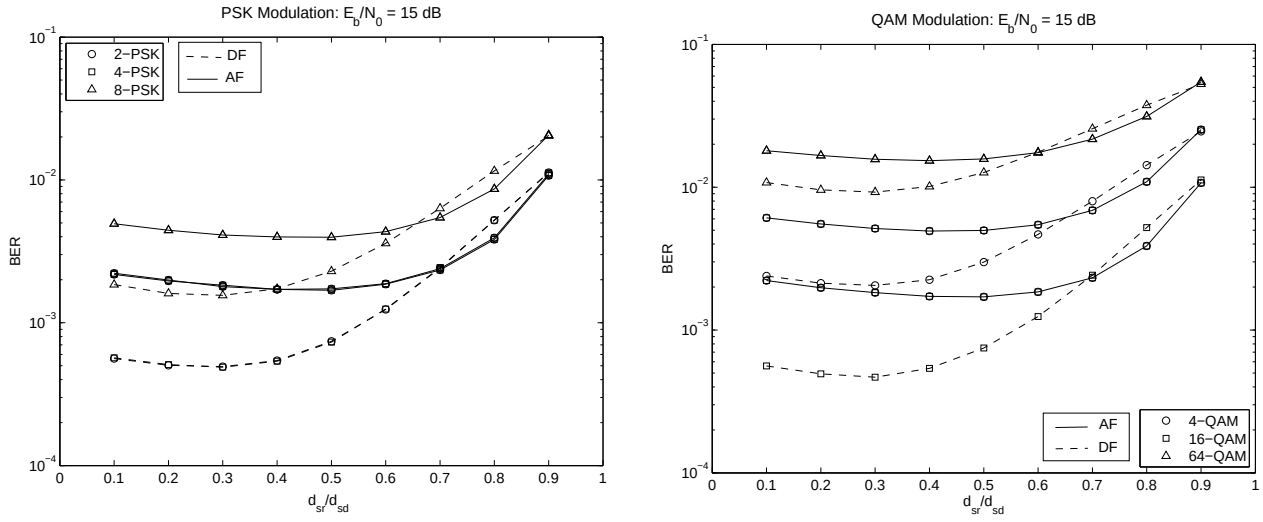


(a) PSK Modulation (b) QAM Modulation

Figure 2.36: Performance of cooperative communication using PSK/QAM modulation transmitted over frequency-flat Rayleigh fading channels, when the relays are at different positions. The other system parameters are summarized in Table 2.18. The attainable BER performance is shown in Fig. 2.35, while the effects of source-relay power allocation are shown in Fig. 2.37.

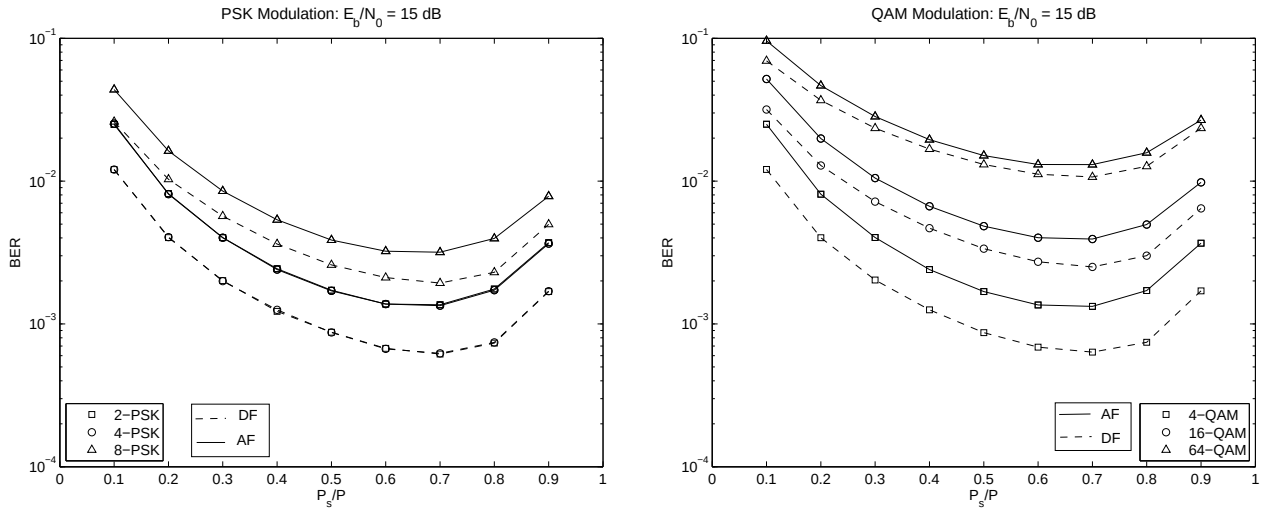


(a) PSK Modulation

(b) QAM Modulation

Figure 2.37: Performance of cooperative communication using PSK/QAM modulation transmitted over frequency-flat Rayleigh fading channels, when different power allocations are employed. The other system parameters are summarized in Table 2.18. The attainable BER performance is shown in Fig. 2.35, while the effects of relay position are shown in Fig. 2.36.

be close to the destination in case of AF relaying. In DF relaying the relay may reduce the number of decoded errors, which are forwarded to the destination, when the relay is close to the source. Hence, the overall BER at the destination is also expected to be reduced. By contrast, in the AF protocol a relay roaming close to the destination may reduce the noise amplification effects and hence the overall BER at the destination may be reduced.

Let us now consider the achievable system's performance when the ratio between the source's transmit power and the system's total transmit power is varied from 0.1 to 0.9. According to Fig. 2.37, most of the transmit power should be allocated to the source in both the AF and DF relaying protocols. The reason for this phenomenon is that using a high transmit power at the source has the potential of reducing the number of decoded errors at the relay in case of DF relaying, while it mitigate the noise amplification at the relay in case of AF relaying.

Below, we will characterises the effect of the number of relays on the overall performance. In this scenario, orthogonal subchannels are created with the aided of TDMA at the cost of a reduced spectral efficiency. The performance of QPSK modulation employing various number of relays is shown in Fig. 2.38. According to the figure, the performance of the system improves upon increasing the number of relays. However, when the total transmit power is kept constant, the incremental improvement is gradually reduce upon increasing the number of relays. The fact is that upon increasing the number of relays, the source's transmit power will be reduced for the sake of keeping the total power the same. Hence, the relays may forward more decoding errors to or amplifying their noise more dramatically.

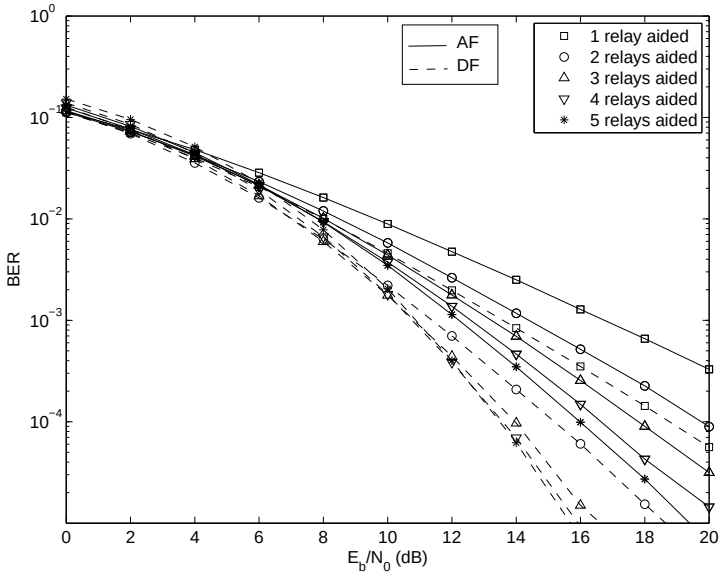


Figure 2.38: Performance of cooperative communication using PSK modulation transmitted over frequency-flat Rayleigh fading channels, when different numbers of relays aided are employed. The other system parameters are summarized in Table 2.18. The effects of relay position and source-relay power allocation are shown in Figs. 2.36(a) and 2.37(a), respectively.

#### 2.3.4.2 Distributed Space-Time Coded Systems

In order to mitigate the interference amongst the signals received at the destination upon increasing the number of relay nodes, the multiple-relay-assisted schemes require orthogonal subchannels for the relay node transmissions. The required orthogonality may be created in the TD, FD or SD with the aid of TDMA, FDMA, CDMA, SDMA, and so on. However regardless of the implementation, this results in a reduction of the system's spectral efficiency. A popular solution is constituted by the so-called distributed space-time coding (DSTC) philosophy [107, 136], where the relays are permitted to simultaneously transmit over the same channel by emulating a classic space-time code. This distributed configuration is capable of retaining the DSTC system's diversity order as well as throughput [107,136].

Fig. 2.39 shows the attainable performance of DF relaying using the orthogonal DSTC of [137,138] and the diagonal DSTC of [139]. Furthermore, the AF relaying aided regime using an orthogonal DSTC, a diagonal DSTC, and distributed linear dispersion coding [136] are also characterized in Fig. 2.39. Again, the DF relaying protocols offer a better BER performance than their AF-aided counterparts, especially in the high $E_b/N_0$ region. Also as seen in the figure, the distributed linear dispersion code perform worst among the DSTC schemes considered, which is a price paid for its flexible system design.

## 2.4 Chapter Summary

In this chapter, several MIMO arrangements designed for wireless communications were considered. We briefly described the well-known transmit and receive diversity techniques. In the context of receive diversity, the MRC, the EGC, the SC and the switched combining were reviewed. By contrast, in

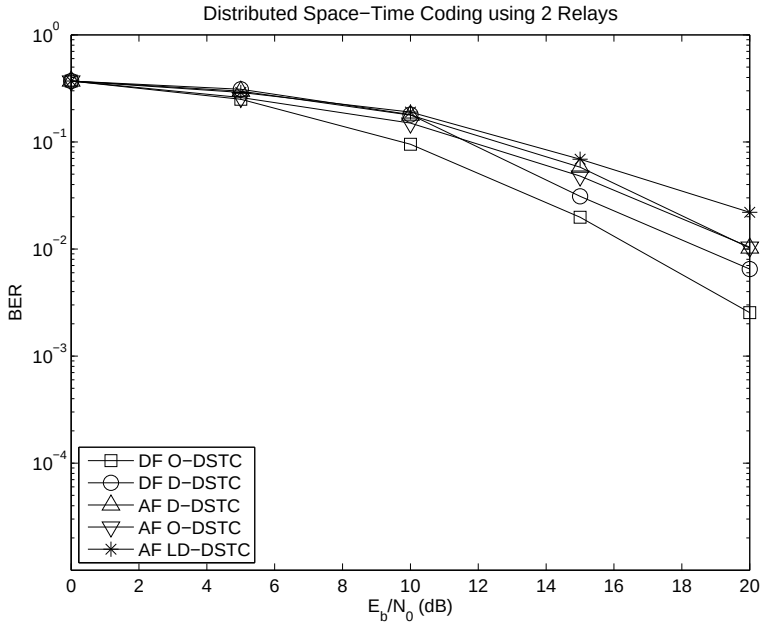


Figure 2.39: Performance of DSTC aided cooperative communication using two relays at the half-way position and communicating over frequency-flat Rayleigh fading channels. The other system parameters are summarized in Table 2.18. The corresponding performances of the uncoded cooperative communication schemes are shown in Figs. 2.35-2.38.

the scenario of transmit diversity schemes, such as STBC and STTC arrangements were summarised. Furthermore, the spatial multiplexing schemes, such as the BLAST family, attains a multiplexing gain. Amalgamating the two transmit MIMO families led to the design of the LDC.

Following the review of the well-known MIMO techniques, we proposed a novel concept, known as STFSK modulation, where a beneficial diversity gain may be gleaned from three different domains, namely the space-, time- and frequency-domain. The STFSK concept offers the following advantages:

- Similar to the STSK [53], the STFSK is capable of achieving both the transmit as well as the receive diversity.
- The single-antenna based detection is possible due to no inter-channel interference.
- Owing to spreading signal on the frequency domain, the STFSK may reduce the negative effect of dispersive channels, which consist of ISI.
- Like the SM/SSK schemes, the STFSK is capable of supporting asynchronous MIMO transmissions.
- Moreover, the STFSK may be configured to support an arbitrary number of transmit and receive antennas without losing substantial information.

Based on the investigations of Section 2.2.4, the following issues should be considered when designing a STFSK system:

- Setting the number of frequencies to two or four constitutes a reasonable choice, which is capable

of mitigating the effects of frequency-selective fading without unduly compromising the spectral efficiency.

- The number of transmit antennas, $n_T$, should be less than or equal to the number of timeslots used since no further capacity gain may be achieved for $n_T > T$.

For a hard-decision based detector, there are additional issued to be considered

- The complexity of the detector is reduced, when the number of frequencies, $K$, increases.
- For a given number of $K$ and a given value of the product $QL$, any possible combination of $Q$ and $L$ results in the same decoding complexity.
- The complexity of a STFSK scheme increases upon increasing the normalized throughput.

For soft-decision based detectors, three further remarks should be considered.

- The complexity of a soft-decision STFSK detector depends only on the product of $Q \times L \times K$, rather than on each component $Q$, $L$ and $K$.
- Increasing the number of frequencies, $K$, may increase the extrinsic information at the cost of extending the bandwidth occupied.
- Increasing the number of dispersion matrices, $Q$, reduces the amount of extrinsic information, when the same number of frequencies, namely $K$, is employed .

The system's performance recorded in Figs. 2.17-2.19 of Section 2.2.4.9 in a single-user interference limited environment showed that STFSK may offer a better performance than the STSK and SFSK schemes, regardless, whether the channel is frequency-selective or frequency-flat. More particularly, observe in Fig 2.18 that for transmission over the 6-tap COST207 channel model, STFSK achieves gains of 5 dB and 6 dB over STSK and SFSK, respectively, as shown in Fig. 2.18 at the BER of $10^{-4}$. Additionally, STSK suffered from the ISI imposed by the frequency-selective fading channel, requiring a 2 dB power boost when changing the channel model from uncorrelated flat-fading to the 6-tap COST207 rural area model. We also concluded that STSK and SFSK constitute special cases of STFSK. A performance summary is detailed in Table 2.19. Finally, we investigated the STFSK performance in the context of iteratively exchanging extrinsic information with the channel decoder. The results of Fig. 2.20 showed that an $E_b/N_0$ gain of 3 dB is achieved at the BER of $10^{-4}$, when the number of iterations between the soft STFSK demapper and the RSC decoder was increased from one to five.

Furthermore, in Section 2.2.4.9 the ASE of the proposed STFSK aided SFHMA system was investigated in the multi-user and multi-cell environment. The results of Table 2.13 showed that the proposed system may double the attainable ASE compared to GMSK aided SFHMA, when the RS(8,4) channel codes are employed for transmission over the 6-tap COST-207 rural area channel model associated with Rayleigh fading and AWGN. Additionally, the soft-decision RSC(23,33) coded STFSK aided SFHMA may approach the maximum achievable ASE in various frequency reuse cluster sizes, as seen in Table 2.13. By contrast, this is only possible for the full-reuse cluster size of 9

Table 2.19: Summary of the space-time-frequency diversity schemes of Table 2.6, where the corresponding performances are shown in Figs. 2.17-2.19.

| | LDC | STSK | SFSK | STFSK |
|---|---|---|---|---|
| Schematic | – | Fig. 2.9 | Fig. 2.10 | Fig. 2.11 |
| Configuration | 4/1/4/16 | 4/1/4/4-4 | 4/1/4/8-2 | 4/1/4/2-4-2 |
| Hard-decision complexity per bit | (2.64): $C^{\times} = 1056$<br>(2.65): $C^{+} = 1052$ | (2.60): $C^{\times} = 1312$<br>(2.61): $C^{+} = 1180$ | (2.62): $C^{\times} = 657$<br>(2.63): $C^{+} = 591$ | (2.58): $C^{\times} = 665$<br>(2.59): $C^{+} = 565$ |
| Channel model | Frequency-flat Rayleigh fading - Fig. 2.17 | | | |
| CSI | perfect | perfect | perfect | perfect |
| $E_b/N_0$ required at $BER = 10^{-5}$ | $\simeq 28$ $dB$ | $\simeq 19$ $dB$ | $\simeq 22$ $dB$ | $\simeq 16$ $dB$ |
| Channel model | Frequency-selective Rayleigh fading - 4-tap ITU-A - Fig. 2.18 | | | |
| CSI | perfect | perfect | perfect | perfect |
| $E_b/N_0$ required at $BER = 10^{-5}$ | | $\simeq 21$ $dB$ | $\simeq 22$ $dB$ | $\simeq 16$ $dB$ |
| Channel model | Frequency-selective Rayleigh fading - 6-tap COST-207RA - Fig. 2.18 | | | |
| CSI | perfect | perfect | perfect | perfect |
| $E_b/N_0$ required at $BER = 10^{-5}$ | | $\simeq 21.5$ $dB$ | $\simeq 22$ $dB$ | $\simeq 17$ $dB$ |
| Channel model | Frequency-selective Rayleigh fading - 6-tap COST-207RA - Fig. 2.19 | | | |
| CSI | CSI error = 10% | CSI error = 10% | CSI error = 10% | CSI error = 10% |
| $E_b/N_0$ required at $BER = 10^{-5}$ | | $\simeq 23$ $dB$ | $\simeq 22$ $dB$ | $\simeq 19.5$ $dB$ |

and for the fractional-reuse cluster size of 21/3 in case of the soft-decision RSC(23,33) coded STFSK aided SFHMA. Furthermore, the system's ASE was compared to that of the soft-decision RSC coded GMSK aided TD/FDMA regime. We demonstrated in Fig. 2.28 and Table 2.14 that the soft-decision RSC(23,33) coded STFSK aided SFHMA system is capable of exceeding the ASE of the RSC(23,33) coded GMSK aided TD/FDMA as well as that of WCDMA. Despite this significant improvement, the ASE of the STFSK aided SFHMA remains only 60 % of that of the more complex LTE system, when the same RSC(23,33) channel code and a system bandwidth of 5 MHz are employed. Hence in our future research we will find appropriate upper-layer techniques for STFSK in the interest of increasing its ASE.

In Section 2.3, we discussed the family of distributed wireless MIMO systems in the context of wireless cooperative communications. Following the system model of Section 2.3.2 and the portrayal of relaying protocols described in Section 2.3.3, our performance results were provided in Figs. 2.36-2.39 of Section 2.3.4. Based on the analysis and results, a number of remarks may be summarized as in Table 2.20 below.

Table 2.20: Summary of the cooperative communication systems of Section 2.3.4, where the corresponding performances are shown in Figs. 2.36-2.39.

| Effect | Figure | Remark |
|---|---|---|
| Relay position | 2.36 | The relay station should be close to the source in order to avoid error propagation, when the DF relaying protocol is employed. By contrast, when the relay station is close to the destination, AF relaying should be preferred. |
| Source-relay power allocation | 2.37 | A significant amount of transmit power allocated to the source station may avoid the errors and/or noise amplification at the relay. |
| The number of relays | 2.38 | The system's performance improves upon increasing the number of the relays at the cost of increasing system complexity as well as reducing the system's spectral efficiency. |
| Space-time codes | 2.39 | The DSTC was proposed in order to avoid wasting the network's resources, such as the time slots and/or frequencies. |

# Chapter 3

# Coherent Detection for H-ARQ Aided Cooperative Wireless Communications

## 3.1 Introduction

Communications over wireless channels in mobile networks typically has to tolerate a higher BER than that in a wireline-based network due to the effects of fading and interference. In order to combat the effects of the BER and to avoid the retransmissions of erroneous data blocks by the transport layer's error-control mechanism, the ARQ protocol is typically combined with channel codes at the physical layer, hence creating a cross-layer H-ARQ protocol. Along with the benefits of cooperative communications, which offers significant diversity and/or multiplexing gains as described in Chapter 2, relay-aided H-ARQ arrangements potentially further improve the integrity of wireless systems.

Hence, relay-aided H-ARQ arrangements have attracted substantial research attention. For example, Zhao and Valenti [140] proposed a relay-aided network including a source, a destination and multiple relays, which retransmitted the packets instead of the more distant source station. This system exhibited a significant improvement in terms of the energy-latency trandoff, when compared to conventional multihop protocols implemented as a cascade of point-to-point links. The outage probability of a cooperative wireless network invoking H-ARQ and coded cooperation amongst the nodes was derived in [141]. Furthermore, Hasan and Aygolu [142] presented a cooperative H-ARQ transmission scheme based on superposition modulation and incremental relaying, while Stanojev *et al.* [143] investigated the energy efficiency of H-ARQ protocols in a single-user link as well as with the assistance of relay stations. Cross-layer operation assisted superposition coding aided multiplexed H-ARQ techniques were studied by Zhang and Hanzo [144]. By contrast, Harsini *et al.* [145] characterized the performance of cross-layer designs conceived for H-ARQ protocols employing adaptive modulation and coding as well as adaptive cooperative diversity. A range of other contributions related to relay-aided ARQ and H-ARQ are summarized in Table 3.1.

In this chapter we combine the advantages of cooperative wireless networks with those of H-ARQ systems employing coherent detection, as illustrated in Fig. 3.1, where perfect CSI is assumed to be available at the receivers. The CSI may be achieved by employing the pilot symbol assisted schemes proposed by Cavers in [146]. We commence in Section 3.2 by investigating the attainable performance

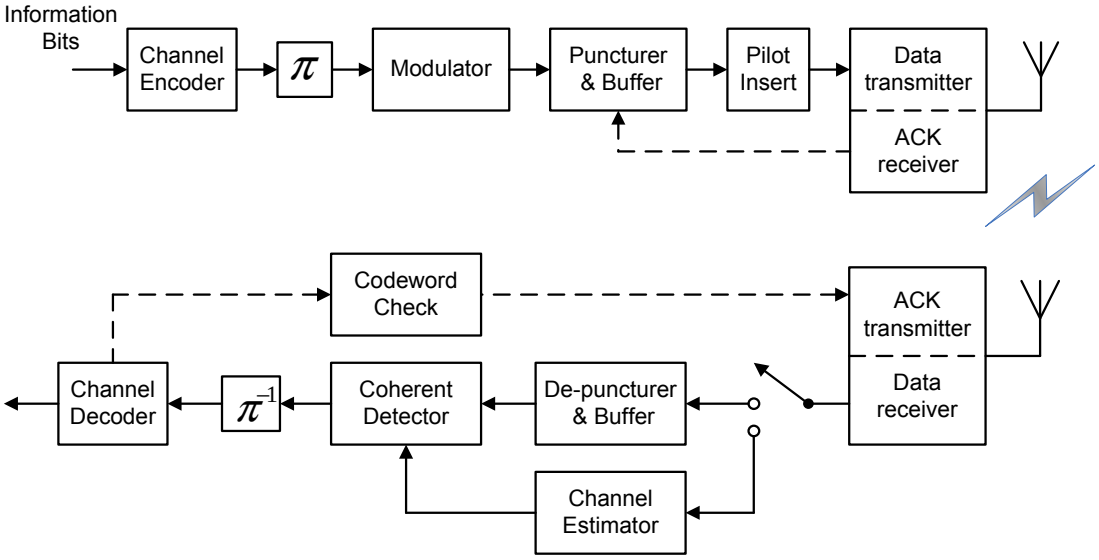


Figure 3.1: Transceiver schematic employing perfect coherent detection aided H-ARQ.

of cooperative ARQ in both uncorrelated and correlated fading channels, where a novel relay-switching regime is proposed for mitigating the detrimental effects of correlated fading without unduly increasing the system's complexity and delay. We demonstrate that the proposed relay-switching scheme not only improves the system's BER and FER performance, but additionally reduces the number of retransmissions. Hence, this proposal may reduce the transmit power, delay as well as interference. Furthermore, in Section 3.3 a novel relay-switching regime is proposed and intrinsically amalgamated with turbo coded H-ARQ schemes for achieving further improvements. In this relay-switching aided turbo coded H-ARQ scheme the Selective-Segment-Repeat (SSR) technique of [23] is employed for transmission over a fading channel.

We continued in Section 3.4 by studying H-ARQ systems employing Systematic Luby Transform codes (SLT) [38, 40], which constitute a family of rateless codes in the context of wireless cooperative networks. We demonstrate that when iterative detection is employed for exchanging *extrinsic* information between the SLT decoder and the demodulator, the proposed system may provide a significant gain for transmission over wireless Rayleigh fading channels, compared to the system where the decoder and demodulator operate independently. This gain is further increased in the presence of assisting relay stations. In Section 3.4.2, a modified relay-aided H-ARQ protocol using incremental redundancy was amalgamated with SLT codes in order to enhance the achievable throughput and energy efficiency of cooperative networks.

Table 3.1: Major cooperative ARQ and H-ARQ contributions.

| | | |
|---|---|---|
| 2005 | Zhao and Valenti [140] | Proposed a practical networks comprising multiple relays operating over orthogonal time slots based on a generalization of H-ARQ. |
| | Nam *et al.* [147] | Proposed cooperative communication through ARQ, attaining both full-diversity and full-rate. |
| 2006 | Dianati *et al.* [148] | Proposed a node-cooperative ARQ scheme for wireless ad-hoc networks, which is suitable for mobile wireless channels with high and correlated frame-error profile. |
| | Yu *et al.* [149] | Analysed and compared the data link layer packet error rate of different ARQ protocols, including the incremental relaying and the selection relaying. |
| 2007 | Krikidis [150] | Proposed a distributed truncated ARQ protocol in user cooperative networks. |
| | Mahinthan *et al.* [151] | Studied the performance of adaptive relaying schemes in cooperative diversity systems equipped with ARQ. |
| | Tomasin *et al.* [141] | Derive the expressions of the outage probability for a wireless network that integrates H-ARQ and coded cooperation among nodes. |
| 2008 | Azarian *et al.* [152] | Analysed the performance of the ARQ-dynamic decode and forward cooperation protocol in the single-relay-dedicated scenario and the two-user-cooperation scenario. |
| | Le and Hossain [153] | Presented an analytical model for a general ARQ cooperative diversity scheme in cluster-based multi-hop wireless networks. |
| | Weng and Murch [154] | Derived the optimal diversity-multiplexing-delay tradeoff in the cooperative broadcast for arbitrary number of receive nodes and arbitrary maximum number of ARQ rounds. |
| 2009 | Mahinthan *et al.* [155] | Proposed a cross-layer design of a wireless communication system where a quadrature signalling-based cooperative diversity system employs truncated stop-and-wait ARQ for error control. |
| | Alcaraz and Garcia [156] | Investigated the performance of cooperative ARQ algorithms in cellular access networks. |
| | Hasan and Aygolu [142] | Presented a cooperative transmission scheme based on superposition modulation and incremental relaying, which is provided by a H-ARQ type feedback channel. |
| | Stanojev *et al.* [143] | Investigated the energy efficiency of truncated H-ARQ protocols in a single-user link or with the assistance of a relay station. |
| 2010 | Choi *et al.* [157] | Proposed an adaptive multi-node incremental relaying technique in cooperative communications with AF relays. |
| | Zhang and Hanzo [144] | Proposed cross-layer super position coding aided multiplexed H-ARQ techniques. |
| | Narasimhan *et al.* [158] | Analysed a two-user uplink interference channel with H-ARQ and base station cooperation. |
| 2011 | Harsini *et al.* [145] | Presented performance analysis and cross-layer design approaches for H-ARQ protocols, employing adaptive modulation and coding and adaptive cooperative diversity. |

## 3.2 ARQ Aided Cooperative Networks

### 3.2.1 System Model

We will consider an ARQ scenario, where the source station (SS) broadcasts its data to both the relay station (RS) and the destination station (DS) in the first time slot and then the RS amplifies and forwards the data to the DS. It is assumed that the Source-to-Relay (SR), Source-to-Destination (SD) and Relay-to-Destination (RD) channels suffer from correlated fading, but there is no correlation among the SD and RD channels, owing to the substantial physical separation of the stations.

The signal received at the RS may be expressed as

$$y_R[i] = G_{SR} h_{SR}[i] x[i] + n_{SR}[i], \tag{3.1}$$

where $i$ is the symbol index; $x[i]$ is the transmit signal of the SS with power $P_S$ and $y_R[i]$ is the signal received at the RS; $n_{SR}[i]$ represents the zero-mean complex-valued AWGN with a variance of $\sigma_n^2$; $h_{SR}[i]$ denotes the non-dispersive CIR between the SS and the RS, which is modelled as a wide-sense stationary (WSS) zero-mean complex Gaussian (ZMCG) random process with variance of $\sigma_{SR}^2$; and $G_{SR}$ is the path-loss-related power gain for the Source-to-Relay (SR) link.

The RS amplifies $y_R[i]$ and forwards it to the DS, which receives

$$y_D[i] = \Big[G_{SD} h_{SD}[i] x[i] + n_{SD}[i]\Big] + \Big[G_{RD} h_{RD}[i] A[i] \Big(G_{SR} h_{SR}[i] x[i] + n_{SR}[i]\Big) + n_{RD}[i]\Big], \tag{3.2}$$

where, again, $y_D[i]$ is the signal received at the DS; $h_{RD}[i]$ is the channel between the $RD$ link, which is modelled as a WSS ZMCG process with a variance of $\sigma_{RD}^2$, while $n_{RD}[i]$ is the zero-mean complex AWGN process having a variance of $\sigma_n^2$. Furthermore, $G_{RD}$ is the path-loss-related power gain for the $RD$ link. Finally, $A_R$ is the fixed relay gain, which is expressed as [159]

$$A_R[i] = \sqrt{\frac{P_R}{P\big[|y_R[i]|^2\big]}} = \sqrt{\frac{G_{SR} P_R}{G_{SR} P_S \sigma_{SR}^2 + \sigma_n^2}}, \tag{3.3}$$

where $P_R$ is the transmit power of the RS.

The received packet is then decoded at the DS's receiver and then checked for the presence of residual bit errors by using error detection codes, such as the classic Cyclic Redundancy Checking (CRC) codes. If no error is detected, a positive acknowledgement is returned to the source to trigger the transmission of a new packet. Otherwise, a negative acknowledgement is fed back in order to ask for the packet's retransmission. Accordingly, the SS sends the packet again. Consequently, the combined signal received at the DS's receiver may be expressed as

$$y_D^L[i] = \sum_{l=0}^{L} \left\{ \Big[G_{SD} h_{SD}^l[i] x[i] + n_{SD}^l[i]\Big] + \Big[G_{RD} h_{RD}^l[i] A_R[i] \Big(G_{SR} h_{SR}^l[i] x[i] + n_{SR}^l[i]\Big) + n_{RD}^l[i]\Big] \right\}, \tag{3.4}$$

where $L$ is the number of retransmissions, hence $L = 0$ indicates that no retransmission is required.

### 3.2.2 Single-Relay Aided ARQ

The single-relay aided ARQ scheme assigns a single fixed relay to assist the SS in its transmission attempts. If the channels are assumed to experience highly correlated fading, there is little difference

between the consecutive values of channel coefficients, which suggests that the retransmitted packets may also be corrupted. As a result, there is no substantial spatial diversity gain. Nonetheless, an improved performance may be attained owing to the power-gain gleaned from the reduced-distance relaying.

### 3.2.3 Relay-Switching Aided ARQ

When the channel experiences slow fading, the single-relay aided ARQ protocol may prove to be ineffective, because the retransmitted versions may be subjected to fading, which is correlated with the versions received before. In order to further improve the attainable performance of the H-ARQ scheme considered, a novel relay-switching philosophy is proposed here. A top-level view of the scheme is illustrated in Fig. 3.2. According to this scheme, the SS will send the retransmitted packet through another RS every time, when a retransmission request is received. As a benefit of the independence of the channels between the SS, the RSs and the DS, there is no correlation between the signals received from the RSs at the DS's receiver. Thus, in addition to achieving a reduced-distance-based power gain, the proposed scheme also achieves a spatial diversity gain for the received signals.

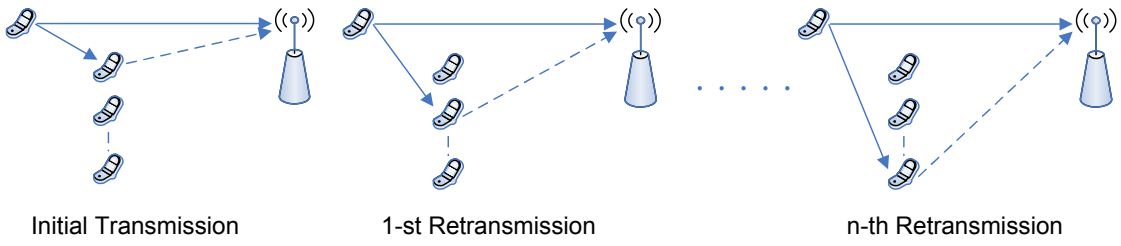


Figure 3.2: Relay-switching aided ARQ

### 3.2.4 Capacity

The instantaneous capacity of the relay-aided ARQ scheme may be formulated as [102]

$$C = min\{C_1, C_2\}, \tag{3.5}$$

where $C_1$ represents the sum capacity of the SD and SR links and $C_2$ represents the sum capacity of the RD and SD links, which are illustrated in Fig. 3.3.

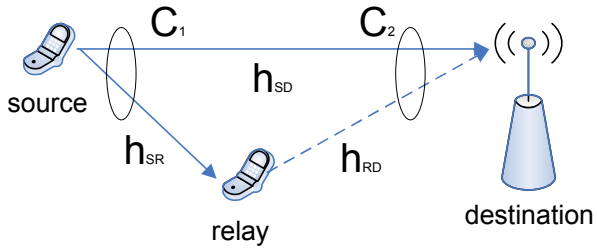


Figure 3.3: Relaying topology used for relay capacity calculation.

According to the Shannon-Hartley's theorem, the channel capacity $C$ is given as

$$C = Blog_2\left(1 + \frac{S}{N}|h|^2\right), \tag{3.6}$$

where $B$ is the channel's bandwidth in Hertz and $S/N$ is the SNR at the receiver, while $h$ represents the channel's fading coefficient. For convenience, we set $B = 1$ in this study and hence $B$ is dropped from the following expressions.

Substituting the Shannon-Hartley formula of Eq. (3.6) into our equivalent system models of Eqs. (3.1) and (3.4), the instantaneous sum capacities may be formulated as

$$C_1 = log_2\left(1 + \frac{P_{source}G_{SD}\sum_{l=0}^{L}|h_{SD}^l|^2}{N_0} + \frac{P_{source}G_{SR}\sum_{l=0}^{L}|h_{SR}^l|^2}{N_0}\right), \tag{3.7}$$

and

$$C_2 = log_2\left(1 + \frac{P_{source}G_{SD}\sum_{l=0}^{L}|h_{SD}^l|^2}{N_0} + \frac{P_{relay}G_{RD}\sum_{l=0}^{L}|h_{RD}^l|^2}{N_0}\right). \tag{3.8}$$

In order to achieve the ergodic capacity, the capacities $C_1$ of Eq. (3.7) and $C_2$ of Eq. (3.7) are weighted by their specific probability of occurrences quantified by the joint Probability Density Function (PDF) of channel coefficients and then they are averaged - i.e. integrated over their entire dynamic range, yielding:

$$\bar{C}_1 = \underbrace{\int_0^\infty \int_0^\infty \cdots \int_0^\infty}_{2(L+1)-fold} C_1 \cdot F\{|h_{SD}^0|, ..., |h_{SD}^L|\} \cdot F\{|h_{SR}^0|, ..., |h_{SR}^L|\} \cdot d_{SD}^0 ... d_{SD}^L \cdot d_{SR}^0 ... d_{SR}^L, \tag{3.9}$$

and

$$\bar{C}_2 = \underbrace{\int_0^\infty \int_0^\infty \cdots \int_0^\infty}_{2(L+1)-fold} C_2 \cdot F\{|h_{SD}^0|, ..., |h_{SD}^L|\} \cdot F\{|h_{RD}^0|, ..., |h_{RD}^L|\} \cdot d_{RD}^0 ... d_{RD}^L \cdot d_{SR}^1 ... d_{SR}^L, \tag{3.10}$$

where $F\{|h_{SD}^0|, ..., |h_{SD}^L|\}$, $F\{|h_{SR}^0|, ..., |h_{SR}^L|\}$ and $F\{|h_{RD}^0|, ..., |h_{RD}^L|\}$ are the joint PDFs of the channel coefficients $h_{SD}^l$, $h_{SR}^l$ and $h_{RD}^l$ ($l = \{0...L\}$ is the number of retransmission), respectively.

Consequently, the ergodic capacity of the system may be formulated as

$$\bar{C} = min\{\bar{C}_1, \bar{C}_2\}. \tag{3.11}$$

***Single-Relay Aided ARQ:*** The joint PDF of the single-relay assisted scheme depends on the correlation of channels encountered, but more specifically on the particular correlation between the retransmitted channel envelopes at the specific instants, when the data packets were actually transmitted.

For example, in case of correlated Rayleigh fading channels and when only a single retransmission is available ($L = 1$), the joint PDF of the channel coefficients $h_{RD}^0$ of the first transmission and $h_{RD}^1$ of the retransmission for the RD link may be formulated as [160]

$$F\{|h_{RD}^0|, |h_{RD}^1|\} = \frac{4|h_{RD}^0||h_{RD}^1|e^{-[\Omega_0|h_{RD}^0|^2 + \Omega_1|h_{RD}^1|^2/\Omega_0\Omega_1(1-\rho)]}}{\Omega_0\Omega_1(1-\rho)\sqrt{\Omega_0\Omega_1\rho}} \cdot I_0\left\{\frac{2\sqrt{\rho}|h_{RD}^0||h_{RD}^1|}{(1-\rho)\sqrt{\Omega_0\Omega_1}}\right\}, \tag{3.12}$$

where we have $\Omega_0 = \overline{|h_{RD}^0|^2}$, $\Omega_1 = \overline{|h_{RD}^1|^2}$ and $\rho = \frac{cov(|h_{RD}^0|^2, |h_{RD}^1|^2)}{\sqrt{var(|h_{RD}^0|^2)var(|h_{RD}^1|^2)}}$ ($0 < \rho < 1$) represents the channel envelope's correlation, which depends on the time-lag between two transmission attempts, i.e on the coefficients $h_{RD}^1$ and $h_{RD}^2$.

***Relay-Switching Aided ARQ:*** As a benefit of the relay-switching action between the retransmissions, there is no correlation between the channel coefficients of the retransmitted and original data packet. Therefore, the joint PDF of the relay switching scheme may be simplified to the product of the individual PDFs. For example, the joint PDF of transmission attempts for the RD link may be formulated as:

$$F\{h_{RD}^0, ..., h_{RD}^L\} = \prod_{l=0}^{L} f(h_{RD}^l), \tag{3.13}$$

where $f(h_{RD}^l)$ is the PDF of the Rayleigh distribution.

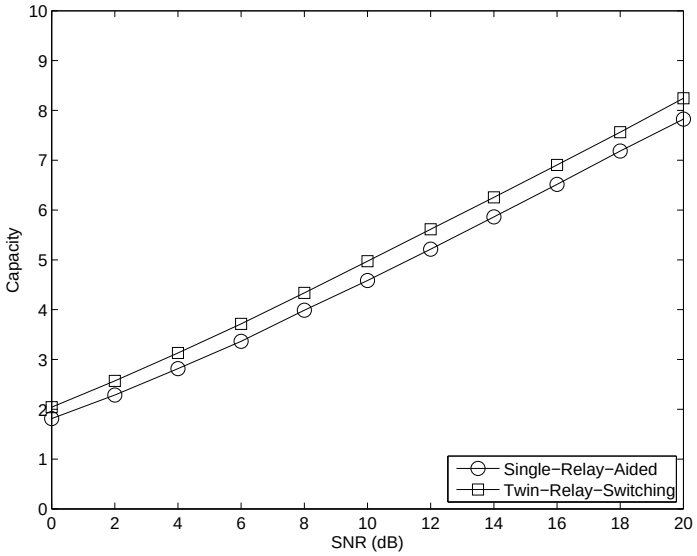


Figure 3.4: Capacity of relay aided H-ARQ

The capacity of both the single-relay-aided and twin-relay-aided schemes is shown in Fig. 3.22. This figure demonstrates that the relay-switching scheme provides a higher capacity than the single-relay scheme.

### 3.2.5 Performance of ARQ Aided Cooperative Networks

The BER and FER performance of the cooperative ARQ, where system's parameters are provided in Table 3.2, over the uncorrelated Rayleigh fading channels are shown in Fig. 3.5. According to the figure, the cooperative ARQ may achieve a power gain of approximately 2 dB at the FER of $10^{-3}$, compared to the conventional direct transmission based ARQ systems. Additionally, as shown in Fig. 3.6(a), the cooperative ARQ systems are capable of reducing the number of retransmissions. Consequently, the system's effective throughput is significantly improved. More particularly, as seen in Fig. 3.6(b), at the $E_b/N_0$ value of 20 dB the DF cooperative ARQ may double the throughput of the direct transmission based ARQ scheme while the AF cooperative ARQ's throughput is 50% higher than that of the direct transmission based ARQ regime.

Note that for the selective-repeat ARQ, the system's throughput may be quantified as [161]

$$\eta_{SR} = M \frac{K_{inf}}{N_{tra}} (1 - P_{frame}), \tag{3.14}$$

where $M$ is the number of bits per modulated symbol; $K_{inf}$ and $N_{tra}$ is the number of information bits

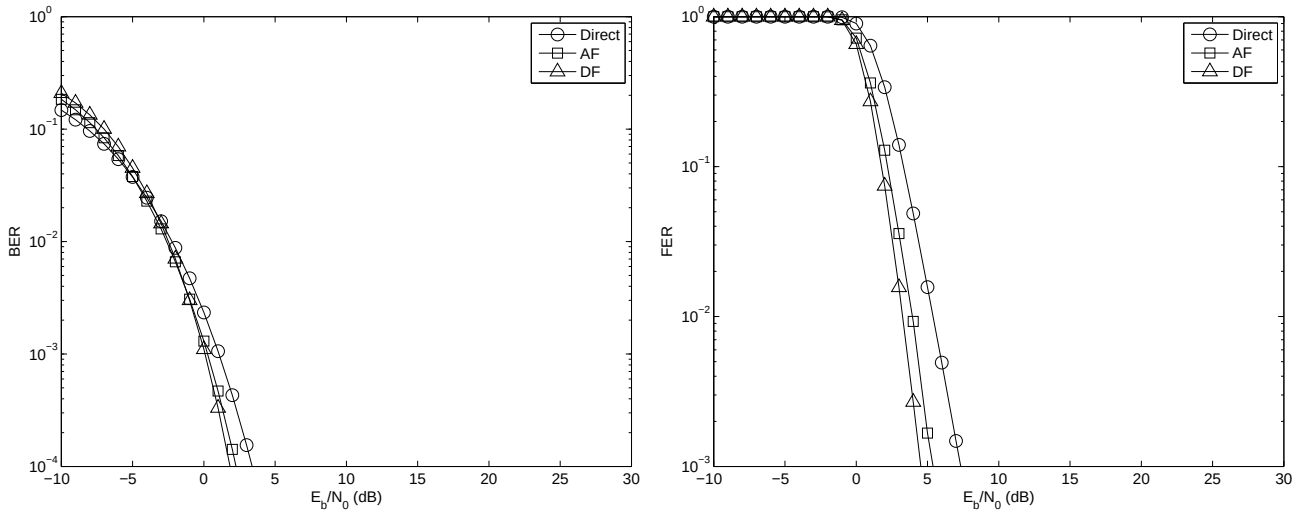


(a) BER vs $E_b/N_0$ (b) FER vs $E_b/N_0$

Figure 3.5: Simulation-based BER and FER performance of ARQ aided direct, AF and DF cooperative transmissions over the uncorrelated Rayleigh fading channels. All other parameters are summarized in Table 3.2.

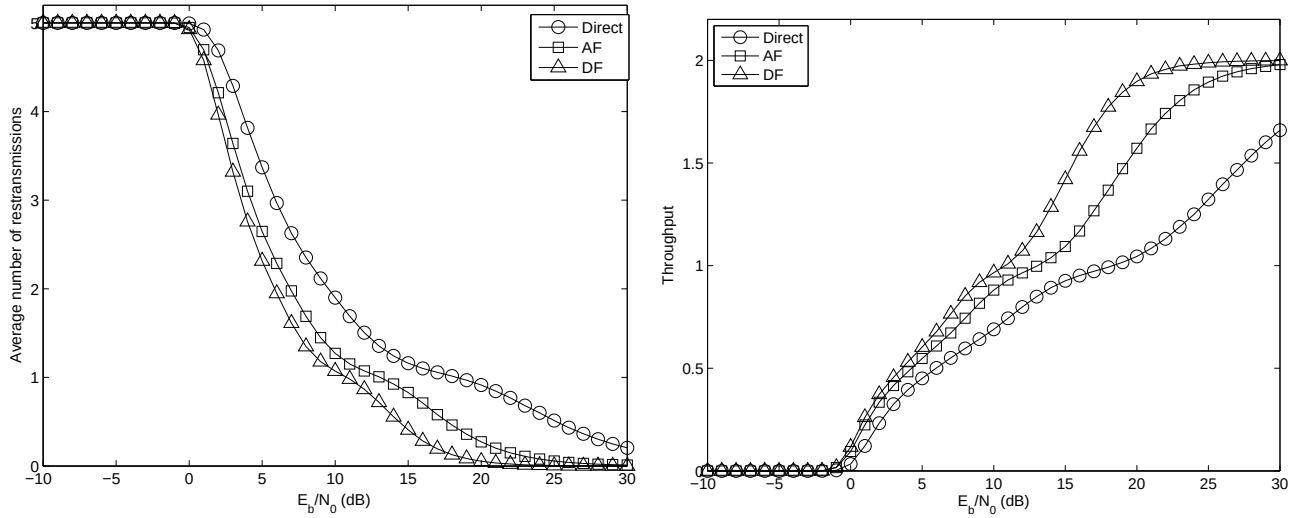


(a) Average number of retransmissions (b) Throughput

Figure 3.6: The average number of retransmissions and the throughput performance of ARQ aided direct, AF and DF cooperative transmissions over the uncorrelated Rayleigh fading channels. All other parameters are summarized in Table 3.2.

Table 3.2: Basic parameters of ARQ aided cooperative networks

| Parameter | Value |
|---|---|
| Information bits per frame | $K_{inf} = 1000$ |
| Modulation type | BPSK |
| Relay type | Direct/AF/DF |
| N$^o$ of relays | L=1 |
| Normalized $d_{SR_l}/d_{R_lD}$ | 0.5/0.5 |
| Source's transmit power | $E_S = \frac{E_b}{G_{rd}+1}$ |
| Relays' transmit power | $E_{R_l} = \frac{G_{rd}E_b}{G_{rd}+1}$ |
| Channel model | frequency-flat Rayleigh fading |
| Maximum number of retransmissions | 5 |

per frame and the number of transmitted bits, which is the product of $K_{inf}$ and the average number of retransmissions, i.e. as in Fig. 3.6(a), while $P_{frame}$ is the FER, i.e. as in Fig. 3.5(b).

Furthermore, we investigate the performance of cooperative ARQ systems for transmission over correlated Rayleigh fading channels. The corresponding BER and FER performance results are shown in Fig. 3.7 and may be contrasted to the uncorrelated fading results of Fig. 3.5. According to Fig. 3.7, the single-relay-aided DF cooperative ARQ achieved a power gain in excess of 5 dB at the FER of $10^{-3}$. When relay switching is employed, a further gain of 5 dB may be gleaned at the same FER value. By contrast, the AF cooperative ARQ only achieved an improved FER performance in the low $E_b/N_0$ region, namely below 10 dB for single-relay aided and below 2 dB for relay-switching aided DF cooperation - fortunately in the region, where it was most needed. For higher $E_b/N_0$, their FER performances were close to the conventional direct ARQ's performance. Again, the average number of retransmissions is shown in Fig. 3.8(a). As seen from the figure, the relay-switching assisted ARQ schemes are capable of reducing the number of retransmissions, compared to the single-relay aided schemes. As a result, their throughput was further improved, as seen in Fig. 3.8(b). Hence, it may be concluded that in correlated fading channels the relay-switching aided ARQ may improve the system's performance in all four aspects considered, namely in terms of the BER, the FER, the number of retransmission as well as the effective throughput.

## 3.3 Relay Switching Aided Turbo Coded Hybrid-ARQ in Correlated Fading Channels

Again, observe by comparing Figs. 3.5 and 3.7 that the channel characteristics substantially affect the attainable system performance. For instance, correlated fading may corrupt consecutive retransmissions, especially when using Chase combining [162], since the transmitted replica may also experience a deep fade. In this scenario the spatial diversity of MIMO systems [23] may mitigate the problem. However, employing co-located MIMO elements at the mobile station, which has compact physical dimensions, may also become ineffective in the presence of spatially correlated fading, even when employing long interleavers. To overcome this potential drawback, we investigate distributed MIMOs relying on single-antenna based mobiles sharing their antennas by invoking cooperative relaying. We

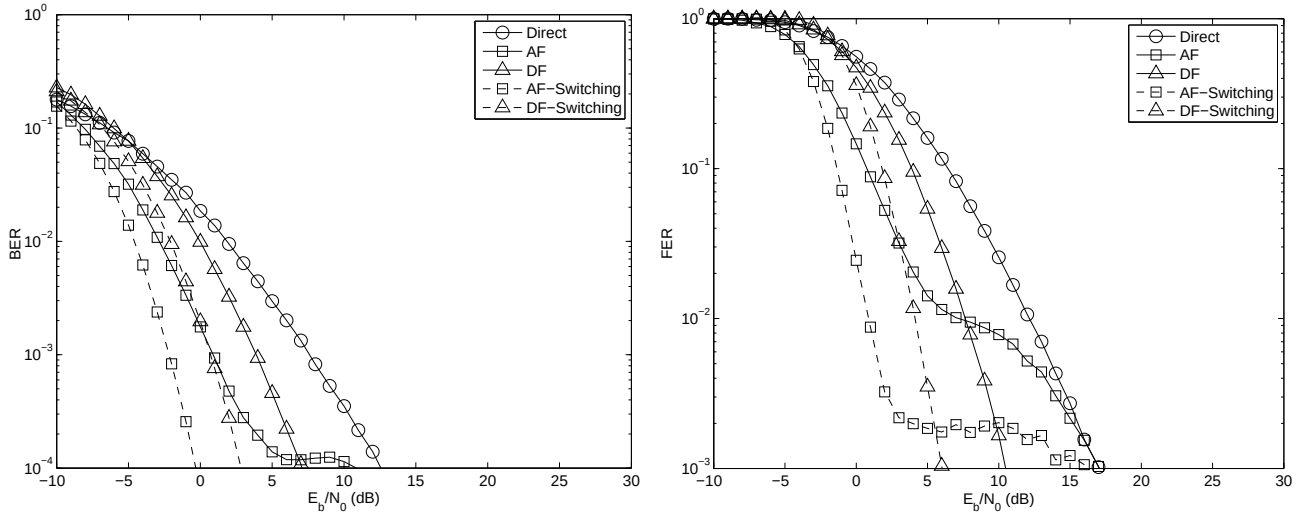


(a) BER vs $E_b/N_0$

(b) FER vs $E_b/N_0$

Figure 3.7: BER and FER performance of ARQ aided direct, AF and DF cooperative transmissions over the correlated Rayleigh fading channels at the normalized Doppler frequency of $10^{-4}$. All other parameters are summarized in Table 3.2. The corresponding uncorrelated fading results are seen in Fig. 3.5.

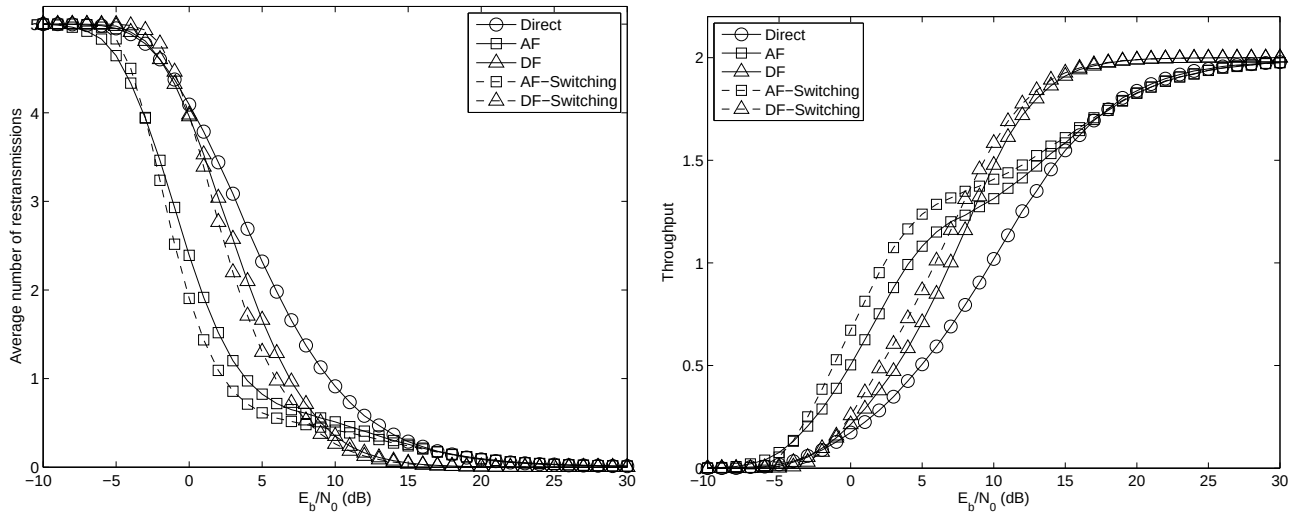


(a) Average number of retransmissions

(b) Throughput

Figure 3.8: The average number of retransmissions and the throughput performance of ARQ aided direct, AF and DF cooperative transmissions over the correlated Rayleigh fading channels at the normalized Doppler frequency of $10^{-4}$. All other parameters are summarized in Table 3.2. The corresponding uncorrelated fading results are seen in Fig. 3.6.

exploit the flexibility of cooperative networks [116, 117] by advocating a novel relay-switching regime, where the specific relay activated is changed after each transmission attempt, in order to overcome the spatial correlation effects. Additionally, we combine the proposed relay-switching regime with the H-ARQ relying on Segment Selective Repeat technique of (SSR) [163], where not all, but only the most error-infested segments are retransmitted, in order to further improve the overall performance of the system.

### 3.3.1 Relay-Switching Aided Turbo Coded Hybrid-ARQ

#### 3.3.1.1 TC-HARQ Using Chase Combining

In the H-ARQ scheme of Fig. 3.1, the ARQ protocol is combined with convolutional turbo coding. A CRC code is used in order to produce a positive or negative acknowledgement. More particularly, at the SS a $Q$-bit CRC code defined over the Galois Field $GF(2)$ is attached to $(K - Q)$ information bits, resulting in the bit sequence of $\mathbf{x} = \{x_1, x_2, ..., x_K\}$. This bit sequence is then passed to a $(K, N)$ turbo encoder, which turns $K$ uncoded input bits into $N$ encoded bits. The resultant bits are then punctured. Following modulation, the packet is transmitted to both the RS and the DS.

In the DS's receiver of Fig. 3.1, the received packet is decoded and checked for bit errors. If there is no decoding error, the SS proceeds by transmitting a new packet. Otherwise, the same packet will be retransmitted. In case of the conventional single-relay aided scheme, the routes of the retransmitted packets are the same as those of the original ones. By contrast, the routes are alternated in case of the relay-switching aided schemes. When the retransmitted packets arrive at the DS's decoder, they are amalgamated with the previous versions using the Chase Combining (CC) technique [162].

#### 3.3.1.2 TC-HARQ using Incremental Redundancy

In contrast to the above-mentioned TC-HARQ arrangement, in case of the TC-HARQ using IR, the SS will send additional parity bits, which are unknown to the DS, whenever a negative ACK is fed back. As a benefit of additional parity bits, a coding gain will be achieved at the DS's channel decoder. However, the studies of [164] demonstrated that the HARQ using IR has an inferior performance in comparison to that of the H-ARQ using CC, when the systematic bits in the first transmission are corrupted by deep fades and no more systematic bits were received during the retransmission sessions. In order to avoid the above-mentioned detrimental effect, the H-ARQ scheme of Fig. 3.1 using IR should include part of the systematic information in the IR transmission.

Indeed, the TC-HARQ scheme of Fig. 3.1 using IR may achieve three different types of gains, including the usual relay-aided reduced-distance-based power gain, a spatial diversity gain achieved by the relay-switching scheme and channel-coding gain, which is also referred to as time-diversity gain.

#### 3.3.1.3 TC-HARQ Using Segment Selective Repeat

The studies provided in Chapter 5 of [165] showed that the residual decoding errors found in turbo codes usually form some error-burst, or clusters in a packet. In order to exploit this phenomenon, the authors of [163] proposed a turbo coded hybrid ARQ scheme relying on segment selective repeat (SSR)

in order to improve the attainable system performance. According to this scheme, the entire packet is divided into smaller segments, each having an identical length. Once the decoder fails, the most severely corrupted segments have to be retransmitted. In the soft-decoding scenarios, our confidence in the symbol-estimates is typically determined by the Log-Likelihood Ratio (LLR). The higher the LLRs, the more confident the symbol-estimates are. Therefore, the LLR values and the number of LLR polarities toggled from one iteration to another is considered to be the specific criterion for determining how severely corrupted a segment is. Hence, the segments having the lowest mean absolute LLR values and/or associated with the highest number of LLR polarity swap operations are likely to be retransmitted.

As analysed in the previous section, the relay-switching scheme is capable of providing an increased spatial diversity gain for the ARQ scheme. Thus, it is of high potential to combine the turbo coded Hybrid-ARQ arrangement of Fig. 3.1 using SSR with the relay-switching scheme in order to further improve the system's performance.

### 3.3.2 Performance of Relay-Switching Aided Turbo Coded Hybrid-ARQ

Table 3.3: The parameters of TC-HARQ schemes of Fig. 3.1. The corresponding scheme outline is shown in Fig. 3.9.

| Parameters | **Scheme A-1** | **Scheme A-2** | **Scheme A-3** | **Scheme B-1** | **Scheme B-2** | **Scheme B-3** |
|---|---|---|---|---|---|---|
| N$^o$ of information bits | 300 | 300 | 300 | 300 | 300 | 300 |
| N$^o$ of bits of 1st trans. | 600 | 600 | 600 | 600 | 600 | 600 |
| N$^o$ of bits per re-/IR-trans. | 200 | 200 | 200 | 200 | 200 | 200 |
| N$^o$ of re-/IR-trans. | 3 | 3 | 3 | 3 | 3 | 3 |
| H-ARQ Combining Type | CC | CC | CC | IR | IR | IR |
| Relaying type | none | AF | AF-switching | none | AF | AF-switching |
| Normalized $P_{source}/P_{relay}$ | 1.0/0.0 | 0.5/0.5 | 0.5/0.5 | 1.0/0.0 | 0.5/0.5 | 0.5/0.5 |
| Normalized $G_{sd}/G_{sr}/G_{rd}$ | 1/4/4 | 1/4/4 | 1/4/4 | 1/4/4 | 1/4/4 | 1/4/4 |

In this section, we will investigate the achievable performance of the relay switching aided TC-HARQ regime of Fig. 3.1 and compare the diverse schemes considered. The generator polynomial of the half-rate Recursive Systematic Convolutional (RSC) turbo code component is given by:

$$G = \frac{1 + D + D^3}{1 + D^2 + D^3}. \tag{3.15}$$

In Scheme A-x, the first transmissions include 300 systematic bits and 300 parity bits, while the 200-bit retransmitted packets include 100 systematic bits and 100 parity bits, as shown in Fig. 3.3. Similarly, the IR transmissions of Scheme B-x contain 100 systematic bits and 100 new parity bits. The remaining parameters of each scheme are detailed in Table 3.3, while the outline of schemes is shown in Fig. 3.9. Observe in the table that the total transmit power is normalized to unity and the

normalized path-loss gains represent a relay positioned halfway between the SS and the DS, which using a path-loss exponent of two.

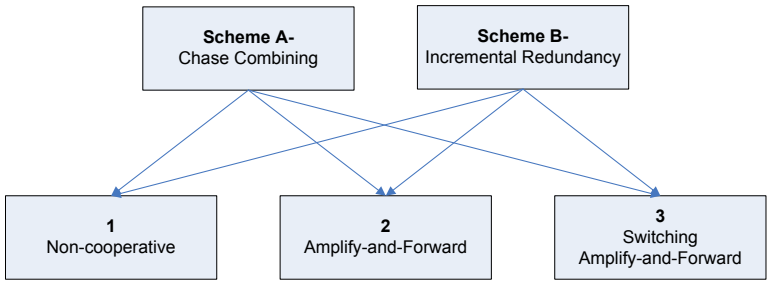


Figure 3.9: Schematic for characterising the comparisons of Table 3.3.

The BER performance of the six schemes characterized in Table 3.3 are shown in Fig. 3.10(a). It may be seen from the figure that the TC-HARQ schemes of Fig. 3.1 using IR, or Scheme B-x of Table 3.3 performs better than the schemes using CC, or Scheme A-x of Table 3.3. Furthermore, the TC-HARQ of Fig. 3.1 assisted by a single relay, namely Scheme A-2 may provide an approximately 5 dB gain at the BER of $10^{-3}$ against Scheme A-1 operating without the assistance of a relay. Observe furthermore from Fig. 3.10(a) that an extra 1 dB may be gleaned by Scheme A-3, where the relays are switched after each retransmission.

The average number of re-/IR-transmissions of the four H-ARQ schemes of Table 3.3 are shown in Fig. 3.11(a). According to the figure, the average number of re-/IR-transmissions is comparable for the considered schemes. This means that the relay-switching schemes do not impose any further delay compared to the conventional single-relay aided scheme. Indeed, the relay-switching aided TC-HARQ schemes not only reduce the BER, but they also increase the attainable throughput of the system without increasing its delay, namely above 2 dB as seen in Fig. 3.11(b).

Fig. 3.12 shows the effect of the channel's correlation on the performance of the systems. According to the figure, the relay-switching schemes, namely Scheme A-3 of Table 3.3, exhibits an improved performance in case of highly correlated channels. Explicitly, at the normalized Doppler frequency of $10^{-3}$, Scheme A-3 may achieve a gain of 1.5 dB at the BER of $10^{-7}$. Furthermore, this gain increased to 2 dB and 3 dB at the same BER value, when the normalized Doppler frequency was $10^{-4}$ and $10^{-5}$, respectively. In other words, the attainable gain improved, when the normalized Doppler frequency was reduced, i.e the channel became more correlated. This was a direct benefit of the increased spatial diversity, when the relays of consecutive retransmissions were switched. At low Doppler frequencies the correlation between the channel envelopes of retransmissions was high, hence the single-relay aided schemes operated less effectively than relay-switching. As a result, the gains of the single-relay schemes recorded for highly correlated channels were lower than those of the less correlated channels.

Finally, we investigated the performance of turbo-coded H-ARQ of Fig. 3.1 using SSR in the relaying network. The detailed parameters are provided in Table 3.4, while the outline of scheme comparison is shown in Fig. 3.13. In the SSR schemes considered, the entire packet was divided into 15 segments, each having a length of 100 bits, where the five segments having the lowest absolute average LLR values were retransmitted. The attainable BER and FER performances are shown in Fig. 3.14, while the average number of retransmission and the throughput performances are shown

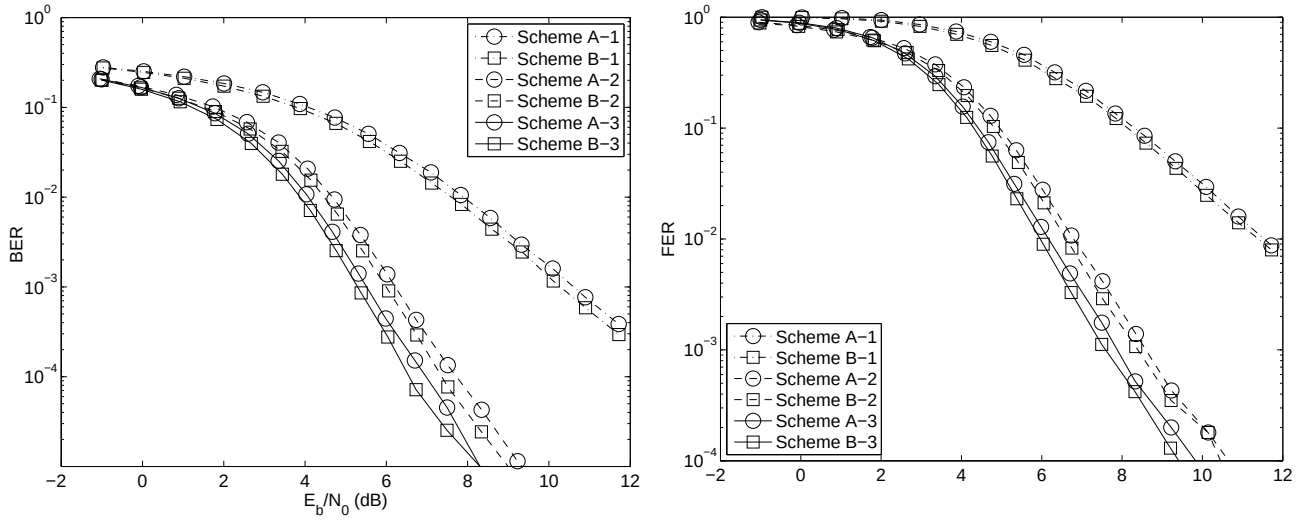


(a) BER vs $E_b/N_0$

(b) FER vs $E_b/N_0$

Figure 3.10: BER and FER performance of turbo coded H-ARQ of Fig. 3.1 employing direct, AF and DF cooperative transmissions over correlated Rayleigh fading channels at the normalized Doppler frequency of $10^{-3}$. All other parameters are summarized in Table 3.3. The corresponding results of the uncoded ARQ are shown in Fig. 3.7.

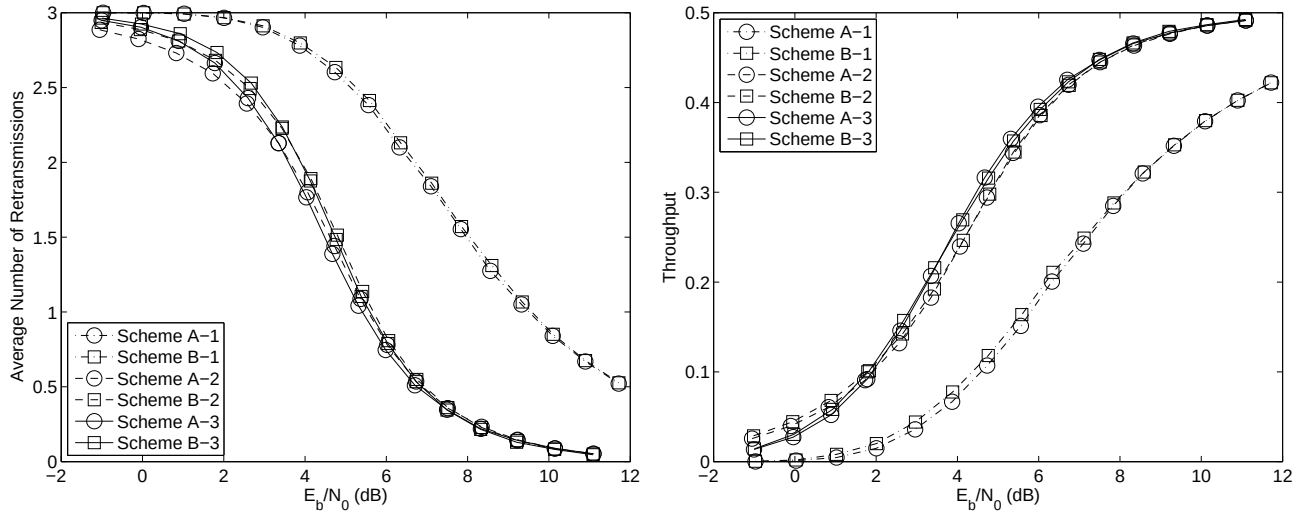


(a) Average number of retransmissions vs $E_b/N_0$

(b) Throughput vs $E_b/N_0$

Figure 3.11: The average number of retransmissions and the throughput performance of turbo coded H-ARQ of Fig. 3.1 employing direct, AF and DF cooperative transmissions over the correlated Rayleigh fading channels at the normalized Doppler frequency of $10^{-3}$. All other parameters are summarized in Table 3.3. The corresponding results of the uncoded ARQ are shown in Fig. 3.8.

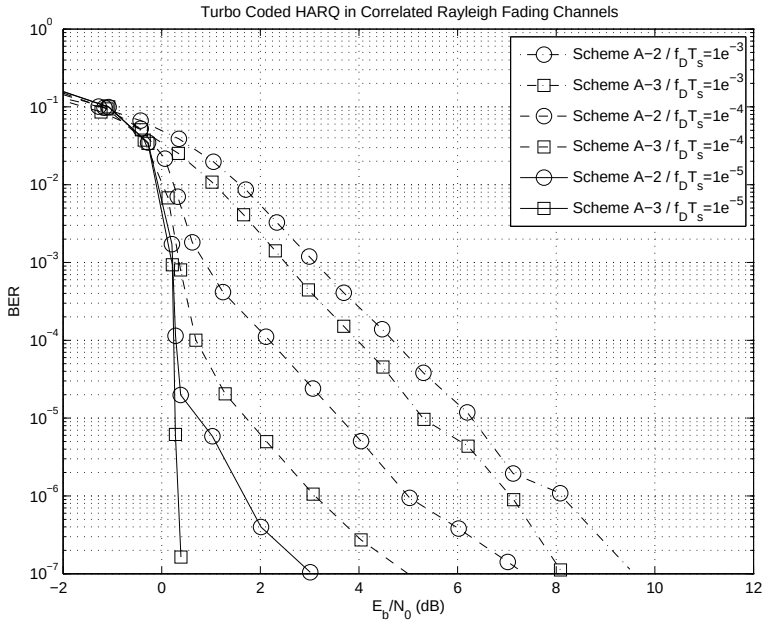


Figure 3.12: BER performance of TC-HARQ of Fig. 3.1, when operating in correlated Rayleigh fading channels at the normalized Doppler frequency of $f_DT_s = \{10^{-3}, 10^{-4}, 10^{-5}\}$. The remaining parameters were provided in Table 3.3.

Table 3.4: Parameters of TC-HARQ schemes of Fig. 3.1, where a third-rate turbo code using CC and SSR is employed instead of a half-rate turbo code using CC and IR of Table 3.3. The corresponding scheme outline is shown in Fig. 3.13.

| Parameters | **Scheme C-1** | **Scheme C-2** | **Scheme C-3** | **Scheme D-1** | **Scheme D-2** | **Scheme D-3** |
|---|---|---|---|---|---|---|
| N$^o$ of information bits | 500 | 500 | 500 | 500 | 500 | 500 |
| N$^o$ of bits of 1st trans. | 1500 | 1500 | 1500 | 1500 | 1500 | 1500 |
| N$^o$ of bits per re-/IR-trans. | 500 | 500 | 500 | 500 | 500 | 500 |
| N$^o$ of re-/IR-trans. | 3 | 3 | 3 | 3 | 3 | 3 |
| H-ARQ Combining Type | CC | CC | CC | SSR | SSR | SSR |
| Relaying type | none | AF | AF-switching | none | AF | AF-switching |
| Normalized $P_{source}/P_{relay}$ | 1.0/0.0 | 0.5/0.5 | 0.5/0.5 | 1.0/0.0 | 0.5/0.5 | 0.5/0.5 |
| Normalized $G_{sd}/G_{sr}/G_{rd}$ | 1/4/4 | 1/4/4 | 1/4/4 | 1/4/4 | 1/4/4 | 1/4/4 |

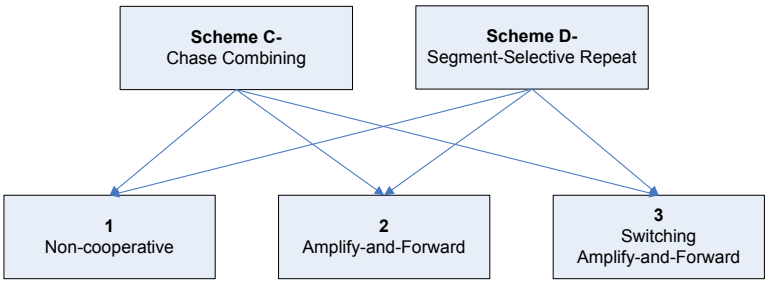


Figure 3.13: Schematic for characterising the comparisons of Table 3.4.

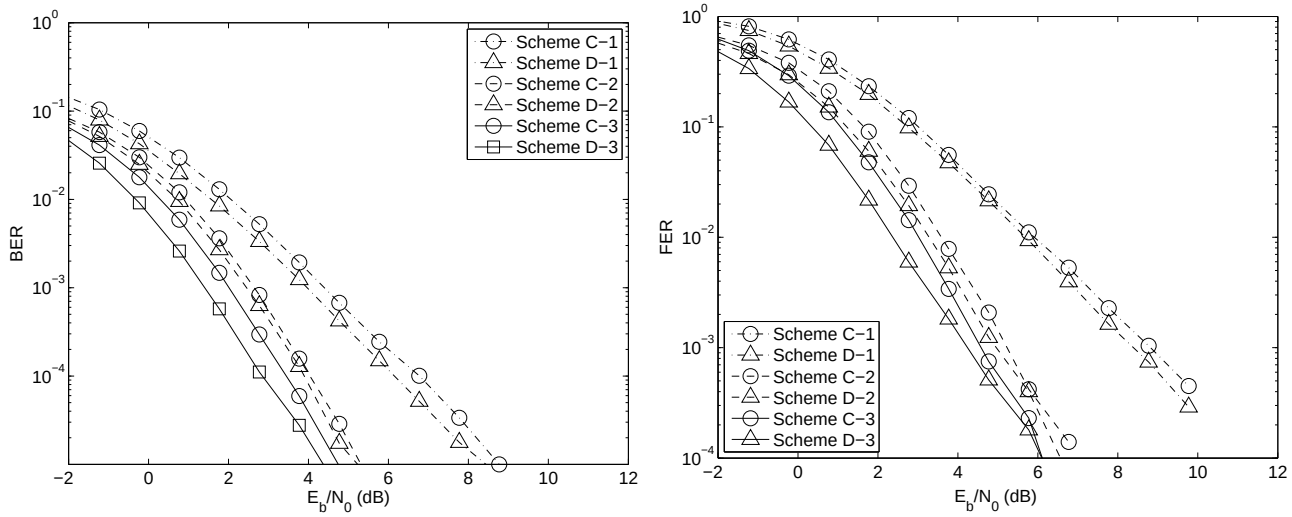


(a) BER vs $E_b/N_0$

(b) FER vs $E_b/N_0$

Figure 3.14: BER and FER performance of turbo coded H-ARQ of Fig. 3.1 employing direct, AF and DF cooperation employing CC and SSR for transmissions over the correlated Rayleigh fading channels at the normalized Doppler frequency of $10^{-3}$. All other parameters are summarized in Table 3.4. The corresponding results of the uncoded ARQ are shown in Fig. 3.7.

in Fig. 3.15. It may be seen from Fig. 3.14(a) that when there is no relay-switching, relay aided H-ARQ using SSR may have a modest gain of 0.5 dB compared to the conventional Scheme C-2 of Table 3.4 using CC. This result is similar to that of the direct transmission Scheme C-1 of Table 3.4. By contrast, Scheme D-3, which employs SSR, may achieve an approximately 1.5 dB gain, when the relays are switched during the retransmission attempts. Furthermore, as seen in Fig. 3.15(b), the throughput curve of Scheme D-3 suggests that an approximately 2 dB lower $E_b/N_0$ is required than that of Scheme C-3 in the $E_b/N_0$ region between 0 dB to 5 dB. This implies that Scheme D-3 may increase the attainable throughput of the system.

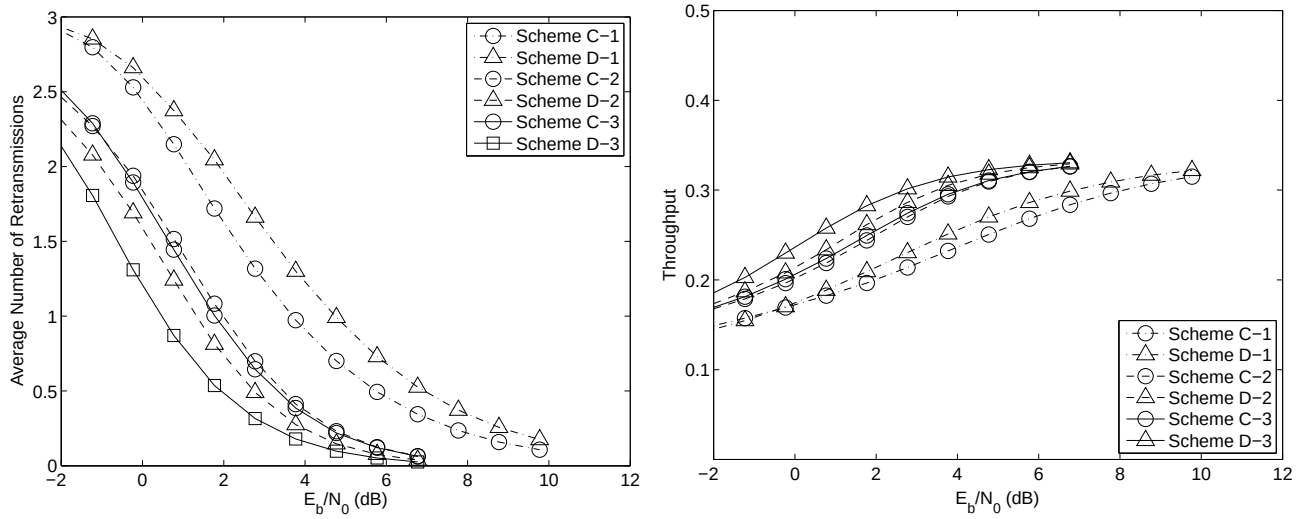


(a) Average number of retransmissions vs $E_b/N_0$

(b) Throughput vs $E_b/N_0$

Figure 3.15: The average number of retransmissions and the throughput performance of turbo coded H-ARQ of Fig. 3.1 employing direct, AF and DF cooperation employing CC and SSR for transmissions over the correlated Rayleigh fading channels at the normalized Doppler frequency of $10^{-3}$. All other parameters are summarized in Table 3.3. The corresponding results of the uncoded ARQ are shown in Fig. 3.8.

## 3.4 Systematic Luby Transform Coded H-ARQ in Wireless Cooperative Network

Recently, a number of researchers have focused their attention on the employment of rateless codes in relay-aided networks for the sake of increasing the achievable communication efficiency and robustness [166–169]. Briefly, a rateless code has a rate determined by the number of transmitted symbols required before the decoder become capable of decoding the received information. In contrast to the fixed-rate block codes, the rate is unknown a priori. Typically, they are characterized by a single parameter $K$, the length of the information block in bits. By comparison, fixed-rate block codes, such as the family of Reed-Solomon and turbo codes, are often characterized by the parameter pair $(K, N)$, where $N$ defines the codeword length. The transmission of a rateless codeword is terminated, when the receiver successfully decodes the message and uses a feedback channel to return an ACK to the transmitter. Therefore, a rateless code does not have a fixed rate, but rather the rate is determined 'on the fly' by the codeword-length, which becomes sufficiently long for the receiver to decode the message.

The family of fountain codes [170] not only has a low complexity, but it is also capable of approaching the capacity for diverse classes of channel models. Luby Transform (LT) codes, introduced by Luby in [38] were shown to approach the capacity of Binary Erasure Channels (BEC). However, LT codes might exhibit an error floor for a small block length $K$. In order to eliminate the error floor, Raptor codes were proposed by Shokrollahi in [39], which invoke LT codes as an inner code, while a high-rate LDPC code is employed as the outer code of a two-stage concatenated architecture. This arrangement is capable of approaching capacity for the BEC, despite its modest linear-time encoding

and decoding complexity. By contrast, Nguyen *et al.* [40] proposed Systematic LT codes (SLT), which invoke iterative decoding for preventing the potential avalanche-like inter-packet error propagation. Other rateless codes have been proposed in [166,171,172] for both the AWGN channel and for various types of fading channels. As shown in [166,171,172], rateless codes are capable of reliably operating for transmissions over diverse classes of channels, since they are capable of adapting their coding rates to the channel quality without any knowledge of the channel state information or even channel statistics at the transmitter.

Since they are capable of adapting to the channel conditions without requiring any channel knowledge at the transmitter, existing rateless codes are beneficial in relay-aided networks. Castura and Mao [166–168] proposed a coding framework for wireless relay channels based on rateless codes. Furthermore, Nikjah and Beaulieu [173, 174] studied the average throughput of DF based half-duplex as well as full-duplex rateless coded relaying schemes under a specific peak power constraint and an average power constraint. The development of rateless codes as well as their applications in relay networks is summarized in Table 3.5. In line with the prevalent trends, in this section we will investigate the performance of SLT codes in the context of cooperative wireless networks. Furthermore, their iterative detection will be proposed in order to improve the relay-aided system's performance, where the soft-output SLT decoder exchanges soft information with the 16-QAM modem.

## 3.4.1 Iterative Decoding Aided Systematic Luby Transform Codes

### 3.4.1.1 Systematic Luby Transform Codes

LT codes [38] were originally designed for the BEC [11], where each packet is either perfectly received, or lost for example owing to network-congestion at one of the routers. The LT codes transmit an appropriately designed number of redundant packets in order to fill these packet erasure events. However, when LT codes are employed for transmission over wireless channels, which impose both fading and inter-symbol interference, in addition to packet erasures, each LT codeword might become corrupted, which results in catastrophic inter-packet error propagation during LT decoding [182]. As illustrated in Fig. 3.16, the errors of the first packet after the first LT decoding cycle are propagated to the second and third packets after five decoding cycles. As a result, more and more decoding errors appear, when the number of decoded packets increases. In order to mitigate the deleterious effects of error propagation, LT codes have been frequently combined with classic physical-layer FEC codes [182, 183]. The idea of combining classic FEC codes with LT codes by directly amalgamating them was proposed in [40], where systematically concatenated parity bits were incorporated in order to create the family of SLT codes.

The soft-output LT decoding process is based on the classic concept of LDPC decoding [37]. Given a LT code $\boldsymbol{C}$, a generator matrix $\boldsymbol{G}$ of $\boldsymbol{C}$ is a matrix whose rows generate all the elements of $\boldsymbol{C}$, i.e., if $\boldsymbol{G} = (g_1\ g_2\ ...\ g_k)^T$, then every codeword $\boldsymbol{w}$ of $\boldsymbol{C}$ can be uniquely represented as

$$\boldsymbol{G} = c_1 g_1 + c_2 g_2 + ... + c_k g_k = \boldsymbol{cG}, \tag{3.16}$$

where we have $\boldsymbol{c} = (c_1\ c_2\ ...\ c_k)$. Then the Parity Check Matrix (PCM) $\boldsymbol{H}$ of a LT code, which checks a codeword $\boldsymbol{c}$ is in $\boldsymbol{C}$ if and only if the following matrix-vector product satisfies $\boldsymbol{Hc} = 0$, which is calculated similarly to procedures of a classic LDPC code. More specifically, a LT code's generator

Table 3.5: Major rateless code contributions and their applications in cooperative wireless communications.

| | | |
|---|---|---|
| 2002 | Luby [38] | Introduced LT codes, the first rateless erasure codes. |
| 2004 | Shokrollahi [39, 175] | Introduced Raptor codes, an extension of LT-codes with linear time encoding and decoding. |
| 2005 | MacKay [170] | Presented Fountain codes that are 'record-breaking' sparse-graph codes for channels subjected to packet erasures. |
| 2006 | Castura and Mao [166] | Proposed a framework for communication over fading channels utilizing rateless codes. |
| 2007 | Castura and Mao [167, 168] | Proposed a coding framework for wireless relay channels based on rateless codes. |
| | Puducheri *et al.* [169] | Designed distributed LT codes for wireless relaying networks. |
| | Nguyen *et al.* [40] | Presented systematic LT codes and their soft decoding. |
| 2008 | Nikjah and Beaulieu [173, 174] | Studied the average throughput of DF half-duplex as well as of DF full-duplex rateless coded relaying schemes under a specific peak power constraint and an average power constraint. |
| | Yuan and Ping [176] | Proposed a family of systematic rateless codes that are capacity-approaching on a binary erasure channel, regardless of the channel's erasure rate. |
| 2009 | Liu and Lim [130] | Discussed cooperative protocols based on Fountain codes in a relay network. |
| | Bonello [177, 178] | Proposed reconfigurable rateless codes, that are capable of varying the block length as well as adaptively modifying their encoding strategy. |
| | Cheng *et al.* [179] | Designed Raptor codes for binary-input AWGN channels using the mean-LLR-EXIT chart approach presented. |
| 2010 | Gong *et al.* [180] | Considered the code design for a half-duplex 4-node joint relay system with two sources, one relay, and one destination, employing superposition coding and Raptor coding. |
| | Fan *et al.* [181] | Studied the performance limits and design principles of rateless codes over MIMO fading channels. |

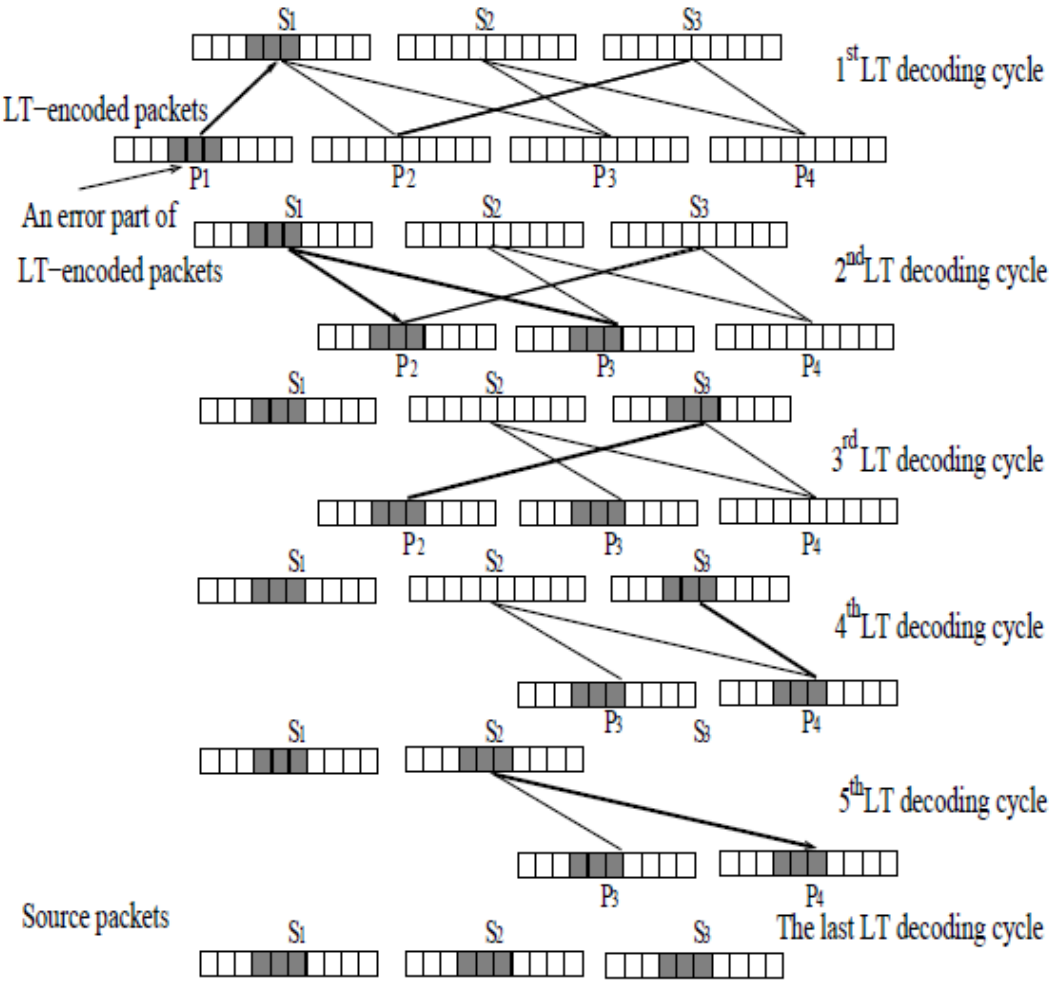


Figure 3.16: An example of error propagation in the LT hard-decoding process, when the LT decoder receive packets corrupted by channel noise (©Nguyen *et al.* [40]).

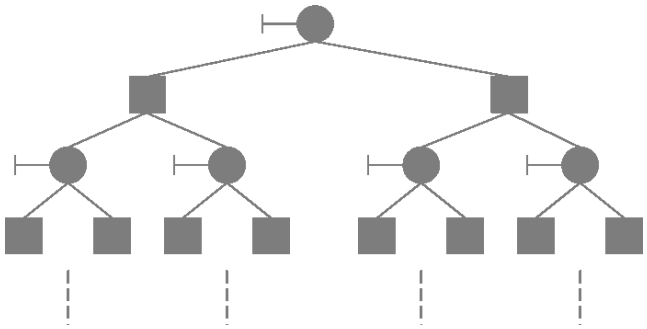

Figure 3.17: Tree-based representation of LT codes

matrix $\boldsymbol{G}_{(K\times N)}$ is partitioned into two matrices, namely $\boldsymbol{A}$ and $\boldsymbol{B}$ having a size of $(K \times K)$ and $(K \times M)$ elements, respectively. If $\boldsymbol{A}$ is a non-singular matrix, then the PCM is calculated as [37]

$$\boldsymbol{H}_{(M\times N)} = [(\boldsymbol{B}^T \cdot (\boldsymbol{A}^T)^{-1})_{(M\times K)} | \boldsymbol{I}_{(M\times M)}], \tag{3.17}$$

where $\boldsymbol{I}_{(M\times M)}$ is $(M \times M)$-element identity matrix.

An LT PCM can be represented by a classic Tanner graph [171]. To elaborate a little further, the filled circles and the filled squares of Fig. 3.17 represent the variable nodes - or synonymously the information nodes - and the parity check nodes of the LT code, respectively, while the horizontal lines connected to the variable nodes correspond to the intrinsic information provided by the channel's output. Let us assume that the circular node at the top of Fig. 3.17 represents the $k^{th}$ variable node in the block of $N$ single-bit LT encoded packets, which is also termed as a root node. The root node receives extrinsic parity-check information from the specific check nodes that are directly connected to it at the tree-level immediately below it, as seen in Fig. 3.17. Similarly, these check nodes also receive extrinsic information from the specific variable nodes they are directly connected to at the next level down in Fig. 3.17, etc. The dotted lines in Fig. 3.17 indicate that the above process is repeated further by expanding the tree. The number of connections associated with a variable node of the LT code - excluding the line representing the intrinsic information - indicates the column weight of this particular message node, while the number of connections associated with an LT check node represent the corresponding row weight. The column weight and row weight of the LT PCM are related to the degree distribution of LT packets. The LT decoding process is implemented in the same way as the classic LDPC decoding procedure. Initially, the LT decoder's soft values are set to a value corresponding to the demodulator's soft output. The decoder's soft values of $R^a_{i,j}$ and $Q^a_{i,j}$, which denote the LLRs - as detailed in Section 2.2.4.4 of Chapter 2 - are then passed from the check nodes to the variable nodes and vice versa, which are then iteratively updated after each decoding iteration as follows [40]:

$$tanh\Big(\frac{R_{i,j}}{2}\Big) = \prod_{n\in\{C_i\}, n\neq i} tanh\Big(\frac{Q_{n,j}}{2}\Big). \tag{3.18}$$

The LT decoder outputs its tentative hard decision values after each iteration and then checks whether the product of the corresponding codeword and the transpose of the PCM $\boldsymbol{H}$ is equal to zero, i.e whether a legitimate codeword was produced. If not, the LT decoding process will be continued in an iterative fashion, until the output codeword becomes legitimate or the maximum affordable number of iterations is exhausted.

In order to improve the achievable performance, the LT code's degree distribution, which will be detailed below, is created by expanding its $(K \times N)$-element generator matrix $\boldsymbol{A}$ with the aid of attaching a unity matrix having a size of $(K \times K)$, resulting in a systematic code [40]. For example, if we have a generator matrix $\boldsymbol{G}_{K\times N} = [\boldsymbol{I}_{K\times K} | \boldsymbol{A}_{K\times M}]$, where $(N = K + M)$, as shown in Fig. 3.18, then the PCM $\boldsymbol{H}$ is calculated as

$$\boldsymbol{H} = [\boldsymbol{A}^T | \boldsymbol{I}']. \tag{3.19}$$

#### 3.4.1.2 Degree Distributions

Each SLT code is characterized by the distributions of the degree of message nodes, $d_m$ and the degree of the parity nodes $d_c$, which represents the number of connections or 'edges' between the received

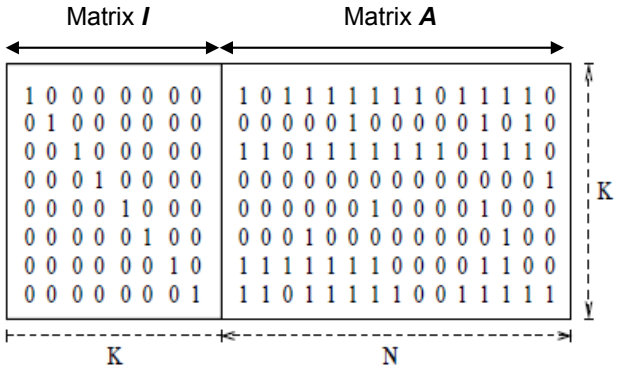


Figure 3.18: SLT generator matrix.

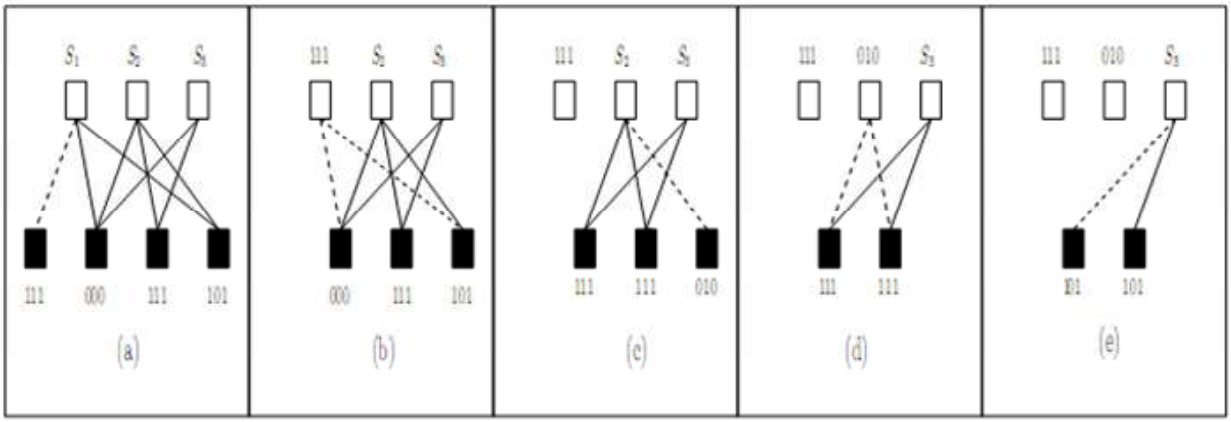


Figure 3.19: Decoding of a LT code having $K = 3$ source packets and $N = 4$ transmitted packet each containing three bits, where the decoding cycles are shown in Fig. 3.16 (©Tee *et al.* [182]).

packets and the original source packets, as seen in Fig. 3.19. A number of different degree distributions have been proposed in [38,182,184] for the parity nodes of LT as well as SLT codes. The most simple distribution termed as the 'ideal soliton distribution' was proposed in [38]

$$\rho(d_c) = \begin{cases} 1/K & \text{for } d_c = 1, \\ \frac{1}{d_c(d_c-1)} & \text{for } d_c = 2, 3, ..., K, \end{cases} . \tag{3.20}$$

When no degree-one packet is recovered at any state of Fig. 3.19 of the consecutive LT decoding cycle seen in Fig. 3.16, the decoding process is terminated and the remaining packets may not be recovered, unless a high number of redundant packets are received. In order to overcome this problem, Luby [38] proposed the so-called 'Robust Solition Distribution' (RSD), which increases the number of degree-one encoded packets to $S \triangleq c \cdot ln(K/\delta)\sqrt{K}$, where the parameter $\delta$ denotes the probability of decoding failure imposed by the lack of the degree-one packets, while $c$ represents a constant. Furthermore, the following term is defined as

$$\tau(d_c) = \begin{cases} \frac{S}{K}\frac{1}{d_c} & \text{for } d_c = 1, 2, .., \frac{K}{S} - 1, \\ \frac{S}{K} ln\left(\frac{S}{\delta}\right) & \text{for } d_c = \frac{K}{S}, \\ 0 & \text{for } d_c > \frac{K}{S}. \end{cases} \tag{3.21}$$

Then the RSD $\mu(d_c)$ is obtained by combining the 'ideal soliton distribution' $\rho(d_c)$ with $\tau(d_c)$ of Eq. (3.21), yielding

$$\mu(d_c) = \frac{\rho(d_c) + \tau(d_c)}{Z}, \tag{3.22}$$

where $Z = \sum_{d_c} \rho(d_c) + \tau(d_c)$ represents the normalization factor of the denominator.

In order to improve the achievable LT coding performance, in [182] the 'Improved Robust Soliton Distribution' (IRSD) was proposed by introducing the extra factor of:

$$\nu = \sum \mu(d_{c,i}) \cdot K, \tag{3.23}$$

where $d_{c,i}$ represents the degree-$i$ term of the distribution, satisfying the following conditions

$$\begin{cases} \frac{\frac{1}{d_c(d_c-1)} + \frac{S}{K}\frac{1}{d_c}}{Z} \cdot K < 1 & \text{for } 2 \leq d_c \leq \frac{K}{S} - 1, \\ \frac{1}{d_c(d_c-1)} \cdot \frac{K}{Z} < 1 & \text{for } \left(\frac{K}{S} + 1\right) \leq d_c \leq K, \end{cases} . \tag{3.24}$$

Consequently, the IRSD is defined as [182]

$$D(d_c) = \begin{cases} \frac{1+S+\nu}{ZK} & \text{for } d_c = 1, \\ \frac{1}{Z}\left(\frac{1}{d_c(d_c-1)} + \frac{S}{K} \cdot \frac{1}{d_c}\right) & \text{for } 2 \leq d_c < \frac{K}{S}, \\ \frac{S}{ZK} \cdot ln\frac{S}{\delta} & \text{for } d_c = \frac{K}{S}, \\ 0 & \text{for } d_c > \frac{K}{S}, \end{cases} . \tag{3.25}$$

where we have $Z = \sum_{d_c} \rho(d_c) + \tau(d_c) + \nu(d_c)$.

In order to achieve further improvements, Nguyen *et al.* [184] proposed the 'Truncated Degree Distribution' (TDD) of

$$\Omega(d_c) = \begin{cases} \frac{1}{Z}\left[1 + \frac{S}{K} + \nu(d_c)\right] & \text{for } d_c = \gamma, \\ \frac{1}{Z}\left[\frac{\gamma}{d(\frac{\gamma}{d}+1)} + \frac{S}{K}\frac{\gamma}{d}\right. & \text{for } d_c = 2\gamma, \cdots, \frac{K\gamma}{S} - 1, \\ \frac{S}{ZK} ln\frac{S}{\delta} & \text{for } d_c = \frac{K\gamma}{S}, \\ 0 & \text{for } d_c > \frac{K\gamma}{S} \text{ or } d_c = 1, \end{cases} . \tag{3.26}$$

where we have $Z = \sum_{d_c}[\rho(d_c) + \tau(d_c)] + \nu(\gamma)$, while $\gamma$ is an integer number higher than one, which is required for ensuring that the degree distribution becomes a truncated degree distribution.

As demonstrated in [184], SLT codes using the TDD achieved a better BER performance than conventional quasi-regular LDPC codes in single-antenna aided systems. Therefore, the TDD will be employed in our investigations in this section.

Finally, the degree distribution of the message nodes $d_m$ is defined as

$$D[d_m(\bar{d}_c)] = \frac{K}{N}, \tag{3.27}$$

where $\bar{d}_c$ denotes the average degree of the parity nodes.

#### 3.4.1.3 ID-SLT Coded 16-QAM Aided H-ARQ

When utilizing Soft Input and Soft Output (SISO) information for iterative decoding, the SLT decoder exchanges extrinsic information with the 16-QAM demodulator, which also uses SISO information in

its bit-to-symbol demapping process, through a pair of interleaver and de-interleaver components. This model is shown in Figure 3.20, where the soft output of the demodulator is fed forward to the SLT decoder. After carrying out SLT decoding using the procedures of Section 2.2.4.4, the resultant extrinsic information is fed back to the demodulator as the *a-priori* information. The demodulator then exploits both the *a-priori* information and the channel's output information, which is demapped to bits and passed to the SLT decoder of Section 3.4.1.1 again. This process continues, until the syndrome checking condition of the SLT decoder is satisfied, indicating that a legitimate SLT codeword was received or the affordable number of iterations was exhausted. The exchange of *extrinsic* information with the demodulator will enhance the attainable decoding performance of the SLT decoder. Consequently, a significant coding gain is achieved by the system. The performance of the iterative decoding process might be beneficially visualized by EXIT charts [89], which was detailed in Section 2.2.4.4.

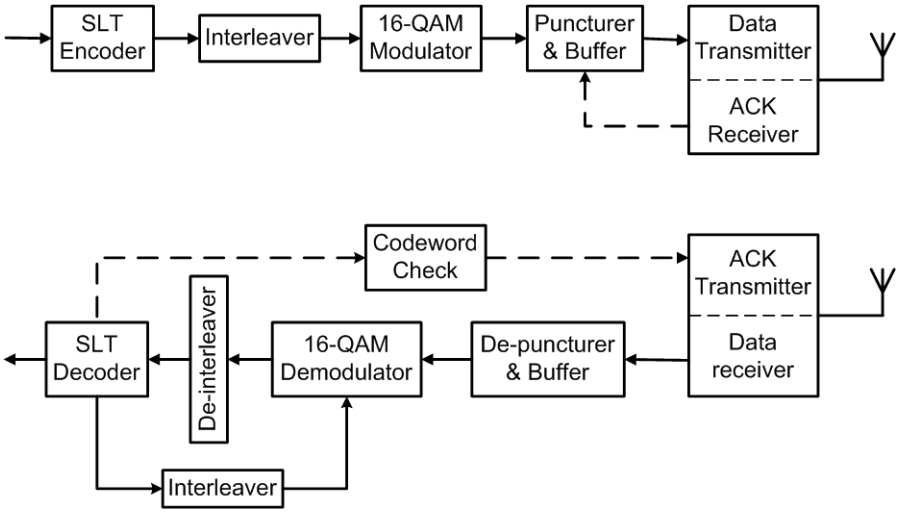


Figure 3.20: Block diagram of the ID-SLT coded 16-QAM H-ARQ scheme, which employs the iterative detection philosophy detailed in Section 2.2.4.4.

Typically, the classic Gray bit-to-symbol mapping scheme is the best in non-iterative arrangements, but it does not benefit from iterative decoding [23]. Hence, in this study a more beneficial bit-to-symbol mapping scheme relying on a philosophy reminiscent of Ungerboeck's classic set-partitioning (SP) [185] based mapping scheme was chosen for the demodulator.

### 3.4.2 H-ARQ with Incremental Redundancy for ID-SLT Coding

As discussed in Chapter 1, there are two basic types of H-ARQ schemes, namely the Type-I H-ARQ and the Type-II H-ARQ. The transmitter of the classic Type-I H-ARQ scheme typically retransmits all the information and parity bits of corrupted packets, when a negative acknowledgement (ACK) is received, while the receiver simply drops erroneous packets [186]. In the H-ARQ type II scheme, the information part and the parity part are sent together during the first transmission attempt. However, during the second transmission attempt no previously sent information is retransmitted - instead, additional parity information is transmitted. There are also two ways of information combining in H-ARQ protocol, namely Chase Combining [162] and Incremental Redundancy (IR-HARQ) [187]

exploitation. When the different received replicas are combined in the soft-value domain, the resultant technique is referred to as the H-ARQ scheme using Chase Combining. In fact, the method simply boosts the received SNR after Chase combining, but it does not provide an additional coding gain nor does it increase the achievable effective throughput. By contrast, the Type-II H-ARQ relies on the above-mentioned IR-HARQ exploitation, where the transmitter sends additional redundancy during the retransmission stages. The receiver combines the additional redundant bits with those received before, in order to recover the original information bits. Naturally, in contrast to Chase combining, this method is expected to provide an increased coding gain at the receiver. Based on these advantages, in this section the SLT coded H-ARQ scheme using IR is invoked for our system.

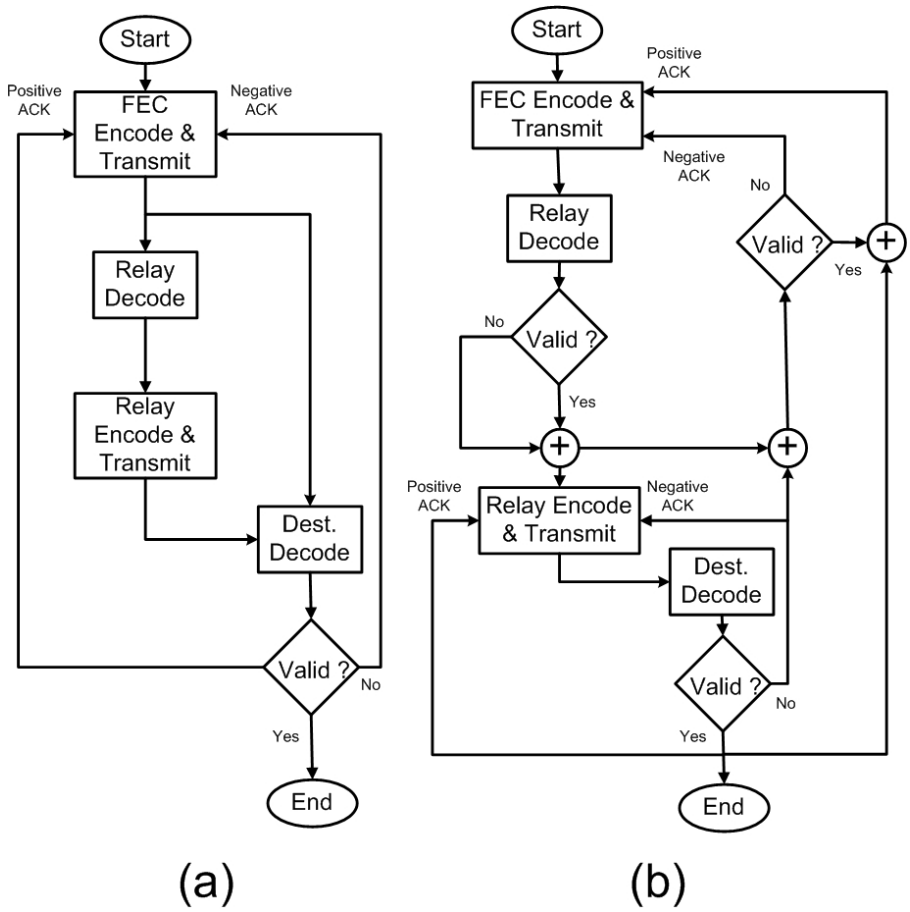


Figure 3.21: IR-HARQ algorithms conceived for cooperative relay networks:
a. The passive-cooperative IR-HARQ,
b. The active-cooperative IR-HARQ, where the relay directly activates retransmission, instead of waiting for retransmitted packets from the relay.

The IR-HARQ aided SLT coding scheme is shown in Fig. 3.20. As shown in this figure, the information bits are FEC encoded and modulated, before they are passed to the puncturing and buffering components. A carefully selected fraction of the parity bits is punctured, i.e. simply not transmitted, in order to achieve the highest possible code rate during the first transmission, while storing the untransmitted punctured bits for later IR transmissions, as and when needed. In the receiver, the SLT decoder and the syndrome checking block will generate a status signal in order to inform the transmitter about the outcome of the CRC check operation. If a positive ACK is received corresponding to a legitimate decoded code word, the buffered parity bits that were previously

punctured will be deleted. Otherwise, additional IR is transmitted, until we reach the maximum affordable number of IR transmissions. In this treatise, the original cooperative IR-HARQ scheme is termed as the *"passively-cooperative IR-HARQ"*.

Additionally, an *"actively-cooperative IR-HARQ"* scheme is proposed for cooperative wireless networks. There, both the relay's and the destination's receivers feed their decoding status back to the source. If negative ACKs are received from both the RS and the DS, the IR transmission is carried out as usual. By contrast, if a negative ACK is received from the DS and a positive ACK is received from the RS, the IR transmissions are activated only at the relay, while the source remains idle. Clearly, this arrangement requires the collaboration among all stations, especially the assistance of the RS. Note that this IR-HARQ procedure is only suitable for the DF cooperative scheme and that the IR transmissions require extra timeslots, which improves the achievable transmission integrity at the cost of reducing the delay.

During the IR transmissions of the actively-cooperative IR-HARQ scheme, only a single version of the signal may have arrived from the RS to the DS. Thus, there may not be any spatial diversity gain. To compensate for the resultant diversity loss, the relay may choose to increase its transmit power. This power allocation may be deemed fair, because the source has not utilized its power during the IR transmissions, provided of course that the total transmit power remains constant. The associated power consumption will be quantified in the next section.

The actively-cooperative scheme here can be seen as an instance of the Harbinger protocol [140]. However, the scheme does not always prove to be more effective than its passively cooperative counterpart. Hence, in the following section we will investigate the conditions under which the actively-cooperative scheme performs better.

### 3.4.3 Achiveable Capacity and Transmit Power

The achievable capacity and power requirements of both the passively- and actively-cooperative IR-HARQ schemes of Fig. 3.21 are quantified in this section. Based on these quantitative results, we will propose measures to assist the "actively-cooperative" scheme in performing more efficiently at a lower transmit power than the "passively-cooperative" one. For the sake of a convenient analysis, in the actively cooperative IR-HARQ scheme, the IR transmissions are divided into two time slots as well. During the first time slot, the RS's transmit power is set to $P'_R$, while in the second slot, it is set to $P_R$.

Let us assume that during the first transmission of the passively-cooperative scheme, the source transmits $m_c$ bits, and in each IR transmission it transmits additional $l_c$ bits, while the number of IR transmissions is $n \in \{1, 2, ...n_{max}\}$, where $n_{max}$ is the maximum number of IR transmissions. For the actively-cooperative scheme, the first transmission is the same as that of the passive cooperative scheme. The number of IR transmissions at both the source and the RS is denoted as $n_s$, while the number of IR transmissions at the RS only is $n_r$. Also note that we have to obey $n_s + n_r = n$ to make the comparison between the two systems a fair one.

#### 3.4.3.1 Achievable Capacity

**Passively-cooperative scheme**

As detailed in Section 3.2.4, the instantaneous capacity of the first transmission of a passively-cooperative single-relay-aided IR-HARQ system in fading channels may be expressed as

$$C_{1^{st},passive} = min\{C^1_{1^{st},passive}, C^2_{1^{st},passive}\}, \tag{3.28}$$

with

$$C^1_{1^{st},passive} = \frac{1}{2}log_2\left(1 + \frac{P_S|h_{sr}|^2}{d^\alpha_{sr}N_0} + \frac{P_S|h_{sd}|^2}{d^\alpha_{sd}N_0}\right), \tag{3.29}$$

$$C^2_{1^{st},passive} = \frac{1}{2}log_2\left(1 + \frac{P_S|h_{sd}|^2}{d^\alpha_{sd}N_0} + \frac{P_R|h_{rd}|^2}{d^\alpha_{rd}N_0}\right). \tag{3.30}$$

Averaging Eqs. (3.29) and (3.30) over the probability density function of the Rayleigh distribution and applying the same processes as in [188], the average capacity of the first transmission becomes

$$\bar{C}_{1^{st},passive} = min\left\{f\left(\frac{P_S}{d^\alpha_{sr}N_0}\right),\ f\left(\frac{P_S}{d^\alpha_{sd}N_0} + \frac{P_R}{d^\alpha_{rd}N_0}\right)\right\}, \tag{3.31}$$

where we have [188]

$$\begin{aligned} f(x) &= -log_2e \cdot e^{-1/x}Ei\left(\frac{-1}{x}\right) \\ &= -log_2e \cdot e^{-1/x}\int_1^\infty \frac{e^{-tx}dt}{t}, \end{aligned} \tag{3.32}$$

with $Ei(y)$ being the exponential-integral function [188].

Similarly, the average capacity of each IR transmission of a passively-cooperative single-relay-aided IR-HARQ system in fading channels is given by

$$\bar{C}_{IR,passive} = min\left\{f\left(\frac{P_S}{d^\alpha_{sr}N_0}\right),\ f\left(\frac{P_S}{d^\alpha_{sd}N_0} + \frac{P_R}{d^\alpha_{rd}N_0}\right)\right\}. \tag{3.33}$$

Hence, the average capacity of a passively-cooperative single-relay-aided IR-HARQ system in fading channels may be expressed as

$$\begin{aligned} \bar{C}_{passive} &= \frac{m_c}{m_c + nl_c}\bar{C}_{1^{st},passive} + \frac{nl_c}{m_c + nl_c}\bar{C}_{IR,passive} \\ &= \frac{m_c}{m_c + nl_c}\bar{C}_{1^{st},passive} + \frac{n_sl_c}{m_c + nl_c}\bar{C}_{IR,passive} + \frac{n_rl_c}{m_c + nl_c}\bar{C}_{IR,passive}. \end{aligned} \tag{3.34}$$

**Actively-cooperative scheme**

When the relay succeeded in decoding a packet correctly and actively transmitted the requested IR information only, the system's instantaneous capacity is given by

$$C_{IR,active} = \frac{1}{2}log_2\left(1 + \frac{P'_R|h'_{rd}|^2}{d^\alpha_{rd}N_0} + \frac{P_R|h_{rd}|^2}{d^\alpha_{rd}N_0}\right). \tag{3.35}$$

Subsequently, its average capacity during the active IR transmission is expressed as

$$\bar{C}_{IR,active} = f\left(\frac{P'_R}{d_{rd}^{\alpha}N_0} + \frac{P_R}{d_{rd}^{\alpha}N_0}\right). \tag{3.36}$$

Noted that the source stop sending IR information only, when the decoding process at the relay is successful. Therefore, the average capacity of an actively-cooperative single-relay-aided IR-HARQ system in fading channels may be expressed as

$$\bar{C}_{active} = \frac{m_c}{m_c + nl_c}\bar{C}_{1^{st},passive} + \frac{n_s l_c}{m_c + nl_c}\bar{C}_{IR,passive} + \frac{n_r l_c}{m_c + nl_c}\bar{C}_{IR,active}. \tag{3.37}$$

**Capacity Comparison of Active and Passive H-ARQ Cooperation**

The difference between Eqs. (3.34) and (3.37) manifests itself in the third term. Therefore, the capacity of the actively-cooperative scheme is higher than or equal to that of the passively-cooperative one, if $\bar{C}_{active} \geq \bar{C}_{passive}$. In other words, the relay's allocated power and its position have to satisfy the following condition,

$$\left\{f\left(\frac{P'_R}{d_{rd}^{\alpha}N_0} + \frac{P_R}{d_{rd}^{\alpha}N_0}\right)\right\} \geq min\left\{f\left(\frac{P_S}{d_{sr}^{\alpha}N_0}\right),\ f\left(\frac{P_S}{d_{sd}^{\alpha}N_0} + \frac{P_R}{d_{rd}^{\alpha}N_0}\right)\right\}. \tag{3.38}$$

### 3.4.3.2 Transmit Power of Active and Passive H-ARQ Cooperation

The average total transmit energy of each symbol of the passive cooperative single-relay-aided IR-HARQ system is expressed as

$$\begin{aligned}\bar{P}_{passive} &= P_S + P_R \\ &= \frac{(m_c + nl_c)(P_S + P_R)}{m_c + nl_c} \\ &= \frac{(m_c + n_s l_c)(P_S + P_R)}{m_c + nl_c} + \frac{n_r l_c (P_S + P_R)}{m_c + nl_c},\end{aligned} \tag{3.39}$$

while that of the actively-cooperative single-relay-aided IR-HAQR system is calculated by replacing $P_S$ in the second term of Eq. (3.39) by $P'_R$, yielding

$$\bar{P}_{active} = \frac{(m_c + n_s l_c)(P_S + P_R)}{m_c + nl_c} + \frac{n_r l_c (P'_R + P_R)}{m_c + nl_c}. \tag{3.40}$$

It may be inferred from Eqs. (3.39) and (3.40) that $\bar{P}_{passive} \geq \bar{P}_{active}$ if the following condition is satisfied

$$P'_R \leq P_S. \tag{3.41}$$

Based on the analysis provided above, it is concluded that both Inequalities (3.38) and (3.41) must be satisfied to allow the "actively-cooperative scheme" achieve a higher capacity with less transmit power compared to the "passively-cooperative scheme", if the three stations collaborate.

The channel capacity of the passively- and actively-cooperative schemes is shown in Figure 3.22, where we have $P_{source} = 0.67$, $P_{relay} = 0.33$, $P'_{relay} = 0.33$ and $d_{sr} = d_{rd} = 0.5d_{sd}$. Clearly, the actively-cooperative scheme may achieve the same or higher capacity than the passively-cooperative

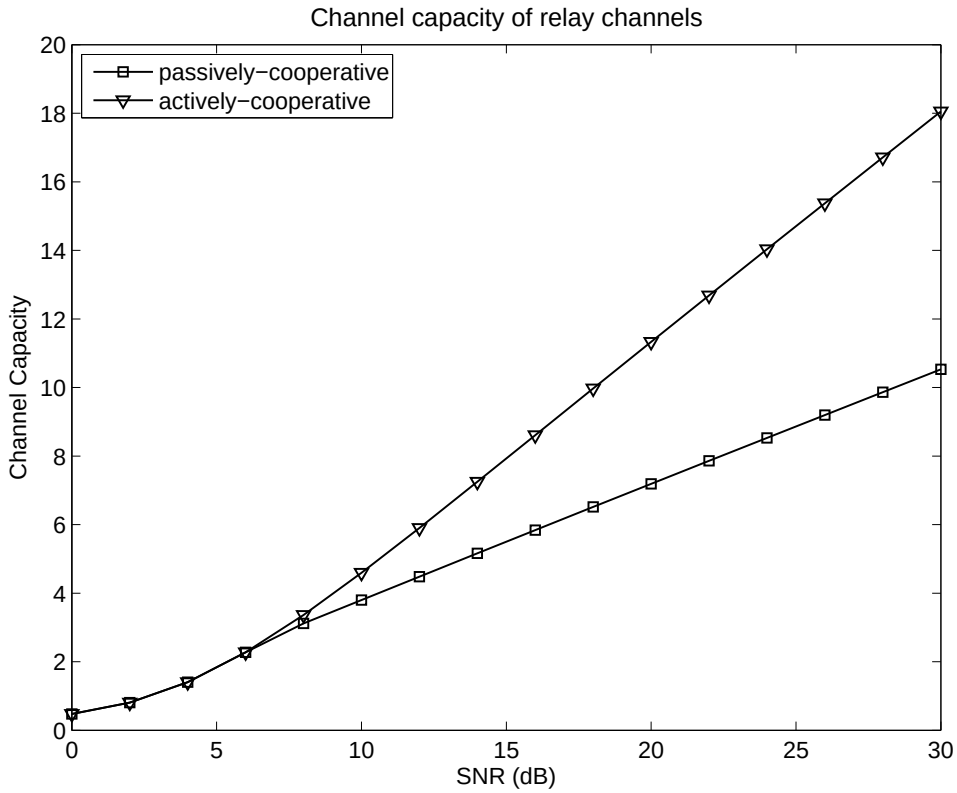


Figure 3.22: Channel capacity of cooperative schemes communicating in uncorrelated Rayleigh fading channels: $P_{source} = 0.67$, $P_{relay} = 0.33$, $P'_{relay} = 0.67$, $d_{sr} = d_{rd} = 0.5d_{sd}$

one. This fact implies that the relay's position and power arrangement in the actively-cooperative scenario indeed satisfied the required conditions.

Both these schemes impose, however, a factor two multiplexing loss due to splitting a time slot into the broadcasting and relaying phases, as described in Section 3.4.2. In order to recover the multiplexing loss, the so-called successive relaying [126, 189], which was described in Section 2.3.3.2, may be applied to our scheme.

### 3.4.4 Performance of Relay-Aided ID-SLT Coded H-ARQ

The BER performance of the ID-SLT coded 16QAM scheme of Figure 3.20 is shown in Figure 3.23. The half-rate SLT code $\{1200, 2400\}$ is used for all three investigated schemes, including the direct transmission, AF and DF arrangements. The detailed parameters of each scheme can be seen in Table 3.6. It is observed in Figure 3.23 that there is an approximately $2.5dB$ gain, when the 16-QAM mapper and the SLT decoder iteratively exchange their extrinsic information in the context Scheme-1 of Table 3.6. Introducing AF relaying in Scheme-2 provides only a slightly improvement of about $0.2dB$. As mentioned before, AF relaying simply amplifies the received signal at the relay and then forwards it. Thus it does not benefit from the coding gain of SLT coding. A clearer view is provided by the EXIT chart [23] of Figure 3.24. There is only a tiny gap between the EXIT functions of Scheme-1 and Scheme-2 of Table 3.6, which explains why AF relaying provides only insignificant benefits for the ID-SLT coded 16-QAM system. By contrast, Scheme-3 of Table 3.6 first recovers and then re-encodes the source's bits at the relay. Thus, this process benefits from the coding gain of the SLT

Table 3.6: ID-SLT coded 16-QAM schemes' parameters. The system architecture is shown in Fig. 3.20.

| Parameters | **Scheme-1** | **Scheme-2** | **Scheme-3** |
|---|---|---|---|
| Relaying type | none | AF | DF |
| N$^o$ of data bits | 1200 | 1200 | 1200 |
| SLT code rate | 1/2 | 1/2 | 1/2 |
| Degree distribution type | TDD | TDD | TDD |
| Modulation type | 16-QAM | 16-QAM | 16-QAM |
| N$^o$ of outer iterations of SLT decoders | 8 | 8 | 8 |
| N$^o$ of inner iterations between SLT decoder & 16-QAM demapper at Relay | unavailable | unavailable | 0, 2 & 4 |
| N$^o$ of inner iterations between SLT decoder & 16-QAM demapper at Destination | 0 & 4 | 0 & 4 | 0 & 4 |
| Channel type | uncorrelated Rayleigh | uncorrelated Rayleigh | uncorrelated Rayleigh |

code. Therefore, its performance becomes substantially better than that of the two previous schemes. More particularly, a $3dB$ gain was achieved for the same system even without inner iterations between the SLT decoder and the 16-QAM symbol-to-bit demapper. There is a further gain of approximately $2.5dB$, when four inner iterations are applied at the relay. Further insights are provided by Figure 3.25. In this figure, the EXIT chart reveals that at $E_b/N_0 = 4dB$ there is a widely open EXIT-tunnel for Scheme-3, which is not the case for Scheme-1 and Scheme-2. This implies that the DF relaying scheme, namely Scheme-3 of Table 3.6, is expected to outperform the two remaining schemes.

Although not explicitly shown here, we found that changing the number of inner decoding iterations at the relay also affects the signal quality at the destination. When increasing the number of inner iterations from one to two without increasing the number of inner iterations at the destination's receiver, the required SNR is reduced by about $1dB$. However, no additional obvious improvements are attained, when the number of iterations is further increased, as evidenced by the two overlapped curves of Scheme 3 in Fig 3.23. This fact may be explained by the EXIT chart of Figure 3.26, where an open tunnel does exist, when there are two or four inner iterations at the relay, while it does not appear for a single iteration. Explicitly, an open tunnel emerges at $2dB$ for two or more iterations. However, the difference between the EXIT functions of two and four iterations is extremely small. This is why the performance does not substantially improve, when there are four iterations between the demapper and SLT decoder of Fig. 3.20 at the relay.

Figure 3.27 illustrates our BER results for Scheme-2 and Scheme-3 of Table 3.6 at different source powers $P_{source}$. We assumed that the total transmit power was fixed to unity, and the position of the RS is fixed right at the mid-point between the source and the DS. In Scheme-2, the BER degrades, when the sources' power is increased. An $E_b/N_0$ difference of 2dB emerges, when increasing the sources' power from 0.33 to 0.80. However, the system performs best at $P_{source} = 0.5$ in the context of Scheme-3. Both increasing and decreasing the sources' power will degrade the BER.

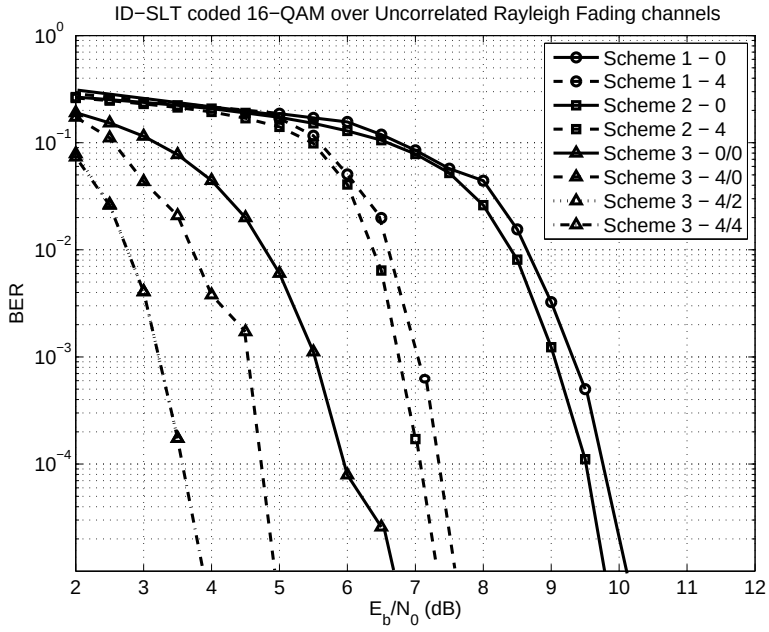


Figure 3.23: BER of the ID-SLT coded 16-QAM schemes as shown in Fig. 3.20 using the parameters of Table 3.6. Notes:

• Scheme A - x: Scheme A uses x inner iterations between the SLT decoder and 16-QAM demapper.

• Scheme B - y/z: Scheme B uses y inner iterations between the SLT decoder and 16-QAM demapper at the DS; and uses z inner iterations between the SLT decoder and 16-QAM demapper at the RS.

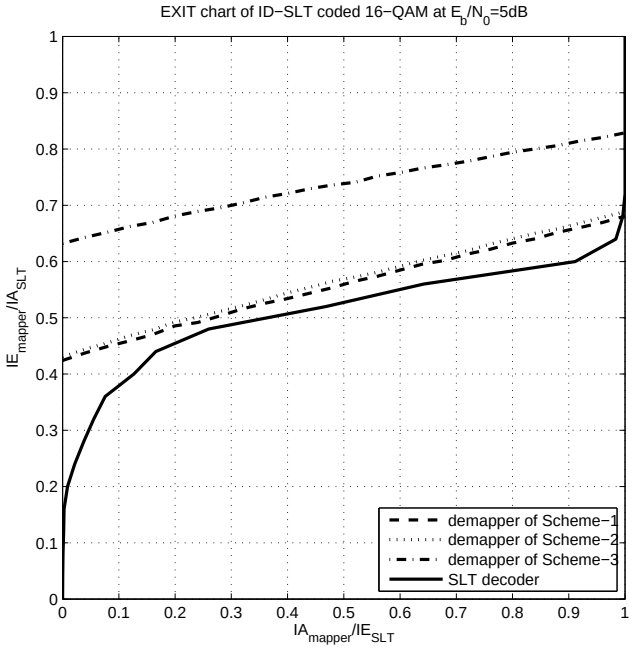


Figure 3.24: EXIT chart for the ID-SLT coded 16-QAM schemes as shown in Fig. 3.20 using the parameters of Table 3.6 for transmissions over uncorrelated Rayleigh fading channels at $E_b/N_0 = 5dB$. The corresponding BER performance is shown in Fig. 3.23.

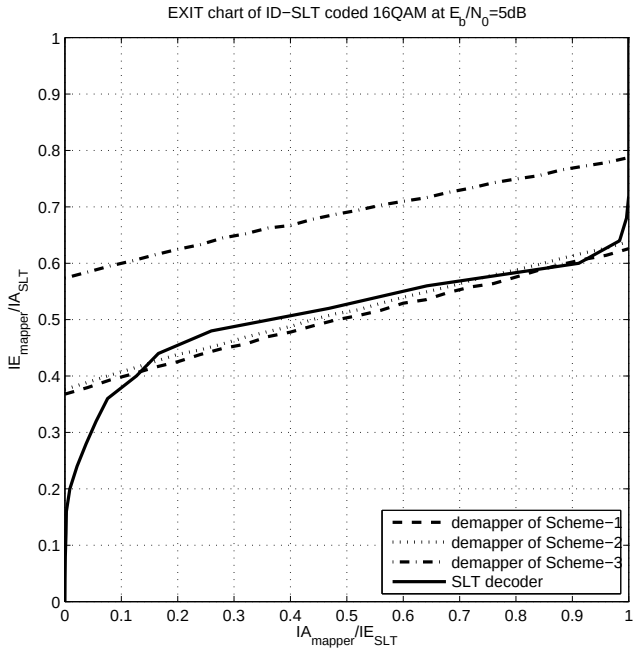


Figure 3.25: EXIT chart for the ID-SLT coded 16-QAM schemes as shown in Fig. 3.20 using the parameters of Table 3.6 for transmissions over uncorrelated Rayleigh fading channels at $E_b/N_0 = 4dB$. The corresponding BER performance is shown in Fig. 3.23.

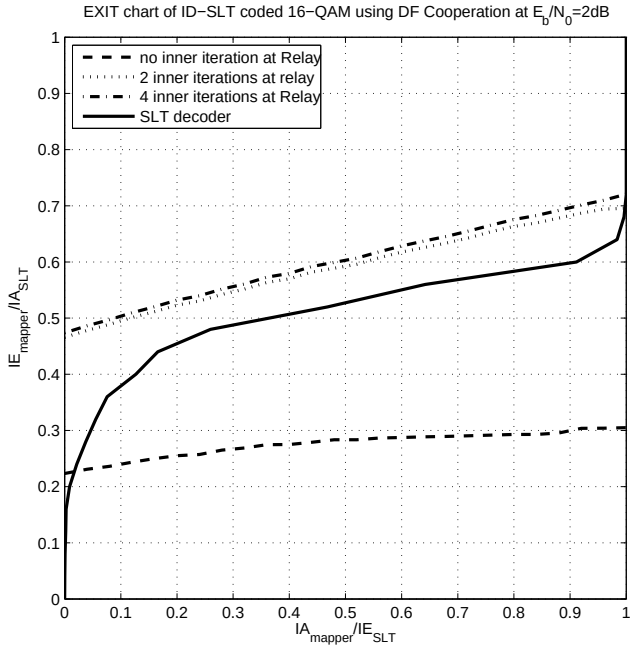


Figure 3.26: EXIT chart for the ID-SLT coded 16-QAM schemes as shown in Fig. 3.20 using the parameters of Table 3.6 as well as DF cooperation (Scheme-3) for transmissions over uncorrelated Rayleigh fading channels at $E_b/N_0 = 2dB$. The corresponding BER performance is shown in Fig. 3.23.

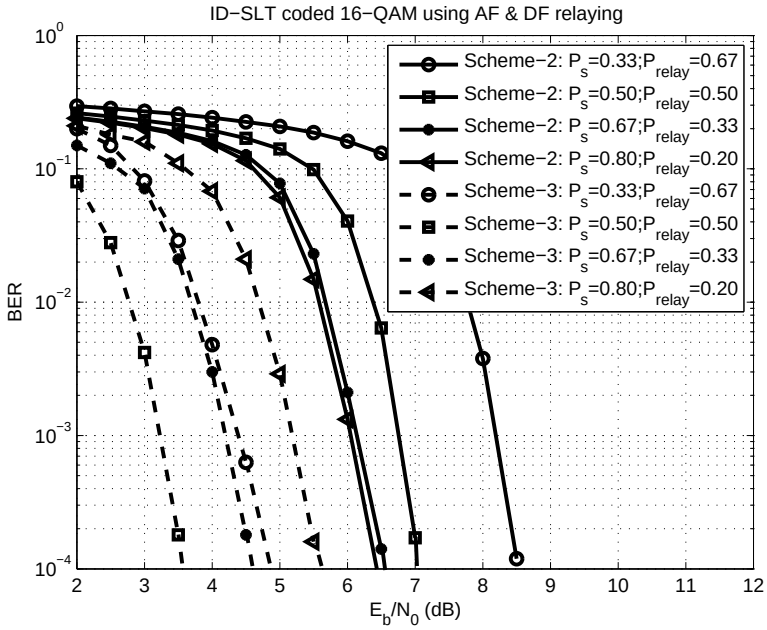


Figure 3.27: BER of the ID-SLT coded 16-QAM scheme as shown in Fig. 3.20 using the parameters of Table 3.6 for transmissions over uncorrelated Rayleigh fading channels in conjunction with AF and DF cooperation using different normalized source powers of $P_{source} = \{0.33, 0.50, 0.67, 0.80\}$ and $P_{relay} = 1 - P_{source}$; and normalized distance of $d_{sr} = 0.5$ and $d_{rd} = 1 - d_{sr}$. The BER performance of the equal source-relay power allocation using relays at the mid-point is shown in Fig. 3.23.

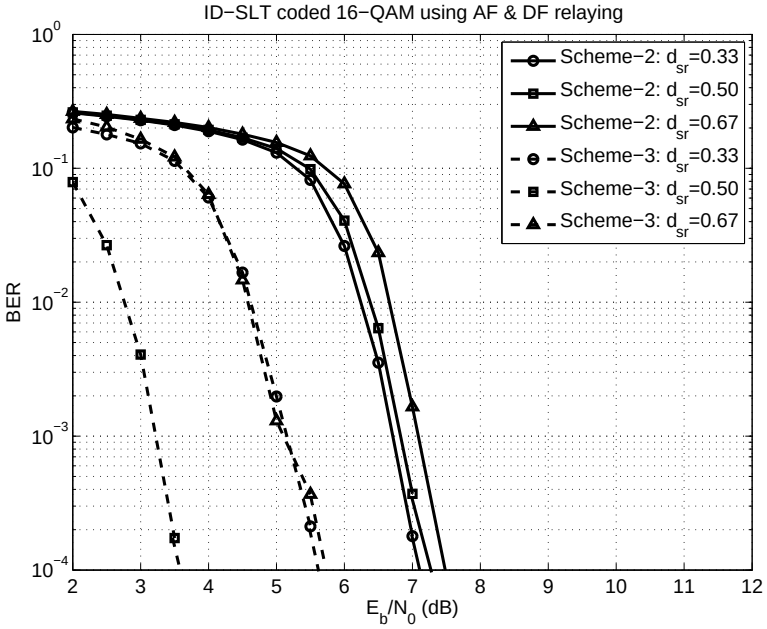


Figure 3.28: BER of the ID-SLT coded modulation scheme as shown in Fig. 3.20 using the parameters of Table 3.6 for transmissions over uncorrelated Rayleigh fading channels in conjunction with AF and DF cooperation using normalized source powers of $P_{source} = 0.50$ and $P_{relay} = 1 - P_{source}$; and different normalized distance of $d_{sr} = \{0.33, 0.50, 0.67\}$ and $d_{rd} = 1 - d_{sr}$. The BER performance of the equal source-relay power allocation using relays at the mid-point is shown in Fig. 3.23.

Table 3.7: HARQ/ID-SLT coded 16-QAM schemes' parameters

| Parameters | **Scheme-A** | **Scheme-B** | **Scheme-C** |
|---|---|---|---|
| Relaying type | none | passive DF | active DF |
| N$^o$ of data bits | 1000 | 1000 | 1000 |
| SLT code rate | 1/3 | 1/3 | 1/3 |
| N$^o$ of bits of $1^{st}$ transmission | 2000 | 2000 | 2000 |
| Maximum n$^o$ of IR transmissions | 5 | 5 | 5 |
| N$^o$ of bits per IR transmission | 200 | 200 | 200 |
| Degree distribution type | TDD | TDD | TDD |
| Modulation type | 16-QAM | 16-QAM | 16-QAM |
| N$^o$ of outer iter. | 8 | 8 | 8 |
| N$^o$ of inner iter. at RS | unavailable | 4 | 4 |
| N$^o$ of inner iter. at DS | 4 | 4 | 4 |
| Rayleigh fading type | uncorrelated | uncorrelated | uncorrelated |

In Figure 3.28 we assumed that the transmit powers at both the source and relay were 0.5, and the normalized distance between the source and the destination is unity. It can be observed in the figure that Scheme-2 performs slightly better, when the relay gets closer to the source, i.e. for $d_{sr} = 0.33$. Explicitly, an $E_b/N_0$ improvement of $0.5dB$ is seen, when changing the source-to-relay distance from 0.67 to 0.33. This observation suggests that Scheme-2 performs better for a relatively high received signal quality than for a lower quality, because in the latter case, it may suffer from excessive noise amplification. By contrast, as observed in Figure 3.28, the best location for Scheme-3 appears at $d_{sr} = 0.5$, where relaying achieves a good balance between correcting errors and avoiding error propagation.

Below we will characterize the attainable performance of IR-HARQ aided SLT coding in our wireless relay network. In these simulations, the SLT code $\{1000, 3000\}$, encoding 1000 uncoded bits into 3000 coded bits was chosen, while the other parameters were provided in Table 3.7. The first transmission employs the SLT code $\{1000, 2000\}$, and each IR transmission includes 200 extra bits. The maximum number of IR transmissions is five, which hence corresponds to the SLT code $\{1000, 3000\}$. The source's and relay's transmit powers are 0.67 and 0.33, respectively. If an IR transmission is required and the codeword recovered at the relay is legitimate, the relay will forward the data at a power of $P'_{relay} = P_{source}$. It is also noted that these parameters allow the system to satisfy the conditions outlined in Section 3.4.3.

Fig. 3.29 shows the frame error ratio (FER) for the three scenarios listed in Table 3.7. According to Fig. 3.29, the performances of the actively- and passively-cooperative schemes are comparable, while they both outperformed the classic H-ARQ scheme dispensing with relaying. More particularly, observe in Fig. 3.29 that a power gain in excess of 3 dB may be achieved by the cooperative schemes of Fig. 3.21 compared to direct H-ARQ transmissions. The number of IR transmissions for these schemes is shown in Fig. 3.30. Despite sending an equal number of IR transmissions from the relay, the actively-cooperative Scheme-C of Table 3.7 is capable of significantly reducing the number of IR transmissions at the source in the low $E_b/N_0$ region, namely below $4dB$. Consequently, the actively-

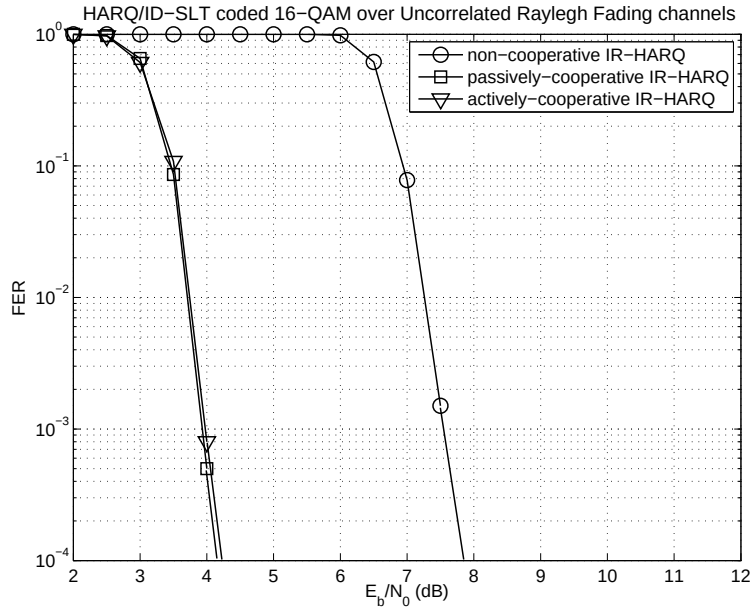


Figure 3.29: FER of the ID-SLT coded 16-QAM schemes as shown in Fig. 3.20 using the parameters of Table 3.7 for transmissions over uncorrelated Rayleigh fading channels.

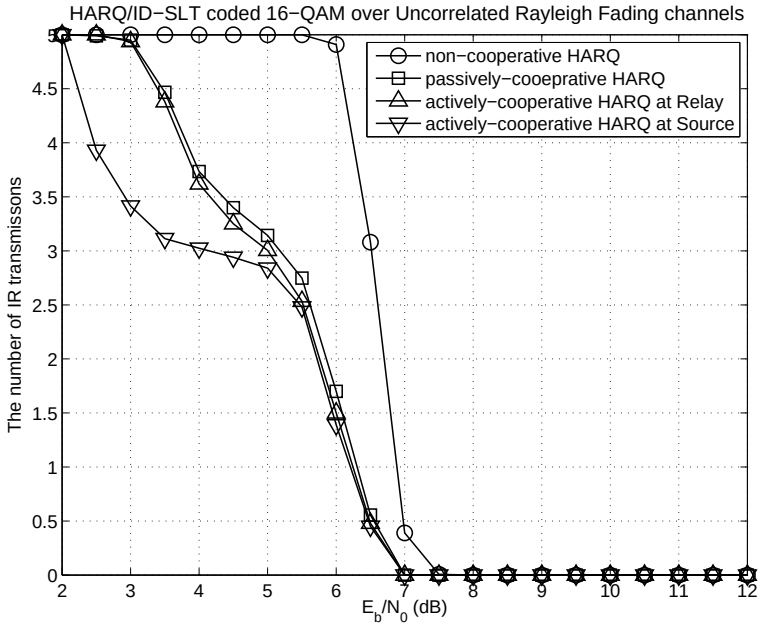


Figure 3.30: The number IR transmissions of the ID-SLT coded 16-QAM schemes as shown in Fig. 3.20 using the parameters of Table 3.7 for transmissions over uncorrelated Rayleigh fading channels. The corresponding FER performance is shown in Fig. 3.29.

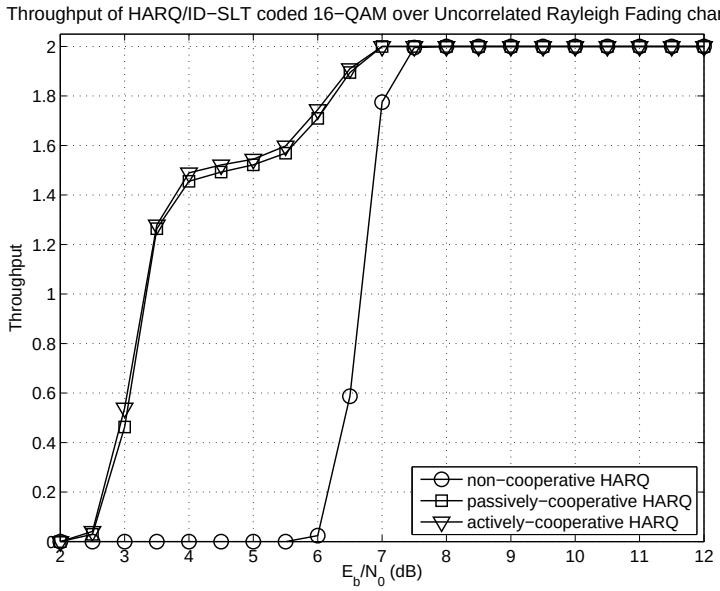


Figure 3.31: Throughput of the ID-SLT coded 16-QAM schemes as shown in Fig. 3.20 using the parameters of Table 3.7 for transmissions over uncorrelated Rayleigh fading channels. The corresponding FER performance is shown in Fig. 3.29, while the number IR transmissions is shown in Fig. 3.30.

cooperative scheme of Fig. 3.21(b) improves both the throughput and transmit power efficiency for the entire system.

The throughput of the three schemes of Table 3.7 is characterized in Fig. 3.31 as a direct consequence of Fig. 3.29 and 3.30. The throughput of Scheme-B and Scheme-C of Table 3.7 is significantly increased in the $E_b/N_0$ region between 3 dB and 7 dB, compared to Scheme-A, where no cooperation was employed. Furthermore, Scheme-C may offer a slightly higher throughput than Scheme-B, despite its lower power consumption. The total transmit power requirements are revealed in Fig. 3.32. In accordance with the number of IR transmission at the source, Scheme-C is capable of reducing the total transmit power by about 5% in the $E_b/N_0$ region between 2 dB and 3.5 dB, but eventually it approaches that of Scheme-C around 6.5 dB.

## 3.5 Chapter Summary

In this chapter the relay-switching scheme aided ARQ system of Fig. 3.2 was proposed for transmission over correlated Rayleigh fading channels, which improved the attainable system performance by reducing the effects of channel envelope correlation, hence providing an increased spatial diversity for signals received at the destination. The results of Figs. 3.5-3.6 demonstrated that the proposed relay-switching scheme not only improves the system's BER as well as FER performance, but additionally reduces the number of retransmissions. Hence, this proposal may beneficially increase the system's performance, reduce transmit power, delay as well as interference. Our performance comparisons amongst the direct as well as relay-aided schemes are briefly summarized in Table 3.8 and Table 3.9.

The relay-switching regimes of Fig. 3.2 was further employed in combination with cooperative TC-HARQ of Fig. 3.1 for transmission over correlated fading channels. The results of Fig. 3.10 showed that an $E_b/N_0$ gain of about 1 dB may be achieved at the BER of $10^{-5}$ at a modestly increased system

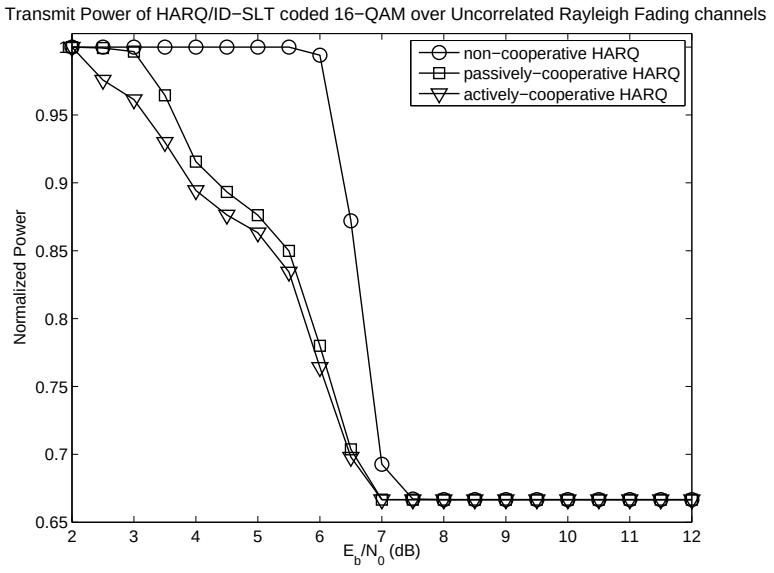


Figure 3.32: Average transmit energy of the ID-SLT coded 16-QAM schemes as shown as shown in Fig. 3.20 using the parameters of Table 3.7 for transmissions over uncorrelated Rayleigh fading channels. The corresponding FER performance and the number IR transmissions are shown in Fig. 3.29 and Fig. 3.30, respectively, while the throughput performance is shown in Fig. 3.31.

Table 3.8: Performance summary of relay-aided ARQ for transmissions over uncorrelated Rayleigh fading channels. The system parameters are provided in Table 3.2.

| | Figure | Direct | AF | DF |
|---|---|---|---|---|
| $E_b/N_0$ at $BER = 10^{-4}$ | 3.5(a) | $\geq$ 3.0 dB | $\geq$ 1.5 dB | $\geq$ 1.5 dB |
| $E_b/N_0$ at $FER = 10^{-3}$ | 3.5(b) | $\geq$ 7.0 dB | $\geq$ 5.1 dB | $\geq$ 4.8 dB |
| $E_b/N_0$ at $\eta_{max} = 2$ | 3.6(b) | $\gg$ 30.0 dB | $\geq$ 30.0 dB | $\geq$ 25.0 dB |

$\eta_{max}$ represents the maximum achievable throughput (bits/symbol).

Table 3.9: Performance summary of relay-switching aided ARQ for transmissions over correlated Rayleigh fading channels at the normalized Doppler of $10^{-3}$. The system parameters are provided in Table 3.2.

| | Figure | Direct | AF | DF | AF-switching | DF-switching |
|---|---|---|---|---|---|---|
| $E_b/N_0$ at $BER = 10^{-4}$ | 3.7(a) | $\geq$ 12.5 dB | $\geq$ 7.0 dB | $\geq$ 7.0 dB | $\geq$ -0.8 dB | $\geq$ 2.5 dB |
| $E_b/N_0$ at $FER = 10^{-3}$ | 3.7(b) | $\geq$ 17.0 dB | $\geq$ 17.0 dB | $\geq$ 10.5 dB | $\geq$ 16.0 dB | $\geq$ 6.0 dB |
| $E_b/N_0$ at $\eta_{max} = 2$ | 3.8(b) | $\geq$ 30.0 dB | $\geq$ 30.0 dB | $\geq$ 25.0 dB | $\geq$ 30.0 dB | $\geq$ 25.0 dB |

$\eta_{max}$ represents the maximum achievable throughput (bits/symbol).

complexity. Additionally, we introduced the TC-HARQ of Fig. 3.1 using SSR and the relay-switching regime of Fig. 3.2 in order to further improve the attainable performance. More particularly, as seen in Fig. 3.14, a gain of approximately 2 dB was achieved across the $E_b/N_0$ region spanning between 0 dB to 5 dB, when the TC-HARQ scheme using SSR was assisted by relay-switching. Our further results are summarized in Table 3.10 and Table 3.11.

Table 3.10: Performance summary of relay-switching aided turbo coded H-ARQ of Fig. 3.1 employing CC and IR combining techniques for transmissions over correlated Rayleigh fading channels at the normalized Doppler of $10^{-3}$. The system parameters are provided in Table 3.3, while the schematic rationale of our comparisons is portrayed in Fig. 3.9.

| | **Figure** | **Scheme** | | | | | |
|---|---|---|---|---|---|---|---|
| | | **A-1** | **A-2** | **A-3** | **B-1** | **B-2** | **B-3** |
| Relaying type | 3.2 | none | AF | AF-switching | none | AF | AF-switching |
| Combining type | | CC | CC | CC | IR | IR | IR |
| $E_b/N_0$ required at $BER = 10^{-4}$ | 3.10(a) | $\geq$ 13.7 dB | $\geq$ 7.8 dB | $\geq$ 7.0 dB | $\geq$ 13.5 dB | $\geq$ 7.5 dB | $\geq$ 6.5 dB |
| $E_b/N_0$ required at $FER = 10^{-3}$ | 3.10(b) | $\gg$ 12.0 dB | $\geq$ 9.0 dB | $\geq$ 7.8 dB | $\gg$ 12.0 dB | $\geq$ 8.8 dB | $\geq$ 7.5 dB |
| $E_b/N_0$ required at $\eta_{max} = 0.5$ | 3.11(b) | $\gg$ 12.0 dB | $\geq$ 12.0 dB | $\geq$ 12.0 dB | $\gg$ 12.0 dB | $\geq$ 12.0 dB | $\geq$ 12.0 dB |

$\eta_{max}$ represents the maximum achievable throughput (bits/symbol).

Furthermore, we conceived the system of Fig. 3.20, which was based on the concatenation of SLT codes and 16-QAM, where the decoder and the demodulator iteratively exchange *extrinsic* information. We demonstrated that the arrangement is capable of providing a significant coding gain for transmission over wireless Rayleigh fading channels, compared to the system where the SLT coding scheme and the demodulator operate independently. More particularly, the simulation results of Figs. 3.23-3.26 showed that when AF and DF relayings were employed along with the proposed SLT coded 16-QAM scheme, the system achieved a gain of about 2.5 dB and 6 dB, respectively, at the BER of $10^{-5}$, compared to the non-iterative detection scheme operating without the relay's assistance. Moreover, we found from Fig. 3.28 that the AF relaying aided SLT coded 16-QAM scheme benefits more substantially, when the relay station is roaming close to the source. By contrast, the DF relaying aided scheme achieves its best performance near the mid-point, as seen in Fig. 3.28. Further results and remarks are provided in Table 3.12. Finally, we improved the system's performance by employing the actively cooperative ARQ protocol of 3.21(b) combined with SLT coding. This arrangement allows the system's total transmit power to be reduced, while increasing its attainable throughput. Specifically, it reduces the number of IR transmissions by approximately 30%, while the total transmit power was reduced by about 5% in the $E_b/N_0$ region between 2 dB and 4 dB. The summary of these actively and passively cooperative is additionally provided in Table 3.13.

Table 3.11: Performance summary of relay-switching aided turbo coded H-ARQ of Fig. 3.1 employing CC and SSR combining techniques for transmissions over correlated Rayleigh fading channels at the normalized Doppler of $10^{-3}$. The system parameters are provided in Table 3.4, while the schematic rationale of our comparisons is portrayed in Fig. 3.13.

| | **Figure** | **Scheme** | | | | | |
|---|---|---|---|---|---|---|---|
| | | **C-1** | **C-2** | **C-3** | **D-1** | **D-2** | **D-3** |
| Relaying type | 3.2 | none | AF | AF-switching | none | AF | AF-switching |
| Combining type | | CC | CC | CC | SSR | SSR | SSR |
| $E_b/N_0$ required at $BER = 10^{-4}$ | 3.14(a) | $\geq$ 7.0 dB | $\geq$ 4.3 dB | $\geq$ 3.5 dB | $\geq$ 6.5 dB | $\geq$ 4.2 dB | $\geq$ 3.0 dB |
| $E_b/N_0$ required at $FER = 10^{-3}$ | 3.14(b) | $\geq$ 9.0 dB | $\geq$ 5.4 dB | $\geq$ 4.5 dB | $\geq$ 8.8 dB | $\geq$ 5.3 dB | $\geq$ 4.2 dB |
| $E_b/N_0$ required at $\eta_{max} = 0.33$ | 3.15(b) | $\geq$ 12.0 dB | $\geq$ 8.0 dB | $\geq$ 8.0 dB | $\geq$ 12.0 dB | $\geq$ 8.0 dB | $\geq$ 8.0 dB |

$\eta_{max}$ represents the maximum achievable throughput (bits/symbol).

Table 3.12: Performance summary of relay-aided ID-SLT coded H-ARQ for transmissions over uncorrelated Rayleigh fading channels. The system parameters are provided in Table 3.6.

| Figure | Parameter | **Scheme-2: AF** | **Scheme-3: DF** | Remark |
|---|---|---|---|---|
| 3.23 | $d_{sr}$ | 0.5 | 0.5 | The AF relaying provided only insignificant benefits for the ID-SLT coded 16-QAM scheme. By contrast, the DF relaying outperforms both the direct and the AF relaying schemes. |
| | $d_{rd}$ | 0.5 | 0.5 | |
| | $P_S$ | 0.5 | 0.5 | |
| | $P_R$ | 0.5 | 0.5 | |
| | $E_b/N_0$ at $BER = 10^{-5}$ | 7.2 dB | 3.9 dB | |
| 3.27 | $d_{sr}$ | 0.5 | 0.5 | For AF scheme, a higher power allocated to the source may avoid the noise amplification, while the equal-power source-relay allocation in DF relaying may strike a balance between the errors being corrected and forwarded. |
| | $d_{rd}$ | 0.5 | 0.5 | |
| | $P_S$ | {0.3,0.5,0.7,0.8} | {0.3,0.5,0.7,0.8} | |
| | $P_R$ | $1 - P_S$ | $1 - P_S$ | |
| | $E_b/N_0$ at $BER = 10^{-5}$ | {8.5,7.0,6.5,6.4} dB | {4.9,3.5,4.6,5.6} dB | |
| 3.28 | $d_{sr}$ | {0.33,0.50,0.67} | {0.33,0.50,0.67} | For AF scheme, the performance slightly changes, when $d_{sr}$ varies from 0.33 to 0.67. By contrast, the relay should stay at the mid-point in the DF scenario. |
| | $d_{rd}$ | $1 - d_{sr}$ | $1 - d_{sr}$ | |
| | $P_S$ | 0.5 | 0.5 | |
| | $P_R$ | 0.5 | 0.5 | |
| | $E_b/N_0$ at $BER = 10^{-5}$ | {7.1,7,2,7.4} dB | {5.6,3.6,5.6} dB | |

Table 3.13: Performance summary of relay-aided ID-SLT coded H-ARQ employing passive- and active-DF-cooperation for transmissions over uncorrelated Rayleigh fading channels. The system parameters are provided in Table 3.7.

| | Figure | **Scheme-A** | **Scheme-B** | **Scheme-C** |
|---|---|---|---|---|
| Relaying type | | none | passive DF | Active DF |
| Algorithm | | | 3.21(a) | 3.21(b) |
| $E_b/N_0$ at $FER = 10^{-3}$ | 3.29 | $\geq$ 7.5 dB | $\geq$ 4.1 dB | $\geq$ 4.1 dB |
| $E_b/N_0$ at $\eta = 1.5$ | 3.31 | $\geq$ 6.8 dB | $\geq$ 4.0 dB | $\geq$ 4.0 dB |
| $E_b/N_0$ at $\eta_{max} = 2$ | 3.31 | $\geq$ 7.5 dB | $\geq$ 7.0 dB | $\geq$ 7.0 dB |

$\eta_{max}$ represents the maximum achievable throughput (bits/symbol).

# Chapter 4

# Imperfect Coherent Detection for H-ARQ Aided Cooperative Wireless Communications

## 4.1 Introduction

Coherent detection is routinely employed in numerous contemporary wireless communication systems, namely in the 3G DS/CDMA [190], HSPA [19] and IEEE 802.11 standards, since it has a 3 dB better power efficiency, than non-coherent schemes. The coherent detectors typically utilize pilot sequences, which are known to both the transmitter and receiver, in order to estimate the channel state information (CSI). The first practical solution was proposed by Cavers [146] in the form of pilot symbol assisted modulation (PSAM). Naturally, the pilots are contaminated by fading, noise and interference. Therefore, the CSI estimation at the receiver is often imperfect, resulting in a degraded performance.

Substantial research efforts have been dedicated to characterising the effects of imperfect detection on the system's performance. For example, the authors of [191, 192] analysed the effects of imperfect Channel Estimation (CE) on the BER of different modulation schemes, such as PSK and QAM. By contrast, [193] concentrated on the wide-band CDMA systems, while that of Sheng and Haimovich [194] investigated the impact of CE errors on Ultra-Wideband (UWB) systems. The authors of [195] and [196] studied the effects of CE on soft decisions in the context of the turbo decoding principle. More recently, the impact of imperfect CSI on ARQ systems was studied in [197, 198] for transmission over Rayleigh fading channels, when using no error correction coding - only an error detection code along with the ARQ protocol was invoked. A number of major contributions, which studied the impact of imperfect CE on the system's performance, are summarized in Table 4.1. In contrast to the systems investigated before, many practical wireless systems employ the H-ARQ protocol combined with a strong FEC code. Therefore, in this chapter we first investigate an H-ARQ scheme using Reed-Solomon (ReS) codes for conventional direct transmission over a block-fading Rayleigh channel. The general transceiver schematic is shown in Fig. 4.1. The proposed arrangement is referred to as the ReS/H-ARQ scheme.

Table 4.1: Major contributions on imperfect-coherent detection.

| Year | Author(s) | Contribution |
|---|---|---|
| 1991 | Cavers [146] | Presented PSAM on a solid analytical basis and provided closed-form expressions for the BER of BPSK and QPSK, as well as a tight upper bound on the SER of 16-QAM. |
| 1998 | Schramm and Muller [191] | Analysed the loss due to imperfect CE and proposed the analytical optimization of pilot symbol spacing for pilot symbol assisted BPSK for fading channels relying on diversity. |
| 1999 | Tang *et al.* [192] | Analysed the BER of M-QAM in flat Rayleigh fading combined with imperfect Channel Estimation (CE), where PSAM was employed. |
| 2000 | Kuo [193] | Derived the analytical BER performance of direct-sequence CDMA, including imperfect CE, while considering the effects of pathloss as well as Rician fading and co-channel interference. |
| | Frenger [195] | Derived a new metric for turbo decoding aided transmissions over Rayleigh fading channels in conjunction with imperfect channel estimates. |
| 2002 | Wang *et al.* [199] | Studied the effects of imperfect channel knowledge on the attainable soft decision performance. |
| 2004 | Cao and Beulieu [200] | Derived the BER of M-QAM relying on PSAM aided CE in static and Rayleigh fading channels for both single branch reception and maximal ratio combining diversity receivers. |
| 2005 | Cai and Giannakis [201] | Analysed the effects of linear Minimum Mean Square Error (MMSE) CE and prediction on the BER of adaptive PSAM. |
| 2006 | Tan and Beaulieu [202, 203] | Analysed the BER of OFDM systems in the presence of CE errors for transmission over Rayleigh and Ricean fading channels. |
| 2007 | Sheng and Haimovich [194] | Investigated the impact of imperfect estimates on ultra-wideband (UWB) system, when path delays and path amplitudes are jointly estimated. |
| 2009 | Cao *et al.* [197, 198] | Evaluated the performance of an ARQ system as a function of the accuracy of CE. |

Table 4.2: Major contributions on imperfect-coherent detection in co-located MIMO communications.

| Year | Author(s) | Contribution |
|---|---|---|
| 2002 | You *et al.* [204] | Provided a time-domain analysis of imperfect CE on OFDM-based spatial multiplexing systems. |
| 2003 | Gu and Leung [196] | Derived closed-form expressions for the BER of the simple Alamouti transmit diversity scheme subjected to receiver CE errors. |
| | Taricco and Biglieri [205–207] | Examined the effects of imperfect CE on the error probability of a frequency-flat slow Rayleigh fading channel in conjunction with multiple transmit and receive antennas. |
| | Ni *et al.* [208] | Analysed the effects of both imperfect CE and of the fading correlation on the performance of ST transmit diversity over correlated Nakagami fading channels. |
| 2004 | Wang and Wang [209] | Studied the effects of imperfect CE on the achievable transmit diversity gain based on STBC for the DL of direct-sequence CDMA. |
| | Chong and Milstein [210] | Analysed the uplink of ST spreading aided CDMA in conjunction with dual transmit and dual receive antennas subjected to the effect of imperfect CE. |
| | Baccarelli and Biagi [211] | Focused on the design and performance evaluation of multiple-antenna aided block-coded systems using imperfect-coherent ML decoding. |
| 2005 | Xiao and Dong [212] | Presented an analysis of diversity selection combining on the attainable performance in Rayleigh fading channels with imperfect CE. |
| 2007 | Li and Kam [213, 214] | Provided the receiver design, performance analysis and code design for STTC for transmission over fading channels with imperfect CSI. |
| 2008 | Bizaki and Falahati [215] | Considered the effect of CE error on Tomlinson-Harashima Precoding (THP) and optimising THP filters together with channel estimators. |
| 2009 | Amihood *et al.* [216] | Evaluated the effects of CE errors on the performance of a system employing THP and the QR decomposition, operating over multiple antenna frequency-flat fading channels. |
| 2010 | Teimouri *at al.* [217] | Provided error probability bounds for concatenated trellis coded modulation or bit-interleaved coded modulation with orthogonal STBC under imperfect CE. |

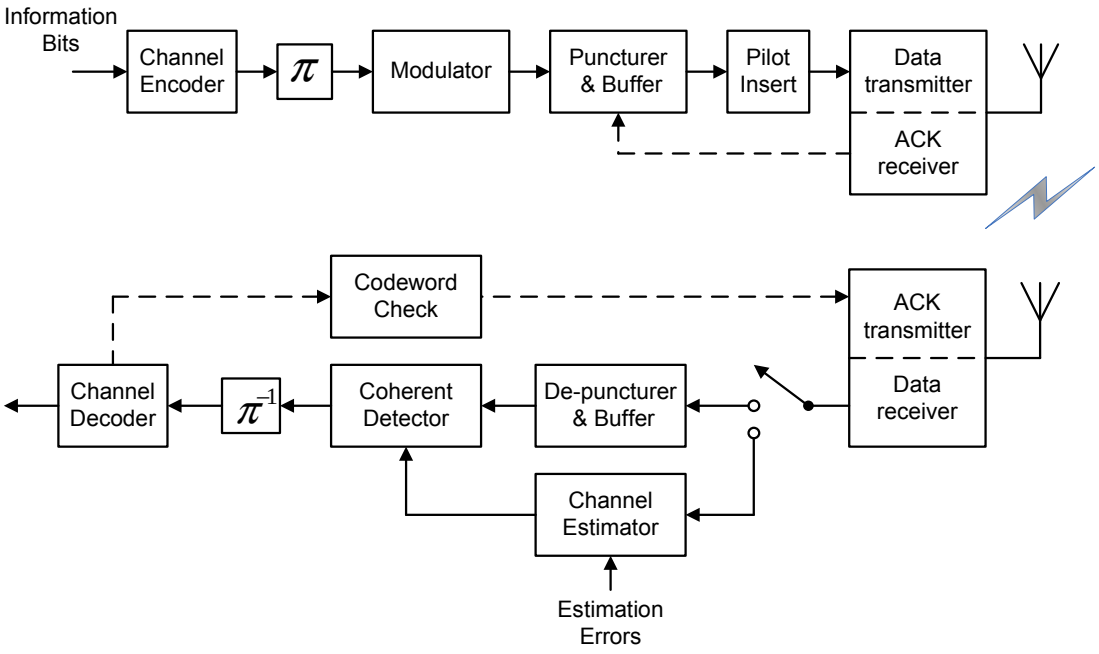


Figure 4.1: Transceiver schematic employing imperfect coherent detection aided H-ARQ. Observe the presence of the channel estimation errors in comparison to Fig.3.1.

We derive the associated goodput equation based on the achievable throughput and the accepted packet error ratio (APER). Due to the dependence of both the throughput and the APER on the CSI, the goodput also varies in accordance with the CSI. Thus, the accuracy of the CSI estimation has an important role in determining the achievable goodput. We use the mean square error (MSE) of the channel estimates as our quality metric. Moreover, it is plausible that the channel estimates' accuracy depends on the energy of pilot symbols. Thus, a power sharing between the uncoded pilot and coded data bits will be proposed in order to maximize the system's goodput.

In the MIMO era, the investigation of imperfect-coherent detection on MIMO systems also attracted a lot of attention. For instance, Cao and Beaulieu [200] investigated the family of imperfect-coherent PSAM systems relying on receive diversity, while Gu and Leung [196] investigated Alamouti's transmit diversity scheme, which was further explored by Wang *et al.* [209] under a more sophisticated system based on STBC and CDMA. Additional contribution are listed in Table 4.2. The investigations have also been further extended to the research area of cooperative MIMO communications. For instance, the authors of [159] have proposed a channel estimator for AF relaying, while a single-relay-aided scenario relying on both orthogonal and non-orthogonal cooperative protocols was considered in [218]. Other major contributions on the imperfect-coherent detection schemes for cooperative communications are provided in Table 4.3. These contributions, however, only considered uncoded systems, albeit all contemporary communication systems employ forward-error-correction (FEC) coding [219].

Against the above-mentioned background, we further investigated the operation of a ReS coded system employed in both AF and DF cooperative networks. Both the Bit Error Probability (BEP) and goodput equations are derived in the context of correlated Rayleigh fading channels in order to analyse the attainable performance of the proposed system. Furthermore, the most appropriate

Table 4.3: Major contributions on imperfect-coherent detection in cooperative MIMO communications.

| Year | Author(s) | Contribution |
|---|---|---|
| 2007 | Patel and Stuber [159] | Addressed the MIMO CE design, the required pilot symbol spacing based upon realistic channel models of cooperative networks, and provided an approximate BER analysis accounting for imperfect CE. |
| 2009 | Gedik and Uysal [218] | Investigated the BER performance of AF relaying with imperfect CE, when a single-relay scenario relying on both orthogonal and non-orthogonal AF cooperative protocols was considered. |
| | Wu and Patzold [220] | Investigated the effects of linear MMSE CE errors on the Symbol-Error-Rate (SER) of a cooperative system operating in AF mode. |
| | Muhaidat *et al.* [221] | Investigated the effects of imperfect CE on the performance of distributed STBCs invoking AF relaying. |
| | Han *et al.* [222] | Evaluated the BER of AF cooperative transmissions using fixed- and variable-gain relaying in the presence of imperfect CE. |
| 2010 | Ikki *et al.* [223, 224] | Investigated the BER performance of a cooperative network using adaptive DF relaying for communication over time-selective frequency-flat Rayleigh fading channels. |
| 2011 | Zhang and Gong [225] | Investigated the impact of imperfect CSI at the transmitter on the diversity gain in dynamic DF relaying and proposed a power control scheme based on imperfect CSI for improving the achievable diversity gain. |
| | Ferdinand and Rajatheva [226] | Presented the performance analysis of a two-hop MIMO beamforming scheme assisted by an AF fixed gain relay system using imperfect CE. |

number of pilot symbols and the corresponding pilot power were determined.

## 4.2 Direct Communications System

### 4.2.1 System Model

We will consider an H-ARQ scheme of Fig. 4.1 operating with the assistance of ReS coding. At the transmitter, the information bits are grouped into blocks of $m$ bits first, generating a symbol. Then a group of $K$ information symbols is forwarded to an $(N, K, t)$ ReS encoder, which is defined over the finite Galois field $GF(2^m)$ and has the code rate of $R = K/N$. Subsequently, the encoded bits are concatenated to $N_p$ pilot bits, which are known to both the transmitter and receiver. No error detection code is required as a benefit of the ReS code's capability of both error detection and

correction [11], provided that the code is sufficiently long [11]. Consequently, as seen in Fig. 4.2, each transmitted packet includes $K$ $m$-bit information symbols, $(N-K)$ $m$-bit parity symbols and $N_p$ pilot bits. Following modulation, the packet is transmitted over the channel. To focus our attention on the H-ARQ scheme, simple BPSK modulation is proposed.

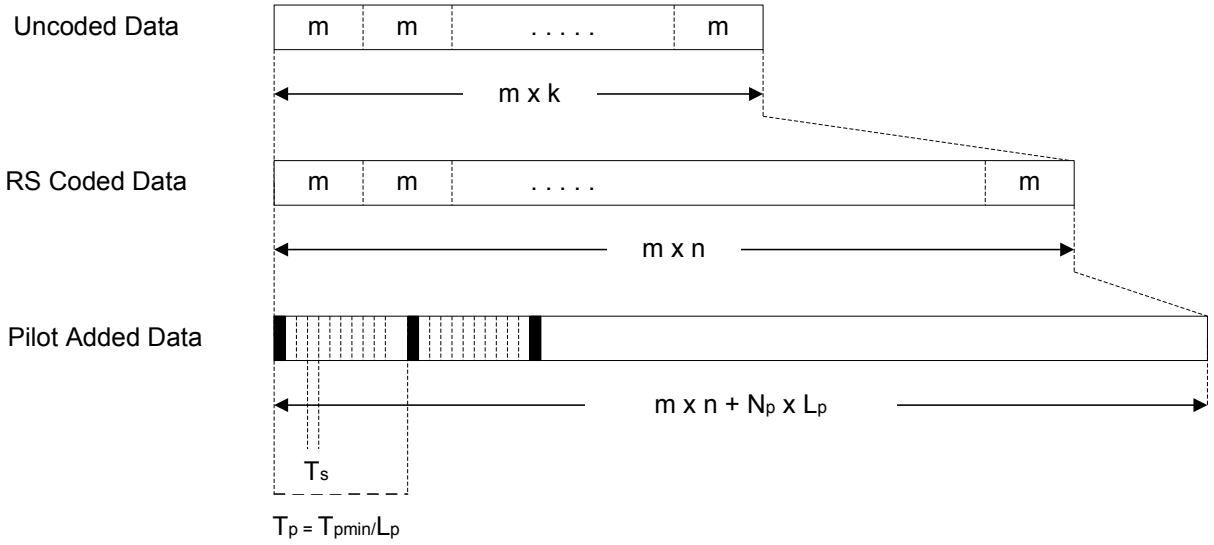


Figure 4.2: Packet structure

The classic Selective Repeat ARQ scheme employing packet buffers both at the transmitter and the receiver is used. Additionally, a block-fading Rayleigh channel is assumed. Then, the received signal may be expressed as

$$\begin{aligned} y_p[k] &= \sqrt{E_p} h x_p[k] + n[k], k = 1, ..., N_p, \\ y_s[k] &= \sqrt{E_s} h x_s[k] + n[k], k = N_p + 1, ..., N_p + n, \end{aligned} \tag{4.1}$$

where $k$ is the symbol index, $y_p[k]$, $y_s[k]$ are the received pilot and data symbols; $x_p[k]$, $x_s[k]$ are the transmitted pilot and data symbols; $n[k]$ is the zero-mean complex AWGN with power spectral density of $N_0$; $h$ represents the Rayleigh fading channel coefficients of having the real part of $Re(h)$ and the imaginary part of $Im(h)$, which are independently and identically distributed (i.i.d) Gaussian random variables with a mean of zero and variance of $\sigma^2/2$. Note that $h$ remains constant during a block, since a block-fading Rayleigh channel is assumed.

At the receiver of Fig. 4.1, the pilot symbols are recovered first in order to estimate the channel gains. Then, the encoded bits are demodulated with the aid of the estimated channel coefficients before being passed to the ReS decoder. The decoder first evaluates the syndromes and checks for errors. If errors are detected, the error correction process is activated. Provided that all errors were successfully corrected, a positive acknowledgement is returned to the transmitter, requesting a new packet. Otherwise, a negative ACK is sent back to request retransmissions.

To recover the channel coefficients, the $N_p$ pilot symbols are fed into the channel estimator, such as a Wiener filter, for generating the estimated version $\hat{h}$ of $h$. According to [227], the minimum mean square error (MMSE) estimate of the Channel Impulse Response (CIR) $\hat{h}$ may be obtained as

$$\hat{h} = \sum_{k=1}^{N_P} w[k] y_p[k], \tag{4.2}$$

where $w[k] = \sigma^2\sqrt{E_p}(N_p\sigma^2E_p+N_0)^{-1}$ is the $k^{th}$ filter coefficient, which remains constant for all values of $k$ due to the block-fading assumption. The resultant CIR estimation MSE is [227]

$$E[|\hat{h}-h|^2] = V^2 = \frac{\sigma^2}{1+N_p\frac{\sigma^2E_p}{N_0}}. \tag{4.3}$$

The estimate $\hat{h}$ is a complex Gaussian random variable with zero mean and a variance of $(\sigma^2 - V^2)$.

### 4.2.2 APER and Goodput

The performance of an ARQ system is typically evaluated in terms of two basic parameters, namely its reliability and throughput. With the assistance of FEC schemes, the reliability of a system may be quantified in terms of the APER, which is defined in [161] as

$$P_E = \frac{P_{ue}}{1-P_{de}}, \tag{4.4}$$

where $P_{ue}$ is the probability of an undetected packet error and $P_{de}$ is the probability of a detected packet error (or probability of retransmission).

The throughput $\eta$ is expressed as [161]

$$\eta = R_e(1-P_{de}) = \frac{Km}{Nm+N_p}(1-P_{de}), \tag{4.5}$$

where $R_e = \frac{Km}{Nm+N_p}$ denotes the effective rate of each packet, since the code-rate of $k/n$ is further reduced by the pilots. Additionally, the probability of retransmission is obtained by subtracting the probability $P_{ue}$ of an undetected packet error from the probability $P_e$ that a received packet contains at least one symbol error. Hence, we have

$$P_{de} = P_e - P_{ue}. \tag{4.6}$$

To evaluate the impact of both the APER and the achievable throughput, the so-called goodput is used, which is defined as the ratio between the expected number of information bits that were correctly received and the number of bits transmitted in a given period of time. In other words, it reflects the ratio of correctly received packets as a fraction of the total throughput, since the latter may contain undetected packet errors. Hence, the goodput $\eta_g$ may be expressed as

$$\eta_g = (1-P_E)\eta. \tag{4.7}$$

### 4.2.3 Impact of Imperfect CE on ReS coded H-ARQ Systems

#### 4.2.3.1 Analysis of CE Error on ReS coded H-ARQ systems

In this section the APER and the goodput of the ReS coded H-ARQ systems subjected to the CE error are derived. The analysis process is based upon the following steps.

- **Step 1.** $P_e$ - Compute the BEP of M-PSK modulated transmission [228].
  $\downarrow$
- **Step 2.** $P_{ue}$ - Estimate the probability of an undetectable codeword error [11].
  $\downarrow$
- **Step 3.** $P_{de}$ - Estimate the probability of retransmission [11].
  $\downarrow$
- **Step 4.** $P_E$ - Calculate the accepted packet error ratio [161].
  $\downarrow$
- **Step 5.** $\eta_g$ - Calculate the goodput [161].

Owing to its direct impact on all of the above-mentioned probabilities, the BEP $p_e$ will be evaluated first. According to [228], if the optimal detection satisfying the minimum symbol error probability criterion is employed at the receiver, the conditional BEP evaluated with the aid of imperfect estimates of the channel gain $\hat{h}$ is given by

$$p_e = \frac{1}{2} erfc\left(\sqrt{\frac{E_s \mid \hat{h} \mid^2 \cdot cos^2\alpha}{E_s V^2 + N_0}}\right), \tag{4.8}$$

where $erfc$ is the complementary error function [66]; $E_s$ is the mean received energy per symbol per diversity channel, $\hat{h}$ is the channel coefficient estimate and $\alpha$ is some angle [228], where the symbol is able to be correctly decoded. For example, $\alpha$ is 0, $\pi/4$ and $3\pi/8$ for BPSK, QPSK and 8-PSK modulation, respectively [229].

We assume that the block-fading channel estimate $\hat{h}$ follows the Rayleigh distribution, which has the Probability Density Function (PDF) of [11]

$$f(\hat{h}) = \frac{\hat{h}}{\sigma^2} e^{-\frac{\hat{h}^2}{2\sigma^2}}. \tag{4.9}$$

Averaging the BEP expression of Eq. (4.8) over the entire range of Rayleigh faded channel estimates, while taking into account their specific probability of occurance described by the PDF of (4.9), the average BEP may be expressed as

$$\begin{aligned} \bar{p_e} &= \int_0^\infty p \cdot f(|\hat{h}|) \cdot d|\hat{h}| \\ &= \int_0^\infty \frac{1}{2} erfc\left(\sqrt{\frac{E_s|\hat{h}|^2}{E_s V^2 + N_0}}\right) \frac{|\hat{h}|}{\sigma^2 - V^2} \cdot e^{-\frac{|\hat{h}|^2}{2(\sigma^2 - V^2)}} d|\hat{h}|. \end{aligned} \tag{4.10}$$

By using the Chernoff bound of $erfc(x) < e^{-x^2}$ [197], the upper bound of the average BEP may be expressed as

$$\bar{p_e} \leq \int_0^\infty \frac{1}{2} e^{-c|\hat{h}|^2} \cdot 2b|\hat{h}| \cdot e^{-b|\hat{h}|^2} d|\hat{h}|, \tag{4.11}$$

where we have

$$b = \frac{1}{2(\sigma^2 - V^2)}, \qquad c = \frac{E_s}{E_s V^2 + N_0}. \tag{4.12}$$

Substituting $z = |\hat{h}|^2$ into the above inequality, we have

$$\bar{p_e} \leq \frac{b}{2} \int_0^\infty e^{-(b+c)z} dz = \frac{-b}{2(b+c)} e^{-(b+c)z} \Big|_0^\infty = \frac{1}{2} \cdot \frac{b}{b+c}. \tag{4.13}$$

A ReS-coded symbol becomes erroneous, when one or more of its $m$ bits is incorrectly received. Thus, the probability of an erroneous ReS-coded symbol is obtained as

$$p_s = 1 - (1 - \bar{p}_e)^m. \tag{4.14}$$

The behaviour of a $(N, K, t)$ ReS code may be analysed by assuming that a specific codeword is transmitted, for example the all-zero codeword. The concept of geometric coding space can be employed for visualizing the decoding situation. For example, Fig. 4.3 demonstrates the coding space containing $(q^t)^N$ words, where only $(q^t)^K$ codewords are legitimate. When the received codeword contains less than $t$ errors, it is within the all-zero codeword's decoding sphere and hence, it is correctable. Thus, the probability of correct decoding is represented by the probability that the received codeword is within the all-zero decoding sphere. By contrast, if the received codewords contains more than $t$ errors, it is uncorrectable, resulting in the incorrect decoding. Then the incorrect decoding is represented by the probability that the received codeword lies within the union of the non-zero codeword sphere. The probability $P_{de}$ of a detectable ReS-codeword now is that of codewords being received outside the union of all the legitimate decoding sphere, yielding

$$P_{de} = 1 - P_{ue} - P_{cd}, \tag{4.15}$$

where $P_{cd}$ is the probability of correct decoding, while $P_{ue}$ represents the undetectable probability of decoding into another legitimate codeword.

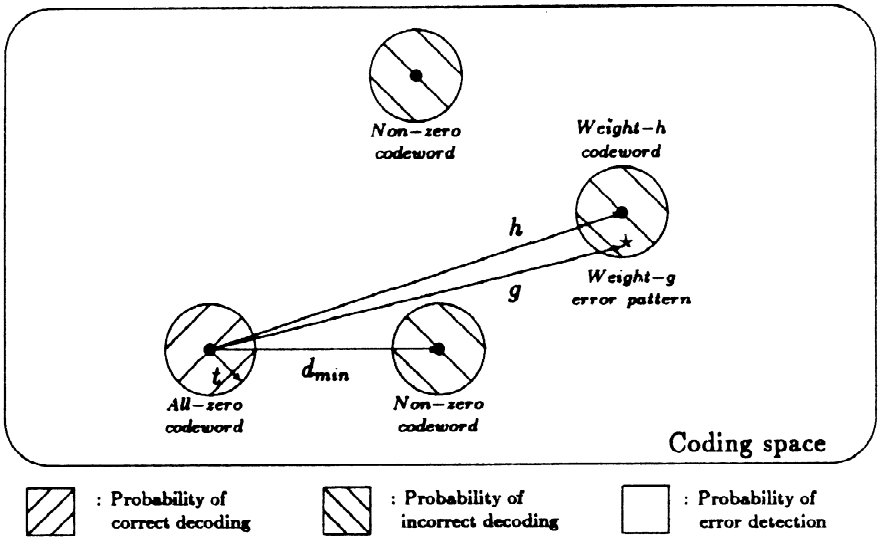


Figure 4.3: Representation of codewords in coding space (©Steele and Hanzo [11], p.445).

An $(N, K, t)$ ReS decoder, designed to correct $t = \lfloor \frac{N-K}{2} \rfloor$ symbol errors, makes a correct codeword decision, when there are less than $t$ symbol errors in a received packet. Therefore, the probability of correct decoding is given as [11]

$$P_{cd} = \sum_{h=0}^{\frac{n-k}{2}} \binom{n}{h} p_s^h (1-p_s)^{n-h}. \tag{4.16}$$

By contrast, the probability of an undetectable ReS-codeword error is obtained as [11]

$$\begin{aligned} P_{ue} &= \sum_{h=d}^{n} \left[ \binom{n}{h} (2^m - 1) \sum_{j=0}^{h-d} (-1)^j \binom{h-1}{j} (2^m)^{h-d-j} \right] \\ &\cdot \sum_{s=0}^{\frac{d-1}{2}} \sum_{g=h-s}^{h+s} \sum_{z=z_{min}}^{z=z_{max}} \binom{h}{h-s+z} \binom{s-z}{g-h+s-2z} \\ &\cdot \binom{n-h}{z} (2^m - 2)^{g-h+s-2z} (2^m - 1)^z \\ &\cdot \frac{1}{(2^m-1)^g} [1-(1-\bar{p}_e)^m]^g [(1-\bar{p}_e)^m]^{n-g}, \end{aligned} \tag{4.17}$$

where we have $d = n - m + 1$, $z_{min} = max\{0, g-h\}$ and $z_{max} = \lfloor \frac{g-h+s}{2} \rfloor$.

Substituting Eq. (4.16) and Eq. (4.17) into Eq. (4.15), the probability $P_{de}$ of retransmission for a given received packet is rewritten as

$$\begin{aligned} P_{de} &= 1 - P_{ue} - \sum_{h=0}^{\frac{n-k}{2}} \binom{n}{h} p_s^h (1-p_s)^{n-h} \\ &= 1 - P_{ue} - \sum_{h=0}^{\frac{n-k}{2}} \binom{n}{h} [1-(1-\bar{p}_e)^m]^h [(1-\bar{p}_e)^m]^{n-h}. \end{aligned} \tag{4.18}$$

Substituting Eqs. (4.14) and (4.17) into Eq. (4.18) yields an explicit formula for the goodput as follows

$$\begin{aligned} \eta_g &= \frac{Km}{Nm+N_p} \left(1 - \frac{P_{ue}}{1-P_{de}}\right)(1-P_{de}) \\ &= \frac{km}{nm+N_p} \sum_{h=0}^{\frac{n-k}{2}} \binom{n}{h} [1-(1-\bar{p}_e)^m]^h [(1-\bar{p}_e)^m]^{n-h}. \end{aligned} \tag{4.19}$$

It may be readily shown that the probability $P_{de}$ of retransmission in Eq. (4.18) is a monotonically decreasing function of the average BEP of $\bar{p}_e$, which will be further elaborated on below. When taking into account the upper bound of the average BEP in Eq. (4.13), the goodput may be shown to be lower bounded by

$$\eta_g \geq \frac{km}{nm+N_p} \sum_{h=0}^{\frac{n-k}{2}} \binom{n}{h} \cdot \left[1 - \left(1 - \frac{b}{2(b+c)}\right)^m\right]^h \left[\left(1 - \frac{b}{2(b+c)}\right)^m\right]^{n-h}. \tag{4.20}$$

#### 4.2.3.2 Power Allocation

Let us assume that the amount of total transmit energy $E_T$ is constant, regardless of the number of pilot symbols transmitted as well as of the number of transmit and receive antennas employed. This assumption implies that the higher the pilot symbols' energy, the lower the data symbols' energy and vice versa. In order to characterize this relationship, let us define a power-allocation factor $\epsilon$, which quantifies the percentage of pilot energy in the total transmit energy. Given this assumption, the amount of energy allocated to pilot symbols becomes $\epsilon E_T = N_p E_p$, while the remaining energy of $(1-\epsilon)E_T = nE_s$ is assigned to the data and parity symbols.

Naturally, assigning a large fraction of the total energy to the pilot symbols, which is equal to the product of $N_p$ and $E_p$, is expected to reduce the MSE of channel estimation. However, this automatically reduces the energy of the useful payload data, hence reducing the average SNR. Consequently, the BEP will increase. Therefore, a specific power allocation scheme is required here, which optimizes the attainable system performance.

As mentioned above, the goodput of the ReS/H-ARQ system is a monotonically decreasing function of the BEP $\bar{p_e}$. However, it may be observed from Eq. (4.13) that the BEP $\bar{p_e}$ is reduced, when the ratio $c/b$ increases. This implies that the goodput is a monotonically increasing function of the variable $c/b$. In order to maximize the goodput of the ReS/H-ARQ system, it is necessary to find the maximum value of $c/b$ in Eq. (4.12). This problem may be simplified to finding the best power-allocation factor of $\epsilon$ by solving the optimization problem of

$$\varepsilon_{opt} = \arg \max_{0<\epsilon<1} \{\eta_g\} = \arg \max_{0<\epsilon<1} \left\{ \frac{c}{b} \right\}. \tag{4.21}$$

This problem was solved in [197] for an uncoded scenario. More particularly, setting the derivative of $c/b$ with respect to $\varepsilon$ equal to zero and solving the resultant quadratic equation, the optimal power-allocation factor $\varepsilon_{opt}$ may be obtained as

$$\varepsilon_{opt} = \frac{n + \gamma - \sqrt{n^2 + n\gamma + n^2\gamma + n\gamma^2}}{-(n\gamma - \gamma)}, \tag{4.22}$$

where $\gamma = E_T\sigma^2/N_0$ represents the ratio of the total transmit power to the noise experienced at the receiver.

As detailed in Appendix IV.A, the value of $\epsilon_{opt}$ is limited as

$$\frac{1-\sqrt{n}}{1-n} \leq \varepsilon_{opt} \leq 0.5. \tag{4.23}$$

### 4.2.4 Numerical Results and Discussions

As mentioned in Section 4.2.2, the goodput reflects the combined impact of both the APER and the throughput. Thus, in this section, we will focus our attention on the goodput results to evaluate the performance of the proposed ReS/H-ARQ system of Fig. 4.1, where the system parameters are provided in Table 4.4.

Fig. 4.4 shows the dependence of the goodput on the normalized CSI MSE and the energy per bit to noise power spectral density ratio for three different code rates, namely for $R = \{0.92, 0.88, 0.84\}$,

Table 4.4: Basic parameters of BPSK aided ReS Coded H-ARQ system of Fig. 4.1.

| Parameters | Value |
|---|---|
| Reed-Solomon code: m/K/N | 8/223/255 |
| Modulation type | BPSK |
| Number of pilot symbols: $N_p$ | 8 |
| Channel model | uncorrelated Rayleigh block-fading |

while fixing the ReS codeword length to 255 symbols ($n = 255$), each of which has 8 bits per symbol ($m = 8$). Fig. 4.4 indicates that the goodput degrades rapidly, when the normalized CSI MSE is above the critical value of $10^{-2}$ for our simulation. This CSI MSE value is achieved at a received $E_b/N_0$ value of around $10dB$, when an equal pilot-data power per symbol is allocated.

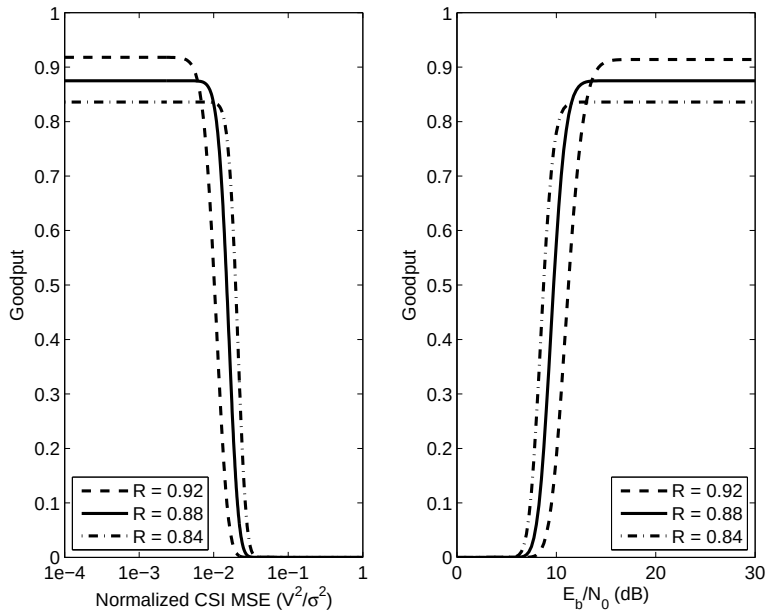


Figure 4.4: Lower bound of the goodput for the ReS/H-ARQ scheme of Fig. 4.1 for transmission over a block-fading, independent Rayleigh channel: $m = 8$, $n = 255$, $N_P = 8$. The system parameters are provided in Table 4.4.

In Fig. 4.5, the goodput of a range of code rates is quantified with the aid of the thin lines for the range of $R = \{0.22, ..., 0.98\}$ in steps of 0.02. The maximum achievable goodput at a specific $E_b/N_0$ value and a given value of $R$ is presented by the bold curve marked with filled circles. A more detailed picture emerges by observing the three-dimensional graph of Fig. 4.6. Clearly, the attainable goodput depends on both the code rate and the $E_b/N_0$. More explicitly, when considering the maximum goodput curve marked by the bold line. Taking a point on the curve and mapping it to the $x$ and $y$ axes, we could identify the best code rate, which provides the maximum goodput at a given value of $E_b/N_0$. It is interesting to note that the goodput does not improve further, when the code rate is reduced below 0.45. Therefore, the code-rate range of $0.45 \div 1$ may be deemed appropriate for the ReS/H-ARQ system associated with $m = 8$ and $n = 255$.

Next, we will investigate the effect of the power allocation regime suggested in Section 4.2.3.2. It can be observed in Fig. 4.7 that the goodput monotonically decreases with the BEP, which has

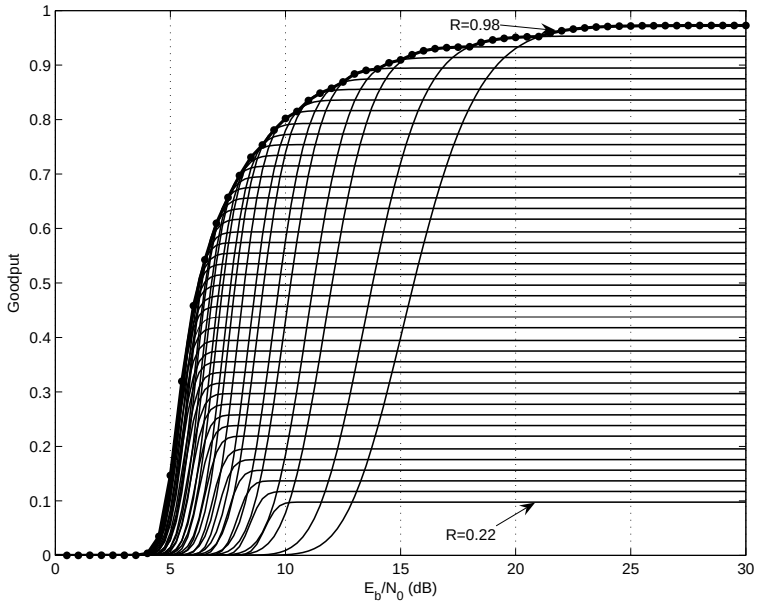


Figure 4.5: Goodput at different ReS code rates for the system of Fig. 4.1 for transmission over a block-fading, independent Rayleigh channel: $m = 8$, $n = 255$, $N_P = 8$, the code rate was varied between $R = 0.22$ and $R = 0.98$ in steps of 0.02. The 3-dimension illustration is shown in Fig. 4.6. The system parameters are provided in Table 4.4.

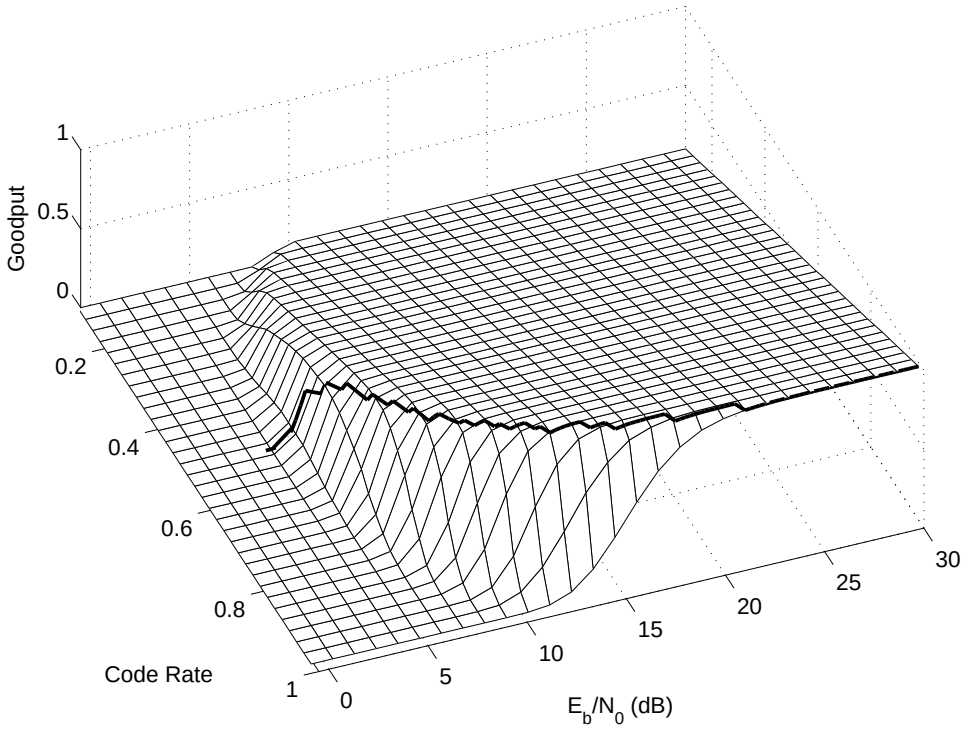


Figure 4.6: Goodput at different ReS code rates for the system of Fig. 4.1 for transmission over a block-fading, independent Rayleigh channel: $m = 8$, $n = 255$, $N_P = 8$, the code rate was varied between $R = 0.22$ and $R = 0.98$ in steps of 0.02. The 2-dimension illustration is shown in Fig. 4.5. The system parameters are provided in Table 4.4.

confirmed our predictions outlined in the previous section. The optimal power-allocation fraction $\epsilon_{opt}$ is shown in Fig. 4.8. Three different ReS codes were investigated, namely the $\{255/223; 97/85; 32/28\}$ codes, which have the same code rate of 0.875 but different codeword lengths. As expected, a larger fraction of the power is assigned to the pilot symbols in the low $E_b/N_0$ region. Additionally, when increasing the codeword length, the system has to assign a larger amount of transmit energy, but relies on the same number of pilot symbols. Hence, this leads to the relative reduction of the power assigned to pilot symbols. This may be observed in Fig. 4.8.

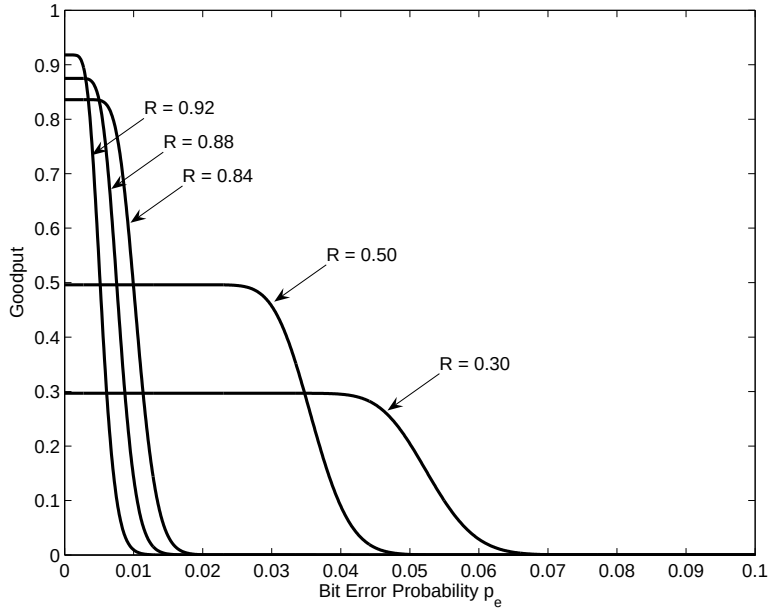


Figure 4.7: The dependence of goodput on the bit error probability for the system of Fig. 4.1 for transmission over a block-fading, independent Rayleigh channel: $m = 8$, $n = 255$, $N_P = 8$. The system parameters are provided in Table 4.4.

Based on using the value of $\epsilon_{opt}$ characterized in Fig. 4.8, the overall goodput performance of ReS/H-ARQ systems is examined in Fig. 4.9. Clearly, the optimized pilot-versus-data power allocation scheme assists the system in achieving an improved goodput. It is also interesting to note that the longer the ReS codeword, the higher the goodput. When the proposed optimum power allocation is employed, there is an approximately $1.75dB$ improvement for the (32/28) ReS code, while this value is about $2.5dB$ for the (255/223) ReS code. Additionally, the longer codewords achieve the maximum attainable goodput at lower $E_b/N_0$ values than the short ones.

## 4.3 Cooperative Communications Systems

### 4.3.1 System Model

- **At the Source Station:** In this section, we will consider an H-ARQ scheme operating with the assistance of ReS coding. The same encoding procedure is applied here as in the direct communications systems of Section 4.2 is applied here. The $N_p$ pilot bits, which are known to both the transmitter and receiver of Fig. 4.1, are inserted into the encoded bit stream. The choice of the pilot symbol spacing $T_p$ will be detailed in Section 4.3.2.1. As a result, each

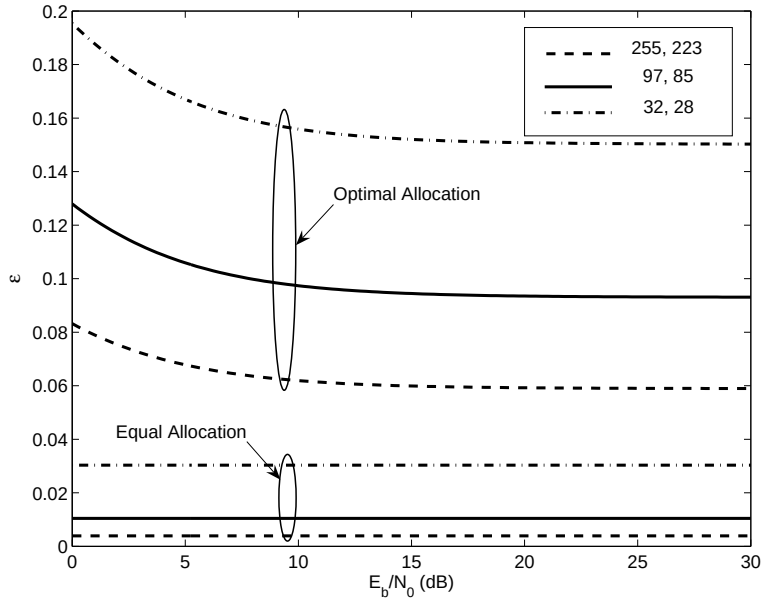


Figure 4.8: The factor of power allocation for the system of Fig. 4.1: $m = 8$, $N_P = 8$. The corresponding goodput is shown in Fig. 4.9. The system parameters are provided in Table 4.4.

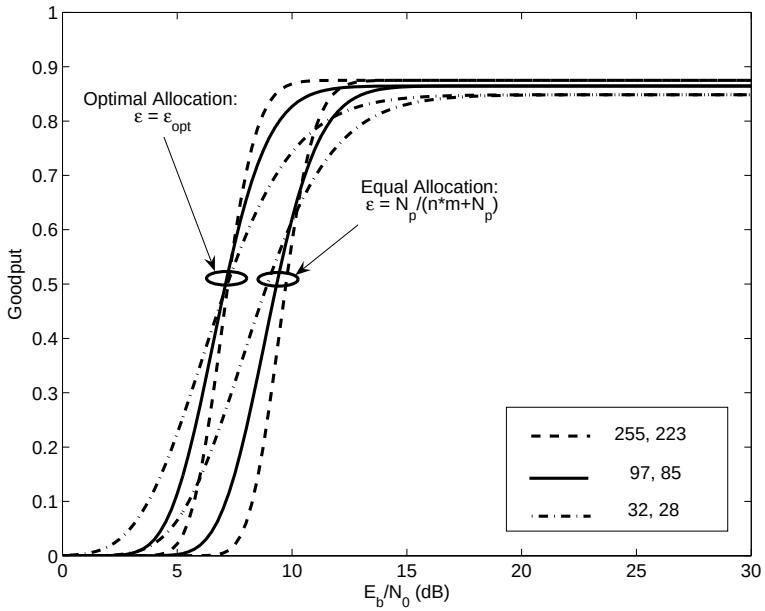


Figure 4.9: Lower bound of goodput based on both equal and optimized power allocation schemes for the system of Fig. 4.1 for transmission over a block-fading, independent Rayleigh channel: $m = 8$, $N_P = 8$. The corresponding power allocation factors are shown in Fig. 4.9. The system parameters are provided in Table 4.4.

transmitted packet of Fig. 4.2 includes $K$ $m$-bit information symbols, $(N-K)$ parity symbols and $N_p$ pilot bits. The packet's structure is shown in Fig. 4.2. Following modulation, the packet is transmitted to the RSs and the DS .

- **At the Relay Station:** The classic SR-ARQ scheme employing packet buffers at all the stations is used. The channels are assumed to be subjected to correlated Rayleigh fading. Then the signals received at the RSs of Fig 4.10 may be expressed as

$$y_{R_l}[k] = G_{SR_l} h_{SR_l}[k] x[k] + n_{SR_l}[k], \tag{4.24}$$

where $k$ is the symbol index, $l = 1, 2, ..., L$ is the RS index; $x[k]$ is the transmit signal at the SS with energy $\sqrt{E_S}$ and $y_{R_l}[k]$ is the signal received at the RS $R_l$; $n_{SR_l}[k]$ represents the zero-mean complex-valued AWGN with a variance of $\sigma_n^2$; $h_{SR_l}[k]$ represents the channel between the SS and the RS $R_l$, modelled as a wide-sense stationary (WSS) zero-mean complex Gaussian (ZMCG) random process with a variance of $\sigma_{SR_l}^2$; finally, $G_{SR_l}$ is the path-loss-related power gain for the $l^{th}$ Source-to-Relay ($SR_l$) link.

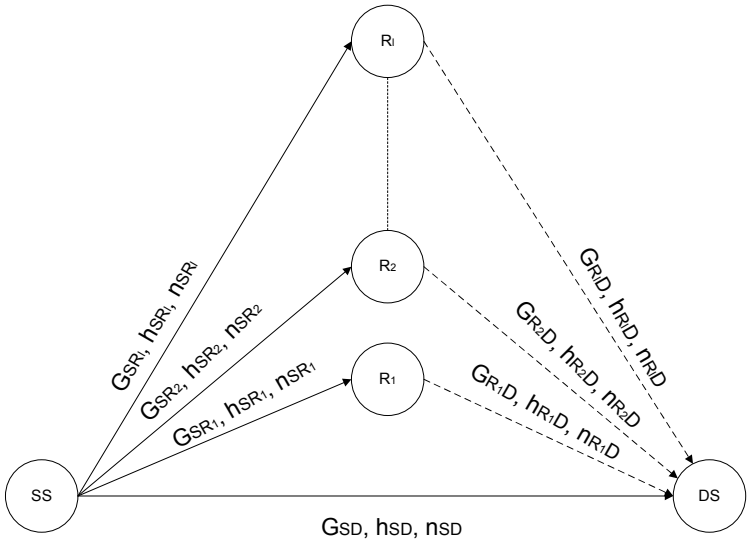


Figure 4.10: Relay schematic using the transceiver of Fig. 4.1.

  - **For AF relaying:** The RSs amplify $y_{R_l}[k]$ and forward them to the DS, which receives

$$\begin{aligned} y_D[k] &= \sum_{l=0}^{L} \omega_l y_{R_l D}[k] \\ &= \sum_{l=0}^{L} \omega_l \Big\{ G_{R_l D} A_{R_l}[k] h_{R_l D}[k] y_{R_l}[k] + n_{R_l D}[k] \Big\} \\ &= \sum_{l=0}^{L} \omega_l \Big\{ G_{R_l D} A_{R_l}[k] h_{R_l D}[k] h_{SR_l}[k] x[k] + G_{R_l D} A_{R_l}[k] h_{R_l D}[k] n_{SR_l}[k] + n_{R_l D}[k] \Big\} \\ &= \sum_{l=0}^{L} \omega_l \Big\{ h_l[k] x[k] + G_{R_l D} A_{R_l}[k] h_{R_l D}[k] n_{SR_l}[k] + n_{R_l D}[k] \Big\}, \end{aligned} \tag{4.25}$$

where, again, $y_D[k]$ is the signal received at the DS; $\omega_l$ is the maximum ratio combining receiver's weighting coefficient; $h_{R_l D}[k]$ represents the channel between the $l^{th}$ Relay-to-Destination ($R_l D$) link, modelled as a WSS ZMCG process with a variance of $\sigma_{R_l D}^2$ and

$n_{R_lD}[k]$ is the zero-mean complex AWGN with a variance of $\sigma_n^2$; finally, $G_{R_lD}$ is the path-loss-related power gain for the $l^{th}$ $R_lD$ link. The overall relay channel is represented by $h_l[k] = G_{R_lD}A_{R_l}[k]h_{R_lD}[k]h_{SR_l}[k]$, where $A[k]$ is the fixed relay gain, which is expressed as [159]

$$A_{R_l}[k] = \sqrt{\frac{E_{R_l}}{E\left[|y_{R_l}[k]|^2\right]}} = \sqrt{\frac{G_{SR_l}E_{R_l}}{G_{SR_l}E_E\sigma_{SR_l}^2 + \sigma_n^2}}. \tag{4.26}$$

In Eq. (4.25), the direct Source-to-Destination link is represented by $l = 0$, where we have $h_{R_0}[k] = h_{SD}[k]$, $G_{R_0D} = G_{SR_0} = 1$, $A_{R_l}[k] = 1$, $n_{SR_0}[k] = n_{SD}[k]$ and $n_{R_0D}[k] = 0$.

– **DF relaying:** At the relays' receivers, the pilot symbols are recovered first in order to estimate the complex-valued channel envelope. Then, the encoded bits are demodulated with the aid of the estimated channel coefficients before being passed to the ReS decoders. The decoders evaluate the ReS code's syndromes and checks for errors. If errors are detected, the relays become idle and wait for new packets from the source. Otherwise, they re-encode the messages and then forward them to the Destination Station (DS). Consequently, the signal received at the DS may be expressed as

$$y_D[k] = \sum_{l=0}^{L} \omega_l \Big\{ G_l h_l[k] x_l[k] + n_l[k] \Big\}. \tag{4.27}$$

- **At the Destination Station:** Similar to the relays' receivers in DF relaying, at the DS's receiver the pilot symbols are recovered first in order to estimate the complex-valued channel envelope. Then, the encoded bits are demodulated with the aid of the estimated channel coefficients, before being passed to the ReS decoder. The DS's decoder evaluates the ReS code's syndromes and checks for errors. In contrast to the relay, the error correction process is activated, if errors are detected. Provided that all errors were successfully corrected, a positive acknowledgement (ACK) is returned to the transmitter, requesting a new packet. Otherwise, a negative ACK is sent to request retransmissions.

### 4.3.2 Impact of Imperfect CE on ReS coded H-ARQ Systems

#### 4.3.2.1 Channel Estimation

- **Pilot Insertion Period:** To estimate the CSI, a certain number of pilot symbols have to be inserted into the data symbol stream using the schematic of Fig. 4.1. However, the pilot-overhead has to be minimized in oder to avoid wasting power as well as to prevent the reduction of the effective data rate. According to the Nyquist sampling theorem, the minimum period for pilot insertion in correlated fading channel must satisfy

$$T_p \leq \left( T_{pmin} = \frac{1}{2F_{max}T_s} \right), \tag{4.28}$$

where $F_{max}$ is the maximum Doppler frequency of the fading channel $h_l[k]$ and $T_s$ is the modulated symbol duration.

– **AF relaying:** When the relays are stationary, the maximum Doppler frequency of the overall channel is equal to the sum of two component Doppler frequencies, while in the case

of mobile relays a lower $T_p$ value, i.e. a high sampling frequency is required due to faster fading. Subsequently, in a down-link scenario the maximum Doppler frequency $F_{max}$ for an AF scheme is equal to [159]

$$F_{max} = \begin{cases} f_{SR_l} + f_{R_lD}, & \text{for stationary relays} \\ 2f_{SR_l} + f_{R_lD}, & \text{for mobile relays} \end{cases} \quad (l = 1, 2..., L), \tag{4.29}$$

where $f_{SR_l}$ and $f_{R_lD}$ are the maximum Doppler frequencies of the $SR_l$ and $R_lD$ links, respectively.

– **DF relaying:** In contrast to the AF relaying, in DF relaying the pilot symbols only cope with a single channel (SR channel or RD channel). Therefore, the value of $F_{max}$ is given by [159]

$$F_{max} = \begin{cases} max\{f_{SR_l}, f_{R_lD}\}, & \text{for stationary relays} \\ 2 \cdot max\{f_{SR_l}, f_{R_lD}\}, & \text{for mobile relays} \end{cases} \quad (l = 1, 2..., L). \tag{4.30}$$

Let us now define the pilot oversampling factor as the ratio between the actual number of inserted pilots $N_p$ and the minimum number of required pilots $N_{pmin}$ of an ReS-codeword, where the latter is determined by the Nyquist theorem:

$$L_p = \frac{N_p}{N_{pmin}} = \frac{T_{pmin}}{T_p}. \tag{4.31}$$

- **Channel Estimation Error:** To recover the channel coefficients, the inserted pilot symbols are fed into the channel estimator of Fig. 4.1, such as a Wiener filter [230], for generating the estimated version $\hat{h}_l[k]$ of $h[k_l]$. According to [227], the filter outputs, which are estimated from $M_1$ preceding and $M_2$ succeeding pilot symbols in Fig. 4.1, are expressed as

$$\hat{h}_l[k] = \sum_{i=-M_1}^{M_2} w_i^* h_l[k-i], \tag{4.32}$$

where the asterisk superscript denotes complex conjugation and $w_i$ represents the filter coefficients. As quantified in [231], the resultant MSE of the channel estimates in a correlated fading channel is obtained as

$$E[|\hat{h_l} - h_l|^2] = \sigma_{e_l}^2 = \frac{\sigma_{h_l}^2}{1 + \frac{1}{2F_{max}T_p} \cdot \frac{E_p}{N_0}}, \tag{4.33}$$

where $\sigma_{h_l}^2$ is the variance of the overall relay channel $\hat{h}_l$.

#### 4.3.2.2 Analysis of CE Error on ReS coded H-ARQ systems

Similar to the system proposed in Section 4.2, the five-step analysis process detailed in Section 4.2.3.1 may be applied here to derive the system's goodput. However, there are a few further considerations:

- For the DF relaying, the last two steps calculating the APER and the goodput are unnecessary at the relay due to the assumption that the relay will refrain from forwarding a packet to the destination, when it detects codeword errors.

- In the direct communication system the PDF-based approach of BEP approximation [67] was employed, while in cooperative communications the Moment Generation Function (MGF) based technique will be employed for approximating the BEP [67] due to the unavailability of the PDF at the destination, where the noise and fading processes no longer follow specific analytically-formulated distributions, such as the Gaussian or Rayleigh distributions.

- **AF relaying:** As a result of the CE error analysed above, Eq. (4.25) may be rewritten as

$$y_D[k] = \sum_{l=0}^{L} \omega_l \Big\{ \hat{h}_{R_l}[k]x[k] + z_{R_lD}[k] \Big\}, \tag{4.34}$$

$$z_l[k] = e_l[k]x[k] + \sqrt{G_{R_lD}} A_{R_l}[k] h_{R_lD}[k] n_{SR_l}[k] + n_{R_lD}[k], \tag{4.35}$$

where $z_l[k]$ is the total AWGN imposed on the received signal, which has the variance defined as

$$\sigma_{z_l} = E_S \sigma_{e_l}^2 + G_{R_lD} A_{R_l}^2 \sigma_{R_lD}^2 \sigma_n^2 + \sigma_n^2. \tag{4.36}$$

Owing to its direct impact on all of the above-mentioned probabilities, the BEP $p_e$ will be evaluated first. As mentioned in [67], the PDF-based approach of BEP approximation has limitations, especially in multi-path fading scenarios. Hence, instead of using the Q-function based solution, we invoke the MGF based technique to approximate the BEP. According to [67], the BEP of M-PSK modulated transmission may be obtained as

$$p_e = \frac{1}{\pi} \int_0^{(M-1)\pi/M} \prod_{l=0}^{L} M_{\gamma_l}\left( s = \frac{1}{sin^2(\theta)} \right) d\theta, \tag{4.37}$$

where $M_{\gamma_l}$ is the MGF of $\gamma$, which is expressed as [159]

$$M_{\gamma_l}(s) = \frac{1}{\bar{\gamma}_l s} exp\Big( \frac{1}{\bar{\gamma}_l s} \Big) \int_{\bar{\gamma}_l s}^{\infty} \frac{e^{-x}}{x} dx, \tag{4.38}$$

and

$$\bar{\gamma}_l = \frac{E_S^2 |\hat{h}_l[k]|^2}{\sigma_{z_l}^2} = \frac{E_S^2 (\sigma_{h_l}^2 - \sigma_{e_l}^2)}{\sigma_{z_l}^2}, \tag{4.39}$$

is the instantaneous received symbols SNR, which is conditioned upon $\hat{h}_l[k]$.

Substituting the value BEP $p_e$ of Eq. (4.37) into Eq. (4.20), we arrive at the goodput expression of the ReS/H-ARQ system for the AF relaying network.

- **DF relaying:**

  - **At the RSs:** The BEP of M-PSK modulated transmissions at a particular RS may be formulated as [67]

$$p_{eR_l} = \frac{2}{max(log_2 M, 2)} \cdot \frac{1}{\pi} \int_0^{(M-1)\pi/M} M_{\gamma_{R_l}}\left( s = \frac{sin^2(\pi/M)}{sin^2(\theta)} \right) d\theta, \tag{4.40}$$

  where $M_{\gamma_{R_l}}$ is the MGF of $\gamma$ corresponding to Rayleigh channels, which is expressed as [67]

$$M_{\gamma_{R_l}}(s) = (1 - s\gamma_{R_l})^{-1}, \tag{4.41}$$

and

$$\bar{\gamma}_{R_l} = \frac{E_S^2 |\hat{h}_{SR_l}[k]|^2}{\sigma^2_{n_{SR_l}}} = \frac{E_S^2(\sigma^2_{h_{SR_l}} - \sigma^2_{e_{SR_l}})}{\sigma^2_{n_{SR_l}}}, \tag{4.42}$$

is the instantaneous received symbols SNR, which is conditioned upon $\hat{h}_l[k]$, and $\sigma^2_{e_{SR_l}}$ is the channel estimation error at the $l^{th}$ RS. Then, the probability of an erroneous ReS-coded symbol at a specific RS is obtained as

$$p_{sR} = 1 - (1 - p_{eR})^m. \tag{4.43}$$

Therefore, the probability of correctly decoding an ReS codeword at a RS is equal to

$$P_{Rc} = \sum_{h=0}^{\frac{n-k}{2}} \binom{n}{h} p_{sR}^h (1 - p_{sR})^{n-h}. \tag{4.44}$$

Finally, the relay will forward the data to the DS with the forwarding probability of

$$P_{Rf} = P_{Rc} + P_{Rue}, \tag{4.45}$$

where $P_{Rue}$ is given by Eq. (4.17).

– **At the DS:** According to Eq. (9.15) of [67] and Eq. (4.45) above, the BEP at the DS may be approximated as

$$\begin{aligned} p_e &= \sum_{L_c=0}^{L} \binom{L}{L_c} P_{Rf}^{L_c} (1 - P_{Rf})^{L-L_c} \cdot \frac{2}{max(log_2 M, 2)} \\ &\cdot \frac{1}{\pi} \int_0^{(M-1)\pi/M} \prod_{l=0}^{L_c} M_{\gamma_l}\left(s = \frac{sin^2(\pi/M)}{sin^2(\theta)}\right) d\theta, \end{aligned} \tag{4.46}$$

where $L_c$ is defined as the number of relays forwarding messages to the DS and $M_{\gamma_l}$ is given by Eq. (4.41). It is noted that when we have $P_{Rf} = 1$, because for example the RSs are extremely close to the DS, the network becomes similar to a classic multiple-input-single-output system. Hence, Eq. (4.46) may be simplified to Eq. (9.15) of [67].

Again, substituting the BEP $p_e$ of Eq. (4.46) into Eq. (4.20), we arrive at the goodput formula of the ReS/H-ARQ system for the DF relaying network.

### 4.3.3 Numerical Results and Discussions

In this section, we investigate the achievable system performance of diverse network configurations. The basic parameters of Table 4.5 are employed for the schematic of Fig. 4.1, unless otherwise stated. To characterize the ReS/H-ARQ system's overall performance, let us consider both the BEP and the achievable goodput.

#### 4.3.3.1 Effect of Doppler frequency

The effects of different Doppler frequencies are shown in Figs. 4.11-4.14. In this case, the normalized Doppler frequencies of the SR link as well as of the RD link were set to {0.001, 0.005, 0.01, 0.02, 0.03}.

Table 4.5: Basic parameters of ReS coded cooperative H-ARQ system of Fig. 4.1.

| **Parameters** | **Values** |
|---|---|
| m/k/n | 8/223/255 |
| Modulation type | BPSK |
| Relay type | fixed |
| N$^o$ of relays | L=2 |
| Normalized $d_{SR_l}/d_{R_lD}$ | 0.5/0.5 for AF<br>0.3/0.7 for DF |
| Data-pilot power allocation scheme | Equal |
| Source's transmit power | $E_{sS} = E_{pS} = \frac{mk}{mn+N_p} \cdot \frac{E_b}{2}$ |
| Relays' transmit power | $E_{sR_l} = E_{pR_l} = \frac{mk}{mn+N_p} \cdot \frac{E_b}{2L}$ |
| Channel model | correlated Rayleigh fading |
| Normalized Doppler freq. of SD link | $f_{SD}T_s = 0.002$ |
| Normalized Doppler freq. of SR$_l$ link | $f_{SR_l}T_s = 0.001$ |
| Normalized Doppler freq. of R$_l$D link | $f_{R_lD}T_s = 0.001$ |
| Pilot oversampling factor | $L_p = 10$ |

Observe in Eq. (4.40), that when the channel was less correlated, the BEP was reduced. This was because each ReS-coded word experienced more-or-less random uniformly distributed errors, which was more beneficial for the ReS code than having some near-error-free and some badly contaminated codewords. It is also interesting to note that Fig. 4.13 may be divided into three $E_b/N_0$ regions based on the cooperation opportunities of the relays. More particularly, the BEP reduced slowly in the first $E_b/N_0$ region, below 10 dB, while it changed more rapidly in the region between 10 dB and 16 dB. This may be explained by considering that due to the high BEP experienced by the relays in the first $E_b/N_0$ region, they cannot successfully recover the messages and thus, they are typically turned off during the cooperative phase. By contrast, they cooperate more frequently in the second $E_b/N_0$ region. Hence, the BEP is significantly reduced. When the SNR is sufficiently high, for instance it is above 16 dB, the relays get involved in forwarding data almost all the time. Therefore, the BEP is gradually decreased in this $E_b/N_0$ region.

On the other hand, the number of pilots has to be increased in order to adequately sample the higher-Doppler channel. As a consequence, the goodput of the entire system was actually reduced. Quantitatively, the goodput was reduced by a factor of two for AF relaying in Fig. 4.12, when the normalized Doppler frequency was increased from 0.001 to 0.03. Meanwhile, the goodput decreased by a third for DF relaying for the same change of the normalized Doppler frequency, as shown in Fig. 4.14.

#### 4.3.3.2 Effect of Pilot Oversampling Factor

In [159], the authors characterized both the effects of pilot spacing and those of the number of pilots separately. Moreover, both of these effects can be treated jointly as those of the pilot power. Therefore, below we characterize the effects of different pilot powers. As shown in Section 4.3.2.1, both the number

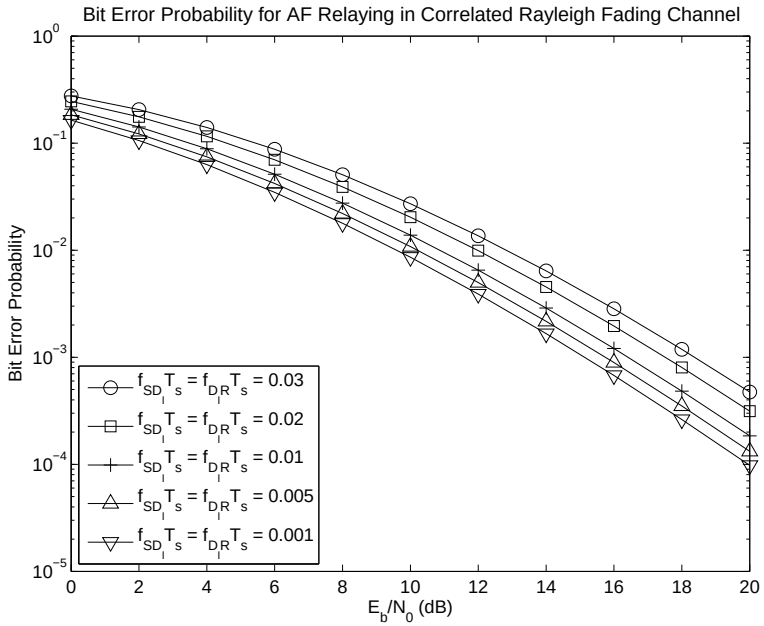


Figure 4.11: Effect of Doppler frequencies on BEP in the ReS coded H-ARQ system of Fig. 4.1 for AF relaying: $f_{SR_l}T_s = f_{R_lD}T_s = \{0.001, 0.005, 0.01, 0.02, 0.03\}$, $f_{SD}T_s = 2f_{SR_l}T_s$, the remaining parameters provided as in Table 4.5. The corresponding goodput results evaluated from Eq. (4.20) are shown in Fig. 4.12.

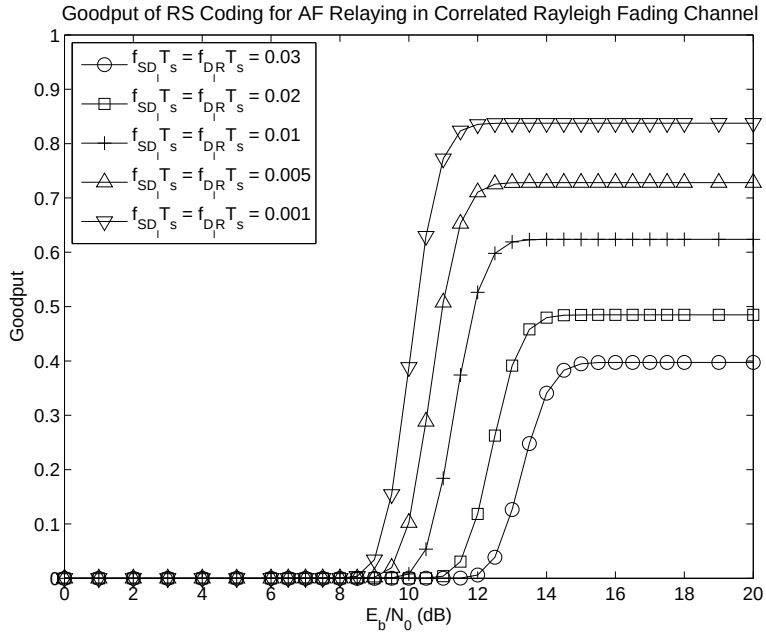


Figure 4.12: Effect of different normalized Doppler frequencies on the achievable goodput in the ReS coded H-ARQ system of Fig. 4.1 using AF relaying, where we have $f_{SR_l}T_s = f_{R_lD}T_s = \{0.001, 0.005, 0.01, 0.02, 0.03\}$, $f_{SD}T_s = 2f_{SR_l}T_s$, the remaining parameters are provided in Table 4.5. The corresponding BEP results evaluated from Eq. (4.37) are shown in Fig. 4.11.

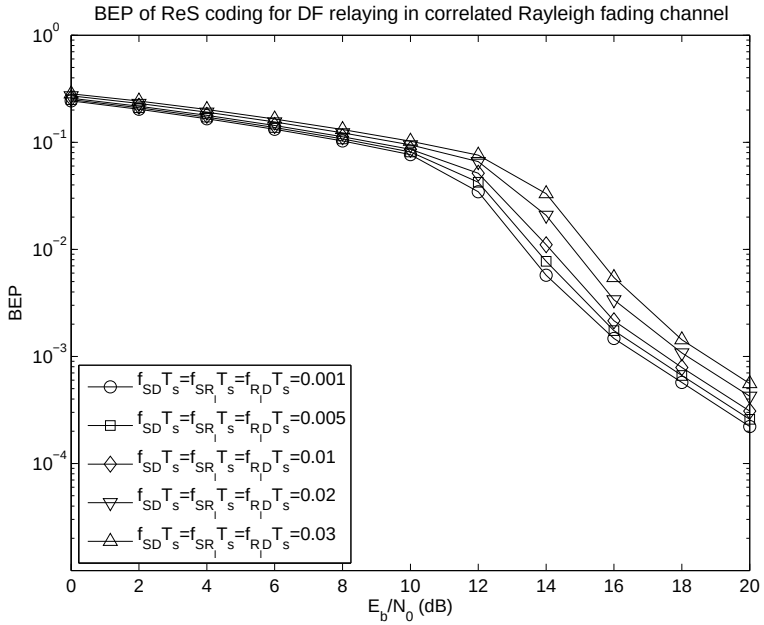


Figure 4.13: Effect of Doppler frequencies on BEP in the ReS coded H-ARQ system of Fig. 4.1 using DF relaying: $f_{SR_l}T_s = f_{R_lD}T_s = \{0.001, 0.005, 0.01, 0.02, 0.03\}$, the remaining parameters provided as in Table 4.5. The corresponding goodput results evaluated from Eq. (4.20) are shown in Fig. 4.14.

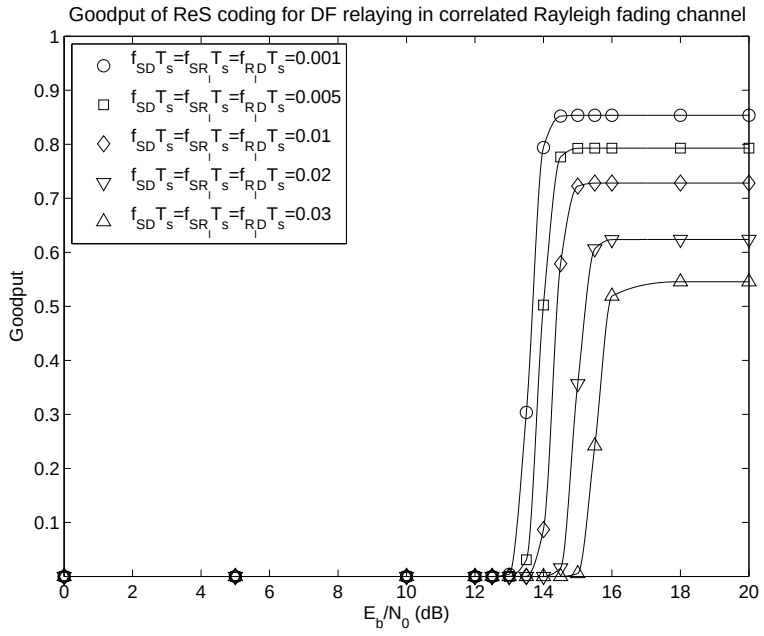


Figure 4.14: Effect of different normalized Doppler frequencies on the achievable goodput in the ReS coded H-ARQ system of Fig. 4.1 using DF relaying, where we have $f_{SR_l}T_s = f_{R_lD}T_s = \{0.001, 0.005, 0.01, 0.02, 0.03\}$, the remaining parameters are provided in Table 4.5. The corresponding BEP results evaluated from Eq. (4.46) are shown in Fig. 4.13.

of pilots and their spacing are related to the pilot oversampling factor of Eq. (4.31). The same power is assigned to all the data and pilot symbols. Hence, we will study the effect of the pilot oversampling factor $L_p$ instead of the pilots' power.

It is plausible that increasing the pilot oversampling factor $L_p$, or - equivalently - the number of pilots, is expected to reduce the CE MSE. However, this automatically reduces the useful data symbols' energy at a fixed total power budget. Consequently, the BEP would be increased. Hence, the optimal pilot oversampling factor $L_{opt}$ has to be determined.

In a mobile relaying aided network, the available number of cooperating nodes, their position and channel characteristics are time-variant. Thus, optimizing the pilot oversampling factor for the SS is feasible. As shown in Eq. (4.40), the BEP is a monotonically decreasing function of the instantaneous received SNR $\bar{\gamma}$. Therefore, we have to find the highest value of $\bar{\gamma}$ in Eq. (4.42) in order to minimize the BEP. As demonstrated in Appendix IV.B, the optimal pilot oversampling factor $L_{popt}$ should be set to

$$L_{popt} = \sqrt{\frac{\sigma_{e_0}^2 \cdot mk \cdot mn \cdot \frac{E_b}{N_0} + (mn)^2}{mk \cdot \frac{1}{2F_{max}T_{pmin}} \cdot \frac{E_b}{N_0}}}. \tag{4.47}$$

The BEP for the proposed AF system of Fig. 4.1 is shown in Fig. 4.15 . It can been seen that there is a gain of 2 dB in the BEP, when the optimization process was employed. The number of pilot symbols required for three different normalized Doppler frequencies is portrayed in Fig. 4.16. As shown in the figure, the number of symbols required decreases in accordance with the increases of the $E_b/N_0$ values and the normalized Doppler frequencies.

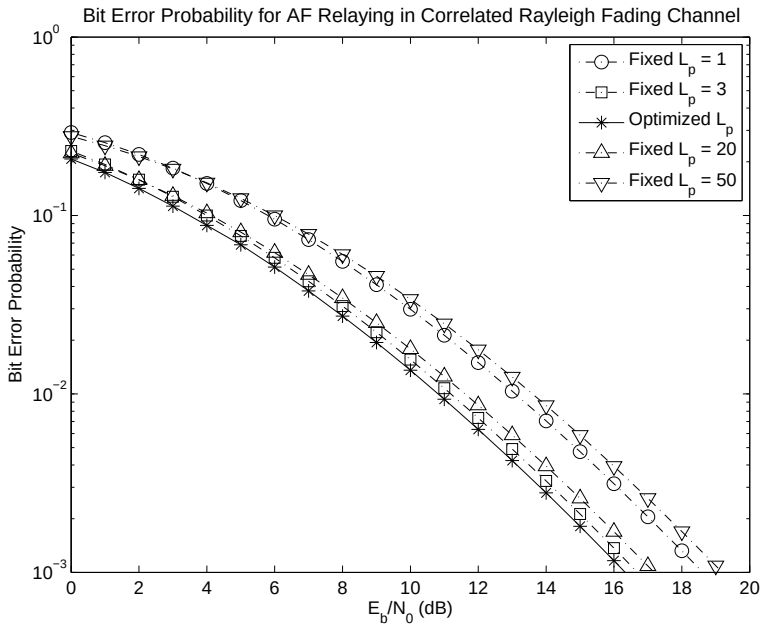


Figure 4.15: Effect of the pilot oversampling factor $L_p$ on BEP in the ReS coded H-ARQ system of Fig. 4.1 using AF relaying, where we have $L_p = \{1, 3, L_{popt}\ for\ BEP, 20, 50\}$, the remaining parameters are provided in Table 4.5. The corresponding goodput results evaluated from Eq. (4.20) are shown in Fig. 4.17 while the corresponding optimized number of pilots is shown in Fig. 4.18.

The goodput performance of the ReS coded AF relaying aided H-ARQ system of Fig. 4.1 is further characterized in Fig. 4.17, but in contrast to Fig. 4.12, it is now parameterized by $L_p$. According to

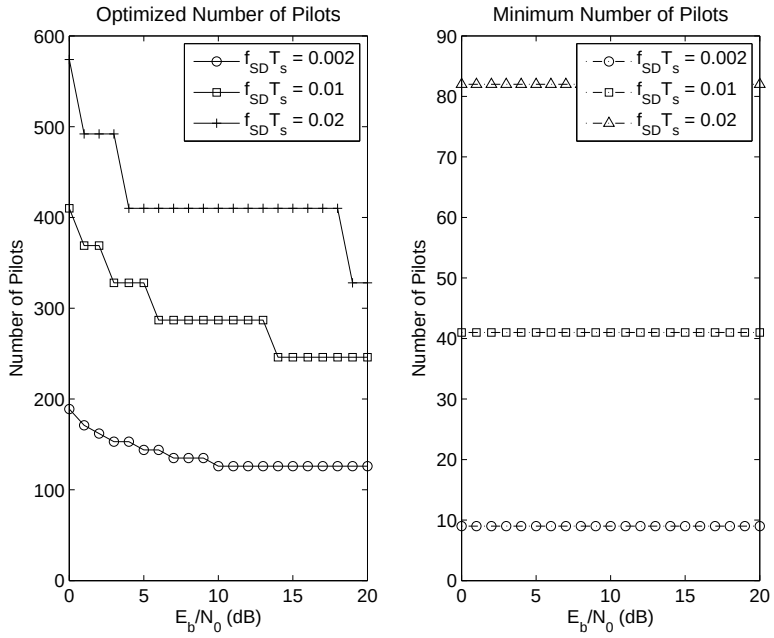


Figure 4.16: Effect of Doppler frequencies on the optimized and minimum number of pilots in the ReS coded H-ARQ system of Fig. 4.1 using AF relaying, where we have $f_{SR_l}T_s = f_{R_lD}T_s = \{0.001, 0.01, 0.02\}$, $f_{SD}T_s = 2f_{SR_l}T_s$, the remaining parameters are provided in Table 4.5.

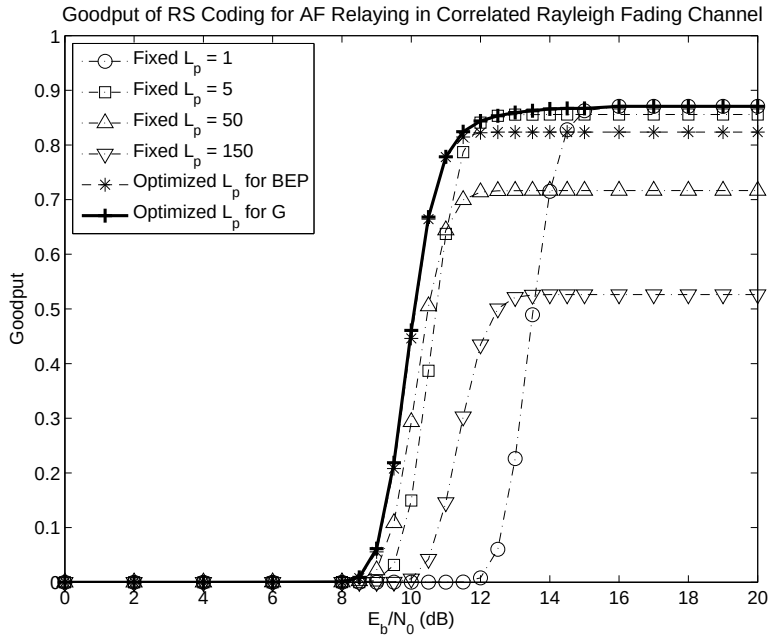


Figure 4.17: Effect of the pilot oversampling factor $L_p$ on the achievable goodput in the ReS coded H-ARQ system of Fig. 4.1 using AF relaying, where we have $L_p = \{1, 3, 50, 150, L_{popt}\ for\ BEP, L_{popt}\ for\ G\}$, the remaining parameters are provided in Table 4.5. The corresponding BEP evaluated from Eq. (4.37) results are shown in Fig. 4.15 while the corresponding optimized number of pilots is shown in Fig. 4.18.

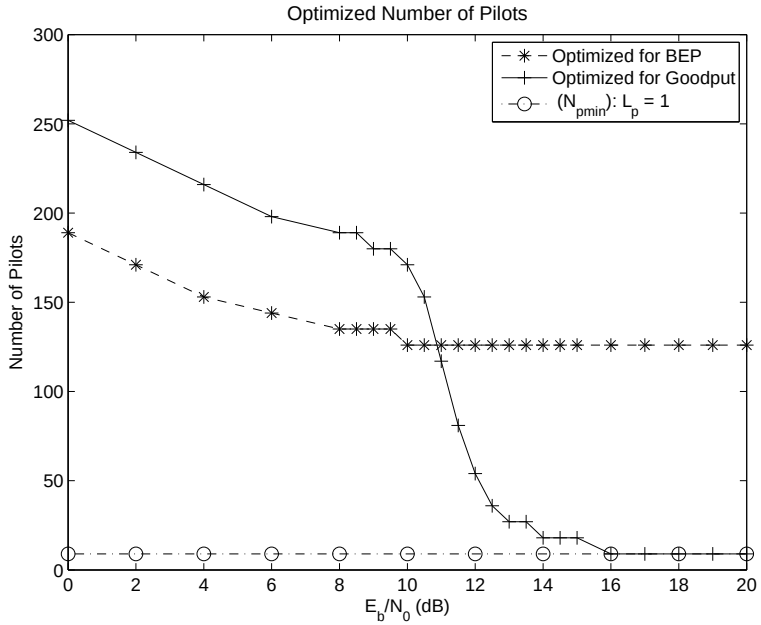


Figure 4.18: Optimized number of pilots in the ReS coded H-ARQ system of Fig. 4.1 using AF relaying, where we have $L_p = \{L_{popt}\ for\ BEP, L_{popt}\ for\ G, 1\}$, the remaining parameters are provided in Table 4.5. The corresponding BEP results evaluated from Eq. (4.37) are shown in Fig. 4.15 while the goodput results evaluated from Eq. (4.20) are shown in Fig. 4.17.

the figure, the optimized value of $L_p$ shifts the goodput curve to the left, which is illustrated by the asterisk-dashed line, but its maximum value is lower than those of $L_p = 1$ and $L_p = 5$. This can be explained by the fact that upon minimizing the BEP by optimizing $L_p$, the effective rate $R_e$ is also reduced. Thus, the goodput of the optimized scenario is also reduced. This problem may be overcome by optimizing the $L_p$ value in Eq. (4.20) instead of that in Eq. (4.40). The results of this optimization process are also shown in Fig. 4.17. Clearly, the optimized goodput curve represented by the bold continuous line in the figure indeed reaches the maximum achievable goodput value of unity. The number of pilot symbols per ReS codeword versus $E_b/N_0$ curves seen in Fig. 4.18 provides a clearer view. During the BEP optimization, the SS kept the number of pilot symbols constant, even when the BEP was low. By contrast, the number of pilots was reduced during the goodput optimization, resulting in an increased goodput.

Similar results were obtained for the DF relaying schemes. As shown in Fig. 4.20, the system may save 2 dB power at a given BEP, when the optimized pilot oversampling factor is employed. However, the goodput, which is represented by the thin continuous line in Fig. 4.20, does not reach its maximum value, when the optimization process is applied. This can be explained by the fact that upon employing the above optimization procedure, the effective rate $R_e$ is also reduced. Therefore, the goodput cannot increase, even when the channel conditions are improved. In order to improve the achievable goodput, a modified optimized pilot oversampling factor should be implemented, which is based on Eq. (4.20). The modified results are also shown in Figs. 4.20, and 4.21. It can be seen from these figures that the value of $L_p$ remains constant in the high-SNR region, namely above 10 dB during the BEP optimization. Meanwhile, during the goodput optimization process the value of $L_p$ continues to be reduced, until reaching its minimum value, resulting in an increased goodput.

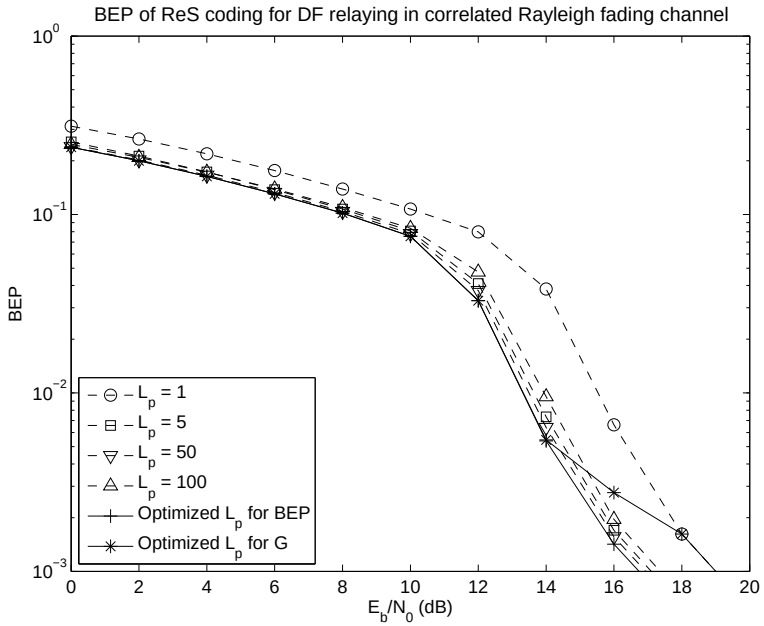


Figure 4.19: Effect of the pilot oversampling factor $L_p$ on BEP in the ReS coded H-ARQ system of Fig. 4.1 using DF relaying, where we have $L_p = \{1, 5, 50, 100, L_{popt}\ for\ BEP, L_{popt}\ for\ G\}$, the remaining parameters are provided in Table 4.5. The corresponding goodput results evaluated from Eq. (4.20) are shown in Fig. 4.20, while the optimized number of pilots is shown in Fig. 4.21.

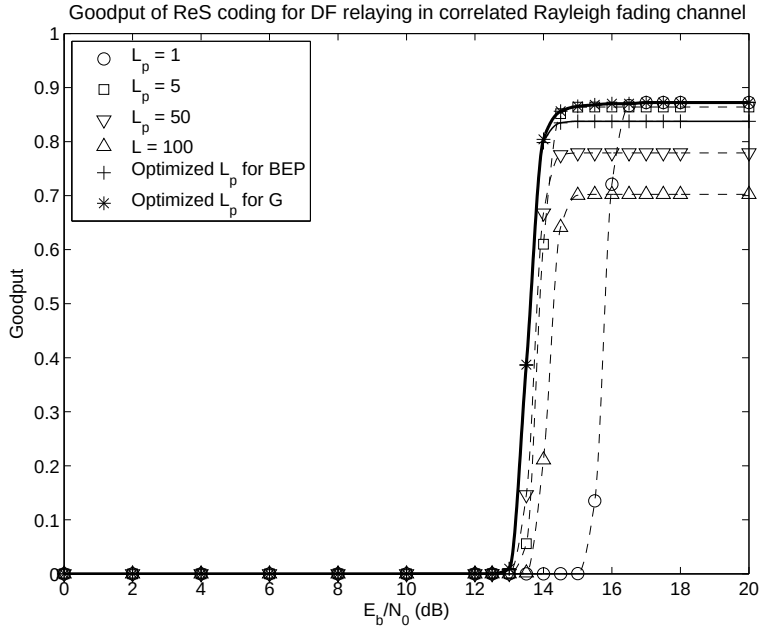


Figure 4.20: Effect of the pilot oversampling factor $L_p$ on the achievable goodput in the ReS coded H-ARQ system of Fig. 4.1 using DF relaying, where we have $L_p = \{1, 5, 50, 100, L_{popt}\ for\ BEP, L_{popt}\ for\ G\}$, the remaining parameters are provided in Table 4.5. The corresponding EBP results evaluated from Eq. (4.46) are shown in Fig. 4.19, while the optimized number of pilots is shown in Fig. 4.21.

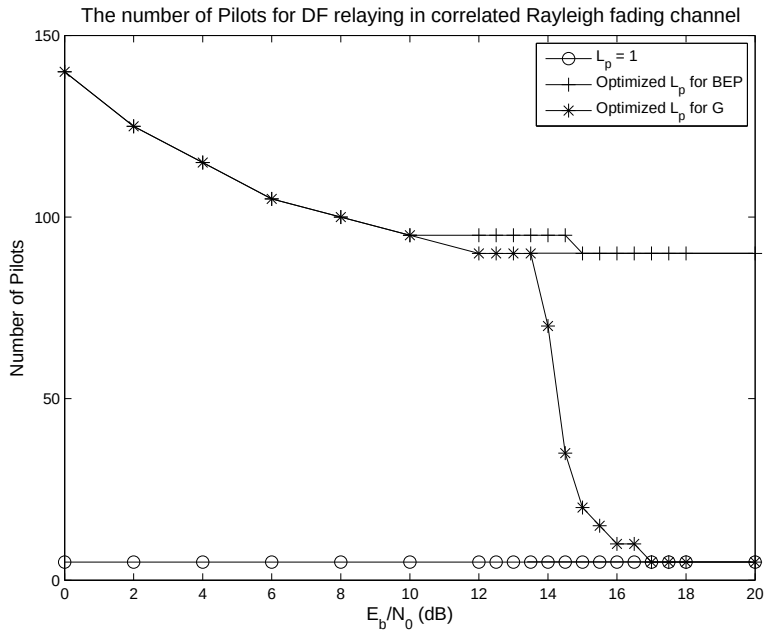


Figure 4.21: Optimized number of pilots in the ReS coded H-ARQ system of Fig. 4.1 using DF relaying where we have $L_p = \{1, L_{popt}\ for\ BEP, L_{popt}\ for\ G\}$, the remaining parameters are provided in Table 4.5. The corresponding goodput results evaluated from Eq. (4.20) are shown in Fig. 4.19, while the corresponding goodput results are shown in Fig. 4.20.

#### 4.3.3.3 Effect of the Number of Relays

In these investigations we assumed for the relay-aided network that the SS was assigned half of the transmit power, compared to the single direct transmission, while the remaining power was equally allocated to the RSs. Fig. 4.22 shows the BEP, when the number of the RSs is increased. Clearly, at each value of $E_b/N_0$, there is an optimal number of relays. For instance, the twin-relay aided scheme provides a lower BER, than the multiple-relay aided schemes, when the $E_b/N_0$ is below 1 dB. The reason for this is that when the number of the RSs increases, the symbols' transmit power at the RSs is reduced according to our assumptions. As a result, the CE MSE increases, while the useful data symbol power decreases. Finally, the BEP may be reduced, even when there are more relays aided.

The trends are similar also in terms of the goodput achieved in Fig. 4.23. It can be observed that there is a cross-over point at 6 dB between the curves of the nine-relay- and fifteen-relay-aided schemes. This is because in the high $E_b/N_0$ region, for example above 6 dB, the higher-order diversity gain may compensate for the relay-power reduction, when relying on an increased number of relays.

In contrast to AF relaying, in the DF relaying scenario the BEP always decreases, when the number of relays increases. The reason for this observation is that in the low $E_b/N_0$ region, namely below 8 dB in Fig. 4.24, the probability that a relay forwards a packet to the destination is low. Owing to the potential presence of errors, this procedure is necessary to avoid propagating more errors to the DS. When the $E_b/N_0$ is high, the relay forwards correct packets more frequently and hence the BEP is reduced at the DS. Consequently, the goodput always improves in accordance with the number of assisting relays, as shown in Fig. 4.25.

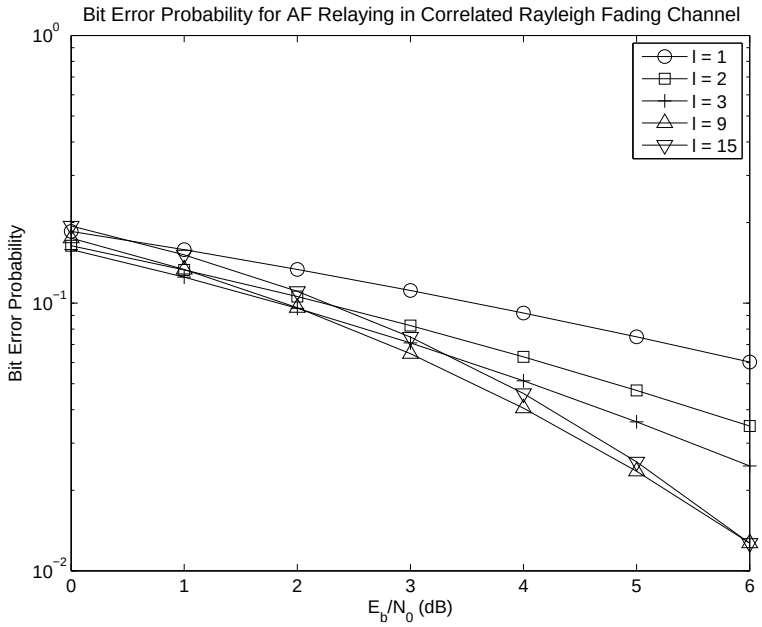


Figure 4.22: Effect of the number of relays on BEP in the ReS coded H-ARQ system of Fig. 4.1 for AF relaying: $L = \{1, 2, 3, 9, 15\}$, the remaining parameters provided as in Table 4.5. The goodput evaluated from Eq. (4.20) results are shown in Fig. 4.23.

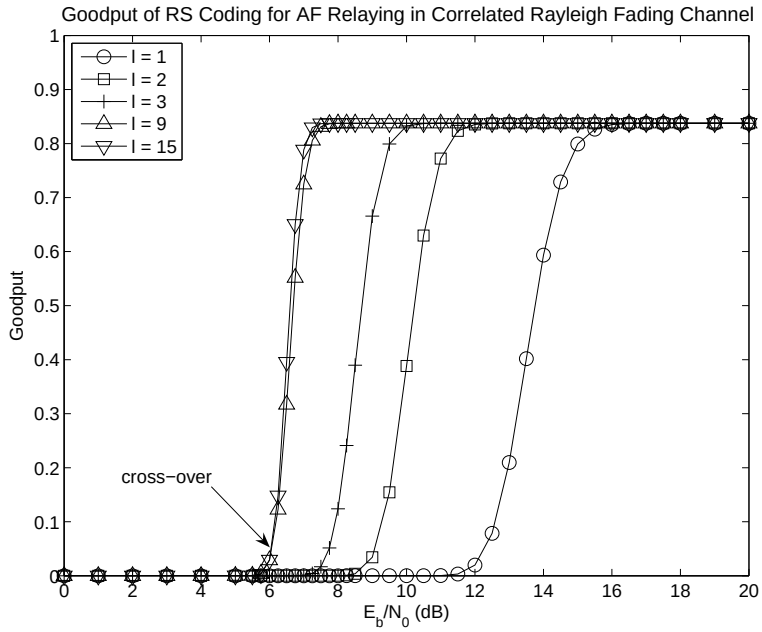


Figure 4.23: Effect of the number of relays on goodput in the ReS coded H-ARQ system of Fig. 4.1 for AF relaying: $L = \{1, 2, 3, 9, 15\}$, the remaining parameters provided as in Table 4.5. The corresponding BEP results evaluated from Eq. (4.37) are shown in Fig. 4.22.

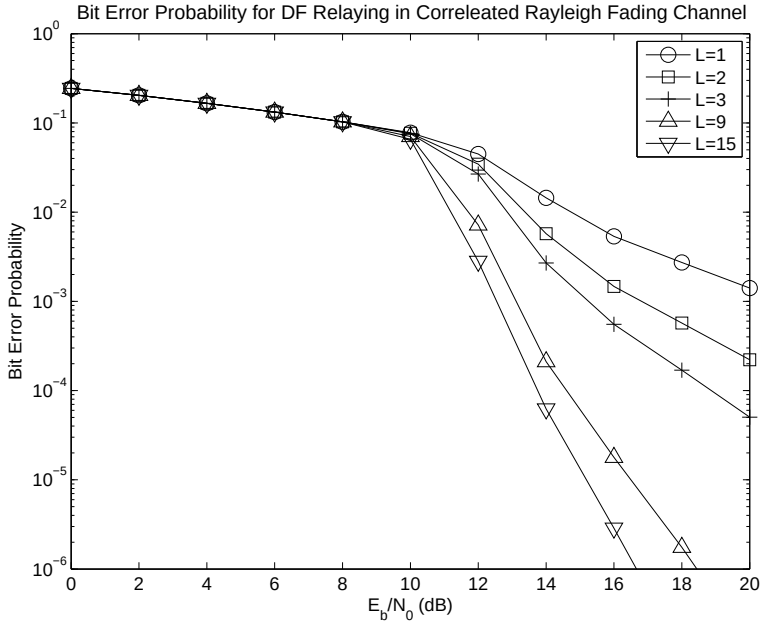


Figure 4.24: Effect of the number of relays on BEP in the ReS coded H-ARQ system of Fig. 4.1 for DF relaying: $L = \{1, 2, 3, 9, 15\}$, the remaining parameters provided as in Table 4.5. The corresponding goodput results evaluated from Eq. (4.20) are shown in Fig. 4.25.

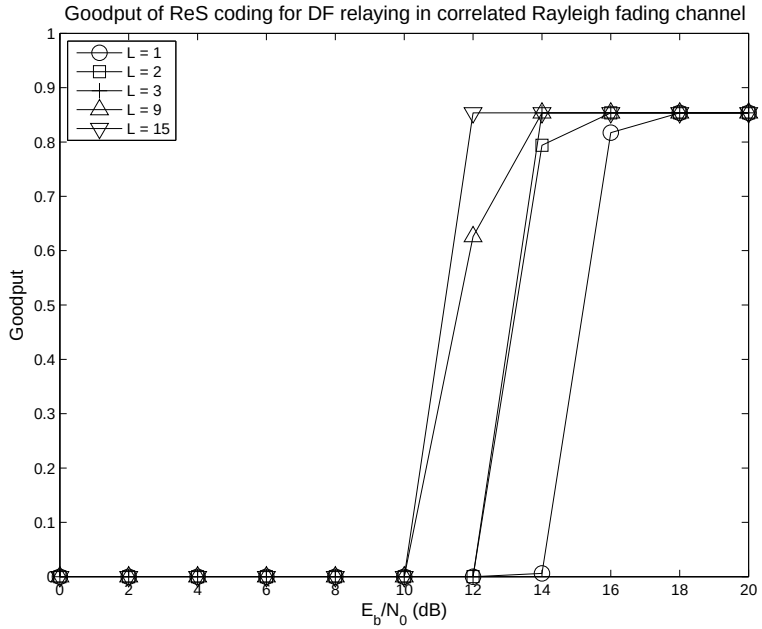


Figure 4.25: Effect of the number of relays on goodput in the ReS coded H-ARQ system of Fig. 4.1 for DF relaying: $L = \{1, 2, 3, 9, 15\}$, the remaining parameters provided as in Table 4.5. The corresponding BEP results evaluated from Eq. (4.46) are shown in Fig. 4.24.

#### 4.3.3.4 Effect of Relay Position

The direct calculation of the optimal positions for the RSs in a relay network based on the pure mathematical process of Eq. (4.40) is challenging. However, if we assume a power allocation scheme similar to that in the previous subsection, the appropriate relay positions may be found by an experimental process. As shown in Fig. 4.26 and Fig. 4.27, the relay position should satisfied the following condition in order to minimize the BEP,

$$d_{R_l D} \approx \frac{1}{1+L}. \tag{4.48}$$

In contrast to the AF relaying schemes, Fig. 4.28 shows that BEP of the DF schemes considered may be minimized at a specific relay position, regardless of the number of assisting relays. More particularly, the normalized Source-Relay distances is around the value of 0.15 in Fig. 4.28, when the number of relays is varied in the range of {1,2,3,9}. The corresponding goodput results may be observed from Fig. 4.29.

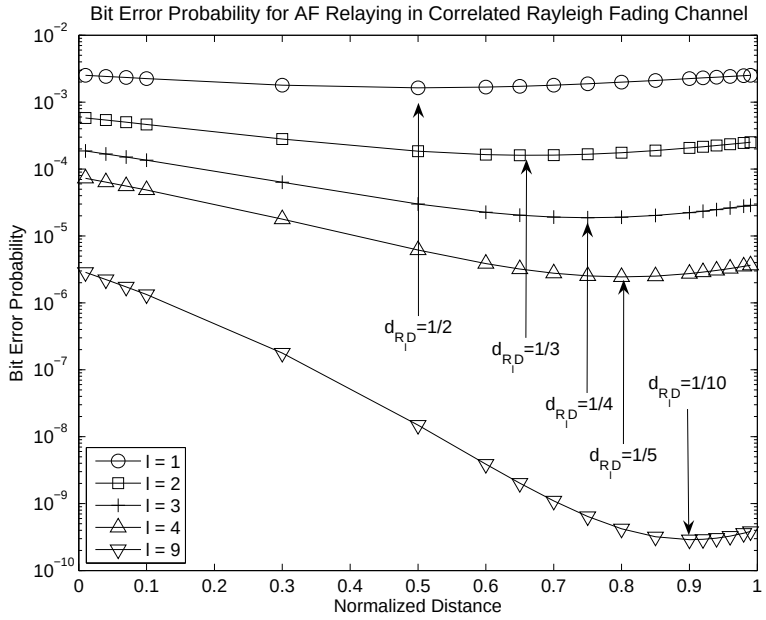


Figure 4.26: Effect of relay positions on BEP in the ReS coded H-ARQ system of Fig. 4.1 for AF relaying: $L = \{1, 2, 3, 4, 9\}$, the remaining parameters provided as in Table 4.5. The corresponding goodput results evaluated from Eq. (4.20) are shown in Fig. 4.27.

#### 4.3.3.5 Effect of Source-Relay Power Allocation

Finding the optimal solution for power allocation among the communication nodes of a relay network is also not challenging. Instead of employing a pure analytical approach, we continue by invoking an experimental process here. For convenience, the power allocation factor $\kappa$, which is defined as the ratio of the source's power to the system's total transmit power, is proposed here. It may be shown that to minimize the BEP, $\kappa$ should satisfy

$$\kappa \approx \frac{1}{1+\sum_{l=1}^{L} d_{R_l D}}. \tag{4.49}$$

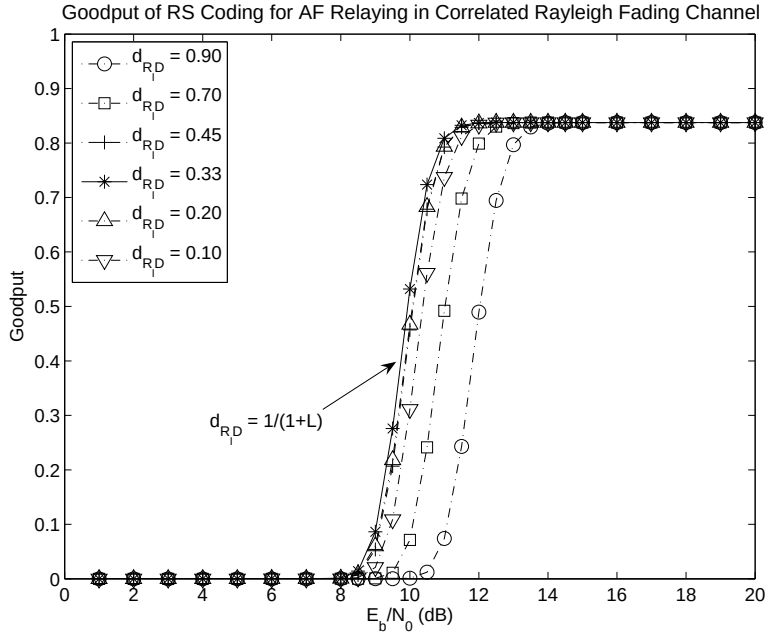


Figure 4.27: Effect of relay positions on goodput in the ReS coded H-ARQ system of Fig. 4.1 for AF relaying: $d_{R_lD} = \{0.90, 0.70, 0.45, 0.33, 0.20, 0.10\}$, the remaining parameters provided as in Table 4.5. The corresponding BEP results evaluated from Eq. (4.37) are shown in Fig. 4.26.

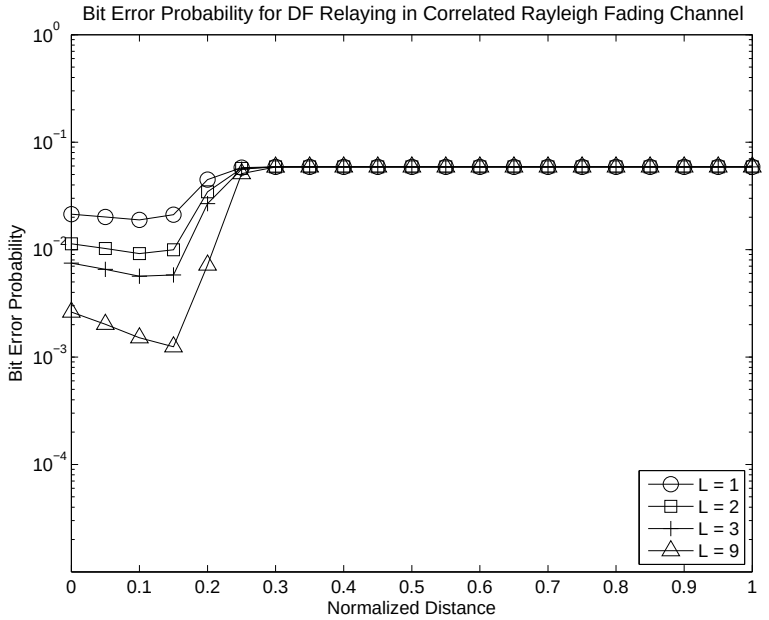


Figure 4.28: Effect of relay positions on BEP in the ReS coded H-ARQ system of Fig. 4.1 for DF relaying: $L = \{1, 2, 3, 4, 9\}$, the remaining parameters provided as in Table 4.5. The corresponding goodput results evaluated from Eq. (4.20) are shown in Fig. 4.29.

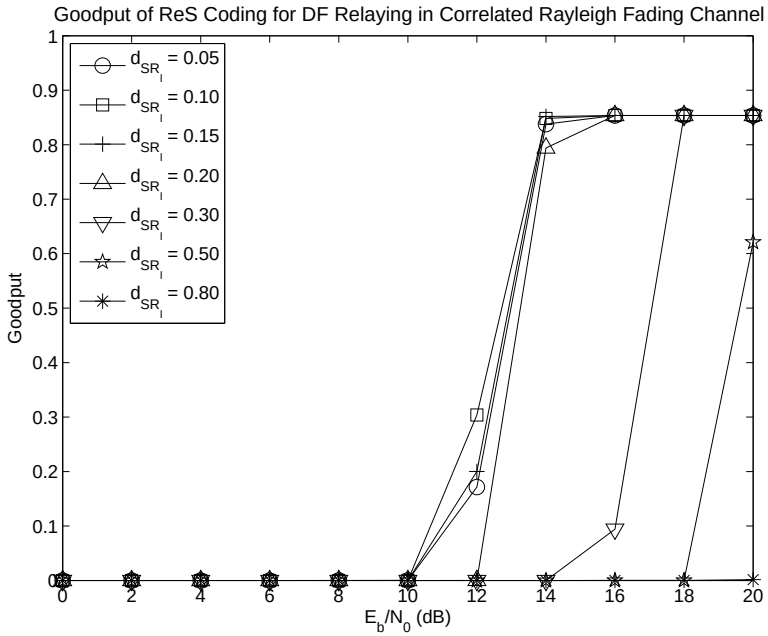


Figure 4.29: Effect of relay positions on goodput in the ReS coded H-ARQ system of Fig. 4.1 for AF relaying: $d_{R_lD} = \{0.05, 0.10, 0.15, 0.20, 0.30, 0.50, 0.80\}$, the remaining parameters provided as in Table 4.5. The corresponding BEP results evaluated from Eq. (4.37) are shown in Fig. 4.24.

Fig. 4.30 portrays the BEP results for the system, where there are one- as well as two-relays and the normalized frequency is equal to $10^{-3}$. Fig. 4.31 showed similar trends, when the normalized Doppler frequency was 0.01. It can be seen from these figures that the proposed scheme's BEP curves indicated by the plus-marker are always beneath those of the others, which implies that the proposed scheme is capable of reducing the BEP. Fig. 4.32 shows the attainable goodput performance. It is clear that the system is capable of achieving an improved goodput, when the proposed power allocation scheme is employed.

#### 4.3.3.6 Effect of Frame Length

Fig. 4.33 characterizes the achievable goodput performance for three different ReS codeword lengths, when the code rate was fixed at 0.87. It was found from Fig. 4.33 that a shorter ReS codeword length of 63 symbols provided a higher goodput in the lower $E_b/N_0$ region, namely below 10 dB, while the longer codeword of 255 symbols proved to be more efficient in the rest of $E_b/N_0$ region. This trend may be explained by the characteristic behaviour of the component $\sum_{h=0}^{\frac{n-k}{2}} \binom{n}{h}[1-(1-p_e)^m]^h[(1-p_e)^m]^{n-h}$ in Eq. 4.20. In terms of the physical interpretation, in the low-SNR region even the longer and hence more potent, but more complex codes fail to correct the errors. It is widely recognized that when the longer codes are overwhelmed by an excessive number of errors, they in fact inflict a more dramatic BER degradation than their shorter counterparts. This is due to opting for the wrong legitimate long codeword, which has a higher minimum distance than a short code.

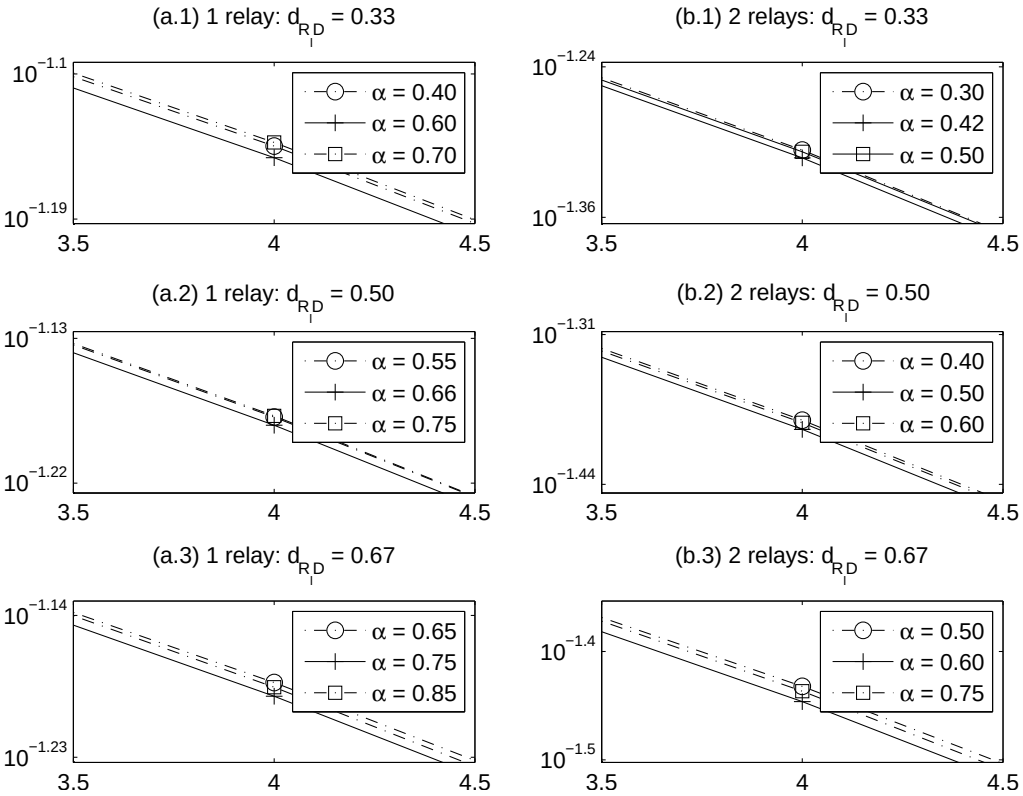


Figure 4.30: Effect of power allocation between nodes on BEP in the ReS coded H-ARQ system of Fig. 4.1 for AF relaying: $f_{R_lD}T_s = 0.001$, $L = \{1, 2\}$, $d_{R_lD} = \{0.33, 0.50, 0.67\}$, the remaining parameters provided as in Table 4.5. The corresponding goodput results evaluated from Eq. (4.20) are shown in Fig. 4.32. By contrat, when $f_{R_lD}T_s = 0.01$, the BEP results evaluated from Eq. (4.37) are shown in Fig. 4.31.

#### 4.3.3.7 Effect of Code Rate

The code rate of $R = k/n$ has a substantial impact on the achievable system performance. Reducing the coding rate provides the system of Fig. 4.1 with a better chance to correct errors imposed during transmissions, but reduces the effective throughput. Therefore, selecting the most appropriate code rate is necessary. Fig. 4.34 and Fig. 4.35 characterize the goodput performance of our ReS coded H-ARQ system of Fig. 4.1, when the code rate is varied from 0.3 to 0.98 in steps of 0.02. It can be observed that the system performs worse, when the code rate is lower than 0.6. Depending on the channel quality, the optimal code rate may be selected from the curve, which ranges from 0.6 to 1, as seen in Fig. 4.35.

#### 4.3.3.8 Comparison between AF and DF Relaying

Furthermore, we compared the performance of the proposed ReS/H-ARQ system of Fig. 4.1 employed in the context of both AF and DF relaying networks. In relaying schemes, the relays' position plays an important role in determining the achievable performance at the destination. For DF relaying, the relays should be close to the source, to avoid avalanche-like error propagation, while upon roaming close to the destination, we should opt for the AF relaying scheme. Therefore, in these investigations we activate specific relays in those particular positions, which may be capable potentially providing

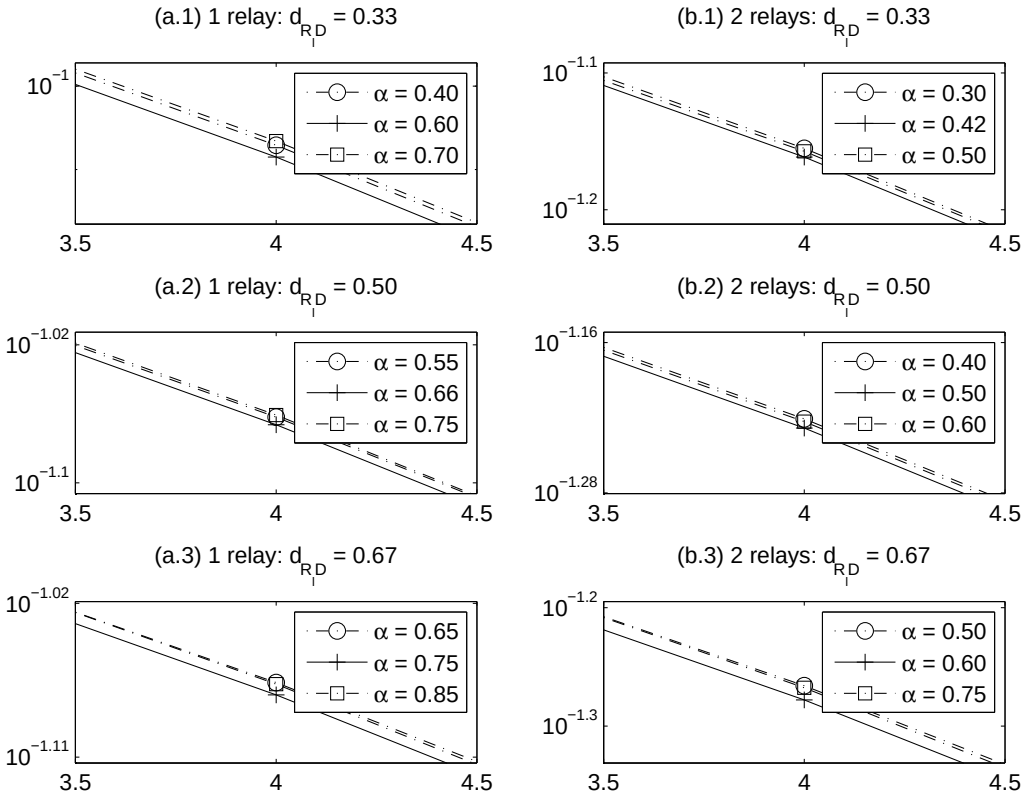


Figure 4.31: Effect of power allocation between nodes on BEP in the ReS coded H-ARQ system of Fig. 4.1 for AF relaying: $f_{R_lD}T_s = 0.01$, $L = \{1, 2\}$, $d_{R_lD} = \{0.33, 0.50, 0.67\}$, the remaining parameters provided as in Table 4.5. By contrast, when $f_{R_lD}T_s = 0.01$, the BEP results evaluated from Eq. (4.37) are shown in Fig. 4.30.

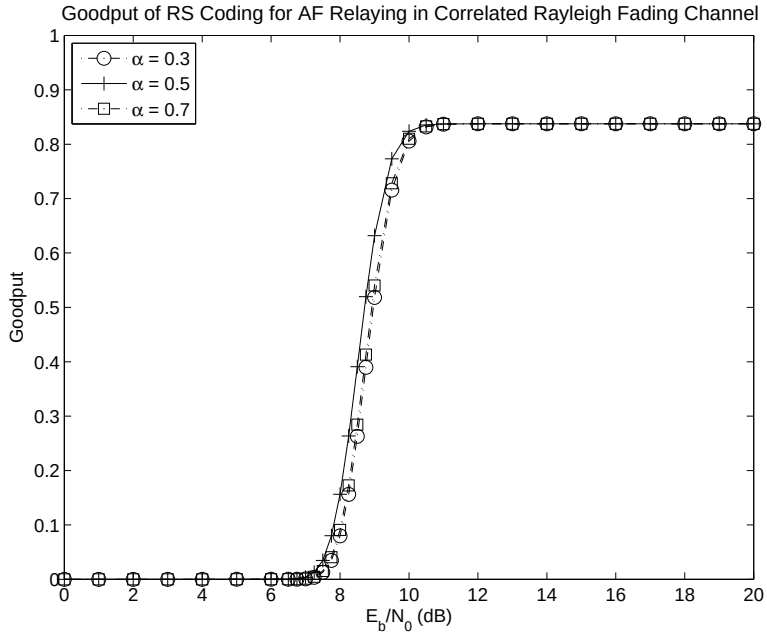


Figure 4.32: Effect of power allocation between nodes on goodput in the ReS coded H-ARQ system of Fig. 4.1 for AF relaying: $f_{R_lD}T_s = 0.001$, $L = 2$, $d_{R_lD} = \{0.33, 0.50, 0.67\}$, the remaining parameters provided as in Table 4.5. The corresponding BEP results evaluated from Eq. (4.37) are shown in Fig. 4.30.

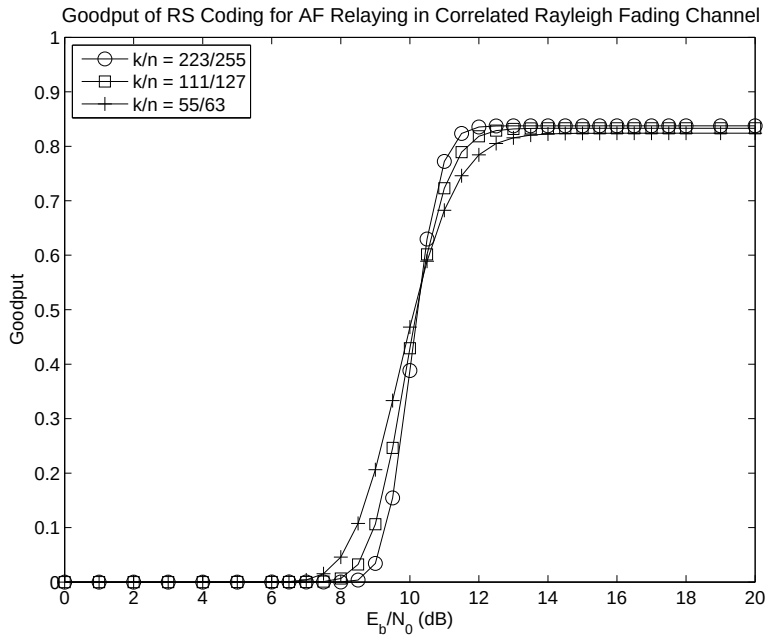


Figure 4.33: Effect of codeword length on the achievable goodput in the ReS coded H-ARQ system of Fig. 4.1 using AF relaying where we have $k/n = \{223/255, 111/127, 55/63\}$, the remaining parameters are provided in Table 4.5.

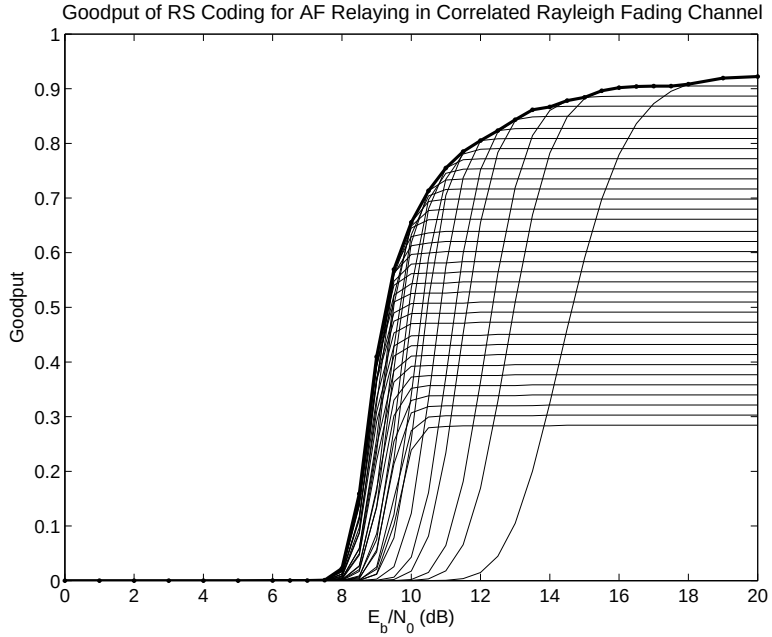


Figure 4.34: Effect of code rate on the achievable goodput in the ReS coded H-ARQ system of Fig. 4.1 using AF relaying where we have $k/n = 0.3 \div 0.98$ in steps of 0.02, the remaining parameters provided in Table 4.5. The corresponding 3-dimensional illustration is shown in Fig. 4.35.

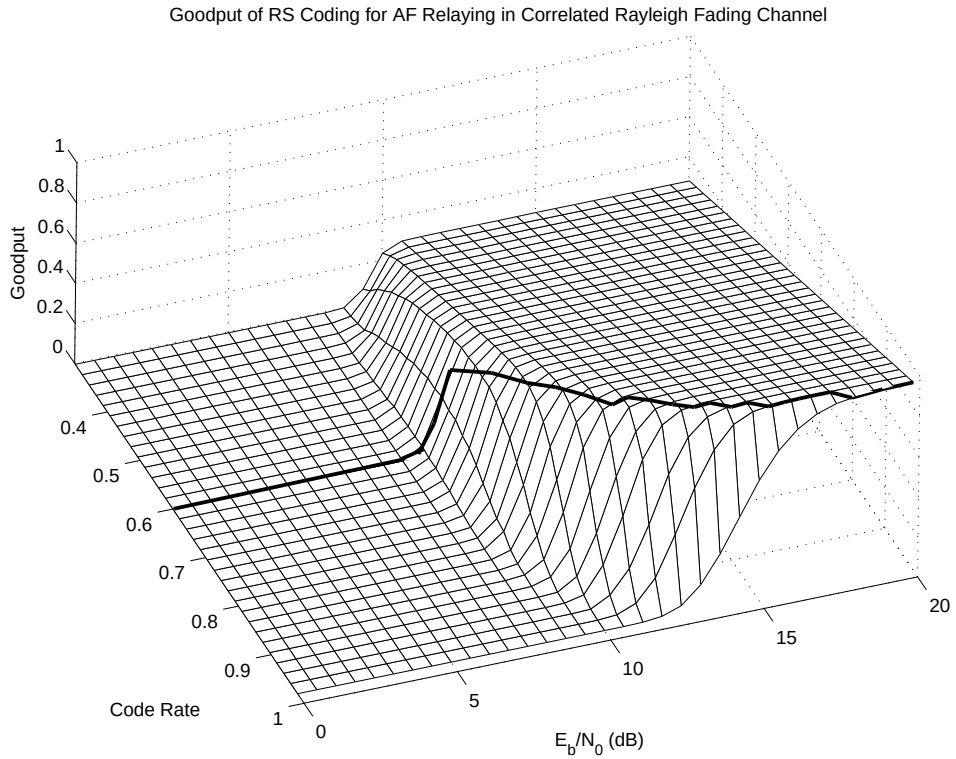


Figure 4.35: Effect of code rate on the achievable goodput in the ReS coded H-ARQ system of Fig. 4.1 using AF relaying where we have $k/n = 0.3 \div 0.98$ in steps of 0.02, while the remaining parameters are provided in Table 4.5. The corresponding 3-dimensional illustration is shown in Fig. 4.34.

the best performance for each scheme. According to Fig. 4.36, the normalized distances $d_{sr}$ should be 0.1 for the DF scenario and 0.7 for the AF relaying. Naturally, since the relays are mobile, a beneficial hybrid relay should activate the DF and AF protocols according to their specific positions. All system parameters are provided in Table 4.5.

Our goodput results were portrayed in Fig. 4.37. As seen in the figure, the AF scheme may achieve a power gain of 2 dB at a given goodput, when compared to the DF regime. However, it becomes slightly inferior to the DF scheme in the high $E_b/N_0$ region, namely above 15 dB. The fact is that in support of the AF scheme, the system has to use an increased number of pilots to deal with the detrimental effects of the combined channel, which included fading of both the SR link and the RD links. This may be observed in Fig. 4.38, where the number of pilots in the AF scheme is three times higher than that in the DF regime in the $E_b/N_0$ region above 15 dB.

## 4.4 Chapter Summary

In Section 4.2 we have studied the effects of imperfect CSI on the achievable goodput of the ReS/H-ARQ system of Fig. 4.1. The associated goodput equation based on the achievable throughput and the APER was derived in Section 4.2.3.1. The results of Fig. 4.9 demonstrated that the accuracy of CSI estimation plays an important role in recovering the received signal. Furthermore, in Section 4.2.3.2 the power allocation between the pilot and data symbols has been optimized for achieving the maximum attainable goodput. More particularly, a power-allocation factor $\epsilon_{opt}$, which ranges from $\frac{1-\sqrt{n}}{1-n}$ to

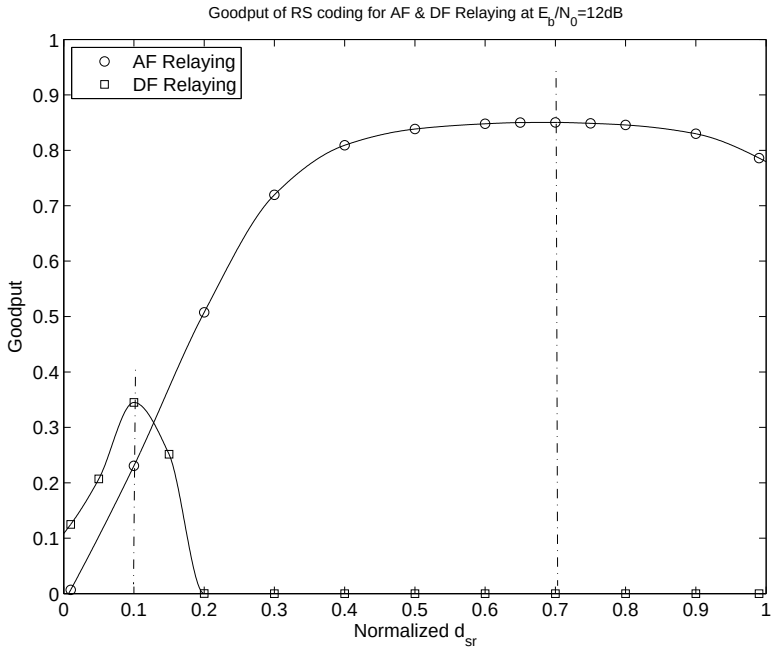


Figure 4.36: Goodput versus normalized distance $d_{sr}$ of the ReS coded H-ARQ system of Fig. 4.1 using Direct, AF and DF relaying communications with pilot optimization at $E_b/N_0 = 12dB$. The remaining parameters are provided in Table 4.5.

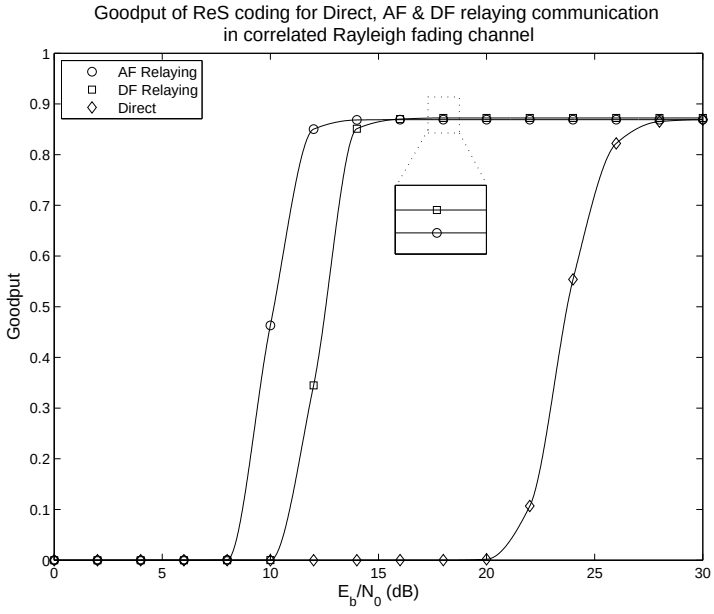


Figure 4.37: Goodput versus $E_b/N_0$ of the ReS coded H-ARQ system of Fig. 4.1 using Direct, AF and DF relaying communications with pilot optimization, where the normalized distance of $d_{sr} = 0.70$ was used for AF, and $d_{sr} = 0.10$ for DF relaying. The remaining parameters are provided in Table 4.5. The corresponding number of pilots employed is shown in Fig. 4.38.

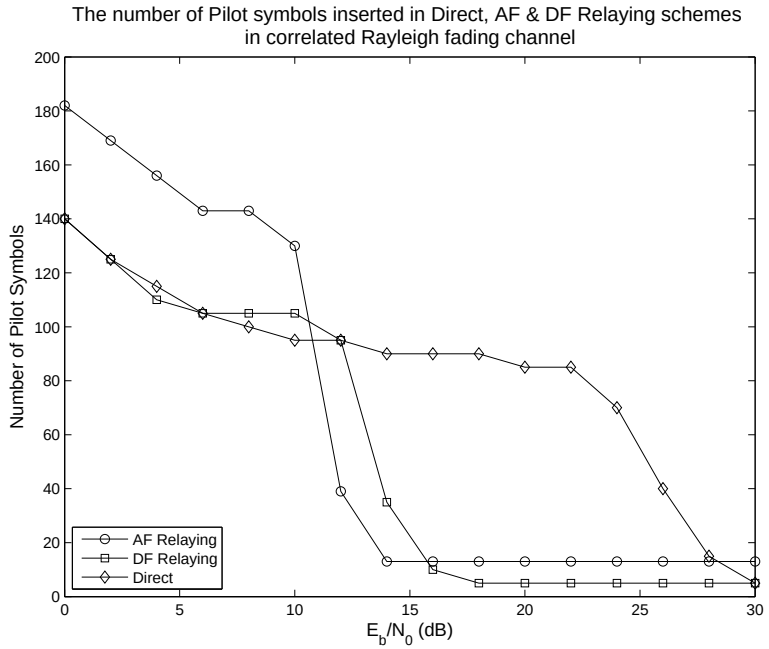


Figure 4.38: The number of pilot symbols employed by the ReS coded H-ARQ system of Fig. 4.1 using Direct, AF and DF relaying communications with pilot optimization, where the normalized distance of $d_{sr} = 0.70$ was used for AF, and $d_{sr} = 0.10$ for DF relaying. The remaining parameters are provided in Table 4.5. The corresponding goodput results evaluated from Eq. (4.20) is shown in Fig. 4.37.

half of the total transmit power, has been defined and optimized in order to maximize the system's goodput. It was found from Fig. 4.9 that the system achieved a $2.5dB$ $E_b/N_0$ gain at a given goodput for the 255/223 ReS code, when the proposed power allocation scheme was utilized.

In Section 4.3 we have further investigated the impact of imperfect CE on the ReS/H-ARQ system of Fig. 4.1, when operating in cooperative wireless networks. Again, the system's BEP and goodput were derived analytically in order to evaluate the achievable performance. Based on these expressions, the pilot-versus-data symbol power allocation was optimized in order to minimize the BEP and to maximize the system's goodput. More particularly, an optimum pilot power allocation scheme was proposed, which reduced the required bit-energy by 4 dB and 2 dB, as seen in Figs. 4.32 and 4.20 when the (255/223) ReS code defined over the Galois field (256) was employed in the AF and DF cooperative networks, respectively. Furthermore, we studied the effects of various factors, such as the Doppler frequency, the number of relays, and so on, on the performance of the proposed ReS/H-ARQ system operating in cooperative networks. The major trends are summarized in Table 4.6 and Table 4.7.

Finally, in Section 4.3.3.8 we compared the performance of the proposed ReS/H-ARQ system of Fig. 4.1, when employed in the context of both AF and DF cooperative networks. As seen in Fig. 4.37, the AF scheme may achieve a power gain of 2 dB in the $E_b/N_0$ region between 8 dB and 12 dB, when compared to the DF regime. However, it becomes slightly inferior to the DF scheme in the high $E_b/N_0$ region, namely above 15 dB, since the AF scheme has to use an increased number of pilots to deal with the detrimental effects of the combined channel, which includes fading of both the SR link and the RD link. This may be observed in Fig. 4.38, when the number of pilots in the AF scheme is three times higher than that of the DF regime in the $E_b/N_0$ region above 15 dB.

Table 4.6: Effects of factors on the performance of imperfect ReS/H-ARQ in cooperative networks.

| Effect | Type | Figure | Remark |
|---|---|---|---|
| Doppler frequency | AF | 4.11-4.12 | Both the BEP and the goodput are significantly reduced when the Doppler frequency decreases. |
| | DF | 4.13-4.14 | In the low $E_b/N_0$ region the BER changes only insignificantly with the Doppler frequency. By contrast, in the high $E_b/N_0$ region the BER is significantly reduced, when the Doppler frequency decreases. When the Doppler frequency increases, the goodput is significantly reduced due to the increase in the number of pilots required. |
| Pilot oversampling factor | AF | 4.15-4.18 | Increasing the pilot oversampling factor, $L_p$, is expected to reduce the CE MSE, but this automatically reduces the useful data symbols' energy at a fixed total power budget. Therefore, the optimal pilot oversampling factor $L_{popt}$ should be set to $$L_{popt} = \sqrt{\frac{\sigma_{e_0}^2 \cdot mk \cdot mn \cdot \frac{E_b}{N_0} + (mn)^2}{mk \cdot \frac{1}{2F_{max}T_{pmin}} \cdot \frac{E_b}{N_0}}}.$$ |
| | DF | 4.19-4.21 | Furthermore, the optimal pilot oversampling factor for the goodput can be achieved by solving Eq. (4.20). |
| Number of relays | AF | 4.22-4.23 | When the transmit power at the relays is identical, there is an optimal number of relays at each value of $E_b/N_0$, which minimizes the BEP as well as maximizes the goodput. |
| | DF | 4.24-4.25 | In contrast to AF relaying, in DF relaying the BEP and goodput always decreases, when the number of relays increases and equal-power allocation is employed among the relays. |
| Relay positions | AF | 4.26-4.27 | The relay position should satisfy the following condition in order to minimize the BEP as well as to maximize the goodput $$d_{R_l D} \approx \frac{1}{1+L}.$$ |
| | DF | 4.28-4.29 | The BEP of the DF schemes considered is minimized at a specific relay position, regardless of the number of assisting relays. |

Table 4.7: Effects of factors on the performance of imperfect ReS/H-ARQ in cooperative networks.

| | | | |
|---|---|---|---|
| Source-relay power location | AF | 4.30-4.32 | To minimize the BEP as well as to maximize the goodput, the power allocation factor $\kappa$, defined as the ratio of the source's transmit power to the system's total transmit power, should satisfy $\kappa \approx \frac{1}{1+\sum_{l=1}^{L} d_{R_l D}}$. |
| Frame length | AF | 4.33 | A shorter ReS codeword provides a higher goodput in the low $E_b/N_0$ region, while longer codewords prove to be more efficient in the high $E_b/N_0$ region. |
| Code rate | AF | 4.34-4.35 | Reducing the coding rate provides system with a better chance of correcting errors imposed during transmissions, but reduces the effective throughput. Observe that the system performs worse, when the code rate is lower than 0.6. Depending on the channel quality, the optimal code rate may be selected from the curve, which ranges from 0.6 to 1, as seen in Fig. 4.35. |

## Appendix IV.A

Let $x = \gamma/n$, then Eq. (4.22) becomes

$$\varepsilon_{opt} = \frac{1 + x - \sqrt{1 + x + nx^2 + nx}}{x - nx}. \tag{4.50}$$

Taking the derivative of $\varepsilon_{opt}$ with respective to $x$, we have

$$\frac{d\varepsilon_{opt}}{dx} = \frac{(n-1)[2\sqrt{1 + x + nx^2 + nx} - (nx + x + 2)]}{2\sqrt{1 + x + nx^2 + nx}(x - nx)^2}. \tag{4.51}$$

It may be readily found that $d\varepsilon_{opt}/dx \leq 0$, since we have the following relationship

$$2\sqrt{1 + x + nx^2 + nx} = 2\sqrt{(1 + x)(1 + nx)} \leq (1 + x) + (1 + nx) = 2 + n + nx. \tag{4.52}$$

Hence, $\varepsilon_{opt}$ is a monotonically decreasing function, which has the upper and lower limits expressed as follows

$$\lim_{x\to\infty} \varepsilon_{opt}(x) \leq \varepsilon_{opt} \lim_{x\to 0} \varepsilon_{opt}(x). \tag{4.53}$$

The lower limit can be obtained as

$$\lim_{x\to\infty} \frac{1 + x^{-1} - \sqrt{x^{-2} + x^{-1} + nx^{-1} + n}}{1 - n} = \frac{1 - \sqrt{(n)}}{1 - n}, \tag{4.54}$$

and applying the L'Hospital rule, the upper limit is expressed as

$$\lim_{x\to\infty} \frac{1 - 0.5(1 + n + 2nx)(1 + nx^2 + nx + x)^{-1/2}}{1 - n} = 0.5. \tag{4.55}$$

## Appendix IV.B

Expressing the value of $\bar{\gamma}$ from Eq. (4.42) for the SS, we have

$$\bar{\gamma} = \frac{\frac{E_{sS}}{N_0}\sigma_{h_{sd}}^2 \cdot \frac{1}{2F_{max}T_p} \cdot \frac{E_{sS}}{N_0}}{\frac{E_{sS}}{N_0}\sigma_{h_{sd}}^2 + 1 + \frac{1}{2F_{max}T_p} \cdot \frac{E_{sS}}{N_0}}. \tag{4.56}$$

If the pilot symbol energy and the encoded data symbol energy are set to be equal, then the received SNR of the SD link can be expressed as

$$\frac{E_{sS}}{N_0} = \frac{E_{pS}}{N_0} = \frac{mk}{mn + N_{pmin}L_p} \cdot \frac{E_b}{N_0}. \tag{4.57}$$

Upon taking into account $T_p = T_{pmin}/L_p$, Eq. (4.56) can be rewritten as

$$\bar{\gamma} = \frac{\left(\frac{mk}{mn+N_{pmin}L_p} \cdot \frac{E_b}{N_0}\right)^2 \cdot \frac{1}{2F_{max}T_{pmin}} \cdot \sigma_{e_0}^2 L_p}{\frac{mk}{mn+N_{pmin}L_p} \cdot \frac{E_b}{N_0} \cdot \left(\sigma_{e_0}^2 + \frac{1}{2F_{max}T_{pmin}} \cdot L_p\right) + 1}. \tag{4.58}$$

Setting the derivative of $\bar{\gamma}$ with respect to $L_p$ equal to zero and solving the resultant equation, we can obtain the optimal value $L_{popt}$ as

$$L_{popt} = \sqrt{\frac{\sigma_{e_0}^2 \cdot mk \cdot mn \cdot \frac{E_b}{N_0} + (mn)^2}{mk \cdot \frac{1}{2F_{max}T_{pmin}} \cdot \frac{E_b}{N_0}}}. \tag{4.59}$$

# Chapter 5

# Non-coherent Detection for H-ARQ Aided Cooperative Wireless Communications

## 5.1 Introduction

In Chapter 3 and Chapter 4 coherent HARQ systems based on PSAM were investigated. However, when rapidly fluctuating fading occurs, the PSAM schemes may become inefficient due to the larger pilot-overhead required for channel estimation. Furthermore, channel estimation imposes a high complexity, which may become unaffordable at the relays. To overcome these impediments, non-coherent detection schemes may be considered as a design alternative, which do not require CSI at the receiver. The general schematic of a non-coherent detection aided H-ARQ system is illustrated in Fig. 5.1.

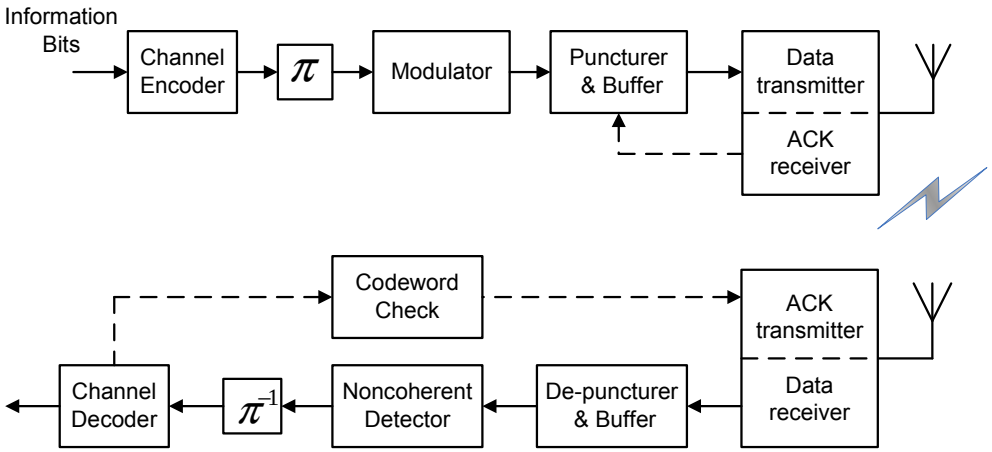


Figure 5.1: Transceiver schematic employing non-coherent detection aided H-ARQ. Observe the absence of the channel estimator in comparison to Fig. 4.1.

Non-coherent systems using differentially encoded modulation designed for cooperative networks were presented for example by Tarasak *et al.* [232], while Yiu *et al.* [233] proposed distributed Differ-

ential STBCs (DSTBC). Jing and Jafarkhani [234] further developed the differential philosophy for employment in cooperative wireless communications, demonstrating that diverse space-time codes, such as Alamouti's scheme [47], the orthogonal design of [59], and the so-called $Sp(2)$ design of [235], may be employed in relay-aided networks. Furthermore, Wang and Hanzo [129] proposed differentially encoded and Multiple-Symbol Differential Sphere-Detection (MSDSD) aided schemes for improving the system's performance, while reducing the decoding complexity of the classic Multiple-Symbol Differential Detector (MSDD) [236]. By contrast, Farhadi and Beaulieu [237] advocated a non-coherent low-complexity detection scheme based on M-FSK modulation. The salient MIMO techniques proposed for cooperative wireless communications are summarized in Table 5.1.

Table 5.1: Major non-coherent distributed MIMO techniques

| Year | Author(s) | Contribution |
|---|---|---|
| 2005 | Tarasak *et al.* [232] | Introduced a differentially encoded modulation scheme for a two-user DF cooperative diversity aided system which, does not require CSI. |
| | Himsoon *et al.* [238] | Proposed a differential AF transmission scheme for a two-user cooperative communications system. |
| | Annavajjala *et al.* [239] | Presented receiver structures of non-coherent AF communication employing on-off keying (OOK) and binary FSK modulation as well as maximum-likelihood (ML) detection. |
| | Yiu *et al.* [233] | Proposed differential distributed space-time block coding. |
| 2006 | Wang *et al.* [240] | Designed differential distributed space-time modulation for cooperative networks. |
| 2008 | Jing and Jafarkhani [234] | Designed distributed space-time coding for wireless relay networks. |
| 2009 | Oggier and Lequeu [241] | Implemented differentially encoded distributed space-time codes for an arbitrary number of relay nodes. |
| 2010 | Farhadi and Beaulieu [237] | Proposed a low-complexity non-coherent system based on M-FSK conceived for AF cooperative wireless networks. |
| | Wang and Hanzo [129] | Proposed sphere-detection for the AF cooperative UL in order to reduce complexity of classic multiple-symbol differential detectors. |

Unfortunately, all of the contributions mentioned above were investigated without the assistance of either the ARQ protocol or channel codes. Hence, in this chapter we will study the performance of HARQ systems employing non-coherent detection in the context of wireless cooperative networks. In Section 5.2, the popular Differential PSK (DPSK) aided HARQ schemes will be studied, where both single- and multiple-symbol detectors will be considered, followed by the comparison of perfect and imperfect channel estimation aided, as well as non-coherent detection schemes in Section 5.2.3. Furthermore, non-coherent FSK aided HARQ arrangements are proposed in Section 5.3. Finally, a novel distributed space-time coding aided HARQ scheme combined with non-coherent detection will be proposed in Section 5.4 for cooperative wireless networks.

## 5.2 Differential Phase Shift Keying Aided H-ARQ

### 5.2.1 Differential Phase Shift Keying Relying on Reed-Solomon Codes

#### 5.2.1.1 Single-Symbol Differential Detection

**a. System Description**

The transceiver of ReS coded DPSK systems is illustrated in Fig. 5.2. The information-bit stream $b(i)$ is ReS encoded and then interleaved in the block $\pi$ of Fig. 5.2 to create the encoded-bit stream $s(i)$. Then $s(i)$ is mapped to the symbols $r(i)$ before differential modulation, which may be described as

$$x(i) = x(i-1) \cdot r(i), \tag{5.1}$$

where $x(i)$ represents the differentially modulated symbols and $x(0)$ is the reference symbol, which is known at both the transmitter and the receiver. Finally, the symbols are transmitted to both the relay and to the destination.

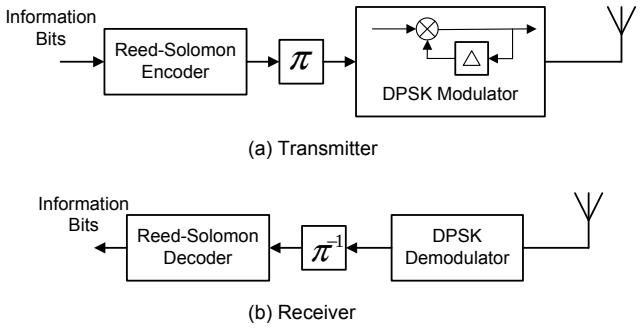


Figure 5.2: Transceiver schematic of ReS coded DPSK scheme

Depending on the specific type of relaying, the signals received at the relay will be appropriately processed. If AF relaying is employed, the signal will be amplified by the gain-factor given in Eq. (4.26) before being forwarded it to the DS. By contrast, in case of DF relaying the signals will be decoded and checked for errors. If errors are detected in the decoded packet, the relay will turn to the idle state. Otherwise, it will re-encode and re-modulate the packet for forwarding it to the DS.

At the destination, the signals received are first passed to the demodulator. For Single Symbol Differential Detection (SSDD), the phase of the two consecutive received symbols is compared and used for determining the value of the symbols. Mathematically, the symbols may be expressed as

$$z(t) = y(t) \cdot y^*(t-1), \tag{5.2}$$

where the superscript * denotes complex conjugation, $y(t)$ represents the symbols received at the destination, which are contaminated by fading and noise, while $z(t)$ denotes the differentially demodulated symbols.

Subsequently, the demodulated signals of both the source and of the relay are combined. In non-coherent detection, the MRC technique cannot be invoked owing to the unavailability of the CSI.

Table 5.2: Basic parameters of DPSK aided ReS coded H-ARQ system

| Parameters | Value |
|---|---|
| Rees-Solomon code: m/k/n | 8/223/255 |
| Modulation type | DBPSK |
| Relay type | fixed |
| N$^o$ of relays | L=1 |
| Normalized $d_{SR_l}/d_{R_lD}$ | 0.7/0.3 for AF<br>0.3/0.7 for DF |
| Source's transmit power | $E_S = \frac{E_b}{G_{rd}+1}$ |
| Relays' transmit power | $E_{R_l} = \frac{G_{rd}E_b}{G_{rd}+1}$ |
| Channel model | correlated Rayleigh fading |
| Normalized Doppler freq. of SD link | $f_{SD}T_s = \{0.001, 0.03\}$ |
| Normalized Doppler freq. of SR$_l$ link | $f_{SR_l}T_s = \{0.001, 0.03\}$ |
| Normalized Doppler freq. of R$_l$D link | $f_{R_lD}T_s = \{0.001, 0.03\}$ |
| Maximum number of retransmissions | 5 |

Thus, typically EGC and SC are employed. After deinterleaving, the combined signal is decoded and checked for the presence of errors. Owing to the ReS codes' capability of detecting errors, the error-detecting codes may be omitted here. If an error is detected, then the retransmissions will be activated. Otherwise, a new packet will be transmitted, as usual.

**b. Performance Results**

In the following, the performance of the DPSK aided ReS coded HARQ system of Fig. 5.2 using non-coherent detection will be investigated. The basic simulation parameters are provided in Table 5.2.

The performance results are shown in Figs. 5.3-5.5. In these figures, the left hand side illustration was recorded for the normalized Doppler frequency of $10^{-3}$ Hz, while the right hand side figures for $3.10^{-2}$ Hz. According to these figures, the relaying schemes provide a better BER performance than conventional direct transmissions. Relaying also reduces the number of retransmissions, whilst increasing the effective throughput.

In case of uncoded ARQ systems, it may be observed from Fig. 5.3 that the AF and DF relaying schemes achieve gains of 2 dB and 3 dB in terms of the $E_b/N_0$, respectively, at the BER of $10^{-5}$, compared to the direct transmission. Additionally, the performance of uncoded systems was only slightly affected, when the Doppler frequency was varied from $10^{-3}$ Hz to $3.10^{-2}$ Hz. However, the results became significantly different in case of the ReS coded schemes. When the Doppler frequency was 0.001 Hz, the ReS coded AF and DF relaying schemes performed similarly and achieved only 1 dB better $E_b/N_0$ than both the non-cooperative ReS coded scheme and the uncoded DF relaying. Meanwhile, ReS coded DF relaying achieved a gain of 2 dB and 3 dB, compared to the ReS coded AF and to the non-cooperative ReS coded schemes, respectively at the BER of $10^{-5}$, although the ReS coded AF relaying and the direct transmission did not perform very differently. Moreover, at the normalized Doppler frequency of 0.03 Hz the coded DF relaying scheme exhibited a BER of $10^{-5}$ at the $E_b/N_0$ of 10 dB, compared to the $E_b/N_0$ value of 12 dB in the same system configuration operating at the Doppler frequency of 0.001 Hz. Hence, we concluded that the cooperative ReS coded HARQ

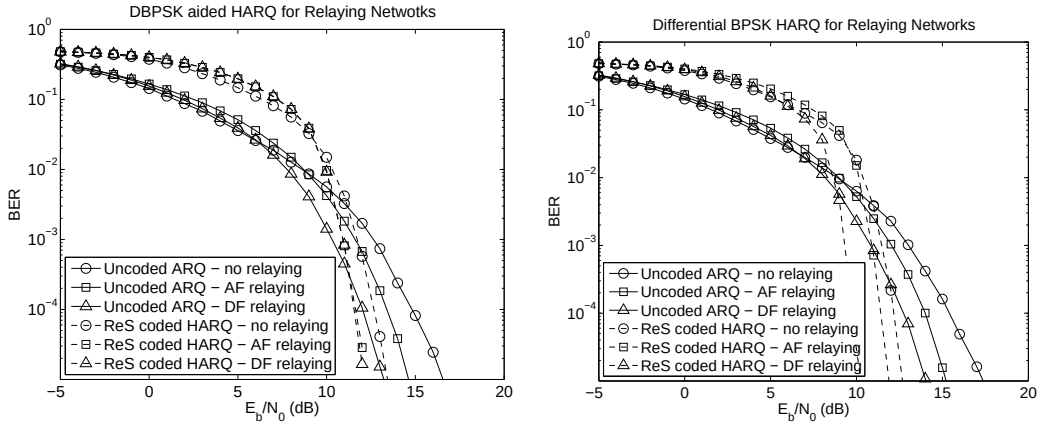


(a) $f_{Doppler} = 10^{-3}$ (b) $f_{Doppler} = 3.10^{-2}$

Figure 5.3: BER performance of DBPSK aided HARQ for non-cooperative and cooperative networks, where the transceiver schematic is shown in Fig. 5.2 and the system parameters are provided in Table 5.2.

schemes were capable of reducing the BER, when the Doppler frequency increased.

Moreover, according to Fig. 5.4, the DF relaying aided ReS coded HARQ is capable of achieving a better BER performance at higher Doppler frequencies at the cost of an increased number of retransmissions. More particularly, at an $E_b/N_0$ of 20 dB all the observed schemes have to double the number of retransmissions in case of $f_D = 0.03\ Hz$, compared to the same schemes operating at $f_D = 10^{-3}\ Hz$. However, the emergent trend is that the relaying schemes are capable of significantly reducing the number of retransmissions required.

As a result of the increased number of retransmissions, the effective throughput of the system significantly decreases, as observed in Fig. 5.5. Similarly, as seen in Fig. 5.5, at the $E_b/N_0$ of 20 dB the throughput was reduced by a third, when the Doppler frequency increased from $10^{-3}$ Hz to $3.10^{-2}$ Hz.

#### 5.2.1.2 Multiple-Symbol Differential Detection

The conventional differential PSK is an appealing simple detection technique, which operates without carrier acquisition and tracking in the receiver. However, it suffers from a performance penalty compared to its higher-complexity coherent counterpart. This performance penalty is further increased for high-Doppler scenarios, when the fading envelope changes substantially between the consecutive symbols. Hence, the Multi-Symbol Differential Detection (MSDD) philosophy was proposed by Divsalar and Simon [236]. In this section, we will study the performance of the MSDD scheme assisting the ReS coded HARQ system in the context of wireless relaying aided networks.

The system structure of the MSDD-aided schemes is similar to the SSDD schemes of Fig. 5.2, except for the demodulator at the receiver. Instead of simply comparing the received phases between two consecutive symbols in order to make a decision, the MSDD detector makes a joint decision based on multiple received symbols. For transmission over fading channels, the ML detector is based on the

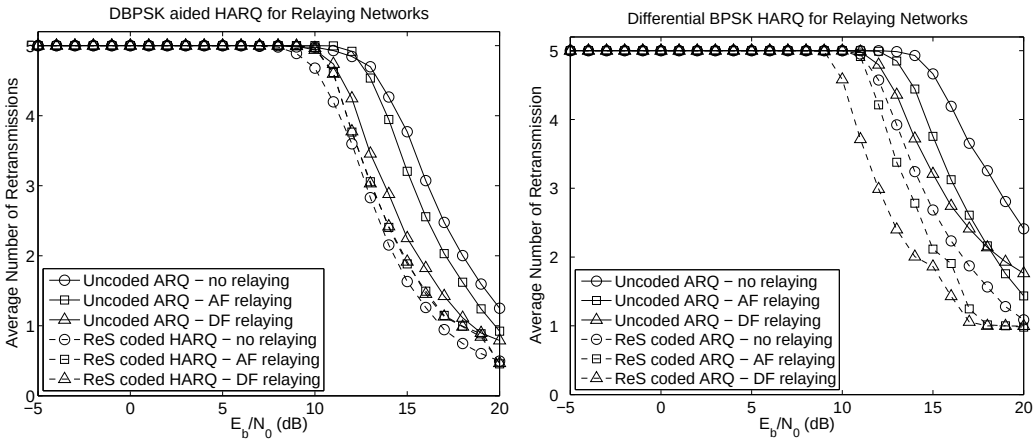


(a) $f_{Doppler} = 10^{-3}$ (b) $f_{Doppler} = 3.10^{-2}$

Figure 5.4: Number of retransmissions of DBPSK aided HARQ for non-cooperative and cooperative networks, where the transceiver schematic is shown in Fig. 5.2 and the system parameters are provided in Table 5.2.

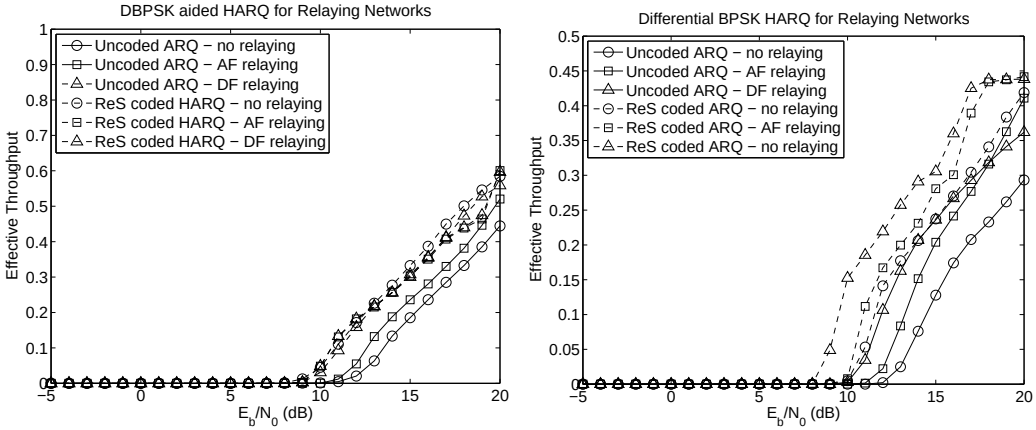


(a) $f_{Doppler} = 10^{-3}$ (b) $f_{Doppler} = 3.10^{-2}$

Figure 5.5: Throughput of DBPSK aided HARQ for non-cooperative and cooperative networks, where the transceiver schematic is shown in Fig. 5.2 and the system parameters are provided in Table 5.2.

following decision [242]

$$\hat{\boldsymbol{s}} = arg \ \min_{\boldsymbol{s}} \left\{ \boldsymbol{y}^H \boldsymbol{R}_{\boldsymbol{yy}} \boldsymbol{y} \right\}, \tag{5.3}$$

where $\hat{\boldsymbol{s}}$ represents the estimated version of the corresponding $N$ symbol vector $\boldsymbol{s}$ and $\boldsymbol{y}$ indicates the vector of $N$ consecutive received symbols, while $\boldsymbol{R}_{\boldsymbol{yy}}$ denotes the correlation matrix, which is given by

$$\boldsymbol{R}_{\boldsymbol{yy}} \triangleq \varepsilon\{\boldsymbol{y}\boldsymbol{y}^H | \boldsymbol{s}\} = diag\{\boldsymbol{s}\}\boldsymbol{C}diag\{\boldsymbol{s}^*\}, \tag{5.4}$$

where $\boldsymbol{C} \triangleq \varepsilon\{\boldsymbol{h}\boldsymbol{h}^H\} + \sigma_n^2 \boldsymbol{I}_N$. Hence, Eq. (5.7) may be rewritten as

$$\hat{\boldsymbol{s}} = arg \ \min_{\boldsymbol{s}} \left\{ (diag\{\boldsymbol{r}\}\boldsymbol{s}^*)^H \boldsymbol{C}^{-1} (diag\{\boldsymbol{r}\}\boldsymbol{s}^*) \right\}. \tag{5.5}$$

The matrix $\boldsymbol{C}$ has real-valued entries and it is symmetric as well as positive definite, hence we may apply the Cholesky decomposition [243] of the inverse matrix, yielding

$$\boldsymbol{C} = \boldsymbol{L}\boldsymbol{L}^H, \tag{5.6}$$

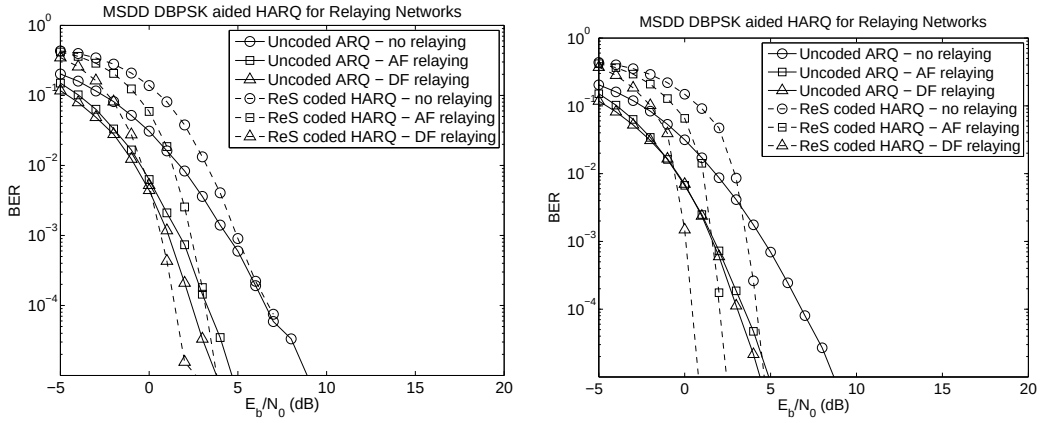


(a) $f_{Doppler} = 10^{-3}$ (b) $f_{Doppler} = 3.10^{-2}$

Figure 5.6: BER performance of MSDD-DBPSK aided HARQ for non-cooperative and cooperative networks, where the MSDD has a window size of 3 and the other system parameters are provided in Table 5.2.

where $\boldsymbol{L}$ is a lower triangular matrix. If we define furthermore $\boldsymbol{U} \triangleq (\boldsymbol{L}^H diag\{\boldsymbol{r}\})^*$, where $\boldsymbol{U}$ is the upper triangular matrix, then the ML decision rule of (5.5) is finally simplified to

$$\hat{\boldsymbol{s}} = arg \min_{\boldsymbol{s}} \left\{ ||\boldsymbol{U}\boldsymbol{s}||^2 \right\}. \tag{5.7}$$

Although the MSDD technique enhances the system's resilience against increased Doppler frequencies, the decoding complexity is exponentially increased with the number of simultaneously detected symbols, or - synonymously - with the width of the detection window. To reduce the associated search complexity, the sphere detection philosophy [244] may be combined with the MSDD scheme in the demodulator.

For a convenient comparison between the SSDD and the MSDD schemes, all the simulation parameters in this part are the same as those of Table 5.2. A detection window size of $N_w = 3$ is chosen for the MSDD.

Based on Figs. 5.6-5.8, we found that most of our discussions provided for the SSDD DPSK aided HARQ systems in Section 5.2.1.1 may also apply to the MSDD scenario. However, an interesting point was observed, namely that the AF relaying aided schemes are capable of outperforming the DF relaying arrangements in terms of both the number of retransmissions and the achievable throughput in the high $E_b/N_0$ region, namely above 12 dB in our simulations. This observation may be explained by the fact that the MSDD receiver is capable of averaging multiple noise samples, hence tending to a zero mean and to a reduced influence.

Comparing the results of Figs. 5.3-5.8, it may be clearly recognized that the MSDD observed in Figs. 5.3 and 5.6 significantly improves the system's performance in all three observed aspects, compared to the SSDD scheme. Numerically, observe in Figs. 5.3 and 5.6 that the MSDD aided HARQ scheme is capable of providing a gain of up to 10 dB over the SSDD ones in terms of reducing the transmit power without degrading the system's performance .

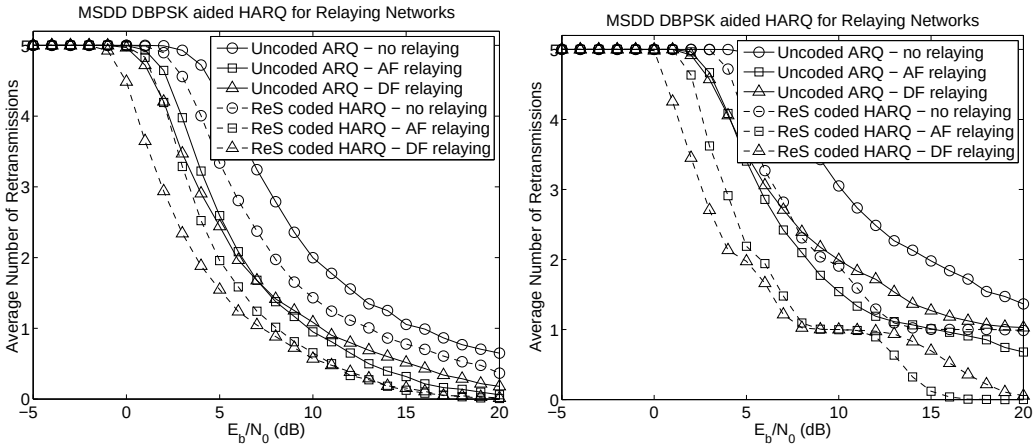


(a) $f_{Doppler} = 10^{-3}$ (b) $f_{Doppler} = 3.10^{-2}$

Figure 5.7: Number of retransmissions of MSDD-DBPSK aided HARQ for non-cooperative and cooperative networks, where the MSDD has a window size of 3 and the other system parameters are provided in Table 5.2.

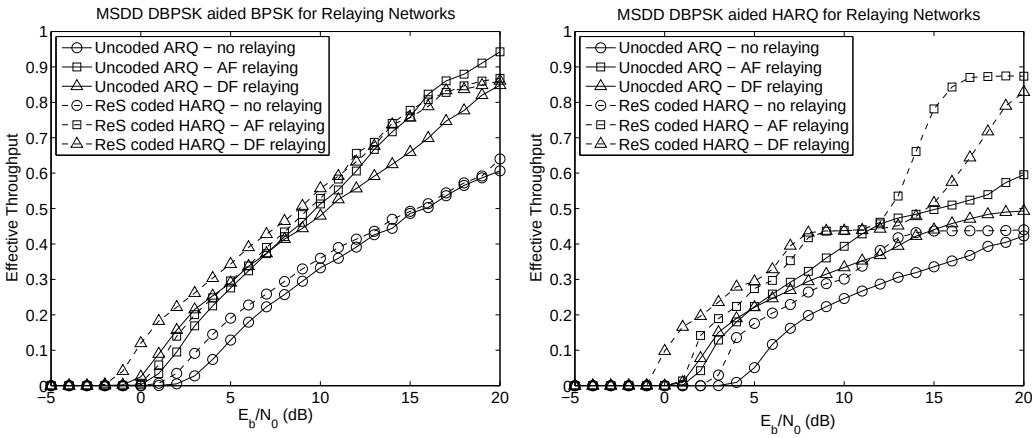


(a) $f_{Doppler} = 10^{-3}$ (b) $f_{Doppler} = 3.10^{-2}$

Figure 5.8: Throughput of MSDD-DBPSK aided HARQ for non-cooperative and cooperative networks, where the MSDD has a window size of 3 and the other system parameters are provided in Table 5.2.

### 5.2.2 Differential Phase Shift Keying with Iterative Decoding

As a further advance, the soft-output MSDD designed for DPSK is combined with convolutional coding [25] in order to exploit the powerful principle of turbo detection. The transceiver schematic of the DPSK aided convolutional coded HARQ system is shown in Fig. 5.9, which may be contrasted to the non-iterative scheme of Fig. 5.2. Additionally, a Unity Rate Code (URC) having an Infinite Impulse Response (IIR) is inserted between the convolutional codec and the DPSK modulator, because it was demonstrated in [25] that URCs substantially improve the convergence of iterative receivers owing to their ability to efficiently spread the extrinsic information without increasing the delay of the turbo interleaver $\pi_1$.

The received signals are detected with the aid of iterative information exchange between the three-detector components, namely the MSDD demodulator, the URC decoder and the convolutional

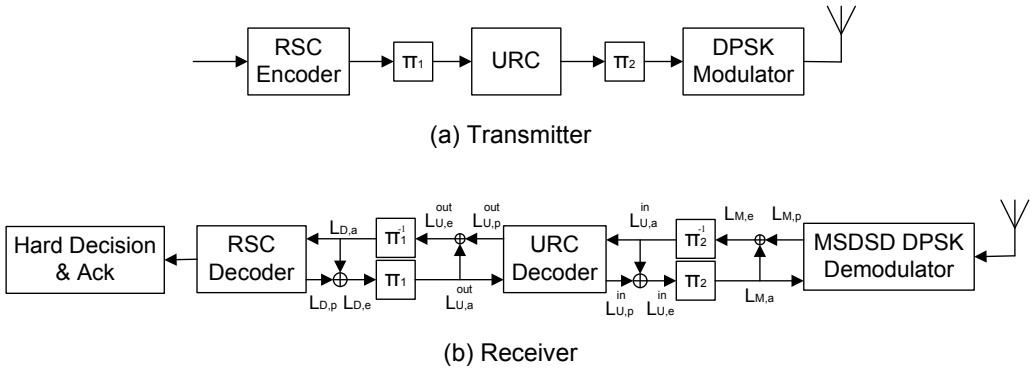


Figure 5.9: Transceiver schematic of convolutional coded DPSK scheme, which may be contrasted to the non-iterative scheme of Fig. 5.2.

decoder of Fig. 5.9.b. Following the last iteration, hard decisions are carried out and are checked for the presence of residual errors. Due to the lack of a reliable error detection capability for the family of convolution codes, an error-detecting code, such as a Cyclic Redundancy Check (CRC) code is concatenated with the detector. The main parameters used in our simulations are shown in Table 5.3, where the half-rate RSC code substitutes for the $(225, 255, 16)$ ReS code as in Table 5.2.

Table 5.3: Basic parameters of DPSK aided convolutional coded H-ARQ system.

| **Parameters** | **Values** |
|---|---|
| information/encoded bits | 500/1000 |
| Modulation type | DBPSK |
| Relay type | fixed |
| N$^o$ of relays | L=1 |
| Normalized $d_{SR_l}/d_{R_lD}$ | 0.7/0.3 for AF<br>0.3/0.7 for DF |
| Source's transmit power | $E_S = \frac{E_b}{G_{rd}+1}$ |
| Relays' transmit power | $E_{R_l} = \frac{G_{rd}E_b}{G_{rd}+1}$ |
| Channel model | correlated Rayleigh fading |
| Maximum number of retransmissions | 5 |

Fig. 5.10 characterizes the attainable performance of the convolution coded HARQ scheme operating in a relaying aided network. According to the figure, in case of an uncoded system the relaying schemes allow the transmit power to be reduced by approximately 6 dB without degrading the attainable BER performance. When convolutional coding is introduced, the power-reduction can be further increased by 3 dB. Furthermore, there is 1 dB performance discrepancy between AF and DF aided relaying.

Similarly, the effective throughput seen in Fig. 5.10(b) is also significantly improved, when the convolutional coding aided relaying schemes are employed. Again, observe in Fig. 5.10(b) that above the $E_b/N_0$ values of 3 dB and 5 dB for the coded and uncoded schemes, respectively, the AF relaying

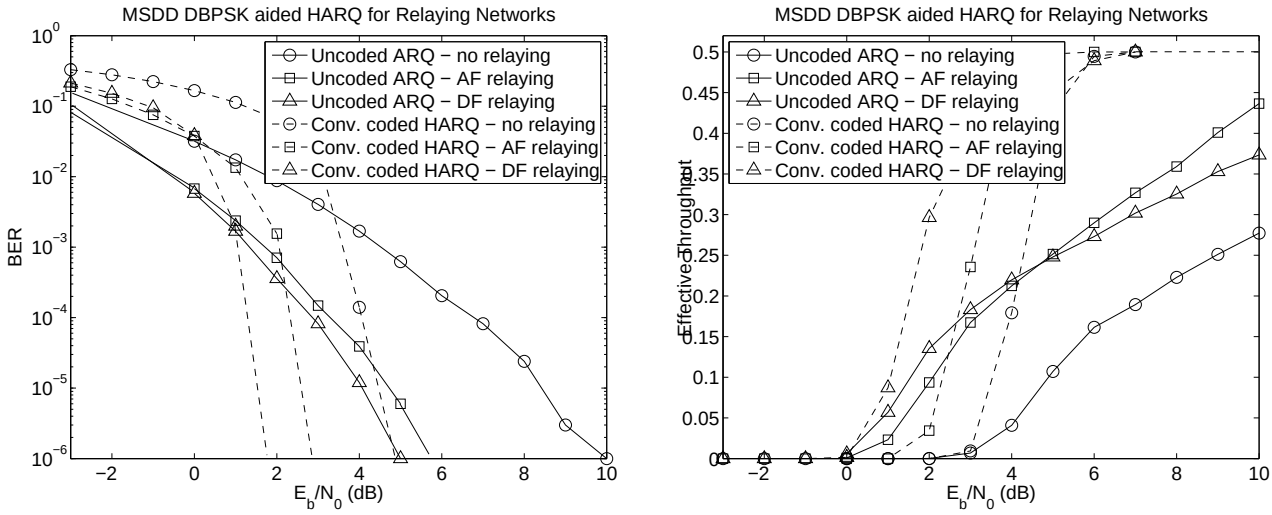


(a) BER

(b) Throughput

Figure 5.10: MSDD DBPSK aided convolutional coded HARQ for non-cooperative and cooperativeAF/DF networks, where the MSDD has a window size of 3 and the other system parameters are provided in Table 5.3.

arrangement achieved a better throughput than the DF regime.

### 5.2.3 Comparison of Coherent and Non-Coherent Detection

The performance of the H-ARQ schemes employing perfect- and imperfect-CSI-based-coherent detection were presented in Chapter 3 and 4, respectively, while a number of the H-ARQ schemes utilizing non-coherent detection were investigated in Sections 5.2.1 and 5.2.2. In order to provide an insightful comparison among these detection schemes in the context of cooperative scenarios, we consider three cases. The first one employs coherent detection with the assistance of pilot symbols, which are assumed to be perfectly recovered at the destination's receiver. More practically, the second scenario assumed that the pilot symbols are imperfectly recovered, resulting in CSI errors at the destination's decoders. Lastly, the non-coherent detection scheme using differential modulation and MSDD is considered. The details of the three schemes are provided in Table 5.4. The channels are assumed to have three different Doppler frequencies, namely $f_D = 10^{-1}$, $10^{-2}$ and $10^{-3}$.

The BER and FER performances of the three considered schemes of Table 5.4 are shown in Fig. 5.11. According to the figure, the performance of the PSA schemes degrades in accordance with the reduction of the channel's correlation. More particularly, the performance of the imperfect-PSA-aided-coherent detection is 1 dB worse than that of the perfect-PSA-based scheme at the BER of $10^{-6}$ as well as at the FER of $10^{-3}$, when the channel's normalized Doppler frequency was $10^{-3}$. When the Doppler frequency increased to $10^{-2}$ and $10^{-1}$, the degradation was approximately 3 dB and 4 dB, respectively. The reason is that upon increasing the channel's normalized Doppler frequency, an increased number of pilot symbols is required to estimate the CSI. Therefore, this reduces the effective SNR of the data bits and hence degrades the performance.

In contrast to the imperfect-coherent detection schemes, at $f_D = 10^{-2}$ the performance of the

Table 5.4: Basic parameters of convolutional coded BPSK aided H-ARQ schemes.

| **Detection Scheme** | **Perfect Coherent** | **Imperfect Coherent** | **Non-Coherent** |
|---|---|---|---|
| Information/Encoded bits | 500/1000 | 500/1000 | 500/1000 |
| Channel code type | RSC | RSC | RSC |
| Generator polynomial | (5,7) | (5,7) | (5,7) |
| Modulation type | BPSK (assisted by Pilot Symbols) | BPSK (assisted by Pilot Symbols) | DBPSK |
| Demodulation type | Coherent with perfect CSI | Coherent with imperfect CSI | MSDD with Window Size of 3 |
| N$^o$ of Pilot Symbols | $1000 \cdot 2 \cdot f_D$ | $1000 \cdot 2 \cdot f_D$ | N/A |
| Detection type | Iterative detection | Iterative detection | Iterative detection |
| Relay type | AF | AF | AF |
| N$^o$ of relays aided | 1 | 1 | 1 |
| Normalized $d_{SR}/d_{RD}$ | 0.7/0.3 | 0.7/0.3 | 0.7/0.3 |
| Source's transmit power | $E_S = \frac{E_b}{G_{rd}+1}$ | $E_S = \frac{E_b}{G_{rd}+1}$ | $E_S = \frac{E_b}{G_{rd}+1}$ |
| Relays' transmit power | $E_R = \frac{G_{rd}E_b}{G_{rd}+1}$ | $E_R = \frac{G_{rd}E_b}{G_{rd}+1}$ | $E_R = \frac{G_{rd}E_b}{G_{rd}+1}$ |
| Channel model | correlated Rayleigh fading | correlated Rayleigh fading | correlated Rayleigh fading |
| Max. n$^o$ of retrans. | 5 | 5 | 5 |

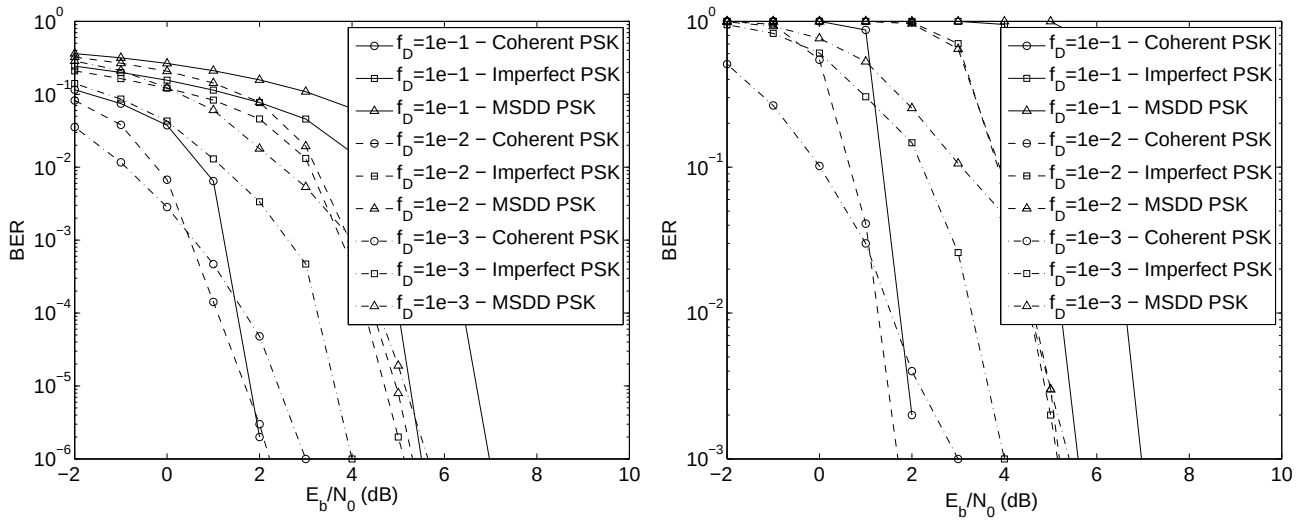


(a) BER versus $E_b/N_0$

(b) FER versus $E_b/N_0$

Figure 5.11: Performance of convolution coded BPSK aided HARQ for cooperative networks employing perfect-, imperfect- and non-coherent MSDD, where the system configurations are detailed in Table 5.4.

non-coherent scheme using MSDD is better than those operating at $f_D = 10^{-1}$ and $f_D = 10^{-3}$. This fact may be explained by noting that the operation of MSDD benefits from the correlation between the channel coefficients. Thus, when the channel's correlation is low, i.e we have $f_D = 10^{-1}$, the MSDD performs inefficiently. By contrast, as analysed in [245], the mutual information penalty of ignoring the phase distortion correlation may be smaller than that of the slower time-varying channel. Therefore, the degraded performance of the MSDD at $f_D = 10^{-3}$ is not unexpected.

Furthermore, it is clearly seen from Fig. 5.11 that the non-coherent MSDD schemes only perform comparably to the imperfect-coherent detection scheme for the moderate-correlation fading channels, namely for $f_D = 10^{-2}$. In the other channels, coherent detection outperforms the non-coherent schemes.

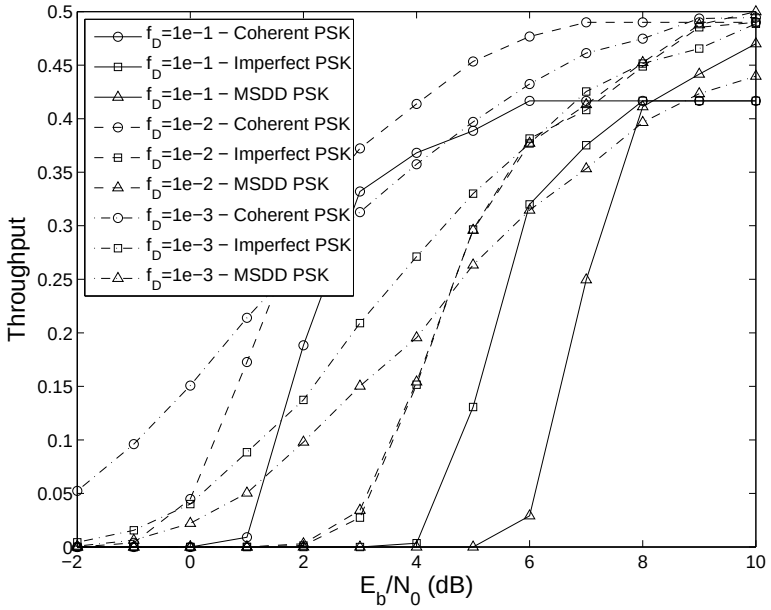


Figure 5.12: The effective throughput of convolution coded BPSK aided HARQ for cooperative networks employing perfect-, imperfect- and non-coherent MSDD, where the system configuration was detailed in Table 5.4.

Furthermore, the effective throughput of the three detection schemes of Table 5.4 is shown in Fig. 5.12. As seen in the figure, for the rapidly time-varying fading channels coherent detection should be employed in the low $E_b/N_0$ region, while the non-coherent MSDD should be utilized in the high $E_b/N_0$ region in order to avoid reducing the system's throughput due to the employment of a large number of pilot symbols. In moderately correlated fading channels, i.e. for $f_D = 10^{-2}$ in the above-mentioned scenarios, the non-coherent MSDD should be chosen due to its ability to perform comparably to the coherent scheme, especially, since it is capable of providing an increased throughput for $E_b/N_0$ values above 6 dB. By contrast, in slow-fading channels, the transmission schemes based on coherent detection have the edge.

## 5.3 Frequency Shift Keying Aided H-ARQ

### 5.3.1 Reed-Solomon Coded Non-coherent Frequency Shift Keying

Frequency Shift Keying (FSK) [66] constitutes another non-coherent detection scheme, which has benefits in the context of wireless cooperative networks. In order to mitigate the performance degradation imposed by the channel noise, interference and fading, FSK may be combined both with FEC, such as the ReS codes, as well as with the Slow Frequency Hoping (SFH) Spread Spectrum (SFH/SS) concept [246–249]. Owing to the FSK's capability of detecting erased and corrupted symbols, the 'error-and-erasure' decoding is preferable to the 'error-correction-only' decoding in the context of ReS coded SFH/SS systems employing $M$-ary FSK modulation, since a reduced BER can be achieved, provided that a reliable erasure insertion scheme is invoked. This is because as detailed in [11], an ReS $(N, K)$ code is capable of correcting $t = \lfloor \frac{N-K}{2} \rfloor$ symbol errors, or alternatively, it can fill $2t = (N-K)$ erased symbols - provided that the receiver can confidently inform the ReS decoder, which symbols were erased by the channel. Several erasure insertion (EI) techniques assisting error-and-erasure ReS decoding were proposed in [250, 251], namely the ratio-threshold test (RTT), the output threshold test (OTT), and the joint maximum output and ratio threshold test (MO-RTT).

In this section, we propose and characterize a the ReS coded SFH M-FSK system, which is subjected to both partial-band interference and Rayleigh fading in the context of a the wireless cooperative network. An EI scheme conceived for error-and-erasure ReS decoding based on the joint MO-RTT technique will be invoked. The related decision statistics will be analysed and the corresponding analytical expressions of the ReS codeword error probability as well as of the bit error ratio (BER) will be derived, after the concept of erasure decoding was introduced. Our results show that the EI ReS decoding scheme may significantly enhance the achievable overall system performance in the context of wireless relaying networks.

Furthermore, we compared the attainable performance of the proposed ReS coded system in wireless cooperative networks to those of convolutional codes and Low Density Parity Check (LDPC) codes [37], which support efficient iterative detection at the cost of relying on sophisticated transceiver designs. Our results demonstrated that although the proposed ReS coding scheme is capable of outperforming convoluational codes in the context of short-packet based transmissions, the LDPC code considered had an edge. Therefore, the ReS coded systems using error-and-erasure decoding may be deemed to constitute an attractive design option for low-complexity as well as low-latency systems.

#### 5.3.1.1 Error Detection Techniques Based on Frequency Shift Keying Modulation

FSK belongs to the family of orthogonal modulation schemes. For example, in M-ary FSK a group of $b = log_2(M)$ information bits is mapped and transmitted by one of $M$ frequencies.

If the signal waveform is represented as

$$s_i(t) = Re[s_{li}(t)e^{j2\pi f_c t}], \qquad (i = 1, 2, ..., M), \tag{5.8}$$

where $s_{li}(t)$ is the equivalent lowpass signal, the matched-filter-type demodulator generates the $M$

complex-valued random variables

$$r_i = r_{ic} + jr_{is} = \int_0^T r_l(t)s_{li}^* dt, \qquad (i = 1, 2, ..., M), \tag{5.9}$$

where $r_l(t)$ is the received equivalent lowpass signal. Then, the optimum detector, such as the square-law detectors illustrated in Fig. 5.13, computes the $M$ squared envelopes as

$$U_i = r_{ic}^2 + r_{is}^2 \qquad (i = 1, 2, ..., M). \tag{5.10}$$

The $M$ squared envelopes generate the decision variables of $\{U_1, U_2, ..., U_M\}$, which may then be subjected to erasure detection.

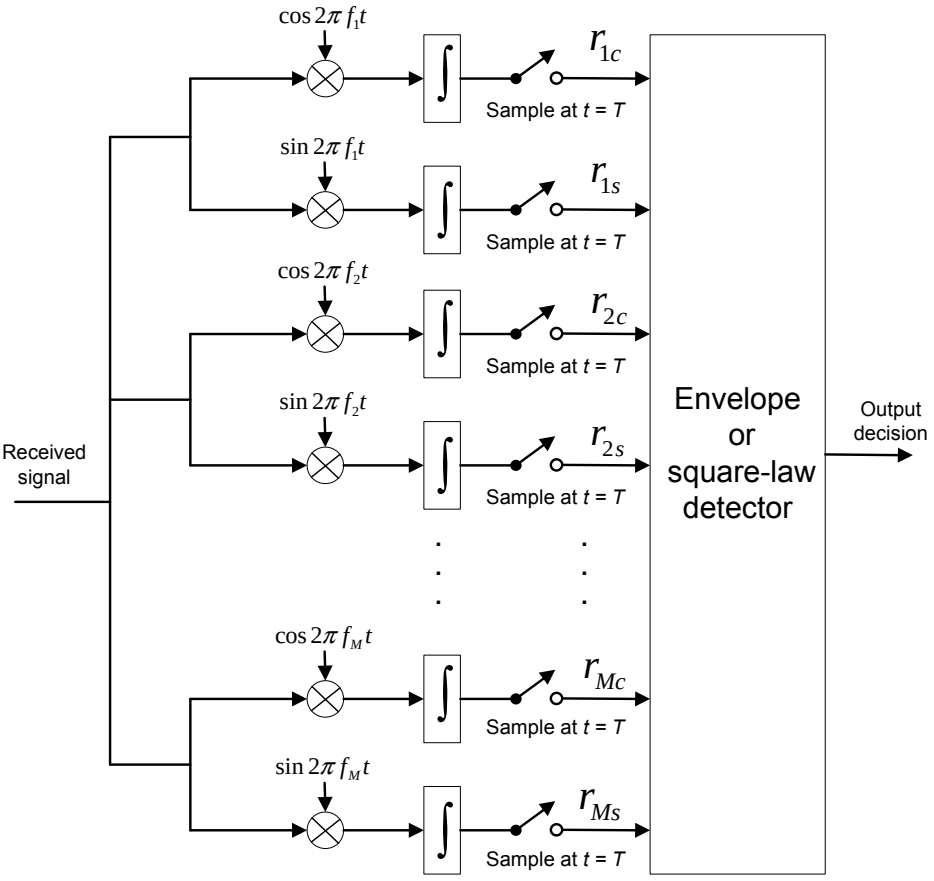


Figure 5.13: Demodulation of M-ary FSK signals for non-coherent detection.

The simplest possible detection philosophy would be to detect the highest of the $M$ decision variables representing the most likely $b$-bits symbol. However, there are more reliable techniques, as discussed in the following sections.

**a. Ratio-Threshold Test**

The Ratio-Threshold Test (RTT) was proposed by Viteri [250] in order to mitigate the effects of tone and partial band jamming imposed on FSK systems. In this test the filter outputs of the M-FSK demodulator are sorted in descending order, yielding

$$Y_{max} = Y_1 > Y_2 > ... > Y_{M-1} > Y_M = Y_{min}. \tag{5.11}$$

Then a pre-set threshold, $\lambda_T$, is chosen and the ratio, $\lambda = Y_2/Y_1$, of the 'second' largest decision variable is compared to the maximum to decide a decision-reliability bit $Q$, as follows

$$Q = \begin{cases} 0: \ \lambda_T \geq \lambda \ (high) \\ 1: \ \lambda_T < \lambda \ (low), \end{cases} \tag{5.12}$$

where $Q = 0$ and $Q = 1$ indicate a high- and low-reliability detection, respectively.

**b. Output Threshold Test**

In contrast to the RTT, the Output Threshold Test (OTT) [252] simply makes decision based on the maximum of the demodulator output, which is defined as

$$Y_1 = Y_{max} = max\{U_1, U_2, ..., U_M\}. \tag{5.13}$$

Therefore, it is not the optimum decision metric. Nonetheless, the results of [252] showed that the OTT may outperform the RTT, when communicating over the dispersive channels, despite its simplicity.

**c. Joint Maximum Output and Ratio Threshold Test**

The joint Maximum Output and Ratio Threshold Test (MO-RTT) proposed by Yang and Hanzo [251] is a further development of the RTT and the OTT. In the context of the joint MO-RTT the erasure detection is based on both the observation of the maximum $Y_1$ and the ratio $\lambda$.

The properties of the erasure detection schemes may be characterized by the joint PDFs of $Y_1$ and $Y_2$, namely by $f_{Y_1,Y_2}(y_1, y_2|H_1)$ and $f_{Y_1,Y_2}(y_1, y_2|H_0)$, given that the associated demodulated symbol is correct ($H_1$) and incorrect ($H_0$), respectively. These PDFs will allow us to evaluate the performance of the erasure insertion scheme in the forthcoming sections. According to [251], the joint PDFs can be expressed as

$$f_{Y_1,Y_2}(y_1, y_2|H_1) = \frac{M-1}{P_{N_n}(H_1)} f_{U_1}(y1) f_{U_m}(y_2) \left[ \int_0^{y_2} f_{U_j}(y)dy \right]^{M-2}, \tag{5.14}$$

$$\begin{aligned} f_{Y_1,Y_2}(y_1, y_2|H_0) = & \frac{M-1}{P_{N_n}(H_0)} \Bigg\{ f_{U_m}(y1) f_{U_1}(y_2) \left[ \int_0^{y_2} f_{U_j}(y)dy \right]^{M-2} \\ & + (M-2) f_{U_m}(y1) f_{U_j}(y_2) \left[ \int_0^{y_2} f_{U_1}(y)dy \right] \left[ \int_0^{y_2} f_{U_k}(y)dy \right]^{M-3} \Bigg\}, \\ & (y_1 \geq y_2 \geq 0; 2 \leq j \leq M, j \neq m; 1 \leq k \leq M, k \neq m, j), \end{aligned} \tag{5.15}$$

where $P_{N_n}(H_1)$ and $P_{N_n}(H_0)$ indicate the probability that the demodulator output is correct and incorrect, respectively, at a given noise value of $N_n$. Furthermore, $f_{U_1}()$ represents the PDF of the decision variable matched to the transmitted symbol, while $f_{U_m}()$ and $f_{U_j}()$ denote the PDFs of the decision variables mismatched to the transmitted symbol.

For the MO-RTT, let $Y_1 = Y$ and $Y_2 = Y\lambda$. Then the above joint PDFs may be rewritten as

$$f_{Y,\lambda}(y, r|H_1) = \frac{(M-1)y}{P_{N_n}(H_1)} f_{U_1}(y) f_{U_m}(yr) \left[ \int_0^{yr} f_{U_j}(x)dx \right]^{M-2}, \tag{5.16}$$

$$\begin{aligned} f_{Y,\lambda}(y, r|H_0) = & \frac{(M-1)y}{P_{N_n}(H_0)} \Bigg\{ f_{U_m}(y) f_{U_1}(yr) \left[ \int_0^{yr} f_{U_j}(x)dx \right]^{M-2} \\ & + (M-2) f_{U_m}(y) f_{U_j}(yr) \left[ \int_0^{yr} f_{U_1}(x)dx \right] \left[ \int_0^{yr} f_{U_k}(x)dx \right]^{M-3} \Bigg\}, \\ & (0 \leq y < \infty; 0 \leq r \leq 1). \end{aligned} \tag{5.17}$$

The PDFs of the RTT may be found by integrating both sides of (5.16) and (5.17) in terms of the variable $\lambda$ from zero to one, while those of the OTT may be evaluated by integrating both sides of (5.16) and (5.17) in terms of the variable $y$ from zero to infinity.

#### 5.3.1.2 Cooperative SFH FSK System Description

The system considered consists of a source station, $L$ relay stations and a destination station, as seen in Fig. 2.29, communicating over Rayleigh fading channels, which are additionally subjected to Partial-Band Gaussian Interference (PBGI). The cooperative communication process is divided into two time slots. In the first slot, the SS broadcasts its packets to all the RSs and the DS. In the second slot, each RS will forward the re-encoded packet to the DS, provided that it correctly decoded the received information. Otherwise, the packet will not be forwarded by RS.

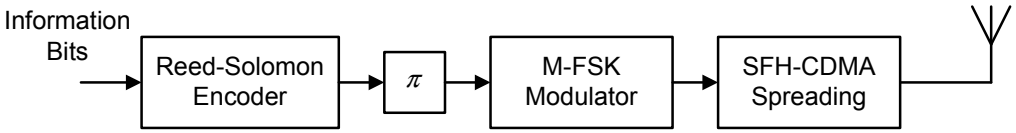


Figure 5.14: The transmitter block diagram of the Source Station using Reed-Solomon coded SFH $M$-ary FSK.

At the SS, the data bits are first encoded by the $(N, K)$ ReS code constructed over the Galois field $GF(2^b)$, which turns $K$ $b$-bit uncoded symbols into $N$ $b$-bit encoded symbols as seen in Fig. 5.14. Subsequently, the encoded symbols are passed to an $M$-ary FSK modulator of Fig. 5.14. We assume that $M = N = 2^b \geq 4$, so that each $b$-bit ReS coded symbol describes an $M$-ary FSK symbol. Finally, the frequency synthesizer of Fig. 5.14, which operates under the control of a pseudo noise (PN) generator, generates a sequence of random hopping frequencies, one of which is activated during each hop interval of duration $T_h$, or symbol interval $T_s$, where we assume $T_h = T_s$. In order to facilitate non-coherent detection at the receiver, the bandwidth of a specific frequency hopping (FH) tone is set to $B = 1/T_h$. The signal transmitted by the SS may be modelled as

$$x_i(t) = \sqrt{2E_s R_c} cos\{2\pi(f_n + f_i)t + \varphi_n + \varphi_i\}, \tag{5.18}$$

where $E_s$ is the bit-energy at the SS, $R_c = K/N$ is the ReS code-rate; $f_n$ is the hopping frequency during the $n^{th}$ FH interval and $f_i$ is the $i^{th}$ tone's frequency associated with the $i^{th}$ transmitted MFSK/ReS symbol. Finally, $\varphi_n$ and $\varphi_i$ are random phases during the $n^{th}$ FH interval and the $i^{th}$ symbol interval.

The modulated signal of each FH tone is assumed to be transmitted over non-dispersive fading channels obeying the Rayleigh distribution having the probability density function of [66]

$$f(|h|) = \frac{2|h|}{\Omega} e^{-|h|^2/\Omega}, \tag{5.19}$$

where $\Omega = E[|h|^2]$.

Furthermore, the communication channels are assumed to be contaminated by both PBGI and additive white Gaussian noise (AWGN). The PBGI occupies a fraction of $\rho \leq 1$ of the total frequency band, having the power spectral density of $N_I/2\rho$, while the AWGN has the power spectral density of

$N_0/2$. Consequently, in the specific portion of the frequency-band interfered by the PBGI, the total noise power spectral density is $N_n/2 = N_0/2 + N_I/2$, while it is $N_n/2 = N_0/2$ in the remainder of the band.

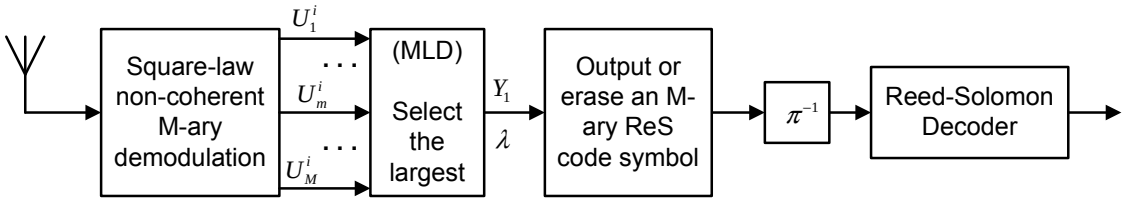


Figure 5.15: The receiver block diagram of the Relay Station using Reed-Solomon coded SFH $M$-ary FSK.

As a result, the signal received at the $l^{th}$ RS may be expressed as

$$r_{il}(t) = G_{sr_l} h_{i,sr_l} \sqrt{2E_s R_c} cos\{2\pi(f_n + f_i)t + \phi_{i,sr_l}\} + n_{i,sr_l}(t), \tag{5.20}$$

where $G_{sr}$ is the path-loss related gain [11], $h_{i,sr_l}$ is the fading coefficient of the $l^{th}$ Source-to-Relay (SR) link, $n_{i,sr_l}$ is the effective noise as defined above and $\phi_{i,sr_l}$ includes all the phases contributing to the received signal's phase due to frequency hopping, carrier and MFSK modulation as well as that induced by the fading.

After demodulation, the RS will carry out demodulate and decode the packet using the schematic of Fig. 5.15. If the packet is correctly decoded, it will be re-encoded, re-modulated and forwarded to the DS. Otherwise, the RS will ignore the packet and becomes idle, awaiting a new packet from the SS. The probability of a packet being forwarded from the RS to the DS will be detailed later.

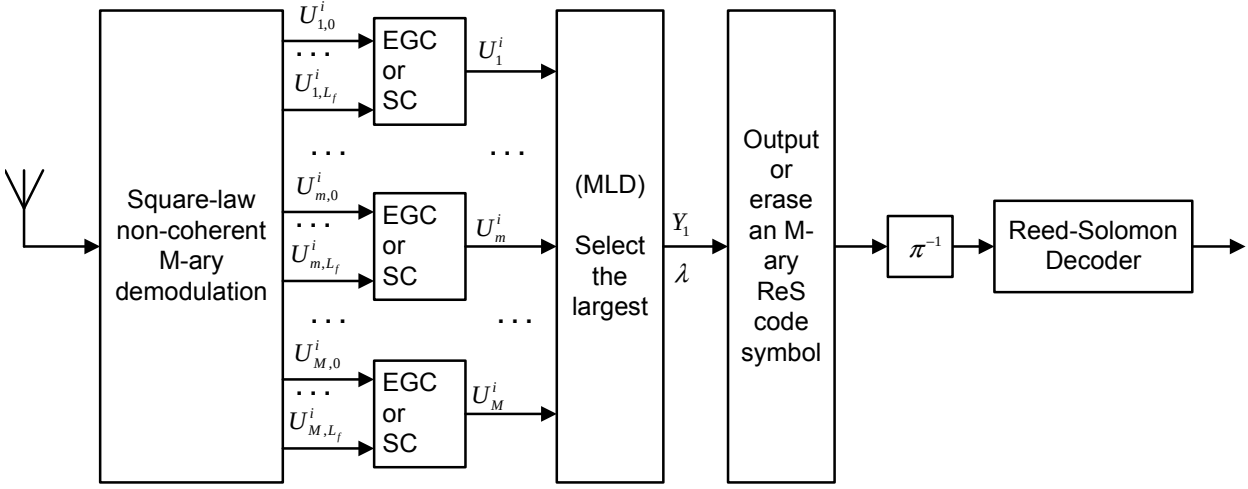


Figure 5.16: The receiver block diagram of the Destination Station using Reed-Solomon coded SFH $M$-ary FSK.

Finally, the signal received at the DS may be expressed as

$$y_i(t) = \sum_{l=0}^{L} G_l h_{i,l} \sqrt{2E_l R_c} cos\{2\pi(f_n + f_i)t + \phi_{i,l}\} + n_{i,l}(t), \tag{5.21}$$

where $G_l$ is the reduced-pathloss-related gain of the $l^{th}$ Relay-to-Destination (RD) link, while $h_{i,l}$ is the fading coefficient of the $l^{th}$ RD link. In Eq. (5.21), the direct Source-to-Destination (SD) link is

represented by $l = 0$, where we have $h_{i,0} = h_{i,sd}$, $G_{i,0} = G_{i,sd}$ and $n_{i,0} = n_{i,sd}$. Again, it is assumed that the fading and noise variances of the RD links are identical. Furthermore, $E_l$ represents the transmit power of the relay. In order to make the comparison between the equal-gain combining technique and the selection combining technique at the destination's receiver convenient, $E_l$ is set to $E_s \frac{G_l}{G_0}$.

The ReS channel decoders at both the RS of Fig. 5.15 and the DS of Fig. 5.16 employ the error-and-erasure decoding [251] in order to improve the achievable performance. In this section, our analysis will be focused on the MO-RTT technique [251], which outperforms both the OTT and the RTT techniques [251, 253].

#### 5.3.1.3 ReS-Coded SFH FSK Using Error-and-Erasure Decoding

In this section we derive the SEP, the BEP as well as the goodput of the proposed ReS-coded SFH FSK scheme using error-and-erasure decoding. Similar to Section 4.2.3.1, the analysis process, which may be applied to both the RS and the DS, is detailed as follows

- **Step 1.** Calculate both the average erroneous probability, $P_{N_0}(H_0)$, and the correct symbol probability $P_{N_0}(H_1)$ of M-FSK [66].
  $\downarrow$
- **Step 2.** Calculate both the symbol erasure probability, $P_e$, and the random symbol error probability, $P_t$, before ReS decoding [251].
  $\downarrow$
- **Step 3.** Compute the Codeword decoding Error Probability (CEP), $P_w$ [254].
  $\downarrow$
- **Step 4.** Compute the SEP, $P_s$ [11].
  $\downarrow$
- **Step 5.** Compute the BEP, $P_b$ [66].
  $\downarrow$
- **Step 6.** Compute the goodput, $\eta_g$, using Eq. (4.20).

Due to the earlier assumption that the packets are only forwarded to the destination, when they are correctly decoded, Steps {4,5,6} will be omitted at the RS.

**a. At the Relay**

The transmissions from the SS to the relays of Fig. 2.29 rely on the schematic of Fig. 5.14, similarly to the traditional direct communication between two nodes. Again, a $t$-error-correction ReS$(N, K, t)$ code can actually correct up to $2t = N - K$ erroneous symbols, provided that the position of the erroneous symbols are known. Hence, according to [254], the codeword decoding error probability after "errors-and-erasures" ReS$(N, K, t)$ decoding at the $l^{th}$ relay can be expressed as:

$$P_w = \sum_{i=0}^{N} \sum_{j=j_0(i)}^{N-i} \binom{N}{i} \binom{N-i}{j} P_{t,l}^i P_{e,l}^j (1 - P_{t,l} - P_{e,l})^{N-i-j}, \tag{5.22}$$

where $j_0(i) = max\{0, N-K+1-2i\}$, while $P_{e,l}$ and $P_{t,l}$ represent the symbol erasure probability and random symbol error probability before ReS decoding, which are given for the MO-RTT as [251]

$$\begin{aligned} P_{e,l} &= (1-\rho)P_{e,l}(N_{0,l}, Y_{T_1,l}, \lambda_{T_1,l}) + \rho P_{e,l}(N_{0,l} + N_{I,l}/\rho, Y_{T_2,l}, \lambda_{T_2,l}) \qquad (5.23)\\ &= (1-\rho)\Bigg[P_{N_{0,l}}(H_1)\int_0^{Y_{T_1,l}}\int_{\lambda_{T_1,l}}^{1} f_{Y_1,\lambda,l}(y,r|H_1)drdy + P_{N_{0,l}}(H_0)\int_0^{Y_{T_1,l}}\int_{\lambda_{T_1,l}}^{1} f_{Y_1,\lambda,l}(y,r|H_0)drdy\Bigg]\\ &\quad +\rho\Bigg[P_{N_{0,l}+N_{I,l}/\rho}(H_1)\int_0^{Y_{T_2,l}}\int_{\lambda_{T_2,l}}^{1} f_{Y_1,\lambda,l}(y,r|H_1)drdy\\ &\qquad + P_{N_{0,l}+N_{I,l}/\rho}(H_0)\int_0^{Y_{T_2,l}}\int_{\lambda_{T_2,l}}^{1} f_{Y_1,\lambda,l}(y,r|H_0)drdy\Bigg],\\ P_{t,l} &= (1-\rho)P_{t,l}(N_{0,l}, Y_{T_1,l}, \lambda_{T_1,l}) + \rho P_{t,l}(N_{0,l} + N_{I,l}/\rho, Y_{T_2,l}, \lambda_{T_2,l}) \qquad (5.24)\\ &= (1-\rho)P_{N_0,l}(H_0)\Bigg[1 - P_{N_{0,l}/\rho}(H_0)\int_0^{Y_{T_2,l}}\int_{\lambda_{T_2,l}}^{1} f_{Y_1,\lambda,l}(y,r|H_0)drdy\Bigg]\\ &\quad + \rho P_{N_0,l+N_{I,l}/\rho}(H_0)\Bigg[1 - P_{N_{0,l}+N_{I,l}/\rho}(H_0)\int_0^{Y_{T_2,l}}\int_{\lambda_{T_2,l}}^{1} f_{Y_1,\lambda,l}(y,r|H_0)drdy\Bigg], \end{aligned}$$

where $P_{N_0,l}(H_0)$ and $P_{N_0,l}(H_1)$ are the average erroneous and correct symbol probabilities of M-ary orthogonal systems at the relay $l$ for a given noise value of $N_{0,l}$, while $f_{Y_1,\lambda,l}(y,r|H_1)$ and $f_{Y_1,\lambda,l}(y,r|H_0)$ present the joint PDFs of (5.16) and (5.17). Finally, $(Y_{T_1,l}, \lambda_{T_1,l})$ and $(Y_{T_2,l}, \lambda_{T_2,l})$ denote the optimized threshold pairs of the MO-RTT, as defined in [251].

Consequently, the probability of the $l^{th}$ relay forwarding packets to the DS is given by

$$P_{Rf} = 1 - P_w. \qquad (5.25)$$

**b. At the Destination**

1. *Symbol Error Probability (SEP):* The choice of the combining technique at the destination's receiver significantly affects the SEP performance. For non-coherent detection aided systems, the EGC and SC are frequently employed. Hence, we will investigate the SEP of these two combining techniques here.

   *EGC*: Based on the assumption detailed in Section 5.3.1.2, the outputs of the square-law detector of Fig. 5.16 employed at the DS's receiver may be expressed as

$$U_1 = \sum_{l=0}^{L_f} |G_l h_l \sqrt{P_l R_c} e^{-j\phi_l} + n_{1,l}|^2, \qquad (5.26)$$

$$U_i = |n_{i,l}|^2, \qquad i = 2, 3, ..., M, \qquad (5.27)$$

   where $L_f$ is the number of relays forwarding packets to the destination.

According to [255], the p.d.fs of the outputs $U_1$ and $U_i$ are given as

$$f_{U_1}(y) = \frac{y^{L_f}}{(1+\bar{\gamma}_l)^{L_f+1} \cdot L_f!} exp\Big( - \frac{y}{1+\bar{\gamma}_l}\Big), \quad y \geq 0, \tag{5.28}$$

$$f_{U_i}(y) = \frac{y^{L_f}}{L_f!} exp(-y), \qquad i = 2, 3...M; \quad y \geq 0, \tag{5.29}$$

where $\bar{\gamma}_l = |\bar{h}|^2 P_s / N_n$.

When $L_f$ relays are capable of forwarding packets to the DS of Fig. 2.29, the average erroneous symbol probability of $P_{N_n,L_f}(H_0)$ encountered at the DS can be expressed as [66]

$$\begin{aligned} P_{N_n,L_f}(H_0) &= 1 - \int_0^\infty f_{U_1}(y) \Big[ \int_0^y f_{U_2}(x) dx \Big]^{M-1} dy \\ &= \frac{1}{L_f!} \sum_{m=1}^{M-1} \frac{(-1)^{M-1} \binom{M-1}{m}}{(1+m+m\bar{\gamma}_l)^{L_f+1}} \\ &\quad \cdot \sum_{k=0}^{mL_f} \beta_{km} (L_f + k)! \Big( \frac{1+\bar{\gamma}_l}{1+m+m\bar{\gamma}_l} \Big)^k, \end{aligned} \tag{5.30}$$

where $\beta_{km}$ is the set of coefficients satisfying the following condition

$$\Big( \sum_{k=0}^{L_f} \frac{U_1^k}{k!} \Big)^k = \sum_{k=0}^{mL_f} \beta_{km} U_1^k. \tag{5.31}$$

*SC:* The outputs of square-law detector at the DS's receiver may be expressed as

$$U_1 = max\{U_{1,l}\}, \qquad l = 0, 1, .., L_f, \tag{5.32}$$

$$U_i = max\{U_{i,l}\}, \qquad i = 2, 3, ..., M, \tag{5.33}$$

where $U_{1,l} = |G_l h_l \sqrt{P_l R_c} e^{-j\phi_l} + n_{1,l}|^2$ and $U_{i,l} = |n_{i,l}|^2$.

According to [256], the p.d.fs of the outputs $U_1$ and $U_i$ are given as

$$f_{U_1}(y) = \frac{L_f + 1}{1+\gamma_l} exp\Big( - \frac{y}{1+\gamma_l}\Big) \Big[ 1 - exp\Big( - \frac{y}{1+\gamma_l}\Big) \Big]^{L_f}, \quad y \geq 0, \tag{5.34}$$

$$f_{U_i}(y) = (L_f + 1) exp(-y)[1 - exp(-y)]^{L_f}, \qquad i = 2, 3...M; \quad y \geq 0. \tag{5.35}$$

Furthermore, when there are $L_f$ relays forwarding packets to the DS, the average erroneous symbol probability of $P_{N_n,L_f}(H_0)$ at the DS can be expressed as [11]:

$$P_{N_n,L_f}(H_0) = 1 - \sum_{l=1}^{L_f+1} (-1)^{l+1} \binom{L_f+1}{l} \prod_{m=1}^{(L_f+1)(M-1)} \frac{m}{m + l/(1+\gamma_c)}. \tag{5.36}$$

*SEP:* The average erroneous symbol probability of $P_{N_n}(H_0)$ at the DS is given by

$$P_{N_n}(H_0) = \sum_{L_f=0}^{L} \binom{L}{L_f} P_{Rf}^{L_c} (1 - P_{Rf})^{L-L_c} \cdot P_{N_n,L_f}(H_0), \tag{5.37}$$

while the correct symbol probability is

$$P_{N_n}(H_1) = 1 - P_{N_n}(H_0). \tag{5.38}$$

Since the fraction $\rho$ of the band is contaminated by the interference, the average erroneous and correct symbol probabilities may finally be expressed as

$$\begin{aligned} P(H_0) &= (1-\rho)P_{N_0}(H_0) + \rho P_{N_0+N_i/\rho}(H_0), & (5.39)\\ P(H_1) &= 1 - P(H_0). & (5.40) \end{aligned}$$

2. *Statistics of the Erasure Insertion Related Variables:* Let $\{U_{1,l}, U_{2,l}, ..., U_{M,l}\}$ represent the decision variables input to the MFSK demodulator of Fig. 5.16. We denote the maximum and the "second" maximum of $\{U_{1,l}, U_{2,l}, ..., U_{M,l}\}$ by

$$\begin{aligned} Y_1 &= max_1\{U_{1,l}, U_{2,l}, ..., U_{M,l}\}, & (5.41)\\ Y_2 &= max_2\{U_{1,l}, U_{2,l}, ..., U_{M,l}\}, & (5.42) \end{aligned}$$

and the ratio of the "second" maximum to the maximum is formulated as

$$\lambda = \frac{Y_2}{Y_1}, \qquad 0 \le \lambda \le 1. \tag{5.43}$$

In the context of the joint MO-RTT, the erasure insertion is based on the observation of both the maximum $Y_1$ of (5.41) and the ratio of $\lambda$ of (5.43). Therefore, the joint p.d.fs of $f_{Y_1,\lambda}(y, r|H_1)$ and $f_{Y_1,\lambda}(y, r|H_0)$ have to be found, in order to evaluate the error-and-erasure ReS decoding performance in terms of the joint MO-RTT erasure insertion scheme.

*EGC:* As shown in the Appendix V, when EGC is employed, the joint p.d.fs of $Y_1$ and $\lambda = Y_2/Y_1$ under the hypotheses $H_1$ of correction decision and $H_0$ of erroneous decision, respectively, can be expressed as

$$\begin{aligned} f_{Y_1,\lambda}(y, r|H_1) &= \frac{(M-1)y}{P_{N_n}(H_1)} \cdot \frac{y^{2L_f} r^{L_f}}{(1+\bar{\gamma}_l)^{L_f+1} \cdot (L_f!)^M} e^{\left(-\frac{1+r+r\bar{\gamma}_l}{1+\bar{\gamma}_l} y\right)} \\ &\quad \cdot \left[ L_f! - e^{-yr} \sum_{k=0}^{L_f} k! \binom{L_f}{k} (yr)^{L_f-k} \right]^{M-2}, \end{aligned} \tag{5.44}$$

and

$$\begin{aligned} f_{Y_1,\lambda}(y, r|H_0) &= \frac{(M-1)y}{P_{N_n}(H_0)} \cdot \frac{y^{2L_f} r^{L_f}}{(1+\bar{\gamma}_l)^{L_f+1} \cdot (L_f!)^M} \Bigg\{ e^{\left(-\frac{1+r+r\bar{\gamma}_l}{1+\bar{\gamma}_l} y\right)} \\ &\quad \cdot \left[ L_f! - e^{-yr} \sum_{k=0}^{L_f} k! \binom{L_f}{k} (yr)^{L_f-k} \right]^{M-2} + (M-2) e^{-(r+1)y} \\ &\quad \cdot \left[ (1+\bar{\gamma}_l)^{L_f+1} L_f! - e^{\left(-\frac{yr}{1+\bar{\gamma}_l}\right)} \sum_{k=0}^{L_f} (1+\bar{\gamma}_l)^{k+1} k! \binom{L_f}{k} (yr)^{L_f-k} \right] \\ &\quad \cdot \left[ L_f! - e^{-yr} \sum_{k=0}^{L_f} k! \binom{L_f}{k} (yr)^{L_f-k} \right]^{M-3} \Bigg\}. \end{aligned} \tag{5.45}$$

*SC:* By contrast, when the SC is employed, the corresponding expressions derived in Appendix V are

$$f_{Y_1,\lambda}(y,r|H_1) = \frac{(M-1)y}{P_{N_n}(H_1)} \cdot \frac{(L_f+1)^2}{1+\gamma_l} e^{\left(-\frac{1+r+r\gamma_l}{1+\gamma_l}y\right)} \left[1-e^{\left(-\frac{y}{1+\gamma_l}\right)}\right]^{L_f}, \cdot[1-e^{-yr}]^{(L_f+1)(M-2)+L_f} \tag{5.46}$$

and

$$\begin{aligned} f_{Y_1,\lambda}(y,r|H_0) = \frac{(M-1)y}{P_{N_n}(H_1)} \cdot \Bigg\{ & \frac{(L_f+1)^2}{1+\gamma_l} e^{\left(-\frac{1+r+r\gamma_l}{1+\gamma_l}y\right)} \left[1-e^{\left(-\frac{y}{1+\gamma_l}\right)}\right]^{L_f} \\ & \cdot[1-e^{-yr}]^{(L_f+1)(M-2)+L_f} + (M-2) \cdot \frac{(L_f+1)^3}{2} e^{(-yr-y)}[1-e^{-y}]^{L_f} \\ & \cdot\left[1-e^{\left(-\frac{yr}{1+\gamma_l}\right)}\right]^2 [1-e^{-yr}]^{(L_f+1)(M-3)+L_f} \Bigg\}. \end{aligned} \tag{5.47}$$

3. *Codeword Error Probability:* Based on the statistics above, the symbol erasure probability, $P_e$, and the random symbol error probability, $P_t$, corresponding to the noise power spectral of $N_n$, and the given thresholds of $Y_T$ and $\lambda_T$, may be expressed as [251]

$$\begin{aligned} P_e(N_n,Y_T,\lambda_T) &= P_{N_n}(H_1)\int_0^{Y_T}\int_{\lambda_T}^1 f_{Y_1,\lambda}(y,r|H_1)drdy \\ &\quad + P_{N_n}(H_0)\int_0^{Y_T}\int_{\lambda_T}^1 f_{Y_1,\lambda}(y,r|H_0)drdy, \end{aligned} \tag{5.48}$$

$$P_t(N_n,Y_T,\lambda_T) = P_{N_n}(H_0)\left[1-\int_0^{Y_T}\int_{\lambda_T}^1 f_{Y_1,\lambda}(y,r|H_0)drdy\right]. \tag{5.49}$$

Due to the effect of the PBGI, the symbol erasure probability and the random symbol error probability after erasure decoding at the destination may be presented as [251]

$$P_e = (1-\rho)P_e(N_0,Y_T,\lambda_T) + \rho P_e(N_0+N_I/\rho,Y_T,\lambda_T), \tag{5.50}$$

$$P_t = (1-\rho)P_t(N_0,Y_T,\lambda_T) + \rho P_t(N_0+N_I/\rho,Y_T,\lambda_T). \tag{5.51}$$

As a result, the codeword error probability $P_w$ at the destination may be expressed as [11]

$$P_w = \sum_{i=0}^{N}\sum_{j=j_0(i)}^{N-i}\binom{N}{i}\binom{N-i}{j}P_t^i P_e^j (1-P_t-P_e)^{N-i-j}, \tag{5.52}$$

where $j_0(i) = max\{0, N-K+1-2i\}$.

Subsequently, the symbol error probability $P_s$ after error-and-erasure ReS decoding may be expressed as [11]

$$P_s = \frac{1}{N}\sum_{i=0}^{N}\sum_{j=j_0(i)}^{N-i}(i+j)\binom{N}{i}\binom{N-i}{j}P_t^i P_e^j (1-P_t-P_e)^{N-i-j}, \tag{5.53}$$

and the bit error probability $P_b$ may be approximated as [66]

$$P_b = \frac{2^{b-1}}{M-1}P_s. \tag{5.54}$$

4. *Goodput:* Employing Eq. (4.20) in Chapter 4 and Eqs. (19) and (20) of [257], the goodput - which was defined in Section 4.2.2 - of the ReS coded HARQ using the SFH FSK scheme of Figs. 5.14-5.16 may be simplified to

$$\eta_g = \frac{k}{n}\left[1 - \sum_{i=0}^{N}\sum_{j=j_0(i)}^{N-i}\binom{N}{i}\binom{N-i}{j}P_t^i P_e^j (1-P_t-P_e)^{N-i-j}\right] = \frac{k}{n}(1-P_w). \tag{5.55}$$

#### 5.3.1.4 Performance of SFH M-ary FSK Aided Reed-Solomon Coded Systems

Based on the expressions of Section 5.3.1.3, we will investigate the performance of the FFH MFSK ReS coded systems operating in the cooperative network. For all the results below, the channels are assumed to be Rayleigh flat-faded. The signal power to interference noise ratio is set to 10 dB, while the portion of the band interfered by the PBGI is set to 0.15. All relays of Fig. 2.29 are assumed to be at the mid-point of the source-to-destination link. The system parameter are provided in Table 5.5.

Table 5.5: Basic parameters of $M$-ary FSK aided ReS coded H-ARQ system

| **Parameters** | **Values** |
|---|---|
| Channel code type | ReS(31,20,6) |
| Modulation type | $M$-ary FSK |
| Relay type | fixed DF |
| N$^o$ of relays | L=1 |
| Normalized $d_{SR_l}/d_{R_lD}$ | 0.5/0.5 |
| Source's transmit power | $E_S = \frac{E_b}{G_{rd}+1}$ |
| Relays' transmit power | $E_{R_l} = \frac{G_{rd}E_b}{G_{rd}+1}$ |
| Channel model | Rayleigh fading |
| Maximum number of retransmissions | 5 |

Fig. 5.17 portrays the relay's codeword error probability at $E_b/N_0 = 8dB$, when utilizing the joint MO-RTT decoding technique, where the 32-ary FSK modulation and $ReS(31, 20)$ code are employed. According to the figure, there exists an optimum threshold value of $Y_T$ or $\lambda_T$, which minimizes the codeword error probability. Observe that at $Y_T = 0$ or $\lambda_T = 1$, the error-and-erasure scheme performs identically to the error-correction-only decoder, since no erasure insertion is employed. If the threshold value of $Y_T$ is too high and simultaneously, the threshold value of $\lambda_T$ is too low, the system will perform worse than the error-correction-only decoder.

The packet forward probabilities versus $E_b/N_0$ at the relay are seen in Fig. 5.18. Three schemes were considered, namely the uncoded scheme, error-correction-only decoding as well as the error-and-erasure decoding. Naturally, both FEC decoding schemes outperform the uncoded scheme. As expected, when the error-and-erasure decoding is employed, a packet has a higher chance of being forwarded, compared to error-correction-only decoding.

Similar to Fig. 5.17, the codeword decoding error probability at the destination is shown in Fig. 5.19, when the value of $E_b/N_0$ is 8dB. It may also be seen from the figure that there is an optimum threshold value of $Y_T$ or $\lambda_T$, which minimizes the decoding error probability.

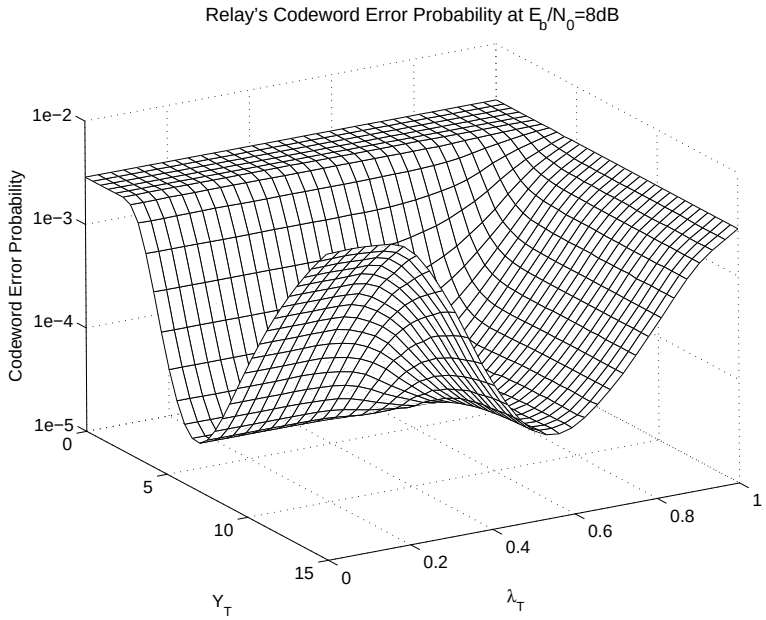


Figure 5.17: Codeword decoding error probability at the relay versus the amplitude threshold, $Y_T$ and the ratio threshold, $\lambda_T$ for the ReS(31,20) FEC coded system of Figs. 5.14 and 5.15 using "error-and-erasure" decoding based on the MO-RTT erasure insertion scheme of Section 5.3.1.2 for transmission over an uncorrelated Rayleigh flat-fading channel, when using the parameters of $\rho = 0.15, M = 32, E_b/N_0 = 8dB, E_b/N_I = 10dB, ReS(31,20), L = 1, G_{sr} = G_{rd} = 4G_{sd}$. The remaining parameters are provided in Table 5.5.

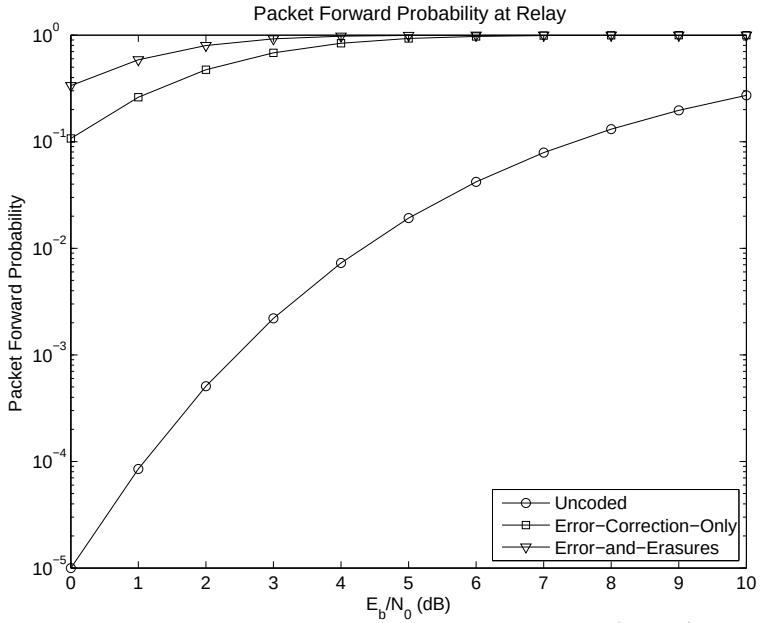


Figure 5.18: Packet forwarding probability at the relay for the ReS(31,20) FEC coded system obeying the schematics of Figs. 5.14 and 5.15 using both "error-correction-only" and "error-and-erasure" decoding based on the MO-RTT erasure insertion scheme of Section 5.3.1.2 for transmission over an uncorrelated Rayleigh flat-fading channel. The results were evaluated from (5.25) using the parameters of $\rho = 0.15, M = 32, E_b/N_I = 10dB,\ ReS(31,20), L = 1, G_{sr} = G_{rd} = 4G_{sd}$. The remaining parameters are provided in Table 5.5.

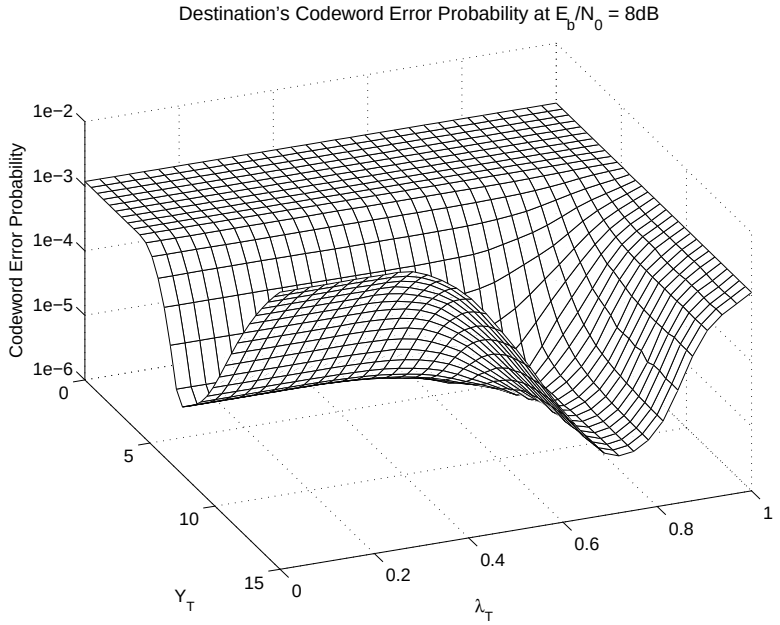


Figure 5.19: Codeword decoding error probability at the destination versus the amplitude threshold, $Y_T$ and the ratio threshold, $\lambda_T$ for the ReS(31,20) FEC coded system obeying the schematics of Figs. 5.14 and 5.16 using "error-and-erasure" decoding based on the MO-RTT erasure insertion scheme of Section 5.3.1.2 for transmission over an uncorrelated Rayleigh flat-fading channel. The results were evaluated from (5.52) using the parameters of $\rho = 0.15, M = 32, E_b/N_0 = 8dB, E_b/N_I = 10dB, ReS(31,20), L = 1, G_{sr} = G_{rd} = 4G_{sd}$. The remaining parameters are provided in Table 5.5.

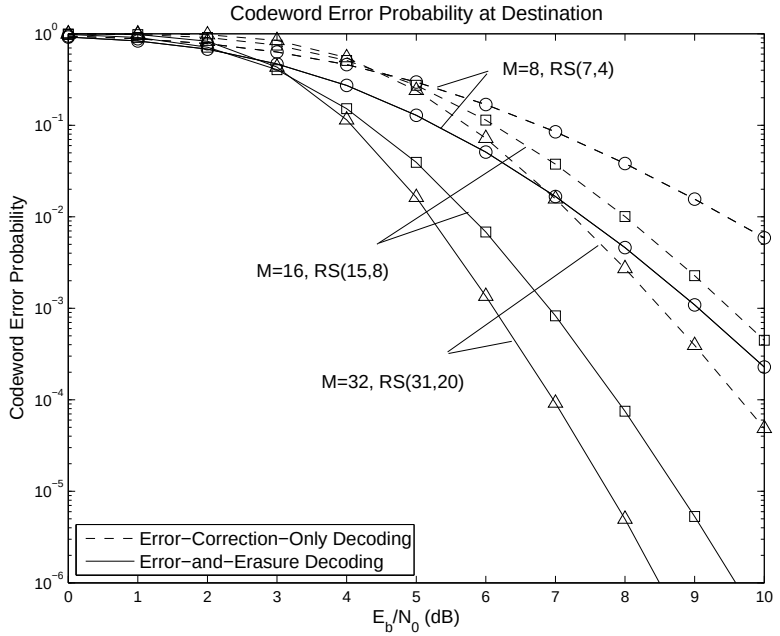


Figure 5.20: Codeword decoding error probability at the destination for the various ReS FEC coded systems obeying the schematics of Figs. 5.14 and 5.16 using both "error-correction-only" and "error-and-erasure" decoding based on the MO-RTT erasure insertion scheme of Section 5.3.1.2 for transmission over an uncorrelated Rayleigh flat-fading channel. The results were evaluated from (5.52) using the parameters of $\rho = 0.15, E_b/N_I = 10dB, L = 1, G_{sr} = G_{rd} = 4G_{sd}$. The remaining parameters are provided in Table 5.5.

Fig. 5.20 compared the performance of the erasure-aided and error-correction-only decoding schemes, when different FSK/ReS schemes are employed. As anticipated, the erasure insertion schemes outperform the error-correction-only arrangements. When employing the $ReS(31, 20)$ code combined with 32-FSK modulation and a single relay, the error-and-erasure decoding scheme achieved 3dB gain at the BER of $10^{-4}$ over the error-correction-only arrangement. Moreover, the ReS codes constructed over high order Galois fields and combined with high-order FSK modulation performed significantly better in the high-$E_b/N_0$ region, namely above 5dB, than those using lower-order Galois field combined with FSK modulation.

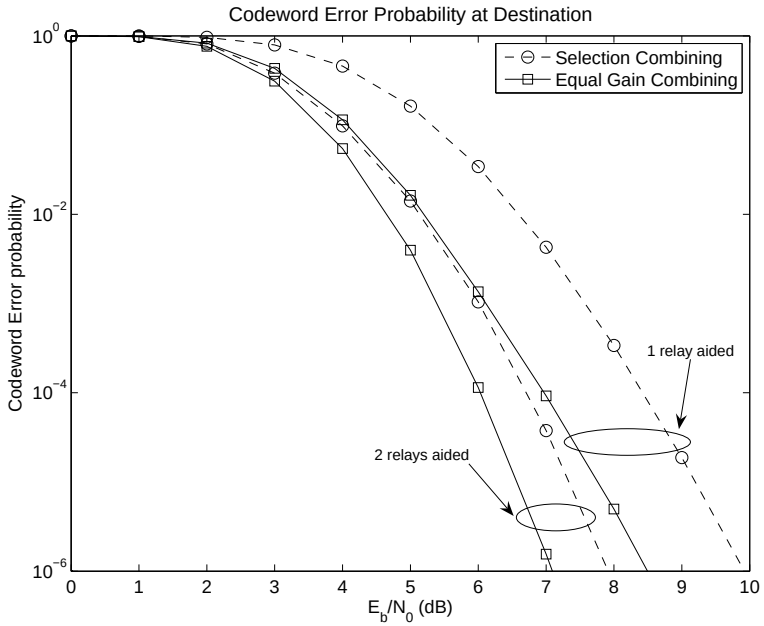


Figure 5.21: Codeword decoding error probability at the destination for the ReS(31,20) FEC coded systems obeying the schematics of Figs. 5.14 and 5.16 using "error-and-erasure" decoding based on the MO-RTT erasure insertion scheme combined with the EGC and SC techniques of Section 5.3.1.2 for transmission over an uncorrelated Rayleigh flat-fading channel. The results were evaluated from (5.52) using the parameters of $\rho = 0.15, M = 32, E_b/N_0 = 8dB, E_b/N_I = 10dB, ReS(31, 20), L = 1, G_{sr} = G_{rd} = 4G_{sd}$. The remaining parameters are provided in Table 5.5.

The system performances of the EGC and SC techniques are compared in Fig. 5.21. According to the figure, the EGC schemes exhibit a lower codeword error probability than SC. More particularly, the EGC scheme may achieve 1.5 dB gain at $E_b/N_0$ of $10^{-6}$, compared to the SC scheme, when assisted by a single relay. Likewise, the resultant gain is 1.0 dB, when there are two assisting relays. This is because the EGC technique is the optimal diversity combining scheme for non-coherent detection.

The beneficial effect of the number of relays is shown in Fig. 5.22. Observe that below $E_b/N_0$ of 2 dB, the schemes relying on a higher number of relays might in fact perform worse than those relying on a lower number of relays. This is because the total available power is distributed amongst the source and the relays for the sake of a fair comparison. As a result, the transmit power of both the source as well as the relays may become insufficient for their successful decoding and hence, the packet forward probability at the relay reduced. In other words, the number of relays forwarding data to the destination is reduced. When the $E_b/N_0$ value increases, more relays forward data to the destination. Thus, the schemes associated with a higher number of relays perform better than those relying on less

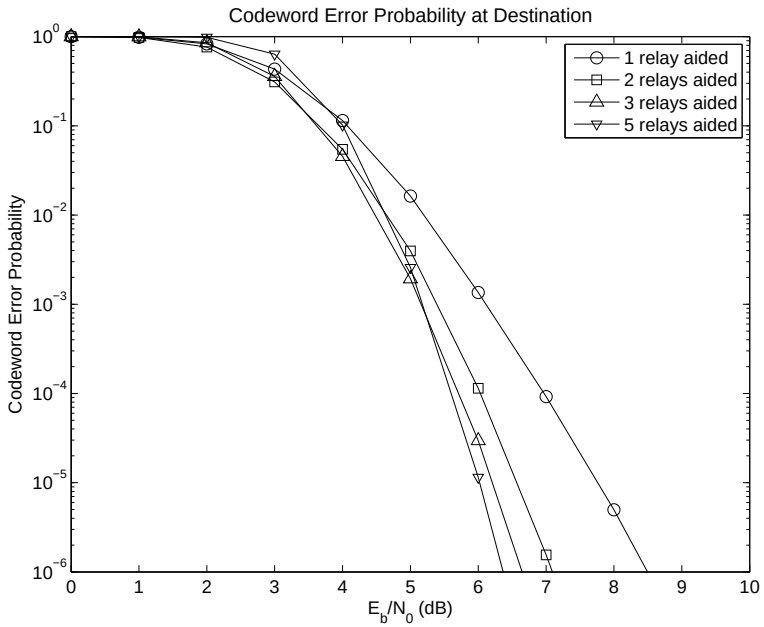


Figure 5.22: Codeword decoding error probability at the destination for the ReS(31,20) FEC coded systems obeying the schematics of Figs. 5.14 and 5.16 using "error-and-erasure" decoding based on the MO-RTT erasure insertion scheme of Section 5.3.1.2 for transmission over an uncorrelated Rayleigh flat-fading channel, when varying the number of relays. The results were evaluated from (5.52) using the parameters of $\rho = 0.15, M = 32, E_b/N_0 = 8dB, E_b/N_I = 10dB$, $ReS(31, 20), L = \{1, 2, 3, 5\}, G_{sr} = G_{rd} = 4G_{sd}$. The remaining parameters are provided in Table 5.5.

relays. However, the BER gain associated with employing more than two relays gradually becomes insignificant upon increasing the number of relays. The attainable performance becomes similar to that of the co-located MIMO system upon increasing the number of transmit antennas.

The effects of interference are characterized in Fig. 5.23, when the partial-band interference fraction $\rho$ is varied. As expected, the codeword error probability increases as a function of $\rho$, i.e when imposing more interference on the signal's band. More particularly, at $E_b/N_0$ of 7 dB and $E_b/N_I$ of 5 dB, $P_W$ increases from $10^{-4}$ to 0.5 upon increasing $\rho$ from 0.1 to 0.9.

Furthermore, we validate the performance of the systems subjected to theoretical analysis in Section 5.3.1.3 by computer simulations. The results of Fig. 5.24 showed that there is a slight gap of approximately 0.5 dB between the analysis and simulations. This can be explained by the fact that the theoretical analysis employs some simplifying approximations, such as those applied to the p.d.fs of the detector's outputs [251, 255], which are given in Eqs. (5.28, 5.29, 5.34, 5.35) or to the average erroneous symbols probability of Eq. (5.30) [66]. Additionally, as seen in Figs. 5.17 and 5.19, the CEP depends on the values of the thresholds, $Y_T$ and $\lambda_T$. For a given received SNR, there is an optimum pair of $Y_T$ and $\lambda_T$ values, which provides the lowest CEP. In the analysis we use the average received SNR for evaluating the CEP, while in the simulations, a given pair of $Y_T$ and $\lambda_T$ values is used for all the instantaneous received SNRs, which varied in accordance with the channel coefficients. Therefore, the simulation results are not perfectly accurate either.

Finally, we compare the performance of the proposed ReS coded scheme using error-and-erasure decoding to that of other coding schemes, such as the classic convolutional and LDPC codes in the context of wireless cooperative networks. The Recursive Systematic Covoluational (RSC) code,

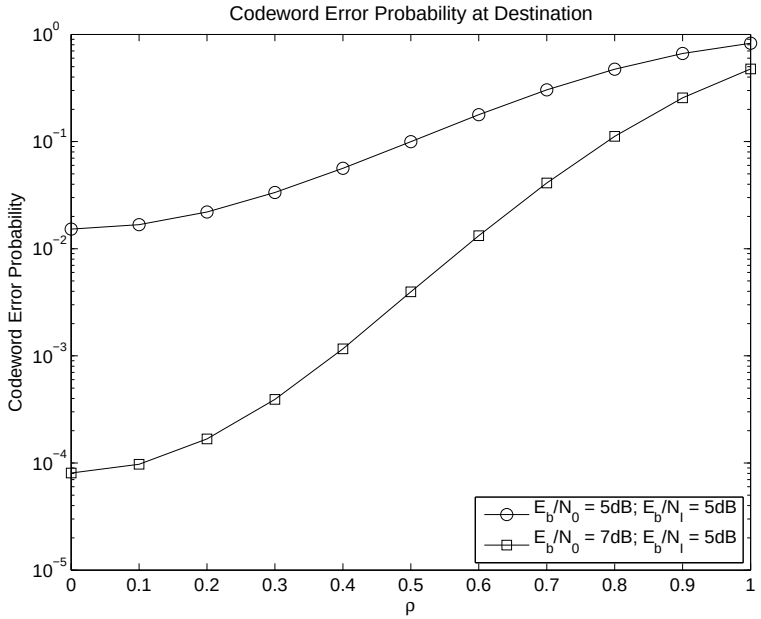


Figure 5.23: Codeword decoding error probability at the destination for the ReS(31,20) FEC coded systems obeying the schematics of Figs. 5.14 and 5.16 using "error-and-erasure" decoding based on the MO-RTT erasure insertion scheme of Section 5.3.1.2 for transmission over an uncorrelated Rayleigh flat-fading channel, when varying the interference fraction $\rho$. The results were evaluated from (5.52) using the parameters of $M = 32, ReS(31, 20), L = \{1, 2, 3, 5\}, G_{sr} = G_{rd} = 4G_{sd}$. The remaining parameters are provided in Table 5.5.

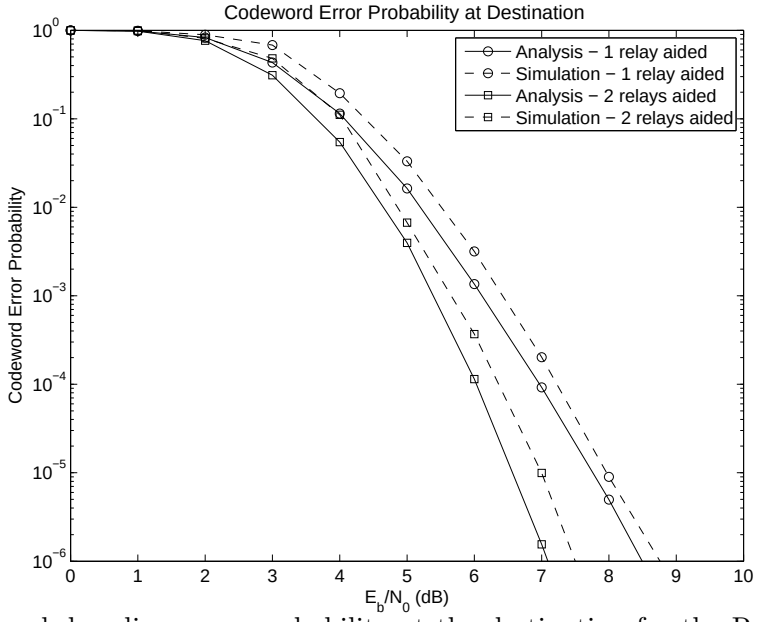


Figure 5.24: Codeword decoding error probability at the destination for the ReS(31,20) FEC coded systems obeying the schematics of Figs. 5.14 and 5.16 using "error-and-erasure" decoding based on the MO-RTT erasure insertion scheme of Section 5.3.1.2 for transmission over an uncorrelated Rayleigh flat-fading channel. The results were generated both by simulations and from (5.52) using the parameters of $\rho = 0.15, M = 32, E_b/N_I = 10dB, ReS(31, 20), L = \{1, 2, \}, G_{sr} = G_{rd} = 4G_{sd}$. The remaining parameters are provided in Table 5.5.

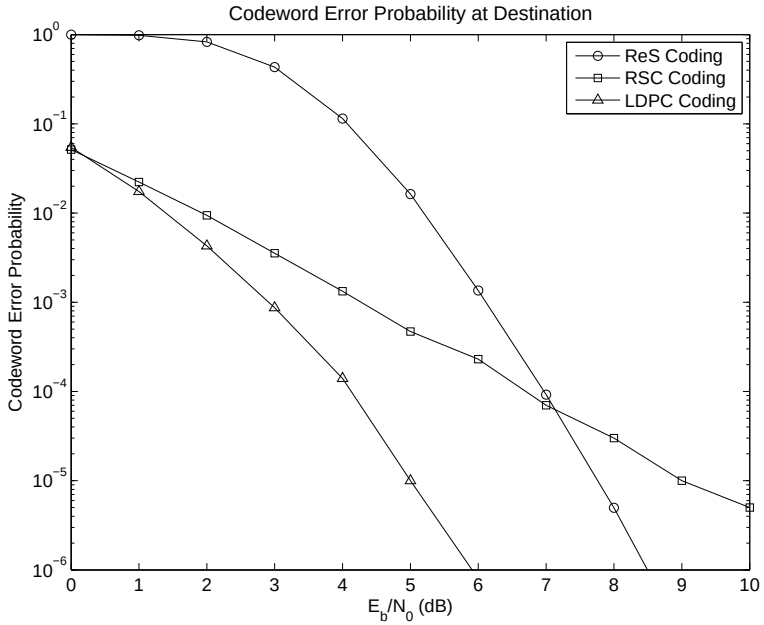


Figure 5.25: Codeword decoding error probability at the destination for the RSC(23,33) coded, LDPC codes and the ReS(31,20) FEC coded systems of Figs. 5.14 and 5.16 using "error-and-erasure" decoding based on the MO-RTT erasure insertion scheme of Section 5.3.1.2 for transmission over an uncorrelated Rayleigh flat-fading channel, when varying the interference fraction $\rho$. The results were evaluated from (5.52) using the parameters of $M = 32, ReS(31, 20), L = \{1, 2, 3, 5\}, G_{sr} = G_{rd} = 4G_{sd}$. The remaining parameters are provided in Table 5.5.

RSC(23,33), using the octally represented generator polynomials of 23 and 33 [66] is considered and a regular LDPC code [37] is employed. For a fair comparison, the same coding rate and the same packet size are employed for all three coding schemes. For the RSC code and the LDPC code, iterative detection is employed at the cost of a potentially increased complexity and latency imposed on the systems. As seen in Fig. 5.25, the LDPC coded scheme outperforms both the ReS coded and the RSC coded scheme. More particularly, it achieves a power gain of 3 dB compared to the ReS coded scheme at the CEP of $10^{-6}$. By contrast, the RSC coded scheme performs better than the ReS coded scheme only in the low $E_b/N_0$ region, namely below 7 dB and no 'turbo cliff' exists, even when iterative detection is employed for the RSC scheme. This may be explained by the fact that the iterative detection aided RSC codes only performs well, when the packet size is long, which is not the case in the cooperative scenario considered.

### 5.3.2 Iterative Decoding Aided Non-coherent Frequency Shift Keying

As a further study, the non-coherent FSK is now combined with convolutional coding in order to carry out iterative detection. The transmitter schematic of the system is the same as that of the ReS coded HARQ seen in Fig. 5.14, albeit the ReS codec was replaced by the convolutional codec. At the receiver, the erasure detecting block is removed and replaced by the iterative decoding structure relying on the convolutional decoder, as shown in Fig. 5.26. The main simulation parameters of the system under our consideration are provided in Table 5.6.

The performance of the convolutional coded HARQ using FSK modulation in our relay-aided

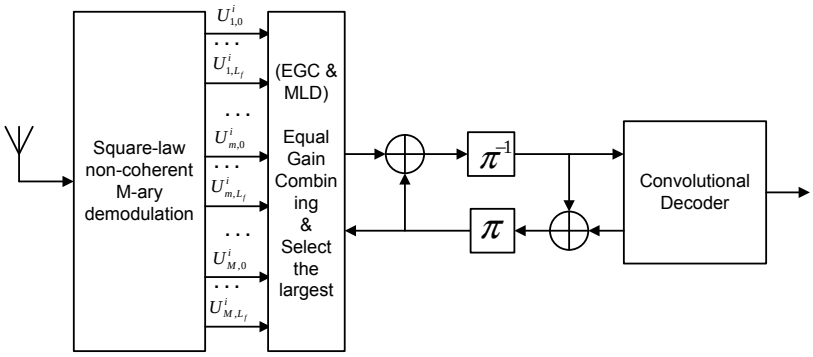


Figure 5.26: The receiver schematic of the convolutional coded FSK system using iterative detection, obeying the transmitter schematics of Fig. 5.14, where the RSC code substitute the ReS code.

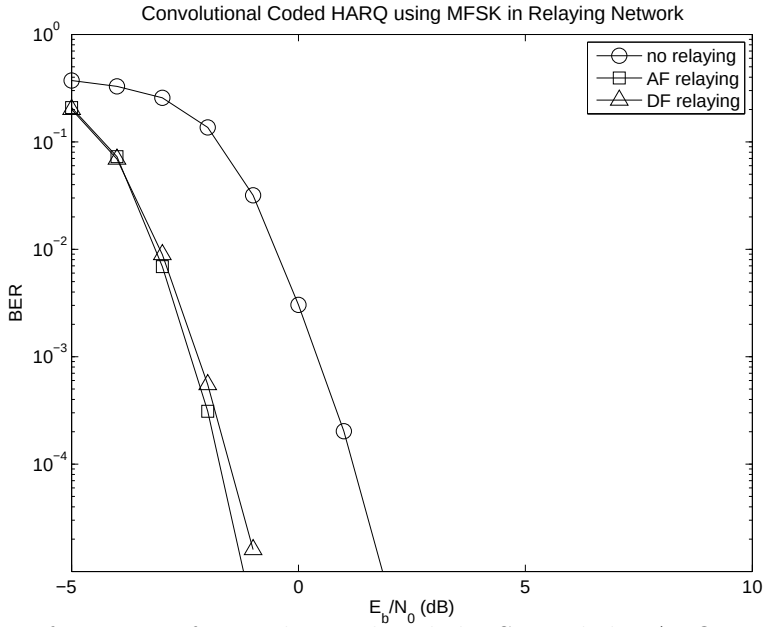


Figure 5.27: BER performance of convolutional coded FSK aided HARQ in AF and DF relaying assisted networks. The receiver schematic is illustrated in Fig. 5.26 and system parameters are provided in Table 5.6.

wireless network is characterized in Figs. 5.27-5.29. According to Fig. 5.27, the AF relaying scheme performs slightly better in BER terms than the DF arrangement, while both of them outperform the direct transmission scheme, achieving a gain of approximately 2.5 dB at the BER value of $10^{-5}$. Despite its slightly better BER performance, the number of retransmissions for the AF relaying scheme is as twice as that of the DF ones in the $E_b/N_0$ region between 2 dB and 6 dB, as shown in Fig. 5.28. Consequently, the AF schemes have a lower throughput than the DF arrangement, as observed in Fig. 5.29.

## 5.4 Distributed Space-Time Coding Aided H-ARQ

In Section 5.2 and Section 5.3, we have investigated the performance of the classic non-coherent detection aided DPSK and FSK techniques in the context of cooperative wireless networks. Albeit they

Table 5.6: Basic parameters of FSK aided convolutional coded H-ARQ system obeying schematics of Figs. 5.14 and 5.26, where the RSC code substitutes the ReS code of Table 5.5. Both the AF and DF relaying schemes were invoked.

| **Parameters** | **Values** |
|---|---|
| Information/encoded bits | 500/1000 |
| Channel code type | RSC(5,7) |
| Modulation type | 4-ary FSK |
| Relay type | fixed |
| N$^o$ of relays | L=1 |
| Normalized $d_{SR_l}/d_{R_lD}$ | 0.7/0.3 for AF<br>0.3/0.7 for DF |
| Source's transmit power | $E_S = \frac{E_b}{G_{rd}+1}$ |
| Relays' transmit power | $E_{R_l} = \frac{G_{rd}E_b}{G_{rd}+1}$ |
| Channel model | Rayleigh fading |
| Maximum number of retransmissions | 5 |

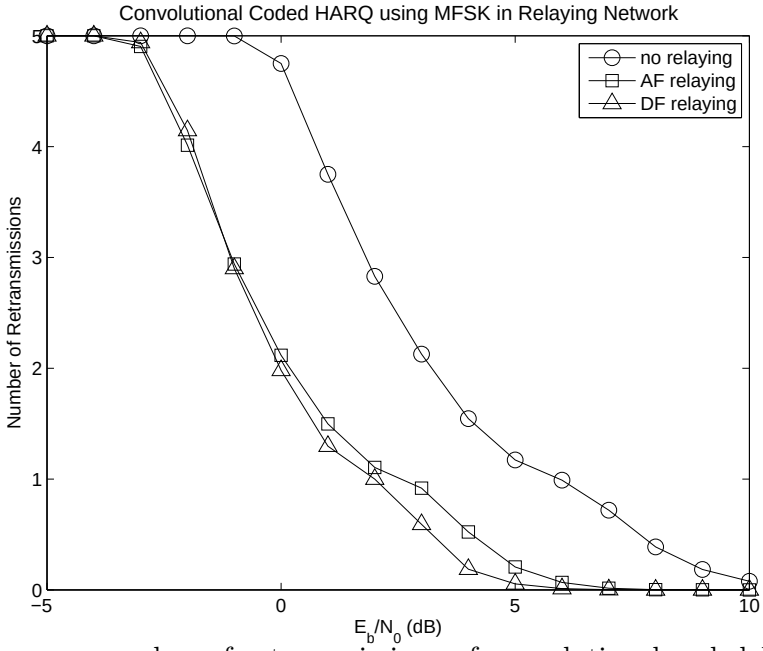


Figure 5.28: The average number of retransmissions of convolutional coded FSK aided HARQ in AF and DF relaying assisted networks. The receiver schematic is illustrated in Fig. 5.26 and system parameters are provided in Table 5.6.

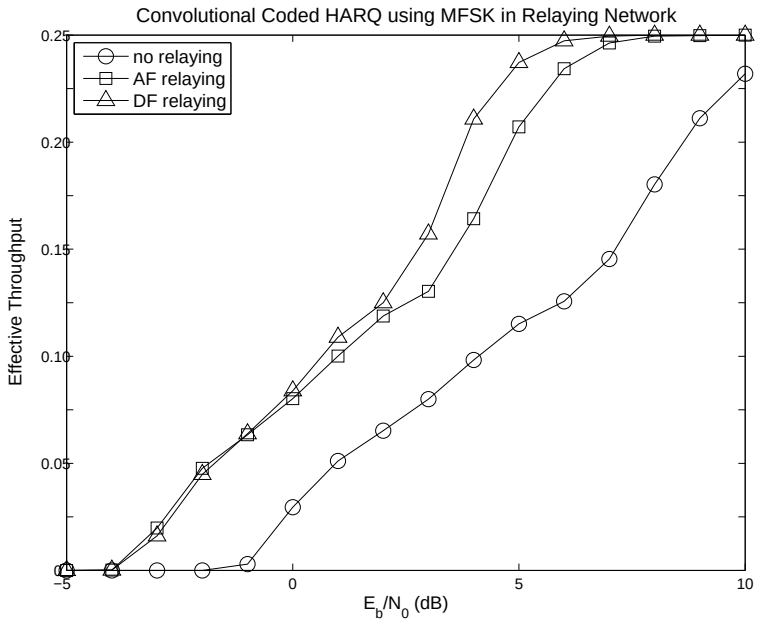


Figure 5.29: The effective throughput of convolutional coded FSK aided HARQ in AF and DF relaying assisted networks. The receiver schematic is illustrated in Fig. 5.26 and system parameters are provided in Table 5.6.

have a low-complexity implementation, when the number of relays increases, orthogonal subchannels have to be created for the relay node's transmissions. These orthogonal relaying subchannels may be created by employing TD, FD or SD subchannels with the aid of TDMA, FDMA, CDMA, SDMA. However, regardless of the specific choice of TD, FD or SD, this results in a reduction of the system's spectral efficiency. A popular solution is constituted by the so-called distributed space-time coding (DSTC) philosophy [107, 136], where the relays are permitted to simultaneously transmit over the same channel by emulating a classic space-time code.

In order to achieve the classic MIMO-aided diversity gain in cooperative networks, the schemes proposed in [233, 234] rely on single-antenna-aided mobiles sharing their antennas in a cooperative fashion. Hence, they rely on two-slot transmissions, invoking the first slot for the source-to-relay transmissions and the second slot for the relay-to-destination transmissions. As a result, a throughput-loss is inevitable. When the ARQ protocol is employed, the throughput loss is further increased. In order to mitigate this drawback, in this section we propose a novel system design based on a combination of DSTBC codes [41] and cooperative HARQ. Furthermore, non-coherent detection is also invoked, in order to reduce the system complexity imposed by the requirement of channel estimation at both the relays as well as at the destination. This proposal allows us to achieve an improved BER as well as throughput.

## 5.4.1 Distributed Differential Space-Time Block Coding

### 5.4.1.1 Conventional Distributed DSTBC Aided H-ARQ

The transmission process of the conventional distributed DSTBC aided H-ARQ is illustrated in Fig. 5.30, which will be further detailed with the aid of Figs. 5.31-5.33. During the first transmission, the source's data packets are encoded by the RSC and URC encoders of Fig. 5.32(a), where

STBC is omitted during the first transmission. Then they are modulated and transmitted to both the relay and to the destination stations, where both the relay and the destination will decode the packet received. If the packet is correctly decoded at the destination, a positive acknowledgement (ACK) is fed back to the source to ask for a new packet. Otherwise, a negative ACK is returned to request a retransmission. When a retransmission is required, the source and the $(N-1)$ relays will carry out DSTBC encoding and then, each node will transmit one column of the $N$-column encoded data matrix as the distributed DSTBC scheme of [234]. The structures of the source's transmitter and the relay's transceiver are provided in Fig. 5.32(a) and Fig. Fig. 5.32(b), while the signal combination and decoding process at the destination's receiver is detailed in Fig. 5.32(c).

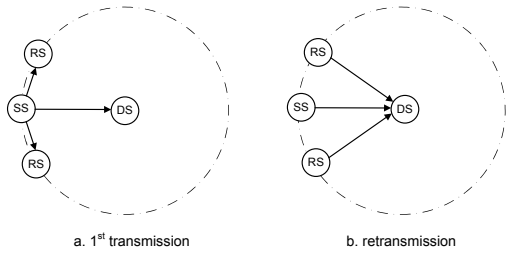


Figure 5.30: Conventional distributed DSTBC aided H-ARQ employing three distributed antennas. In the $1^{st}$ phase, the SS broadcasts both to the RS and to the DS, while in the $2^{nd}$ phase the distributed DSTBC codeword is transmitted to DS, for example using the three-antenna based orthogonal STBC (DG3) scheme of [41].

#### 5.4.1.2 Enhanced distributed DSTBC Aided H-ARQ

In contrast to the conventional distributed DSTBC HARQ scheme of Fig. 5.30, the data packets are encoded by the channel encoder and transmitted by the modulator with the aid of DSTBC encoding, as detailed in Fig. 5.33. Specifically, observe in the figure that the first column of the $N$-column encoded data matrix is transmitted to both the relays' and to the destination's receivers. If a negative ACK is received, the source will send the second column of the DSTBC encoded data matrix, while the $(N-2)$ relays will forward the remaining $(N-2)$ columns of the matrix to the destination, as shown in Fig. 5.31. For instance, when using the DSTBC scheme of Fig. 5.33 relying on three transmit antennas ($N=3$), the source will transmit the first column during its first transmission. During the retransmission session, the source continues by transmitting the second column, while the relay transmits the third column of the DSTBC encoded matrix, as illustrated in Fig. 5.33.

At the destination's receiver, the signals are combined, as shown in Fig. 5.32(d). Our novel design may be summarized as follows:

- The signal received after the first transmission is combined with the retransmitted signal before its decoding in order to create the full DSTBC signal for the second decoding process.
- The received signal corresponding to the first transmission is decoded and then fed into the RSC decoder during the retransmitted information's decoding process. This arrangement allows the RSC to receive more reliable *extrinsic* information during the retransmission phase.
- As described above the first column of the $N$-column encoded matrix is transmitted during the first transmission phase, while the remaining $(N-1)$ columns of the $N$-column encoded matrix

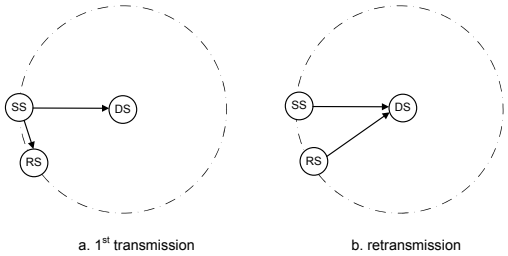


Figure 5.31: Enhanced distributed DSTBC aided H-ARQ employing three distributed antennas: In the $1^{st}$ phase, the SS broadcasts the first column of the DG3 distributed DSTBC to both the RS and to the DS, while in the $2^{nd}$ phase the two remaining columns of the DG3 distributed DSTBC codeword are transmitted to the DS.

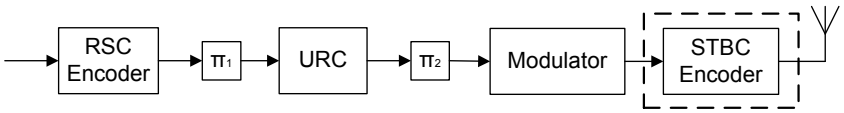


(a) Source's Transmitter

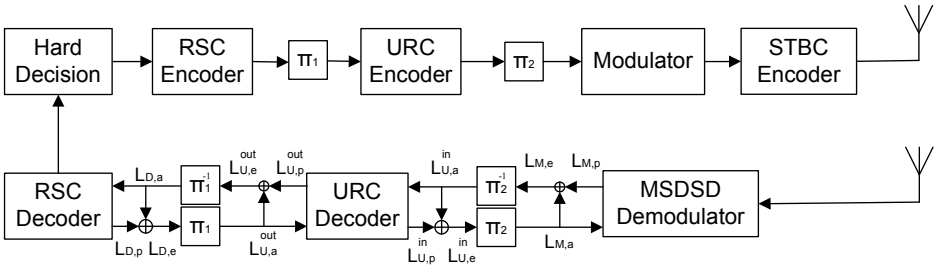


(b) Relay's Transceiver

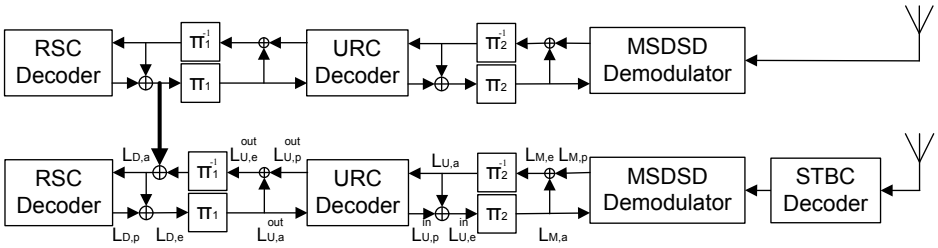


(c) Destination's Receiver for Conventional DSTBC HARQ

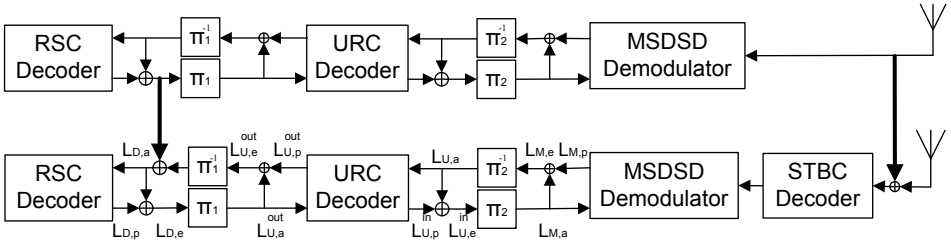


(d) Destination's Receiver for Novel DSTBC HARQ

Figure 5.32: Tranceiver's structures

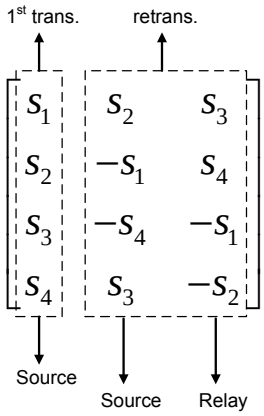


Figure 5.33: The DSTBC encoded matrix of the three-transmit-antenna scheme.

are transmitted during the retransmission slot, while requiring $N-2$ relays. Hence, the proposed scheme requires one less relay, compared to the conventional distributed DSTBC, which require $(N-1)$ relays during the retransmission phase.

#### 5.4.1.3 Performance of Distributed DSTBC Aided H-ARQ

In this section, we will characterize the performance of the conventional distributed DSTBC HARQ, the novel DSTBC HARQ and the non-cooperative HARQ, where the source simply retransmits the same packet upon receiving a negative ACK. In the DSTBC schemes, the DSTBC codes relying either three or four distributed antennas (DG3 and DG4) [41] are employed. Binary phase shift keying (BPSK) modulation is used for all the considered schemes. All nodes are assumed to have the same distance from the destination, as indicated in Figs. 5.30 and 5.31. The channels are correlated Rayleigh fading links having a normalized Doppler frequency of 0.03 Hz, but they are independent of each other. At the receivers, multiple-symbol differential sphere detection (MSDSD) [258, 259] is employed. We opted for a detection-window width of $N_w = 3$. The remaining system parameters are detailed in Table 5.7. It is also assumed that the distance from the source to the relay stations is sufficiently low to allow error-free communications between them in the first transmission.

The BER and FER performance of the five schemes detailed in Table 5.7 are shown in Fig. 5.34. Clearly, the conventional cooperative DSTBC HARQ may achieve 1.5 dB and 3 dB gain over the non-cooperative scheme at the BER value of $10^{-5}$ as well as at the FER value of $10^{-3}$ for both the DG3 and the DG4 schemes. By contrast, our proposed scheme of Fig. 5.31 may further reduced the transmit power by approximately 3 dB and 5 dB at the same BER and FER value.

Fig. 5.35 compared the achievable effective throughput of the schemes considered, which is formulated as

$$\eta = \frac{K}{M} \cdot (1 - P_f), \tag{5.56}$$

where $K$ and $M$ are the number of information bits and the total number of transmitted bits, while $P_f$ is the frame error ratio. According to the figure, both the cooperative schemes have a better performance than the non-cooperative ones in terms of the effective throughput. Additionally, it may be seen from Fig. 5.35 that the proposed cooperative scheme is capable of outperforming the conventional one, since a 3 dB difference was observed between the two scheme at the $E_b/N_0$ value

Table 5.7: Basic parameters of distributed DSTBC aided H-ARQ schemes

| | **Scheme A** | **Scheme B-1** | **Scheme C-1** | **Scheme B-2** | **Scheme C-2** |
|---|---|---|---|---|---|
| Inf./Enc. bits | 500/1000 | 500/1000 | 500/1000 | 500/1000 | 500/1000 |
| Channel code | RSC (5,7) | RSC (5,7) | RSC (5,7) | RSC (5,7) | RSC (5,7) |
| Modulation | DBPSK | BPSK | BPSK | BPSK | BPSK |
| Space-Time code | N/A | DSTBC-DG3 | DSTBC-DG3 | DSTBC-DG4 | DSTBC-DG4 |
| Demodulation | MSDD - 3 | MSDD - 3 | MSDD - 3 | MSDD - 3 | MSDD - 3 |
| Detection type | Iterative det. | Iterative det. | Iterative det. | Iterative det. | Iterative det. |
| Relay type | N/A | DF | DF | DF | DF |
| N$^o$ of relays aided | N/A | 2 | 1 | 3 | 2 |
| $d_{RD}/d_{SD}$ | N/A | 1.0/1.0 | 1.0/1.0 | 1.0/1.0 | 1.0/1.0 |
| Source-Relay Tx power allocation | N/A | Equal | Equal | Equal | Equal |
| Channel model | correlated Rayleigh fad. | correlated Rayleigh fad. | correlated Rayleigh fad. | correlated Rayleigh fad. | correlated Rayleigh fad. |

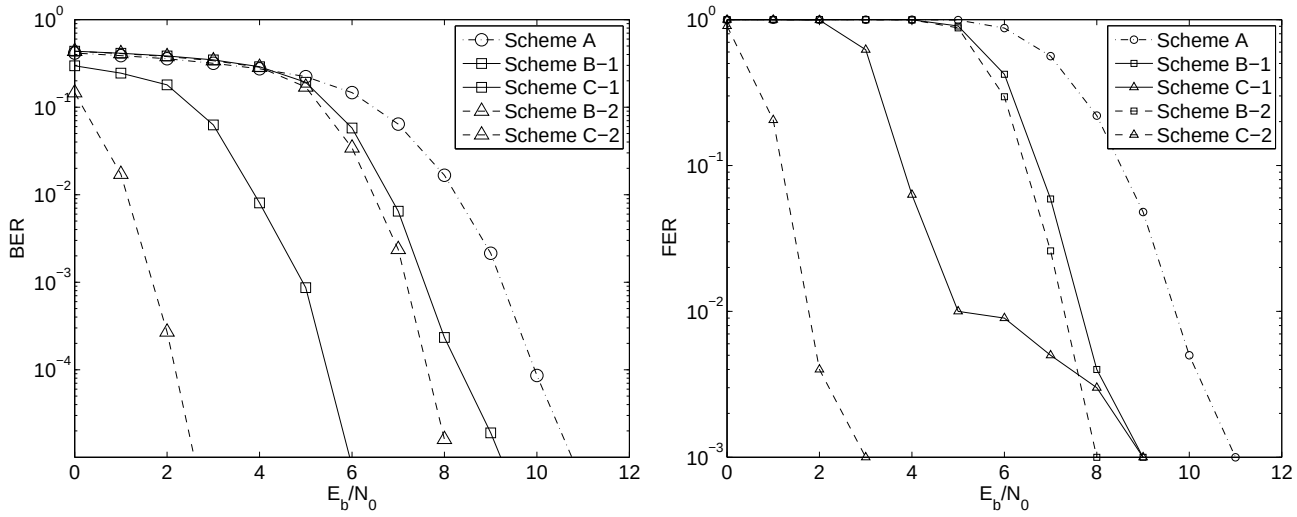


(a) BER versus $E_b/N_0$

(b) FER versus $E_b/N_0$

Figure 5.34: BER and FER performance of the direct transmission H-ARQ and of the distributed DSTBC aided H-ARQ schemes. The transceiver schematics employing distributed DSTBC are shown in Fig. 5.32 and system parameters are detailed in Table 5.7.

below 3 dB.

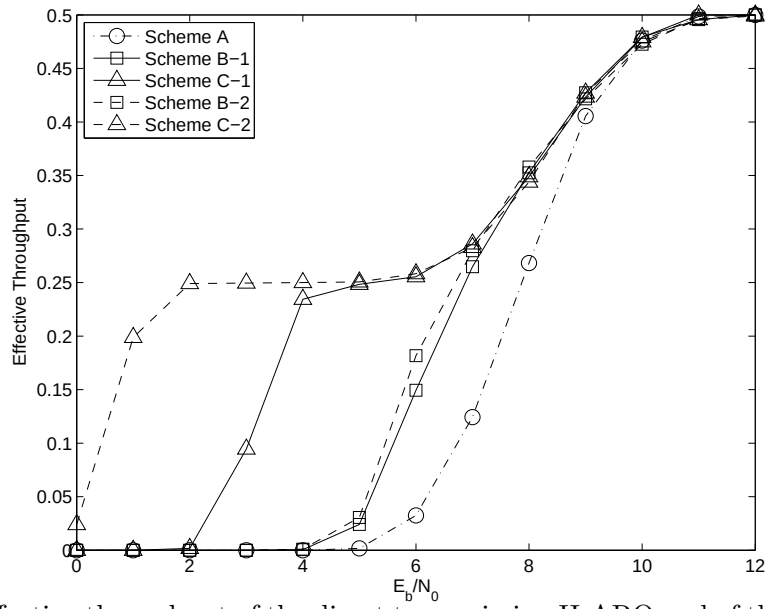


Figure 5.35: The effective throughput of the direct transmission H-ARQ and of the distributed DSTBC aided H-ARQ schemes. The transceiver schematics employing distributed DSTBC are shown in Fig. 5.32 and system parameters are detailed in Table 5.7.

## 5.5 Chapter Summary

In this chapter we investigated the performance of diverse non-coherent detection aided H-ARQ systems in the context of wireless relaying network, which operated without any channel knowledge. First, the popular DPSK aided H-ARQ scheme was studied. Section 5.2.1.1 characterized the performance of the DBPSK aided ReS coded H-ARQ scheme employing SSDD, when an assisting relay was employed. The results of Fig. 5.3 showed that as a benefit of the relay station's assistance, the system's BER performance was improved, while the number of retransmissions was reduced. Accordingly, observe in Fig. 5.5 the overall system's throughput was increased. The system was then further extended by employing MSDD in Section 5.2.1.2. The performance trends quantified in terms of BER, the number of retransmissions as well as the system's throughput were characterized in Figs. 5.6-5.8, when MSDD and a relaying station were employed. Observe from Fig. 5.6 that the MSDD allows the transmit power to be reduced by approximately 10 dB compared to conventional SSDD, without degrading the system's BER performance. A brief comparison between the two above-mentioned systems is provided in Table 5.8.

In contrast to the DPSK aided H-ARQ employing hard demodulation in Section 5.2.1, the DPSK aided H-ARQ employing soft demodulation and iterative decoding for cooperative communications was presented in Section 5.2.2. The performance results of Fig. 5.10 demonstrated that in the context of the convolutional coded HARQ scheme of Fig. 5.9 using the parameters of Table 5.3 for the AF aided cooperative HARQ scheme may achieve a higher throughput than its DF cooperative counterpart, despite its higher BER. Furthermore, our comparison between the perfect- and imperfect-PSA as well as non-coherent detection schemes was presented in Section 5.2.3. According to Fig. 5.11 and Fig. 5.12, when the Doppler frequency increases, the performance discrepancy between the perfect-

Table 5.8: Performance comparison of SSDD and MSDD detection aided HARQ employing ReS coding, obeying the schematics of Fig. 5.2 where the system parameters are detailed in Table 5.2 and the corresponding performance results are shown in Figs. 5.3-5.8.

| | $f_D = 0.001$ | | | | | |
|---|---|---|---|---|---|---|
| Detection scheme | SSDD | | | MSDD | | |
| Relaying type | no | AF | DF | no | AF | DF |
| $E_b/N_0$ required | $\geq 13.0$ $dB$ | $\geq 13.0$ $dB$ | $\geq 13.0$ $dB$ | $\geq 8.0$ $dB$ | $\geq 4.0$ $dB$ | $\geq 2.0$ $dB$ |
| Throughput achieved | $\simeq 0.22$ | $\simeq 0.18$ | $\simeq 0.18$ | $\simeq 0.30$ | $\simeq 0.22$ | $\simeq 0.22$ |
| at $BER = 10^{-5}$ | | | | | | |
| $E_b/N_0$ required at | $\gg 20.0$ $dB$ | $\gg 20.0$ $dB$ | $\gg 20.0$ $dB$ | $\gg 20.0$ $dB$ | 20.0 $dB$ | 20.0 $dB$ |
| Maximum throughput | 0.875 | 0.875 | 0.875 | 0.875 | 0.875 | 0.875 |
| | $f_D = 0.030$ | | | | | |
| Detection scheme | SSDD | | | MSDD | | |
| Relaying type | no | AF | DF | no | AF | DF |
| $E_b/N_0$ required | $\geq 12.50$ $dB$ | $\geq 12.0$ $dB$ | $\geq 10.1$ $dB$ | $\geq 4.8$ $dB$ | $\geq 2.0$ $dB$ | $\geq 0.5$ $dB$ |
| Throughput achieved | $\simeq 0.13$ | $\simeq 0.14$ | $\simeq 0.15$ | $\simeq 0.17$ | $\simeq 0.17$ | $\simeq 0.17$ |
| at $BER = 10^{-5}$ | | | | | | |
| $E_b/N_0$ required at | $\gg 20.0$ $dB$ | $\gg 20.0$ $dB$ | $\gg 20.0$ $dB$ | $\gg 20.0$ $dB$ | 22.0 $dB$ | 17.0 $dB$ |
| Maximum throughput | 0.875 | 0.875 | 0.875 | 0.875 | 0.875 | 0.875 |

PAS-based-coherent detection schemes and the imperfect-PSA-based-coherent schemes as well as the non-coherent arrangement also increases. Encountering rapidly fading channels makes the degradation of the system's performance more severe, as observed in Fig. 5.12. Moreover, it was found in Fig. 5.11 and Fig. 5.12 that in the slow fading scenario of $f_D = 0.001$, the imperfect-PSA-based-coherent detector may achieve a better performance than the differential non-coherent ones in terms of both the BER and the throughput attained. When the Doppler fading frequency is moderate, say $f_D = 0.01$, the performance of the two detection schemes was found comparable in Fig. 5.11 and Fig. 5.12. By contrast, in the fast fading scenario of $f_D = 0.1$, the imperfect-PSA-based-detection scheme only performs better than the differential ones in the low $E_b/N_0$ region, while it is inferior in the high $E_b/N_0$ region of Fig. 5.12, because a high pilot overhead is required. A brief summary of the comparison among the pilot-assisted perfect-, imperfect- and differential non-coherent detectors is provided in Table 5.9.

In Section 5.3, the non-coherent HARQ based M-FSK scheme of Figs. 5.14-5.16 was investigated. In order to exploit the M-FSK scheme's capability of detecting erased symbols, an ReS-coded system using error-and-erasure decoding was proposed in Section 5.3.1. The corresponding mathematical expressions were derived in Section 5.3.1.3 in order to quantify the attainable performance of the proposed system. The results of Fig. 5.20 showed that the error-and-erasure ReS decoding scheme outperforms the error-correction-only ReS decoding arrangement. More particularly, the $ReS(31, 20)$ coded system combined with 32-FSK modulation employing error-and-erasure decoding may achieve an $E_b/N_0$ gain of approximately 3dB at a CEP $P_w$ of $10^{-4}$, compared to the same system using error-correction-only decoding. Moreover, we have compared the achievable performance of the system,

when employing both the EGC and the SC techniques at the receiver. It was found in Fig. 5.21 that the EGC scheme assisted by one or two relays, is capable of achieving an $E_b/N_0$ gain of 1.5 dB or 1.0 dB, respectively, at $P_w$ of $10^{-6}$, compared to the SC scheme. Additionally, we demonstrated in Fig. 5.25 that the performance of the proposed ReS coded scheme is inferior to that of the LDPC codes considered, but it is capable of outperforming convolutional codes, when short packet transmissions are considered. Furthermore, non-coherent FSK aided HARQ was considered in Section 5.3.2. For the convolutional coded H-ARQ arrangement detailed in Table 5.6, the relaying scheme may achieve a gain of 3 dB in terms of transmit power without degrading the system's performance.

Finally, the novel distributed DSTBC scheme of Fig. 5.31 was proposed for a cooperative HARQ-aided system in Section 5.4. In contrast to the conventional distributed DSTBC, the proposed solution not only improved the system's performance, but also reduced the number of relays required by one. More particularly, as shown in Fig. 5.34, the proposed distributed DSTBC scheme achieved a gain of 3 dB and 5 dB in terms of the transmit power at the BER of $10^{-5}$, compared to the conventional distributed DSTBC, when the DG3 and DG4 DSTBCs are employed, respectively. Consequently, the attainable throughput is significantly increased in the $E_b/N_0$ region below 6 dB, as seen in Fig. 5.35.

Table 5.9: Performance comparison of perfect-, imperfect- and non-coherent detection schemes, where system parameters are detailed in Table 5.4 and plots are shown in Fig. 5.11 and Fig. 5.12.

| | $f_D = 0.001$ | | | $f_D = 0.01$ | | | $f_D = 0.1$ | | |
|---|---|---|---|---|---|---|---|---|---|
| Detection scheme | Perfect-Coherent | Imperfect-Coherent | Non-Coherent | Perfect-Coherent | Imperfect-Coherent | Non-Coherent | Perfect-Coherent | Imperfect-Coherent | Non-Coherent |
| Detection type | perfect CSI | imperfect CSI | differential | perfect CSI | imperfect CSI | differential | perfect CSI | imperfect CSI | differential |
| $E_b/N_0$ required<br>Throughput achieved<br>at $BER = 10^{-6}$ | $\geq 3.0\ dB$<br>$\simeq 0.31$ | $\geq 4.0\ dB$<br>$\simeq 0.27$ | $\geq 5.6\ dB$<br>$\simeq 0.30$ | $\geq 2.2\ dB$<br>$\simeq 0.31$ | $\geq 5.1\ dB$<br>$\simeq 0.38$ | $\geq 5.2\ dB$<br>$\simeq 0.20$ | $\geq 2.1\ dB$<br>$\simeq 0.23$ | $\geq 5.4\ dB$<br>$\simeq 0.27$ | $\geq 6.9\ dB$<br>$\simeq 0.25$ |
| $E_b/N_0$ required<br>Throughput achieved<br>at $FER = 10^{-3}$ | $\geq 3.0\ dB$<br>$\simeq 0.31$ | $\geq 4.0\ dB$<br>$\simeq 0.27$ | $\geq 5.3\ dB$<br>$\simeq 0.27$ | $\geq 1.8\ dB$<br>$\simeq 0.29$ | $\geq 5.1\ dB$<br>$\simeq 0.38$ | $\geq 5.1\ dB$<br>$\simeq 0.20$ | $\geq 2.1\ dB$<br>$\simeq 0.23$ | $\geq 5.5\ dB$<br>$\simeq 0.27$ | $\geq 6.9\ dB$<br>$\simeq 0.25$ |
| $E_b/N_0$ required at<br>Maximum throughput | $\geq 9.0\ dB$<br>$\simeq 0.499$ | $\geq 10.0\ dB$<br>$\simeq 0.499$ | $\geq 14.0\ dB$<br>0.500 | $\geq 7.0\ dB$<br>$\simeq 0.490$ | $\geq 10.0\ dB$<br>$\simeq 0.490$ | $\geq 10.0\ dB$<br>0.500 | $\geq 6.0\ dB$<br>$\simeq 0.417$ | $\geq 8.0\ dB$<br>$\simeq 0.417$ | $\geq 12.0\ dB$<br>0.5 |

## Appendix V

In this appendix we drive the joint conditional p.d.fs of $Y_1$ and $\lambda = Y_2/Y_1$ in the context of the MO-RTT, when the relay-aided SFH-MFSK system operates in non-dispersive Rayleigh fading channels.

According to [251], the joint conditional p.d.fs $f_{Y_1,\lambda}(y,r|H_1)$ and $f_{Y_1,\lambda}(y,r|H_0)$ associated with the MO-RTT based erasure insertion scheme may be expressed as

$$\begin{aligned} &f_{Y_1,\lambda}(y,r|H_1) = \\ &\frac{(M-1)y}{P_{N_n}(H_1)} f_{U_1}(y) f_{U_m}(yr) \left[\int_0^{yr} f_{U_j}(x)dx\right]^{M-2}, \\ &\qquad 0 \le y < \infty, 0 \le r \le 1 \end{aligned} \tag{5.57}$$

and

$$\begin{aligned} &f_{Y_1,\lambda}(y,r|H_0) = \\ &\frac{(M-1)y}{P_{N_n}(H_0)} \Bigg\{ f_{U_m}(y) f_{U_1}(yr) \left[\int_0^{yr} f_{U_j}(x)dx\right]^{M-2} \\ &+(M-2) f_{U_m}(y) f_{U_j}(yr) \left[\int_0^{yr} f_{U_1}(x)dx\right] \\ &\cdot \left[\int_0^{yr} f_{U_k}(x)dx\right]^{M-3} \Bigg\}, \quad 0 \le y < \infty, 0 \le r \le 1, \end{aligned} \tag{5.58}$$

where $f_{U_1}(y)$ presents the p.d.f of (5.28) and (5.34), while, $f_{U_m}(y)$, $f_{U_j}(y)$ and $f_{U_k}(y)$ represent the p.d.f of (5.29) and (5.35).

### Equal Gain Combining:

Substituting (5.28) and (5.29) into Eqs. (5.57) and (5.58) above and employing the function (2.321.2) of [260], we have

$$\begin{aligned} f_{Y_1,\lambda}(y,r|H_1) &= \frac{(M-1)y}{P_{N_n}(H_1)} \cdot \frac{y^{2L_f} r^{L_f}}{(1+\bar{\gamma}_l)^{L_f+1} \cdot (L_f!)^2} e^{\left(-\frac{1+r+r\bar{\gamma}_l}{1+\bar{\gamma}_l} y\right)} \left[\int_0^{yr} \frac{x^{L_f}}{L_f!} e^{-x} dx\right]^{M-2} \\ &= \frac{(M-1)y}{P_{N_n}(H_1)} \cdot \frac{y^{2L_f} r^{L_f}}{(1+\bar{\gamma}_l)^{L_f+1} \cdot (L_f!)^M} e^{\left(-\frac{1+r+r\bar{\gamma}_l}{1+\bar{\gamma}_l} y\right)} \\ &\quad \cdot \left[L_f! - e^{-yr} \sum_{k=0}^{L_f} k! \binom{L_f}{k} (yr)^{L_f-k}\right]^{M-2}, \end{aligned} \tag{5.59}$$

and

$$\begin{aligned} f_{Y_1,\lambda}(y,r|H_0) &= \frac{(M-1)y}{P_{N_n}(H_0)}\Bigg\{\frac{y^{2L_f}r^{L_f}}{(1+\bar{\gamma_l})^{L_f+1}\cdot(L_f!)^2}e^{\left(-\frac{r+1+\bar{\gamma_l}}{1+\bar{\gamma_l}}y\right)}\left[\int_0^{yr}\frac{x^{L_f}}{L_f!}e^{-x}dx\right]^{M-2} \\ &\quad +(M-2)\frac{y^{2L_f}r^{L_f}}{(L_f!)^2}e^{-(r+1)y}\left[\int_0^{yr}\frac{x^{L_f}}{(1+\bar{\gamma_l})^{L_f+1}\cdot L_f!}e^{\left(-\frac{x}{1+\bar{\gamma_l}}\right)}dx\right] \\ &\quad \cdot\left[\int_0^{yr}\frac{x^{L_f}}{L_f!}e^{-x}dx\right]^{M-3}\Bigg\} \\ &= \frac{(M-1)y}{P_{N_n}(H_0)}\cdot\frac{y^{2L_f}r^{L_f}}{(1+\bar{\gamma_l})^{L_f+1}\cdot(L_f!)^M}\Bigg\{e^{\left(-\frac{1+r+r\bar{\gamma_l}}{1+\bar{\gamma_l}}y\right)} \\ &\quad \cdot\left[L_f!-e^{-yr}\sum_{k=0}^{L_f}k!\binom{L_f}{k}(yr)^{L_f-k}\right]^{M-2}+(M-2)e^{-(r+1)y} \\ &\quad \cdot\left[(1+\bar{\gamma_l})^{L_f+1}L_f!-e^{\left(-\frac{yr}{1+\bar{\gamma_l}}\right)}\sum_{k=0}^{L_f}(1+\bar{\gamma_l})^{k+1}k!\binom{L_f}{k}(yr)^{L_f-k}\right] \\ &\quad \cdot\left[L_f!-e^{-yr}\sum_{k=0}^{L_f}k!\binom{L_f}{k}(yr)^{L_f-k}\right]^{M-3}\Bigg\}. \end{aligned} \tag{5.60}$$

**Selection Combining:**

Substituting (5.34) and (5.35) into Eqs. (5.57) and (5.58), we have

$$\begin{aligned} f_{Y_1,\lambda}(y,r|H_1) &= \frac{(M-1)y}{P_{N_n}(H_1)}\cdot\frac{L_f+1}{1+\gamma_l}e^{\left(-\frac{y}{1+\gamma_l}\right)}\left[1-e^{\left(-\frac{y}{1+\gamma_l}\right)}\right]^{L_f}(L_f+1)e^{(-yr)}[1-e^{(-yr)}]^{L_f} \\ &\quad \cdot\left[\int_0^{yr}(L_f+1)e^{-x}(1-e^{-x})^{L_f}dx\right]^{M-2} \\ &= \frac{(M-1)y}{P_{N_n}(H_1)}\cdot\frac{(L_f+1)^2}{1+\gamma_l}e^{\left(-\frac{1+r+r\gamma_l}{1+\gamma_l}y\right)}\left[1-e^{\left(-\frac{y}{1+\gamma_l}\right)}\right]^{L_f}[1-e^{-yr}]^{(L_f+1)(M-2)+L_f}, \end{aligned} \tag{5.61}$$

and

$$\begin{aligned} f_{Y_1,\lambda}(y,r|H_0) &= \frac{(M-1)y}{P_{N_n}(H_0)}\Bigg\{(L_f+1)e^{-y}(1-e^{-y})^{L_f}\cdot\frac{L_f+1}{1+\gamma_l}e^{\left(-\frac{yr}{1+\gamma_l}\right)}\left[1-e^{\left(-\frac{yr}{1+\gamma_l}\right)}\right]^{L_f} \\ &\quad \cdot[1-exp(-yr)]^{(L_f+1)(M-2)}+(M-2)\cdot(L_f+1)e^{-y}(1-e^{-y})^{L_f} \\ &\quad \cdot(L_f+1)e^{(-yr)}[1-e^{(-yr)}]^{L_f}\cdot[1-e^{(-yr)}]^{(L_f+1)(M-3)} \\ &\quad \cdot\int_0^{yr}\frac{L_f+1}{1+\gamma_l}e^{\left(-\frac{x}{1+\gamma_l}\right)}\left[1-e^{\left(-\frac{x}{1+\gamma_l}\right)}\right]dx\Bigg\} \\ &= \frac{(M-1)y}{P_{N_n}(H_1)}\cdot\Bigg\{\frac{(L_f+1)^2}{1+\gamma_l}e^{\left(-\frac{1+r+r\gamma_l}{1+\gamma_l}y\right)}\left[1-e^{\left(-\frac{y}{1+\gamma_l}\right)}\right]^{L_f} \\ &\quad \cdot[1-e^{-yr}]^{(L_f+1)(M-2)+L_f}+(M-2)\cdot\frac{(L_f+1)^3}{2}e^{(-yr-y)}[1-e^{-y}]^{L_f} \\ &\quad \cdot\left[1-e^{\left(-\frac{yr}{1+\gamma_l}\right)}\right]^2[1-e^{-yr}]^{(L_f+1)(M-3)+L_f}\Bigg\}. \end{aligned} \tag{5.62}$$

# Chapter 6

# Conclusions and Future Research

In this concluding chapter, a summary of the thesis and the main findings of our investigations will be presented. This will be followed by a number of research topics for potential future studies.

## 6.1 Summary and Conclusions

In this treatise, we have investigated the family of H-ARQ systems in the context of cooperative wireless communications. More particularly, diverse MIMO techniques were combined with cooperative H-ARQ protocols, where various detection schemes were compared, namely both perfect- and realistic imperfect-coherent detection as well as non-coherent detection were investigated, as outlined in Fig. 1.5.

- **Chapter 1:**

  Chapter 1 provided a rudimentary overview of wireless communication systems and of the classic H-ARQ protocol. More particularly, we described the operation of typical wireless systems and then various wireless channel models were discussed in Section 1.1.1, followed by the historic development of commercial wireless systems in Section 1.1.2, which were summarized in Fig. 1.8. A brief introduction to classic co-located MIMO techniques was offered in Section 1.1.3.1, while MIMO-aided cooperative communications was introduced in Section 1.1.3.2. Furthermore, Section 1.2.1 described the ARQ protocol and its common types, namely the Stop-and-wait ARQ, Go-Back-N ARQ and Selective Repeat ARQ. The H-ARQ protocol, where the ARQ is combined with channel codes was introduced in Section 1.2.2. Finally, the thesis' organization, which was outlined in Fig. 1.5, and the main investigations were highlighted in Section 1.3.

- **Chapter 2:**

  Chapter 2 further detailed the co-located as well as distributed MIMO techniques. In Section 2.2.1.1 receive diversity techniques, namely MRC, EGC, SC and SwC were described, while the class of transmit diversity techniques employing space-time codes, such as STBC and STTC were reviewed in Section 2.2.1.2. In contrast to the spatial transmit and receive diversity techniques, multiplexing schemes, such as the HLST and VLST arrangements were detailed in Section 2.2.2. The trade-offs between the achievable diversity gain of the spatial diversity schemes

and the multiplexing gain of the multiplexing schemes were detailed in Section 2.2.3, leading to the introduction of LDC codes.

In order to conceive more flexible MIMO designs, we proposed the novel STFSK concept, where the signals are spread in the three domains, namely the TD, FD and SD. The STFSK system concept was detailed in Section 2.2.4.3. Furthermore, the soft-output STFSK demodulator was proposed in Section 2.2.4.4 for iterative detection, which was investigated by EXIT charts in Section 2.2.4.5. Since the STFSK schemes spread the transmit signal across three domains, their normalized throughput was quantified in Section 2.2.4.6. Additionally, the decoding complexity of both hard-decision and soft-decision aided STFSK schemes was studied in Section 2.2.4.7. Finally, the system parameters were detailed in Section 2.2.4.8 based on the aspects considered in the previous sections. The STFSK schemes' features were summarized in Table 2.6, while their relationship to other MIMO techniques is outlined here in Fig. 6.1.

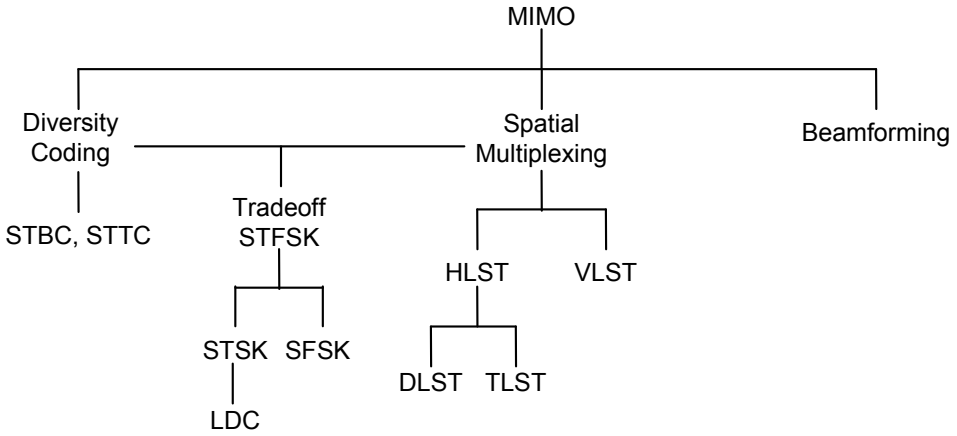


Figure 6.1: MIMO techniques.

The performance of the STFSK schemes is studied in Section 2.2.4.9 in single-user interference-limited environments, both for frequency-flat Rayleigh fading channels as well as for frequency-selective fading channels, using the COST-207 and the ITU channel models of Chapter 1. The results of Figs. 2.17-2.19 demonstrated that STFSK offered a better performance than the STSK, the SFSK as well as the LDC schemes, regardless whether the channel was frequency-selective or frequency-flat. Moreover, an iterative detection aided the soft-output STFSK was conceived. The results of Fig. 2.20 showed that an $E_b/N_0$ gain of 3 dB is achieved at the BER of $10^{-4}$, when the number of iterations between the soft STFSK demapper and the RSC decoder was increased from one to five. Fig. 2.22 also demonstrated that at a fixed number of bits per symbol, using an increased number of frequencies $K$ results in an improved BER performance. Naturally, this improvement is achieved at the cost of a throughput loss due to increasing the bandwidth occupied.

Furthermore, the STFSK schemes is also investigated in terms of its ASE, when it is combined with the SFHMA system of Section 2.2.4.9 for operating in a multi-user and multi-cell environment. The results of Table 2.13 showed that the proposed system may double the attainable ASE compared to GMSK aided SFHMA, when the ReS(8,4) channel code is employed for transmission over the 6-tap COST-207 rural area channel model associated with Rayleigh fading and AWGN. Additionally, the soft-decision RSC(23,33) coded STFSK aided SFHMA of

Table 6.1: Summary of STFSK schemes

| **Aspects** | **Figure, Table & Equation** | **Remarks** |
|---|---|---|
| System design | Figs. 2.9-2.11; Table 2.2 | Each STFSK scheme relies on the parameters $(n_T, n_R, T, Q, L, K)$, which are defined as follows:<br>• The values $(n_T, n_R, T, Q)$ describe an LDC scheme, where $n_T$ transmit antennas and $n_R$ receive antennas are employed to transmit $Q$ symbols spread across $T$ timeslots;<br>• The value of $L$ specifies $L$-PSK/QAM modem conveying $log_2(L)$ bits;<br>• The value $K$ specifies $K$-FSK component representing $log_2(K)$ bits.<br>For $L = 1$, STFSK becomes STSK [53]. By contrast, when $K = 1$, STFSK becomes SFSK [261]. |
| Soft STFSK demodulator & EXIT chart | Figs. 2.12-2.15; Eqs.2.38-2.48; Table 2.3 | • Increasing the number of FSK frequencies, $K$, may increase the *extrinsic* information at the cost of extending the bandwidth used.<br>• Increasing the number of dispersion matrices, $Q$, reduces the *extrinsic* information, when the same number of frequencies, $K$, is employed. |
| Throughput | Eqs. 2.50-2.51, Table 2.4 | • As the value of $K$ or $T$ increases, the throughput of the system linearly decreases.<br>• By contrast, the throughput is increased relatively slowly, namely as a function of $log_2(K \cdot L \cdot Q)$ with the product $(K \cdot L \cdot Q)$. |
| Decoding complexity | Fig. 2.16; Eqs. 2.52-2.73; Tables 2.4-2.5 | • For hard-decisions, the complexity of the decoder is reduced, when the number of frequencies, $K$, is increased.<br>• For a given value of $K$ and for a given value of the product $QL$, all possible combinations of $Q$ and $L$ exhibit the same decoding complexity when hard-decision is employed.<br>• In case of hard-decision, the complexity of a STFSK scheme increases upon increasing the normalized throughput.<br>• The complexity of a soft-decision STFSK demodulator depends only on the product of $Q \times L \times K$, rather than on each individual parameter $Q$, $L$ and $K$. |
| Parameter selection | | • The values of $K = \{2, 4\}$ constitute reasonable choices in order to mitigate the effects of frequency-selective fading, while maintaining a high throughput.<br>• The number of transmit antennas employed should obey $n_T \leq T$, since no further capacity gain may be achieved for $n_T > T$.<br>• To maintain orthogonality, the frequency between the adjacent signalling tones of the FSK modulator has to be separated by at least $1/T_s$ Hz. |

Section 2.2.4.9 may approach the maximum achievable ASE in various frequency reuse cluster sizes, as seen in Table 2.13. For further study, the STFSK system's ASE was compared to that of the soft-decision assisted RSC coded GMSK aided TD/FDMA regime. As demonstrated in Fig. 2.28 and Table 2.14, the soft-decision RSC(23,33) coded STFSK aided SFHMA system is capable of outperforming the RSC(23,33) coded GMSK aided TD/FDMA as well as WCDMA in terms of its ASE. Despite this significant improvement, the ASE of the STFSK aided SFHMA remains only 60 % of that of the more complex LTE system, when the same RSC(23,33) channel code and a system bandwidth of 5 MHz are employed.

As a conceptual extension of the class of co-located MIMO techniques, the family of wireless MIMO systems relying on the distributed antenna elements of the single-antenna mobiles was introduced in Section 2.3 in the context of wireless cooperative communications. The system model and the various popular cooperation types, such as the AF, DF and CF were described in Section 2.3.2. They were followed by a discussion of the associated relaying protocols in Section 2.3.3, including traditional relaying, successive relaying, network coding aided three-phase relaying as well as two-phase relaying. The performance results provided in Figs. 2.36-2.39 of Section 2.3.4 demonstrated that cooperative communication exhibits a number of benefits over conventional direct communications. More particularly, in order to achieve a good performance, the relay station should be close to the source for avoiding DF-relaying-induced error propagation, when the DF relaying protocol is employed. By contrast, in AF relaying the relay station is less prone to error propagation, even when it roams close to the destination. Furthermore, the results of Fig. 2.39 suggested that the DSTC of Section 2.3.4.2 should be employed in order to avoid wasting network resources, such as time slots and/or frequencies occupied for the sake of improving the achievable performance.

- **Chapter 3:**
  In Chapter 3 we focused our attention on coherent detection, exploiting the idealized simplifying assumption that perfect CSI was available at the receiver for H-ARQ aided cooperative communications. We commenced in Section 3.2 by investigating the attainable performance of cooperative ARQ in both correlated and uncorrelated fading channels, where a novel relay-switching regime was proposed for mitigating the detrimental effects of correlated fading without unduly increasing the system's complexity and delay. More particularly, the system model and its rationale were introduced in Sections 3.2.1-3.2.3. They were followed by our capacity derivation, where the relay-switching aided ARQ outperformed the single-relay aided ARQ in term of its achievable capacity. The performance of relay-switching aided ARQ was characterized in Section 3.2.5. According to the results of Figs. 3.5-3.8, the proposed relay-switching scheme improved both the system's BER and FER performance, and additionally, it reduced the number of retransmissions. Hence, our solution reduced the transmit power, delay as well as the interference it inflicted. Furthermore, in Section 3.3 a novel relay-switching regime was proposed, which was intrinsically amalgamated with turbo coded H-ARQ schemes for the sake of achieving further improvements. The TC-HARQ concept using Chase combing, IR and SSR was described in Section 3.3.1, while its performance characterization followed in Section 3.3.2. As seen in Figs. 3.10-3.15, the relay-aided schemes significantly improved the system's performance in terms of all metrics considered, namely the BER, the FER, the number of retransmissions

as well as the achievable throughput. The results of Figs. 3.10, 3.11, 3.14, 3.15 also showed that the TC-HARQ schemes employing both the IR and the SSR techniques may outperform the TC-HARQ using Chase combining. Our related comparisons are further summarised in Table 6.2.

Table 6.2: Summary of relay-switching aided TC-HARQ.

| TC-HARQ schemes | Parameters | BER | FER | Throughput |
|---|---|---|---|---|
| Comparison between CC and IR | Table 3.3 | Fig. 3.10(a) | Fig. 3.10(b) | Fig. 3.15(b) |
| Comparison between CC and SSR | Table 3.4 | Fig. 3.14(a) | Fig. 3.14(b) | Fig. 3.15(b) |

Inspired by the benefits of rateless codes [170], which are capable of adapting to time-variant channel conditions without requiring channel knowledge at the transmitter, in Section 3.4.1 we conceived a novel system based on the concatenation of SLT codes and 16-QAM, where the decoder and the demodulator iteratively exchange *extrinsic* information. The SLT codes [40] were briefly reviewed in Section 3.4.1.1, while their degree distributions, which play an important role in predetermining their performance were characterized in Section 3.4.1.2. The ID-SLT coded 16-QAM aided H-ARQ design of SLT codes and 16-QAM was detailed in Section 3.4.1.3, followed by the proposal of an actively-cooperative ID-SLT H-ARQ scheme employing IR in Section 3.4.2. The achievable capacity and transmit power equations were formulated in Section 3.4.3 for a convenient comparison between the proposed passively- and actively-cooperative schemes. Our comparisons showed that the actively-cooperative scheme improves the achievable throughput despite reducing the total transmit power, hence also reducing the interference imposed by it. The performance of the ID-SLT coded 16-QAM aided H-ARQ arrangement was evaluated in Section 3.4.4. More particularly, the simulation results of Figs. 3.23-3.26 showed that when AF and DF relayings were combined with the proposed SLT coded 16-QAM scheme, the system achieved a gain of about 2.5 dB and 6 dB, respectively, at the BER of $10^{-5}$, compared to the non-iterative detection scheme operating without the relay's assistance. Moreover, we found from Fig. 3.28 that the AF relaying aided SLT coded 16-QAM scheme benefits more substantially, when the relay station is roaming close to the source. By contrast, the DF relaying aided scheme achieves its best performance near the mid-point, as seen in Fig. 3.28. Observe in Fig. 3.31 and 3.32 that the actively cooperative ARQ protocol of 3.21(b) combined with SLT coding reduced the number of IR transmissions by approximately 30%, while the total transmit power was reduced by about 5% in the $E_b/N_0$ region between 2 dB and 4 dB.

- **Chapter 4:**
  Chapter 3 investigated the class of coherent detection aided cooperative H-ARQ schemes, where the CSI was assumed to be perfectly known at the receiver. Naturally, this idealized simplifying assumption is unrealistic. A large number of researchers have considered the impact of imperfect CSI [191–198], but none of them studied it in the context of H-ARQ. Therefore, in Section 4.2 of Chapter 4, we proposed a framework for investigating the impact of imperfect CSI on the performance of ReS coded H-ARQ systems. Our system model was presented in Section 4.2.1, while the APER and the goodput metrics employed for evaluating the attainable performance of H-ARQ systems in the context of imperfect CSI were defined in Section 4.2.2.

Table 6.3: Summary of the factors affecting the performance of imperfect ReS/H-ARQ in the context of cooperative networks.

| Effect | Type | BEP | Goodput |
|---|---|---|---|
| Doppler frequency | AF | Fig. 4.11 | Fig. 4.12 |
| | DF | Fig. 4.13 | Fig. 4.14 |
| Pilot oversampling factor | AF | Fig. 4.15 | Fig. 4.18 |
| | DF | Fig. 4.19 | Fig. 4.21 |
| Number of relays | AF | Fig. 4.22 | Fig. 4.23 |
| | DF | Fig. 4.24 | Fig. 4.25 |
| Relay positions | AF | Fig. 4.26 | Fig. 4.27 |
| | DF | Fig. 4.28 | Fig. 4.29 |
| Source-relay power location | AF | Fig. 4.30 | Fig. 4.32 |
| Frame length | AF | Fig. 4.33 | |
| Code rate | AF | Fig. 4.34 | Fig. 4.35 |

The redefinitions were followed by the derivation of mathematical expressions for characterising the effects of imperfect CSI on the system's APER and on the goodput in Section 4.2.3.1. Based on these expressions, an optimized pilot-versus-data power-allocation scheme was proposed in Section 4.2.3.2. The analysis was verified by the simulation results of Section 4.2.4, which showed that the results showed that for a specific $E_b/N_0$ value, there is an optimized code rate, which maximizes the achievable goodput. The optimized power allocation allows the system to significantly reduce the total transmit power without degrading the APER as well as the achievable goodput.

The impact of imperfect CSI was further analysed then in the scenario of the cooperative wireless communications in Section 4.3. Again, the system model was presented in Section 4.3.1, while the analysis of both AF and DF relaying was provided in Section 4.3.2. The associated performance results were provided in Section 4.3.3. Our related findings are summarised in Table 6.3.

Furthermore, a comparison between the AF and DF relaying cast in the context of imperfect CSI was studied in Section 4.3.3.8. The results of this section showed that AF relaying outperforms DF relaying in the low $E_b/N_0$ region, while in the high $E_b/N_0$ region the AF scheme is inferior to its DF counterpart, since it requires a higher number of pilot symbols.

- **Chapter 5:**

  In contrast to the coherent detection based PSAM schemes of Chapter 3 and Chapter 4, Chapter 5 investigated the performance of non-coherent detection aided H-ARQ in cooperative wireless communications. Section 5.2 considered the popular DPSK aided H-ARQ, where both the SSDD and MSDD schemes were employed. More particularly, the DPSK aided ReS coded H-ARQ scheme employing hard-decisions was detailed in Section 5.2.1. The results of Figs. 5.3-5.5 in Section 5.2.1.1 showed that as a benefit of relaying, the DPSK aided cooperative H-ARQ may reduce both the BER as well as the number of retransmissions, hence increasing the achievable throughput. When employing MSDD, the system's transmit power was further reduced, while

the BER and the throughput remained unaffected, as seen from Figs.5.6-5.8 of Section 5.2.1.2. By contrast, DPSK aided cooperative H-ARQ employing soft-demodulation aided iterative decoding was detailed in Section 5.2.2. The performance results of Fig. 5.10 demonstrated that in the context of the convolutional coded HARQ scheme of Fig. 5.9 using the parameters of Table 5.3 the AF aided cooperative HARQ may achieve a higher throughput than its DF based cooperative counterpart, despite its lower BER. In order to evaluate the performance of various detection schemes in the context of cooperative wireless networks, our comparison between the perfect- and imperfect-PSA as well as non-coherent detection schemes was presented in Section 5.2.3. According to Fig. 5.11 and Fig. 5.12, the performance discrepancy between the perfect-PAS-based-coherent detection schemes and the imperfect-PSA-based-coherent schemes as well as the non-coherent arrangement also increases upon increasing of the Doppler frequency. The results also suggested that in slow fading scenarios the imperfect-PSA-based-coherent detector is preferred, while in fast fading channels, the differential detection might be preferred, since there is no throughput loss due to a high pilot overhead. For moderate Doppler frequencies, the imperfect-PSA and the differential non-coherent schemes perform comparably in terms of both their BER and their achievable throughput. Our comparisons are summarised in Table 6.4.

Table 6.4: Summary of coherent versus non-coherent detection schemes in the context of cooperative H-ARQ

| Detection types | Schematic | BER | FER | Throughput |
|---|---|---|---|---|
| Perfect coherent detection aided H-ARQ | Fig. 3.1 | | | |
| Imperfect coherent detection aided H-ARQ | Fig. 4.1 | Fig. 5.11(a) | Fig. 5.11(b) | Fig. 5.12 |
| Non-coherent detection aided H-ARQ | Fig. 5.1 | | | |

In Section 5.3, non-coherent HARQ based M-FSK schemes were investigated in the context of cooperative wireless networks. In order to exploit the M-FSK scheme's capability of detecting erased symbols, an ReS-coded system using error-and-erasure decoding was proposed in Section 5.3.1. The corresponding mathematical expressions derived for relaying networks using EGC and SC diversity reception techniques were derived in Section 5.3.1.3 in order to quantify the attainable performance of the proposed system. The results of Fig. 5.20 showed that the error-and-erasure ReS decoding scheme outperforms the error-correction-only ReS decoding arrangement. Moreover, we have compared the achievable performance of the system, when employing both EGC and SC techniques at the receiver. It was found in Fig. 5.21 that the EGC scheme assisted by one or two relays is capable of outperforming the SC scheme. Additionally, we demonstrated in Fig. 5.25 that despite the employment of error-and-erasure decoding, the performance of the proposed ReS coded scheme remained inferior to that of the LDPC codes, when the same system parameters were considered. However, the ReS coded system using EI decoding was capable of outperforming convolutional codes, when short packet transmissions are considered. Furthermore, non-coherent FSK aided HARQ employing iterative detection was considered in Section 5.3.2. For the convolutional coded H-ARQ arrangement detailed in Table 5.6, the relaying scheme may halve the required transmit power without degrading the system's performance, compared to the non-iterative benchmark detection schemes.

Finally, the novel distributed DSTBC scheme of Fig. 5.31 was proposed for a cooperative H-ARQ aided system in Section 5.4. For the proposed DSTBC scheme the first column of the $N$-column encoded matrix was sent during the first transmission slot, while the remaining $(N-1)$ columns of the $N$-column encoded matrix were transmitted during the retransmission slots, while requiring $(N-2)$ relays. At the receiver the $N$-column signals were combined for DSTBC decoding. In contrast to the conventional distributed DSTBC, the proposed solution not only improved the system's performance, but also reduced the number of relays required by one. More particularly, as shown in Fig. 5.34, the proposed distributed DSTBC scheme achieved a gain of 3 dB and 5 dB in terms of the transmit power at the BER of $10^{-5}$, compared to the conventional distributed DSTBC, when the DG3 and DG4 DSTBCs were employed, respectively. Consequently, the attainable throughput was significantly increased in the $E_b/N_0$ region below 6 dB, as seen in Fig. 5.35.

Based on the investigations of Chapters 1-5, our design guide-lines inferred for an H-ARQ aided cooperative systems may be summarized as follows:

- **Select an appropriate channel code**: Specifically, in the system requiring a low-complexity and low latency, maximum-minimum-distance block codes, such as ReS codes, may be employed. By contrast, more sophisticated but often more complex channel codes, such as convolutional codes, turbo codes and LDPC codes, which are capable of exploiting the power of soft-decision algorithms and iterative decoding, may be employed in order to reduce the BER at the destination. Furthermore, as discussed in Section 3.4, the family of rateless codes, such as LT, SLT codes, etc., are also attractive channel codes in the context of H-ARQ systems owing to their capability of adapting to time-variant channel conditions without requiring any channel knowledge at the transmitter.

- **Select a detection type**: In Chapters 3-5, we have investigated the family of coherent as well as non-coherent detection aided cooperative H-ARQ schemes. We demonstrated that the pilot symbol assisted coherent detection aided H-ARQ schemes proposed in Chapters 3 and 4 provide a low-complexity solution at the cost of reducing the effective throughput due to employing pilot symbols. By contrast, the non-coherent schemes proposed in Chapter 5 may avoid the pilot-related throughput loss, which partially offsets their typical 3 dB power loss. Alternatively, the frequency bandwidth employed has to be extended in case of non-coherent FSK. Our comparisons between the perfect- and imperfect-PSA as well as non-coherent detection schemes provided in Section 5.2.3 demonstrated that the performance discrepancy between the perfect-PAS-based-coherent detection schemes and the imperfect-PSA-based-coherent schemes as well as the non-coherent arrangement also increases upon increasing the Doppler frequency. In slow-fading scenarios the imperfect-PSA-based-coherent detector is preferred, while in fast fading channels, differential detection might be preferred, since there is no throughput loss due to a high pilot overhead. However, differentially detection systems also exhibit an eroded performance at high Doppler frequencies, which may require the employment of multiple-symbol sphere detection [23]. For moderate Doppler frequencies, the imperfect-PSA and the differential non-coherent schemes perform comparably in terms of both their BER and their achievable throughput.

- **Select an ARQ-retransmission type**: As mentioned in Section 1.2.1, there are three main ARQ protocol types, namely Stop-and-wait ARQ, Go-Back-N ARQ and Selective Repeat ARQ. Owing to their capability of improving the system throughput, Selective Repeat ARQ is preferred to its other two counterparts, which has been extensively employed in contemporary H-ARQ aided communication systems.

- **Select a HARQ-combining type**: As detailed in Section 3.3.1.1, the specific choice of the H-ARQ receiver combining techniques plays a crucial role in predetermining the performance of H-ARQ schemes. By combining multiple version of the same transmit packet, the CC technique of Section 3.3.1.1 offers a simple power-gain based combining solution, albeit its simplicity comes at the cost having no coding gain. By contrast, the IR techniques achieve a beneficial coding gain owing to the additional parity bits gleaned from retransmissions. However, the HARQ scheme using IR has an inferior performance in comparison to that of the H-ARQ arrangement using CC, when the systematic bits in the first transmission are corrupted by deep fades and no more systematic bits were received during the retransmission sessions [164]. For some channel codes, such as turbo codes, the residual decoding errors may occur in error-bursts, or in error clusters of a received packet [165]. In this scenario H-ARQ schemes relying on SSR may be invoked in order to improve the attainable system performance.

- **Choice of the cooperation type**: The cooperation type of relay station plays an important role in predetermining the performance of H-ARQ systems in the context of cooperative networks. As described in Section 2.3.2, AF relaying constitutes a low-complexity cooperative scheme, where the relay simply amplifies and forwards its received signal to the destination. By contrast, DF relaying imposes a higher complexity on the relay during the decoding and re-encoding process, in the hope of improving the signal quality. Our investigations in Section 2.3.4 demonstrated that the relay station should invoke the the DF relaying, when it roams close to the source in order to avoid error propagation. By contrast, when the relay station is close to the destination, AF relaying should be activated.

- **Choice of the relaying protocol**: The relaying protocol, which was discussed in Section 2.3.3 constitutes another important aspect to be considered in the design of a cooperative system. The traditional four-phase relaying protocol attains a high diversity gain and hence an improved link quality at the cost of halving the effective throughput. The throughput loss imposed by four-phase relaying may be reduced by utilizing the successive relaying technique of Section 2.3.3.2. A specific drawback of this protocol is the potential presence of interference imposed. Furthermore, network coded two-phase relaying may be employed to reduce the number of transmission phases required, albeit this is achieved at the cost of degrading the signal quality.

- **Choice of the cooperative multiple access scheme**: In order to mitigate the interference amongst the signals received at the destination upon increasing the number of relay nodes, the multiple-relay-assisted schemes require orthogonal subchannels for the relay node transmissions. The required orthogonality may be created in the TD, FD or SD with the aid of TDMA, FDMA, CDMA, SDMA, and so on. However regardless of its specific implementation, this results in a reduction of the system's spectral efficiency. A popular solution is constituted by the so-called distributed space-time coding (DSTC) philosophy [107, 136], where the relays are permitted to

simultaneously transmit over the same channel by emulating a classic space-time code having co-located antenna elements. This distributed configuration is capable of retaining the DSTC system's diversity order as well as throughput [107, 136].

All of the factors affecting the cooperative H-ARQ system design are illustrated in Fig. 6.2.

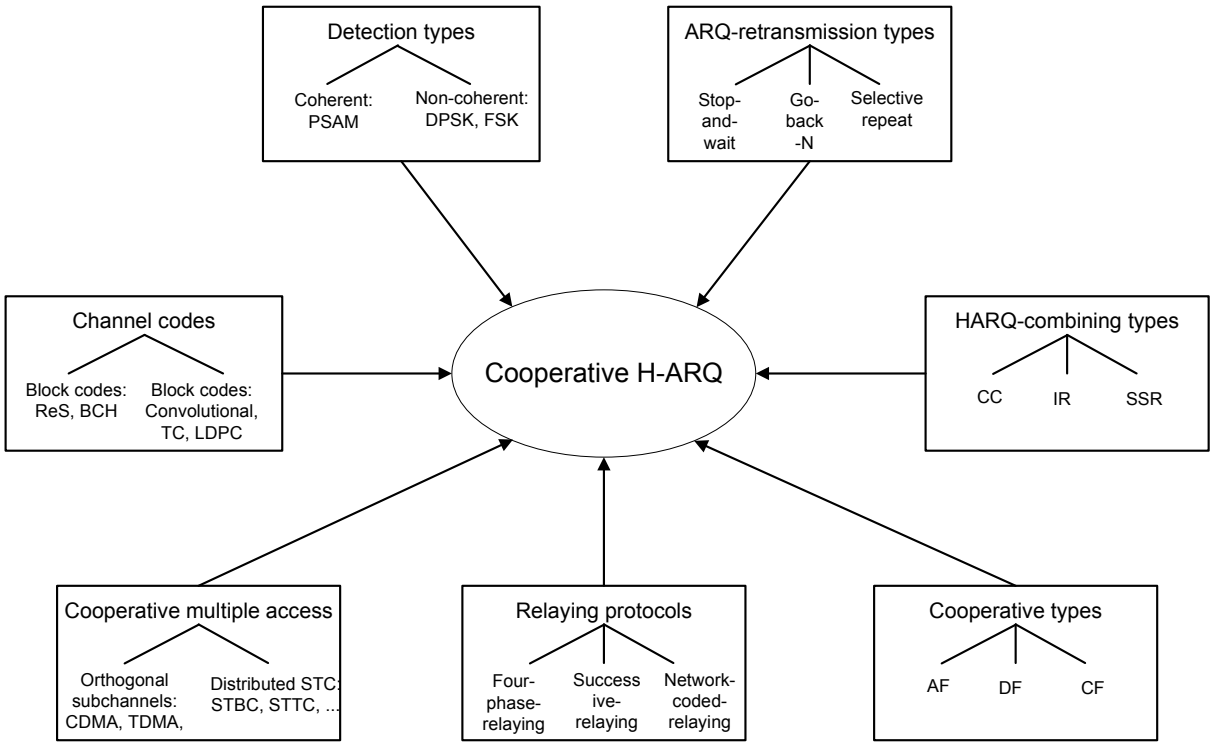


Figure 6.2: Factor affecting a cooperative H-ARQ system design.

## 6.2 Suggestions for Future Research

### 6.2.1 Capacity of Space-Time-Frequency Shift Keying

The STFSK concept was proposed in Section 2.2.4. Our related investigations included its system design, decoding complexity as well as performance. However, the capacity of STFSK is still unknown and hence require further study. This investigation will be based on the combination of the capacity of the STFSK scheme characterized in [53] and that of MIMO channels relying on multi-dimensional signal sets, as detailed in [262]. The knowledge of the capacity, along with the associated decoding complexity, will allow us to optimize parameter selection in order to achieve the best possible performance.

### 6.2.2 Space-Time-Frequency Shift Keying Optimization

In our STFSK schemes proposed in Chapter 2, we employ the combination of PSK/QAM symbol sets and LDC dispersion matrices, where the latter is based on a random search method for the

sake of simplicity. Therefore, the optimized combination of the signalling alphabet and dispersion matrix is worth investigating in order to improve the overall performance. A number of dispersion-matrix optimization approaches have been proposed. For example, the Generic Algorithm of [263] may be useful for optimizing the dispersion matrices of the LDC codes of Section 2.2.3. Diverse QAM arrangements were detailed in [230], while their soft detection was presented in [230, 264]. Hence, the combined joint optimization of the components requires further research.

### 6.2.3 STFSK Aided SFHMA for Multi-user, Multi-cell Data Networks

In Section 2.2.4.9 we investigated the performance of STFSK aided SFHMA in a multi-user, multi-cell environment and compared it to other networks, such as the 2G TD/FDMA GSM, the 3G WCDMA and well as the advanced LTE system in the context of voice services. However, both the LTE and the forthcoming future networks tend to employ the all-IP based techniques. Therefore, a new framework has to be proposed in order to investigate the packet data services of these networks.

### 6.2.4 Pilot-Assisted Soft Decoding Aided H-ARQ

As detailed in Chapter 3, pilot symbol assisted modulation schemes [146] potentially improve the achievable BER performance at the cost of reducing the effective throughput. In order to exploit the benefits of pilots further, the authors of [265] proposed a so-called pilot symbol assisted coding scheme. In this proposal instead of inserting pilots after the modulation stage as in classic PSAM [146], the pilot symbols are combined with the information bits at a predefined rate before carrying out channel encoding. At the receiver employing iterative decoding, the pilots not only provide CSI but also provide valuable parity information for the decoder. As a result, the achievable decoding performance may be further improved.

In the context of cooperative networks and HARQ protocols, the pilot symbol assisted coding scheme is particularly worthwhile investigating, since it may be exploited for quantifying, when there are beneficially contributing relays. Secondly, the H-ARQ scheme using different retransmission techniques, such as the CC, IR and SSR arrangements of Section 3.3, also requires further investigations, when combined with pilot symbol assisted coding [265].

### 6.2.5 Cross Layer Optimization for Cooperative Communications

All of the operational data networks rely on the seven-layer Open Systems Interconnection (OSI) model [266] or on the four-layer TCP/IP model [266], where the layers exchange information through common interfaces, but the performance of a specific layer is independent of that of the others. These models were conceived for wireline-based computer networks in the 1980s. When they are applied to wireless networks, some problems arise due to the characteristics of the hostile wireless channel. These problems degrade the overall performance of the wireless networks. Recently, a vast number of researchers focused their efforts on cross layer optimization [267–269] in order to improve the performance of networks, especially that of relay-aided wireless networks.

The investigations provided in this thesis on the H-ARQ protocol conceived for cooperative com-

munications may be considered a cross-layer optimization process, where the physical and MAC layers are involved. More particularly, in Chapter 3 and 4 we considered the benefits of pilot symbols as well as of channel codes on the physical layer performance of the system employing the H-ARQ protocol, which is a constituent component of the MAC layer. Then the pilot-symbol power allocation as well as channel code rate optimization was proposed in order to maximize the achievable BER and FER performance, while reducing the number of retransmission. However, in cooperative networks, the reliability of the signalling and routing messages amongst the cooperative nodes play a crucial role in the network's high-integrity operation. Therefore, cross layer operation between the physical, the MAC, the network as well as the application layers must be jointly studied for the sake of achieving further improvements.

### 6.2.6 H-ARQ Performance in Multi-User Cooperation

In practice all mobile stations operate in multi-user environments, where co-channel interference is unavoidable. The authors of [107] proposed repetition-based cooperative protocols for a multi-user network by allowing each user to collaborate with all other users. However, the full-scale exploitation of this assumption is unrealistic and therefore, it was modified by the authors of [270] to the scenario, where each user can limit his/her attention to a group of partners. Furthermore, Shan *et. al.* [114] proposed a distributed cooperative MAC for multihop wireless networks.

The HARQ protocol is part of the MAC layer. Therefore, investigating the performance of H-ARQ schemes in multi-user environments is vital. Moreover, the actively-cooperative HARQ scheme of Chapter 2 has to be further investigated in order to understand how effective it might remain when there are multiple users simultaneously communicating.

### 6.2.7 Network Coding Aided Cooperative H-ARQ

Recently, network coding [271, 272] has attracted substantial research efforts. The network coding schemes conceived for cooperative communication [112] allow the communication nodes to transmit their own information as well as to forward the other's data simultaneously. Hence. they are attractive for cooperative communications. The analysis of network coded cooperative wireless networks was considered, for example in [273, 274].

A joint network/channel coding scheme was conceived in [275] for multi-user H-ARQ, where network coding was employed for combining the retransmission of the source to multiple users. In this paper, the authors demonstrated that the proposed scheme using iterative network-channel decoding significantly improved the attainable throughput compared to separate decoding, while the per-user complexity was also reduced at the same time. However, this study only focused on the classic direct communication scenario. Hence, a similar approach applied to cooperative wireless communications is worth adopting.

### 6.2.8 Base Station Cooperation Aided H-ARQ

The cooperative networking philosophy is not limited to mobile station cooperation. Recently, base station (BS) cooperation, or multi-cell cooperation, has also attracted intense research efforts [276]. The multi-cell cooperation approach implies that a number of different BSs preprocessed jointly transmit their signals to the MSs. The collaborating BSs may significantly improve the attainable spectral efficiency. Multi-cell cooperation may be arranged, for example using dirty paper coding [276, 277], Tomlinson-Harashima precoding [278], etc. Hence, HARQ aided multi-cell cooperation holds substantial promise.

# Glossary

| | |
|---|---|
| **1G** | First Generation of mobile communuication network |
| **2G** | Second Generation of mobile communuication network |
| **3G** | Third generation |
| **4G** | Fourth Generation of mobile communuication network |
| **ACK** | Acknowledgement |
| **AMPS** | Advanced Mobile Phone System |
| **AMR** | Advanced Multi-Rate |
| **APER** | Accepted Packet Error Ratio |
| **ARQ** | Automatic-Repeat-reQuest, Automatic request for retransmission of corrupted data |
| **AWGN** | Additive White Gaussian Noise |
| **BEC** | Binary Erasure Channel |
| **BEP** | Bit Error Probability |
| **BER** | Bit error ratio, the number of the bits received incorrectly |
| **CC** | Chase Combining |
| **CDMA** | Code Division Multiple Access |
| **CE** | Channel Estimation |
| **CIR** | Channel Impulse Response |
| **CRC** | Cyclic Redundancy Check codes |
| **CSI** | Channel State Information |
| **DL** | Downlink |
| **DLST** | Diagonal Layered Space-Time |
| **DNF** | Denoise-and-Forward |

| | |
|---|---|
| **DPSK** | Differential Phase Shift Keying |
| **DS** | Direct Sequence |
| **DSTBC** | Differential Space Time Block Codes |
| **DSTC** | Distributed Space-Time Coding |
| **EDGE** | Enhanced Data rate for Global Evolution |
| **EGC** | Equal Gain Combining |
| **EI** | Erasure Insertion |
| **Email** | Electronic mail services |
| **EXIT** | EXtrinsic Information Tranfer chart |
| **FEC** | Forward Error Correction |
| **FER** | Frame error rate |
| **FSK** | Frequency Shift Keying |
| **GPRS** | General Packet Radio Service |
| **GSM** | A Pan-European digital mobile radio standard, operating at 900MHz. |
| **H-ARQ** | Hybrid-Automatic-Repeat-reQuest |
| **HLST** | Horizontal Layered Space-Time |
| **HSDPA** | Higher-Speed Downlink Packet Access |
| **HSUPA** | Higher-Speed Uplink Packet Access |
| **IRSD** | Improved Robust Soliton Degree distribution |
| **ISI** | Intersymbol Interference |
| **ITU** | International Telecommunications Union, formerly the CCITT, standardisation group |
| **LDC** | Linear Dispersion Codes |
| **LDPC** | Low Density Parity Check codes |
| **LLR** | Log Likelihood Ratio |
| **LOS** | Light-Of-Sight |
| **LST** | Layered Space Time |
| **LT** | Luby Transform codes |
| **LTE** | Long Term Evolution |

**MGF** Moment Generating Function

**MIMO** Multi-Input Multi-Output

**ML** Maximum Likelihood

**MMSE** Minimum Mean Square Error

**MO-RTT** Maximum Output and Ratio Threshold Test

**MRC** Mixed Radix Conversion

**MS** A common abbreviation for Mobile Station

**MSDD** Multiple-Symbol-Defferential Detection

**MSDSD** Multiple-Symbol-Defferential Sphere Detection

**MSE** Mean Square Error, a criterion used to optimised the coefficients of the equalizer such that the ISI and the noise contained in the received signal is jointly minimised.

**NC** Network Coding

**OFDM** Orthogonal Frequency Division Multiplexing

**OTT** Output Threshold Test

**PDF** Probability Density Function

**PSAM** Pilot symbol assisted modulation, a technique where known symbols (pilots) are transmitted regularly. The effect of channel fading on all symbols can then be estimated by interpolating between the pilots

**PSK** Phase Shift Keying

**RD** Relay-to-Destination link

**ReS** Reed-Solomon codes

**RS** Relay Station

**RSC** Recursive Systematic Convolutional

**RSD** Robust Soliton Degree distribution

**RTT** Ratio Threshold Test

**SC** Selective Combining

**SD** Soft Decision

**SER** Symbol Error Ratio

**SFH** Slow Frequency Hopping

| | |
|---|---|
| **SFH/SS** | Slow Frequency Hopping/Spread Spectrum |
| **SFHMA** | Slow Frequency Hopping Multiple Access |
| **SFSK** | Space-Frequency Shift Keying modulation |
| **SISO** | Soft-Input-Soft-Output |
| **SLT** | Systematic Luby Transform codes |
| **SM** | Spatial Modulation |
| **SMS** | Short Message Services |
| **SP** | Set Partitioning |
| **SR** | Source-to-Relay link |
| **SS** | Source Station |
| **SSDD** | Single-Symbol-Defferential Detection |
| **SSK** | Space Shift Keying modulation |
| **SSR** | Segment Selective Repeat |
| **STBC** | Space-Time Block Coding |
| **STF** | Space-Time-Frequency |
| **STFSK** | Space-Time-Frequency Shift Keying modulation |
| **STSK** | Space-Time Shift Keying modulation |
| **SwC** | Switched Combining |
| **TDD** | Time Division Duplex |
| **TDMA** | Time Division Multiple Access |
| **TLST** | Threaded Layered Space-Time |
| **UL** | Uplink |
| **UMTS** | Universal Mobile Telecommunication System |
| **URC** | Unity Rate Codes |
| **VLST** | Vertical Layered Space-Time |
| **WCDMA** | Wideband CDMA |
| **WiFi** | Wireless Fidelity |
| **WiMAX** | Worldwide Interoperability for Microwave Access |

**WLAN** Wireless Local Area Network

**WMAN** Wireless Metropolitan Area Network

**XOR** The logical operation Exclusive Disjunction

**ZF** Zero Forcing, a criterion used to optimised the coefficients of the equalizer such that the ISI contained in the received signal is totally eliminated.

# Bibliography


[1] H. A. Ngo and L. Hanzo, "Impact of imperfect channel state information on Reed-Solomon coding aided Hybrid-ARQ in Rayleigh fading channels," in *Proceedings of the IEEE International Conference on Communications (ICC'10)*, pp. 1 –5, may 2010.

[2] H. A. Ngo, T. Stevens, R. G. Maunder, and L. Hanzo, "A systematic LT coded arrangement for transmission over correlated shadow fading channels in 802.11 ad-hoc wireless networks," in *Proceedings of the IEEE 71st Vehicular Technology Conference (VTC 2010-Spring)*, pp. 1–5, may 2010.

[3] H. A. Ngo and L. Hanzo, "Amplify-and-forward relaying aided Reed-Solomon coded Hybrid-ARQ relying on realistic channel estimation," in *Proceedings of IEEE Vehicular Technology Conference - Spring 2010 (VTC'10-Spring)*, 2010.

[4] H. A. Ngo, T. D. Nguyen, and L. Hanzo, "HARQ aided systematic LT coding for amplify-forward and decode-forward cooperation," in *Proceedings of the IEEE 72nd Vehicular Technology Conference Fall (VTC 2010-Fall)*, pp. 1 –5, sept. 2010.

[5] H. A. Ngo, C. Xu, S. Sugiura, and L. Hanzo, "Space-time-frequency shift keying for dispersive channels," *IEEE Signal Processing Letters*, vol. 18, no. 3, pp. 177–180, 2011.

[6] H. A. Ngo, T. D. Nguyen, and L. Hanzo, "Amplify-forward and decode-forward cooperation relying on systematic Luby transform coded hybrid automatic-repeat-request," *IET Communications*, vol. 5, pp. 1096 –1106, may 2011.

[7] H. A. Ngo, R. Maunder, and L. Hanzo, "Relay switching aided turbo coded Hybrid-ARQ for correlated fading channel," in *Proceedings of the IEEE Wireless Conference on Networking and Communications (WCNC'11)*, March 2011.

[8] H. A. Ngo, S. Ahmed, L.-L. Yang, and L. Hanzo, "Erasure insertion in Reed-Solomon coded SFH M-ary FSK with partial-band interference and Rayleigh fading for non-coherent cooperative communications," in *Proceedings of the IEEE 74nd Vehicular Technology Conference Fall (VTC 2010-Fall)*, pp. 1–5, July 2011.

[9] "Measuring the information society 2011." International Telecommunication Union (ITU), 2011.

[10] "New data from TeleGeography's GlobalComms Database shows record mobile subscriber growth in Q4 2010." TeleGeography Research, PriMetrica Inc., 15 Mar. 2011. http://www.telegeography.com/cu/article.php?article_id=36470&email=html.

[11] R. Steele and L. Hanzo, *Mobile Radio Communications: Second and Third-generation Cellular and WATM Systems*. John Wiley - IEEE Press, 2nd ed., May 1999.

[12] S. O. Rice, "Mathematical analysis of random noise," *Bell System Technical Journal*, vol. 24, pp. 282–332, 1945.

[13] M. Patzold, *Mobile Fading Channels: Modelling, Analysis and Simulation*. New York, NY, USA: John Wiley & Sons, Inc., 2001.

[14] A. F. Molisch, H. Asplund, R. Heddergott, M. Steinbauer, and T. Zwick, "The COST259 directional channel model-part i: Overview and methodology," *IEEE Transactions on Wireless Communications*, vol. 5, no. 12, pp. 3421–3433, 2006.

[15] H. Asplund, A. A. Glazunov, A. F. Molisch, K. I. Pedersen, and M. Steinbauer, "The COST-259 directional channel model-part ii: Macrocells," *IEEE Transactions on Wireless Communications*, vol. 5, pp. 3434 –3450, december 2006.

[16] "Technical specifications and technical reports for a GERAN-based 3GPP system," 2003. http://www.3gpp.org/ftp/Specs/html-info/41101.htm.

[17] "GSM 02.60 - GPRS Stage-1 Service Description," 1998. http://www.3gpp.org/ftp/Specs/html-info/0260-CRs.htm.

[18] "Digital cellular telecommunications system (Phase 2+): High Speed Circuit Switched Data (HSCSD) - Stage 2 - GSM(03-34)," 1997. http://www.3gpp.org/ftp/Specs/html-info/0334.htm.

[19] L. Hanzo, J. S. Blogh, and S. Ni, *3G, HSPA and FDD versus TDD Networking: Smart Antennas and Adaptive Modulation*. Wiley, 2nd ed., Feb. 2008.

[20] "3GPP Specifications - Series 25: Radio aspects of 3G, including UMTS," 2001. http://www.3gpp.org/ftp/Specs/html-info/25-series.htm.

[21] "Introduction to cdma2000 standards for spread spectrum systems," 2002. http://www.3gpp2.org/public_html/specs/C.S0001-C_v1.0.pdf.

[22] "cdma2000 high rate packet data air interface specification," 2005. http://www.3gpp2.org/Public_html/specs/C.S0024-A_v2.0_050727.pdf.

[23] L. Hanzo, O. Alamri, M. El-Hajjar, and N. Wu, *Near-Capacity Multi-Functional MIMO Systems: Sphere-Packing, Iterative Detection and Cooperation*. John Wiley - IEEE Press, May 2009.

[24] "3GPP Specifications - Series 36: LTE (Evolved UTRA) and LTE-Advanced radio technolgy - Release 8," 2007. http://www.3gpp.org/ftp/Specs/html-info/36-series.htm.

[25] L. Hanzo, Y. Akhtman, M. Jiang, and L. Wang, *MIMO-OFDM for LTE, WIFI and WIMAX: Coherent versus Non-Coherent and Cooperative Turbo-Transceivers*. John Wiley & Sons, 2010.

[26] "Supplement to IEEE standard for information technology telecommunications and information exchange between systems - local andmetropolitan area networks - specific requirements. part 11: wireless LAN medium access control (MAC) and physical layer (PHY) specifications: High-speed physical layer in the 5 ghz band," 1999.

[27] "IEEE standard for information technology - telecommunications and information exchange between systems - local and metropolitan area networks - specific requirements. Part 11: Wireless LAN medium access control (MAC) and physical layer (PHY) specifications," 2007.

[28] "IEEE standard for information technology–telecommunications and information exchange between systems–local and metropolitan area networks–specific requirements Part 11: Wireless LAN medium access control (MAC) and physical layer (PHY) specifications amendment 5: Enhancements for higher throughput," 2009.

[29] "IEEE standard for local and metropolitan area networks. Part 16: Air interface for fixed and mobile broadband wireless access systems," 2005.

[30] T. Ali-Yahiya, *Understanding LTE and Its Performance*. Springer, 2008.

[31] J. M. Wozencraft and M. Horstein, "Coding for two-way channels," tech. rep., Research Laboratory of Electronics, M.I.T, 1961.

[32] J. M. Wozencraft and M. Horstein, "Digitalised communication over two-way channels," in *The Fourth London Symposium of Information Theory*, (London, England), Aug. 29 - Sep. 3 1960.

[33] R. Comroe and D. J. Costello, "ARQ schemes for data transmission in mobile radio systems," *IEEE Journal on Selected Areas in Communications*, vol. 2, pp. 472–481, July 1984.

[34] S. Lin and P. Yu, "A hybrid ARQ scheme with parity retransmission for error control of satellite channels," *IEEE Transactions on Communications*, vol. 30, pp. 1701–1719, Jul 1982.

[35] Y.-M. Wang and S. Lin, "A modified selective-repeat Type-II hybrid ARQ system and its performance analysis," *IEEE Transactions on Communications*, vol. 31, no. 5, pp. 593–608, 1983.

[36] C. Berrou, A. Glavieux, and P. Thitimajshima, "Near shannon limit error-correcting coding and decoding: Turbo-codes.," in *IEEE International Conference on Communications ICC 93. Geneva. Technical Program, Conference Record*, vol. 2, pp. 1064–1070, 23–26 May 1993.

[37] R. G. Gallager, "Low-density parity-check codes," *MA: MIT Press*, 1963.

[38] M. Luby, "LT codes," in *Proceedings of the 43rd Annual IEEE Symposium on Foundations of Computer Science, 2002*, pp. 271–280, 16-19 Nov. 2002.

[39] A. Shokrollahi, "Raptor codes," in *Proceedings of International Symposium on Information Theory (ISIT-2004)*, p. 36, 27 June-2 July 2004.

[40] T. D. Nguyen, L.-L. Yang, and L. Hanzo, "Systematic Luby transform codes and their soft decoding," in *IEEE Workshop on Signal Processing Systems*, pp. 67–72, 17-19 Oct. 2007.

[41] M. Tao and R. S. Cheng, "Differential space-time block codes," in *Proceedings of IEEE Global Telecommunications Conference (GLOBECOM '01)*, vol. 2, pp. 1098–1102, 2001.

[42] H. A. Ngo, S. Ahmed, L.-L. Yang, and L. Hanzo, "Non-coherent cooperative communications dispensing with channel estimation relying on erasure insertion aided Reed-Solomon coded SFH M-ary FSK subjected to partial-band interference and Rayleigh fading," in *IEEE Transactions on Communications*, pp. 1–5, 2012. Submitted.

[43] H. A. Ngo and L. Hanzo, "Area spectral efficiency of soft-decision space-time-frequency shift keying aided slow frequency hopping multiple access," in *IEEE Transactions on Vehicular Technology*, pp. 1–5, 2012. Submitted.

[44] H. A. Ngo, S. Sugiura, and L. Hanzo, "Iterative soft-detection of space-time-frequency shift keying," in *Proceedings of the IEEE International Conference on Communications (ICC'12)*, pp. 1–5, 2012. Submitted.

[45] H. A. Ngo and L. Hanzo, "Area spectral efficiency of soft-decision space-time-frequency shift keying aided slow frequency hopping multiple access," in *Proceedings of the 75th IEEE Vehicular Technology Conference (VTC'12-Spring)*, pp. 1–5, 2012. Submitted.

[46] G. J. Foschini, "Layered space-time architecture for wireless communication in a fading environment when using multi-element antennas," *Bell Laboratories Technical Journal*, vol. 1, pp. 41–59, 1996.

[47] S. M. Alamouti, "A simple transmit diversity technique for wireless communications," *IEEE Journal on Selected Areas in Communications*, vol. 16, no. 8, pp. 1451–1458, 1998.

[48] V. Tarokh, N. Seshadri, and A. R. Calderbank, "Space-time codes for high data rate wireless communication: Performance criterion and code construction," *IEEE Transaction on Information Theory*, vol. 44, pp. 744–765, 1998.

[49] B. Hassibi and B. Hochwald, "High-rate codes that are linear in space and time," *IEEE Transactions on Information Theory*, vol. 48, no. 7, pp. 1804–1824, 2002.

[50] R. Mesleh, H. Haas, C. W. Ahn, and S. Yun, "Spatial modulation - a new low complexity spectral efficiency enhancing technique," in *Proceedings of the First International Conferance on Communications and Networking (ChinaCom '06), China*, pp. 1–5, 2006.

[51] R. Mesleh, H. Haas, C. W. Ahn, and S. Yun, "Spatial modulation," *IEEE Transactions on Vehicular Technology*, vol. 57, no. 4, pp. 2228–2241, 2008.

[52] J. Jeganathan, A. Ghrayeb, L. Szczecinski, and A. Ceron, "Space shift keying modulation for MIMO channels," *IEEE Transactions on Wireless Communications*, vol. 8, no. 7, pp. 3692–3703, 2009.

[53] S. Sugiura, S. Chen, and L. Hanzo, "Coherent and differential space-time shift keying: A dispersion matrix approach," *IEEE Transactions on Communications*, vol. 58, pp. 3219–3230, Nov. 2010.

[54] D. G. Brennan, "Linear diversity combining techniques," *Proceedings of the IRE*, vol. 47, no. 6, pp. 1075–1102, 1959.

[55] A. Wittneben, "Base station modulation diversity for digital simulcast," in *Proceedings of the 41st IEEE Vehicular Technology Conference: Gateway to the Future Technology in Motion, St. Louis, MO, USA*, pp. 848–853, May 1991.

[56] A. Wittneben, "A new bandwidth efficient transmit antenna modulation diversity scheme for linear digital modulation," in *Proceedings of the IEEE International Conference on Communications (ICC'93). Geneva.*, vol. 3, pp. 1630–1634, May 1993.

[57] J. H. Winters, "The diversity gain of transmit diversity in wireless systems with rayleigh fading," in *Proceedings of the IEEE International Conference on Communications (ICC '94), New Orleans, LA, USA*, pp. 1121–1125, May 1994.

[58] P. W. Wolniansky, G. J. Foschini, G. D. Golden, and R. A. Valenzuela, "V-BLAST: an architecture for realizing very high data rates over the rich-scattering wireless channel," in *Proceedings of URSI International Symposyum on Signals, Systems, and Electronics - ISSSE'98*, pp. 295–300, 1998.

[59] V. Tarokh, H. Jafarkhani, and A. R. Calderbank, "Space-time block codes from orthogonal designs," *IEEE Transactions on Information Theory*, vol. 45, no. 5, pp. 1456–1467, 1999.

[60] V. Tarokh, A. Naguib, N. Seshadri, and A. R. Calderbank, "Space-time codes for high data rate wireless communication: performance criteria in the presence of channel estimation errors, mobility, and multiple paths," *IEEE Transactions on Communications*, vol. 47, no. 2, pp. 199–207, 1999.

[61] V. Tarokh, H. Jafarkhani, and A. R. Calderbank, "Space-time block coding for wireless communications: performance results," *IEEE Journal on Selected Areas in Communications*, vol. 17, no. 3, pp. 451–460, 1999.

[62] J.-C. Guey, M. P. Fitz, M. R. Bell, and W.-Y. Kuo, "Signal design for transmitter diversity wireless communication systems over Rayleigh fading channels," *IEEE Transactions on Communications*, vol. 47, no. 4, pp. 527–537, 1999.

[63] B. Hochwald, T. L. Marzetta, and C. B. Papadias, "A transmitter diversity scheme for wideband cdma systems based on space-time spreading," *IEEE Journal on Selected Areas in Communications*, vol. 19, no. 1, pp. 48–60, 2001.

[64] H. Jafarkhani, "A quasi-orthogonal space-time block code," *IEEE Transactions on Communications*, vol. 49, no. 1, pp. 1–4, 2001.

[65] S. Sugiura, S. Chen, and L. Hanzo, "Space-time shift keying: A unified mimo architecture," in *Proceedings of the IEEE Global Telecommunications Conference (GLOBECOM'10), Miami, Florida, USA*, pp. 1–5, 6-10 December 2010.

[66] J. G. Proakis, *Digital communications*. McGraw-Hill, 4th ed., 2001.

[67] M. K. Simon and M.-S. Alouini, *Digital communication over fading channels*. Wiley-IEEE Press, 2nd ed., Nov. 2004.

[68] W. C. Jakes and D. C. Cox, eds., *Microwave Mobile Communications*. Wiley-IEEE Press, 1994.

[69] G. Ganesan and P. Stoica, "Space-time block codes: a maximum snr approach," *IEEE Transactions on Information Theory*, vol. 47, no. 4, pp. 1650–1656, 2001.

[70] H. Wang and X.-G. Xia, "Upper bounds of rates of complex orthogonal space-time block codes," *IEEE Transactions on Information Theory*, vol. 49, no. 10, pp. 2788–2796, 2003.

[71] E. Biglieri, D. Divsalar, M. K. Simon, and P. J. McLane, *"Introduction to Trellis-Coded Modulation with Applications"*. Upper Saddle River, NJ, USA: Prentice-Hall, Inc., 1st ed., 1991.

[72] A. R. J. Hammons and H. El-Gamal, "On the theory of space-time codes for PSK modulation," *IEEE Transactions on Information Theory*, vol. 46, no. 2, pp. 524–542, 2000.

[73] A. Paulraj, R. Nabar, and D. Gore, *Introduction to Space-Time Wireless Communications*. New York, NY, USA: Cambridge University Press, 2003.

[74] G. D. J. Forney, "The viterbi algorithm," *Proceedings of the IEEE*, vol. 61, pp. 268 – 278, march 1973.

[75] H. El-Gamal and A. R. Hammons, "A new approach to layered space-time coding and signal processing," *IEEE Transactions on Information Theory*, vol. 47, no. 6, pp. 2321–2334, 2001.

[76] E. Viterbo and J. Boutros, "A universal lattice code decoder for fading channels," *IEEE Transactions on Information Theory*, vol. 45, no. 5, pp. 1639–1642, 1999.

[77] O. Damen, A. Chkeif, and J. C. Belfiore, "Lattice code decoder for space-time codes," *IEEE Communications Letters*, vol. 4, no. 5, pp. 161–163, 2000.

[78] G. Strang, *Linear Algebra and Its Applications*. Brooks Cole, February 1988.

[79] B. Vucetic and J. Yuan, *Space-Time Coding*. New York, NY, USA: John Wiley & Sons, Inc., 2003.

[80] G. J. Foschini, G. D. Golden, R. A. Valenzuela, and P. W. Wolniansky, "Simplified processing for high spectral efficiency wireless communication employing multi-element arrays," *IEEE Journal on Selected Areas in Communications*, vol. 17, no. 11, pp. 1841–1852, 1999.

[81] B. Hassibi and B. Hochwald, "Linear dispersion codes," in *Proceedings of IEEE International Information Theory Symposium*, 2001.

[82] B. Hassibi and B. Hochwald, "High-rate linear space-time codes," in *Proceedings of IEEE International Conference on Acoustics, Speech, and Signal Processing, 2001 - (ICASSP '01)*, vol. 4, pp. 2461–2464, 7-11 May 2001.

[83] R. W. J. Heath and A. J. Paulraj, "Linear dispersion codes for mimo systems based on frame theory," *IEEE Transactions on Signal Processing*, vol. 50, no. 10, pp. 2429–2441, 2002.

[84] J. Jeganathan, A. Ghrayeb, and L. Szczecinski, "Spatial modulation: optimal detection and performance analysis," *IEEE Communications Letters*, vol. 12, no. 8, pp. 545–547, 2008.

[85] T. L. Marzetta and B. M. Hochwald, "Capacity of a mobile multiple-antenna communication link in Rayleigh flat fading," *IEEE Transactions on Information Theory*, vol. 45, no. 1, pp. 139–157, 1999.

[86] B. M. Hochwald and W. Sweldens, "Differential unitary space-time modulation," *IEEE Transactions on Communications*, vol. 48, no. 12, pp. 2041–2052, 2000.

[87] L. Hanzo, L.-L. Yang, E.-L. Kuan, and K. Yen, *Single and Multi-Carrier DS-CDMA: Multi-User Detection, Space-Time Spreading, Synchronisation, Networking and Standards.* Wiley-IEEE Press, Aug. 2003.

[88] P. Robertson, "Illuminating the structure of code and decoder of parallel concatenated recursive systematic (turbo) codes," in *Proceedings of the IEEE Global Telecommunications Conference (GLOBECOM '94)*, vol. 3, pp. 1298–1303, 1994.

[89] S. ten Brink, "Convergence of iterative decoding," *Electronics Letters*, vol. 35, pp. 806–808, May 1999.

[90] P. Robertson, E. Villebrun, and P. Hoeher, "A comparison of optimal and sub-optimal map decoding algorithms operating in the log domain," in *Proceedings of the IEEE International Conference on Communications (ICC '95), Seattle*, vol. 2, pp. 1009–1013, 1995.

[91] S. ten Brink, "Convergence behavior of iteratively decoded parallel concatenated codes," *IEEE Transactions on Communications*, vol. 49, no. 10, pp. 1727–1737, 2001.

[92] J. Hagenauer, E. Offer, and L. Papke, "Iterative decoding of binary block and convolutional codes," *IEEE Transactions on Information Theory*, vol. 42, no. 2, pp. 429–445, 1996.

[93] T. M. Cover and J. A. Thomas, *Elements of information theory.* New York, NY, USA: Wiley-Interscience, 1991.

[94] X. Li and J. A. Ritcey, "Trellis-coded modulation with bit interleaving and iterative decoding," *IEEE Journal on Selected Areas in Communications*, vol. 17, no. 4, pp. 715–724, 1999.

[95] E. Geraniotis and M. Pursley, "Error probabilities for slow-frequency-hopped spread-spectrum multiple-access communications over fading channels," *IEEE Transactions on Communications*, vol. 30, no. 5, pp. 996–1009, 1982.

[96] D. Verhulst, "Spectrum efficiency analysis of the digital system SFH900," in *Proceedings of the 2nd Nordic Seminar Digital Land Mobile, Stockholm, Sweden*, 14–16, Oct., 1986.

[97] J. L. Dornstetter and D. Verhulst, "Cellular efficiency with slow frequency hopping: Analysis of the digital SFH900 mobile system," *IEEE Journal on Selected Areas in Communications*, vol. 5, no. 5, pp. 835–848, 1987.

[98] L. Hanzo, C. Somerville, and J. Woodard, *Voice and Audio Compression for Wireless Communications*. Wiley-IEEE Press, 2nd ed., Oct. 2007.

[99] European Telecommunications Standards Institute, *Digital cellular telecommunications system (Phase 2+): Channel coding*, 8.5.1 ed., 1999.

[100] International Telecommunication Union - ITU, *Teletraffic Engineering Handbook*, ITU-D SG 2/16 & ITC ed., June 2001.

[101] E. C. van der Meulen, "Three-terminal communication channels," *Advance Applied Probability*, vol. 3, pp. 120–154, 1971.

[102] T. Cover and A. El-Gamal, "Capacity theorems for the relay channel," *IEEE Transactions on Information Theory*, vol. 25, no. 5, pp. 572–584, 1979.

[103] A. Sendonaris, E. Erkip, and B. Aazhang, "Increasing uplink capacity via user cooperation diversity," in *Proceedings of the IEEE International Symposium on Information Theory*, 1998.

[104] J. N. Laneman, D. N. C. Tse, and G. W. Wornell, "An efficient protocol for realizing cooperative diversity in wireless networks," in *Proceedings of the IEEE International Symposium on Information Theory*, 2001.

[105] T. E. Hunter and A. Nosratinia, "Cooperation diversity through coding," in *Proceedings of the IEEE International Information Theory Symposium*, 2002.

[106] M. Dohler, E. Lefranc, and H. Aghvami, "Virtual antenna arrays for future wireless mobile communication systems," in *IEEE ICT 2002*, Beijing, China, June 2002. [CD Rom].

[107] J. N. Laneman and G. W. Wornell, "Distributed space-time-coded protocols for exploiting cooperative diversity in wireless networks," *IEEE Transactions on Information Theory*, vol. 49, no. 10, pp. 2415–2425, 2003.

[108] J. N. Laneman, D. N. C. Tse, and G. W. Wornell, "Cooperative diversity in wireless networks: Efficient protocols and outage behavior," *IEEE Transactions on Information Theory*, vol. 50, no. 12, pp. 3062–3080, 2004.

[109] R. Nabar, H. Bolcskei, and F. Kneubuhler, "Fading relay channels: Performance limit and space-time signal design," *IEEE Journal on Selected Areas in Communications*, vol. 22, pp. 1099–1109, 2004.

[110] H. H. Sneessens and L. Vandendorpe, "Soft decode and forward improves cooperative communications," in *Proceedings of the 6th IEE International Conference on 3G and Beyond*, pp. 1–4, 7-9 Nov. 2005.

[111] T. Bui and J. Yuan, "A decode and forward cooperation scheme with soft relaying in wireless communication," in *Proceedings of the IEEE 8th Workshop Signal Processing Advances in Wireless Communications (SPAWC 2007)*, pp. 1–5, 2007.

[112] L. Xiao, T. Fuja, J. Kliewer, and D. Costello, "A network coding approach to cooperative diversity," *IEEE Transactions on Information Theory*, vol. 53, no. 10, pp. 3714–3722, 2007.

[113] L. Wang, O. Alamri, and L. Hanzo, "K-best sphere detection for the sphere packing modulation aided SDMA/OFDM uplink," in *Proceedings of the IEEE Global Telecommunications Conference (GLOBECOM'08)*, pp. 1–5, Nov. 30 2008-Dec. 4 2008.

[114] H. Shan, W. Zhuang, and Z. Wang, "Distributed cooperative MAC for multihop wireless networks," *IEEE Communications Magazine*, vol. 47, no. 2, pp. 126–133, 2009.

[115] F. Willems and E. van der Meulen, "The discrete memoryless multiple-access channel with cribbing encoders," *IEEE Transactions on Information Theory*, vol. 31, no. 3, pp. 313–327, 1985.

[116] A. Sendonaris, E. Erkip, and B. Aazhang, "User cooperation diversity. Part I. System description," *IEEE Transactions on Communications*, vol. 51, pp. 1927 – 1938, November 2003.

[117] A. Sendonaris, E. Erkip, and B. Aazhang, "User cooperation diversity. Part II. Implementation aspects and performance analysis," *IEEE Transactions on Communications*, vol. 51, pp. 1939–1948, November 2003.

[118] A. Stefanov and E. Erkip, "Cooperative coding for wireless networks," *IEEE Transactions on Communications*, vol. 52, no. 9, pp. 1470–1476, 2004.

[119] K. Azarian, H. El-Gamal, and P. Schniter, "On the achievable diversity-multiplexing tradeoff in half-duplex cooperative channels," *IEEE Transactions on Information Theory*, vol. 51, no. 12, pp. 4152–4172, 2005.

[120] R. Hu and J. Li, "Exploiting Slepian-Wolf codes in wireless user cooperation," in *Proceedings of the IEEE 6th Workshop on Signal Processing Advances in Wireless Communications*, pp. 275–279, 2005.

[121] T. E. Hunter and A. Nosratinia, "Diversity through coded cooperation," *IEEE Transactions on Wireless Communications*, vol. 5, no. 2, pp. 283–289, 2006.

[122] T. E. Hunter, S. Sanayei, and A. Nosratinia, "Outage analysis of coded cooperation," *IEEE Transactions on Information Theory*, vol. 52, no. 2, pp. 375–391, 2006.

[123] R. Hu and J. Ti, "Practical compress-forward in user cooperation: Wyner-Ziv cooperation," in *Proceedings of the IEEE International Information Theory Symposium*, pp. 489–493, 2006.

[124] M. N. Khormuji and E. G. Larsson, "Improving collaborative transmit diversity by using constellation rearrangement," in *Proceedings of the IEEE Wireless Communications and Networking Conference (WCNC 2007)*, pp. 803–807, 2007.

[125] X. Bao and J. Li, "Efficient message relaying for wireless user cooperation: Decode-Amplify-Forward (DAF) and hybrid DAF and coded-cooperation," *IEEE Transactions on Wireless Communications*, vol. 6, no. 11, pp. 3975–3984, 2007.

[126] Y. Fan, C. Wang, J. Thompson, and H. V. Poor, "Recovering multiplexing loss through successive relaying using repetition coding," *IEEE Transactions on Wireless Communications*, vol. 6, pp. 4484–4493, Dec. 2007.

[127] G. Yue, X. Wang, Z. Yang, and A. Host-Madsen, "Coding schemes for user cooperation in low-power regimes," *IEEE Transactions on Signal Processing*, vol. 56, no. 5, pp. 2035–2049, 2008.

[128] H. Ochiai, P. Mitran, and V. Tarokh, "Design and analysis of collaborative diversity protocols for wireless sensor networks," in *Proceedings of IEEE 60th Vehicular Technology Conference, 2004. VTC2004-Fall*, vol. 7, pp. 4645–4649, 26-29 Sept. 2004.

[129] L. Wang, L. Kong, S. X. Ng, and L. Hanzo, "To cooperate or not: A capacity perspective," in *Proceedings of IEEE 71st Vehicular Technology Conference (VTC 2010-Spring)*, pp. 1–5, 2010.

[130] K. J. R. Liu, A. K. Sadek, W. Su, and A. Kwasinski, *Cooperative Communications and Networking*. New York, NY, USA: Cambridge University Press, 2009.

[131] Y. Li and B. Vucetic, "On the performance of a simple adaptive relaying protocol for wireless relay networks," in *Proceedings of IEEE Vehicular Technology Conference VTC-Spring 2008*, pp. 2400–2405, 2008.

[132] B. Rankov and A. Wittneben, "Spectral efficient protocols for half-duplex fading relay channels," *IEEE Journal on Selected Areas in Communications*, vol. 25, no. 2, pp. 379–389, 2007.

[133] Y. Wu, P. A. Chou, and S.-Y. Kung, "Information exchange in wireless networks with network coding and physical-layer broadcast," in *Proceedings of 39th Annual Conference on Information Science and Systems*, [CD-ROM], Mar. 2005.

[134] P. Larsson, N. Johansson, and K. E. Sunell, "Coded bi-directional relaying," in *Proceedings of IEEE 63rd Vehicular Technology Conference (VTC 2006-Spring)*, vol. 2, pp. 851–855, 2006.

[135] S. J. Kim, P. Mitran, and V. Tarokh, "Performance bounds for bi-directional coded cooperation protocols," in *Proceedings of the 27th International Conference on Distributed Computing Systems Workshops (ICDCSW '07)*, 2007.

[136] Y. Jing and B. Hassibi, "Distributed space-time coding in wireless relay networks," *IEEE Transactions on Wireless Communications*, vol. 5, no. 12, pp. 3524–3536, 2006.

[137] T. Kiran and B. S. Rajan, "Distributed space-time codes with reduced decoding complexity," in *Proceedings of IEEE International Symposium on Information Theory*, pp. 542–546, 2006.

[138] Y. Jing and H. Jafarkhani, "Using orthogonal and quasi-orthogonal designs in wireless relay networks," *IEEE Transactions on Information Theory*, vol. 53, no. 11, pp. 4106–4118, 2007.

[139] S. Yiu, R. Schober, and L. Lampe, "Distributed space-time block coding," *IEEE Transactions on Communications*, vol. 54, no. 7, pp. 1195–1206, 2006.

[140] B. Zhao and M. Valenti, "Practical relay networks: A generalization of hybrid-ARQ," *IEEE Journal on Selected Areas in Communications*, vol. 23, pp. 7–18, 2005.

[141] S. Tomasin, M. Levorato, and M. Zorzi, "Analysis of outage probability for cooperative networks with HARQ," in *Proceedings of the IEEE International Symposium on Information Theory (ISIT 2007)*, pp. 2716–2720, 2007.

[142] C. Hasan and U. Aygolu, "An incremental relaying approach for superposition modulated cooperative transmission," in *Proceedings of the IEEE Wireless Communications and Networking Conferance (WCNC'09)*, pp. 1–6, 2009.

[143] I. Stanojev, O. Simeone, Y. Bar-Ness, and D. H. Kim, "Energy efficiency of non-collaborative and collaborative Hybrid-ARQ protocols," *IEEE Transactions on Wireless Communications*, vol. 8, no. 1, pp. 326–335, 2009.

[144] R. Zhang and L. Hanzo, "A unified treatment of superposition coding aided communications: Theory and practice," *IEEE Communications Surveys & Tutorials*, no. 99, pp. 1–18, 2010. Early Access.

[145] J. S. Harsini, F. Lahouti, M. Levorato, and M. Zorzi, "Analysis of non-cooperative and cooperative Type II Hybrid ARQ protocols with AMC over correlated fading channels," *IEEE Transactions on Wireless Communications*, vol. 10, no. 3, pp. 877–889, 2011.

[146] J. K. Cavers, "An analysis of pilot symbol assisted modulation for Rayleigh fading channels," *IEEE Transactions on Vehicular Technology*, vol. 40, no. 4, pp. 686–693, 1991.

[147] Y. H. Nam, K. Azarian, H. El-Gamal, and P. Schniter, "Cooperation through ARQ," in *Proceedings of the IEEE 6th Workshop on Signal Processing Advances in Wireless Communications*, pp. 1023–1027, 2005.

[148] M. Dianati, X. Ling, K. Naik, and X. Shen, "A node-cooperative ARQ scheme for wireless ad hoc networks," *IEEE Transactions on Vehicular Technology*, vol. 55, no. 3, pp. 1032–1044, 2006.

[149] G. Yu, Z. Zhang, and P. Qiu, "Cooperative ARQ in wireless networks: Protocols description and performance analysis," in *Proceedings of the IEEE International Confernence on Communications (ICC '06)*, vol. 8, pp. 3608–3614, 2006.

[150] I. Krikidis, "Distributed truncated ARQ protocol for cooperative diversity networks," *IET Communications*, vol. 1, no. 6, pp. 1212–1217, 2007.

[151] V. Mahinthan, H. Rutagemwa, J. W. Mark, and X. Shen, "Performance of adaptive relaying schemes in cooperative diversity systems with arq," in *Proceedings of the IEEE Global Telecommunications Conference (GLOBECOM '07)*, pp. 4402–4406, 2007.

[152] K. Azarian, H. El-Gamal, and P. Schniter, "On the optimality of the ARQ-DDF protocol," *IEEE Transactions on Information Theory*, vol. 54, no. 4, pp. 1718–1724, 2008.

[153] L. Le and E. Hossain, "An analytical model for arq cooperative diversity in multi-hop wireless networks," *IEEE Transactions on Wireless Communications*, vol. 7, no. 5, pp. 1786–1791, 2008.

[154] L. Weng and R. D. Murch, "Achievable diversity-multiplexing-delay tradeoff for ARQ cooperative broadcast channels," *IEEE Transactions on Wireless Communications*, vol. 7, no. 5, pp. 1828–1832, 2008.

[155] V. Mahinthan, h. Rutagemwa, J. W. Mark, and X. Shen, "Cross-layer performance study of cooperative diversity system with ARQ," *IEEE Transactions on Vehicular Technology*, vol. 58, no. 2, pp. 705–719, 2009.

[156] J. J. Alcaraz and J. Garcia-Haro, "Performance of single-relay cooperative ARQ retransmission strategies," *IEEE Communications Letters*, vol. 13, no. 2, pp. 121–123, 2009.

[157] W. Choi, D. I. Kim, and B.-H. Kim, "Adaptive multi-node incremental relaying for hybrid-ARQ in AF relay networks," *IEEE Transactions on Wireless Communications*, vol. 9, no. 2, pp. 505–511, 2010.

[158] R. Narasimhan, "Hybrid-ARQ interference channels with receiver cooperation," in *Proceedings of the IEEE International Conference on Communications (ICC'10)*, pp. 1–5, 2010.

[159] C. S. Patel and G. L. Stuber, "Channel estimation for amplify and forward relay based cooperation diversity systems," *IEEE Transactions on Wireless Communications*, vol. 6, pp. 2348–2356, June 2007.

[160] C. C. Tan and N. C. Beaulieu, "Infinite series representations of the bivariate Rayleigh and Nakagami-m distributions," *IEEE Transactions on Communications*, vol. 45, pp. 1159 –1161, oct 1997.

[161] S. B. Wicker, *Error Control Systems for Digital Communication and Storage*. Prentice Hall, Oct 1994.

[162] D. Chase, "Code combining: A maximum-likelihood decoding approach for combining an arbitrary number of noisy packets," *IEEE Transactions on Communications*, vol. 33, pp. 385 – 393, may 1985.

[163] L. Cao and T. Shi, "Turbo codes based hybrid ARQ with segment selective repeat," *Electronics Letters*, vol. 40, pp. 1140 – 1141, sept. 2004.

[164] P. Frenger, S. Parkvall, and E. Dahlman, "Performance comparison of HARQ with Chase combining and incremental redundancy for HSDPA," in *Proceedings of the 54th IEEE Vehicular Technology Conference (VTC'01-Fall)*, vol. 3, pp. 1829 –1833, 2001.

[165] L. Hanzo, T. Liew, B. Yeap, R. Tee, and S. X. Ng, *Turbo Coding, Turbo Equalisation and Space-Time Coding: EXIT-Chart Aided Near-Capacity Designs for Wireless Channels*. John Wiley & Sons, 2nd ed., 2010.

[166] J. Castura and Y. Mao, "Rateless coding over fading channels," *IEEE Communications Letters*, vol. 10, no. 1, pp. 46–48, 2006.

[167] J. Castura and Y. Mao, "A rateless coding and modulation scheme for unknown Gaussian channels," in *Proceedings of the 10th Canadian Workshop on Information Theory*, pp. 148–151, 6-8 June 2007.

[168] J. Castura and Y. Mao, "Rateless coding for wireless relay channels," *IEEE Transactions on Wireless Communications*, vol. 6, no. 5, pp. 1638–1642, 2007.

[169] S. Puducheri, J. Kliewer, and T. E. Fuja, "The design and performance of distributed LT codes," *IEEE Transactions on Information Theory*, vol. 53, no. 10, pp. 3740–3754, 2007.

[170] D. J. C. MacKay, "Fountain codes," *IEE Proceedings-Communications*, vol. 152, pp. 1062–1068, 9 Dec. 2005.

[171] R. Palanki and J. S. Yedidia, "Rateless codes on noisy channels," in *Proceedings of International Symposium on Information Theory, ISIT 2004*, 2004.

[172] O. Etesami and A. Shokrollahi, "Raptor codes on binary memoryless symmetric channels," *IEEE Transactions on Information Theory*, vol. 52, no. 5, pp. 2033–2051, 2006.

[173] R. Nikjah and N. C. Beaulieu, "Achievable rates and fairness in rateless coded decode-and-forward half-duplex and full-duplex opportunistic relaying," in *Proceedings of the IEEE International Conference on Communications (ICC'08)*, pp. 3701–3707, 19-23 May 2008.

[174] R. Nikjah and N. C. Beaulieu, "Novel rateless coded selection cooperation in dual-hop relaying systems," in *Global Telecommunications Conference, 2008. IEEE GLOBECOM 2008. IEEE*, pp. 1–6, Nov. 30 2008-Dec. 4 2008.

[175] A. Shokrollahi, "Raptor codes," *IEEE Transactions on Information Theory*, vol. 52, no. 6, pp. 2551–2567, 2006.

[176] X. Yuan and L. Ping, "On systematic LT codes," *IEEE Communications Letters*, vol. 12, no. 9, pp. 681–683, 2008.

[177] N. Bonello, R. Zhang, S. Chen, and L. Hanzo, "Reconfigurable rateless codes," *IEEE Transactions on Wireless Communications*, vol. 8, no. 11, pp. 5592–5600, 2009.

[178] N. Bonello, S. Chen, and L. Hanzo, "Low-density parity-check codes and their rateless relatives," *IEEE Communications Surveys and Tutorials*, vol. 13, no. 1, pp. 3–26, 2011.

[179] Z. Cheng, J. Castura, and Y. Mao, "On the design of Raptor codes for binary-input gaussian channels," *IEEE Transactions on Communications*, vol. 57, no. 11, pp. 3269–3277, 2009.

[180] C. Gong, G. Yue, and X. Wang, "Analysis and optimization of a rateless coded joint relay system," *IEEE Transactions on Wireless Communications*, vol. 9, no. 3, pp. 1175–1185, 2010.

[181] Y. Fan, L. Lai, E. Erkip, and H. V. Poor, "Rateless coding for MIMO fading channels: performance limits and code construction," *IEEE Transactions on Wireless Communications*, vol. 9, no. 4, pp. 1288–1292, 2010.

[182] R. Y. S. Tee, T. D. Nguyen, S. X. Ng, L.-L. Yang, and L. Hanzo, "Luby transform coding aided bit-interleaved coded modulation for the wireless Internet," in *Proceedings of the 6th IEEE Vehicular Technology Conference (VTC'07-Fall)*, pp. 2025–2029, Sept. 30 2007-Oct. 3 2007.

[183] R. Y. S. Tee, T. D. Nguyen, L.-L. Yang, and L. Hanzo, "Serially concatenated Luby transform coding and bit-interleaved coded modulation using iteratlive decoding for the wireless Internet," in *Proceedings of IEEE 63rd Vehicular Technology Conference, VTC 2006-Spring*, vol. 1, pp. 22–26, 7–10 May 2006.

[184] T. D. Nguyen, L.-L. Yang, S. X. Ng, and L. Hanzo, "An optimal degree distribution design and a conditional random integer generator for the systematic Luby transform coded wireless Internet," in *IEEE Wireless Communications and Networking Conference (WCNC'08)*, pp. 243–248, March 31- April 3 2008.

[185] G. Ungerboeck, "Channel coding with multilevel/phase signals," *IEEE Transactions on Information Theory*, vol. 28, pp. 55 – 67, jan 1982.

[186] S. Lin and D. J. Costello, *Error Control Coding.* Prentice Hall, 2nd ed., 2004.

[187] J. Hagenauer, "Rate-compatible punctured convolutional codes (RCPC codes) and their applications," *IEEE Transactions on Communications*, vol. 36, no. 4, pp. 389–400, 1988.

[188] W. C. Y. Lee, "Estimate of channel capacity in Rayleigh fading environment," *IEEE Transactions on Vehicular Technology*, vol. 39, no. 3, pp. 187–189, 1990.

[189] L. Kong, S. X. Ng, R. G. Maunder, and L. Hanzo, "Maximum-throughput irregular distributed space-time code for near-capacity cooperative communications," *IEEE Transactions on Vehicular Technology*, vol. 59, no. 3, pp. 1511–1517, 2010.

[190] L. Hanzo, M. Mnster, B. J. Choi, and T. Keller, *OFDM and MC-CDMA for Broadcasting Multi-User Communications, WLANs and Broadcasting.* Wiley-IEEE Press, 2003.

[191] P. Schramm and R. R. Muller, "Pilot symbol assisted BPSK on Rayleigh fading channels with diversity: performance analysis and parameter optimization," *IEEE Transactions on Communications*, vol. 46, no. 12, pp. 1560–1563, 1998.

[192] X. Tang, M. A. Alouini, and A. J. Goldsmith, "Effect of channel estimation error on M-QAM BER performance in Rayleigh fading," *IEEE Transactions on Communications*, vol. 47, no. 12, pp. 1856–1864, 1999.

[193] W.-Y. Kuo, "Analytic forward link performance of pilot-aided coherent DS-CDMA under correlated Rician fading," *IEEE Journal on Selected Areas in Communications*, vol. 18, no. 7, pp. 1159–1168, 2000.

[194] H. Sheng and A. M. Haimovich, "Impact of channel estimation on ultra-wideband system design," *IEEE Journal of Selected Topics in Signal Processing*, vol. 1, no. 3, pp. 498–507, 2007.

[195] P. Frenger, "Turbo decoding for wireless systems with imperfect channel estimates," *IEEE Transactions on Communications*, vol. 48, no. 9, pp. 1437–1440, 2000.

[196] D. Gu and C. Leung, "Performance analysis of transmit diversity scheme with imperfect channel estimation," *Electronics Letters*, vol. 39, no. 4, pp. 402–403, 2003.

[197] L. Cao, P. Y. Kam, and M. Tao, "Impact of imperfect channel state information on ARQ schemes over Rayleigh fading channels," in *Proceedings of IEEE International Conference on Communications (ICC '09)*, pp. 1–5, 14–18 June 2009.

[198] L. Cao and P.-Y. Kam, "On the performance of packet ARQ schemes in Rayleigh fading: The role of receiver channel state information and its accuracy," *IEEE Transactions on Vehicular Technology*, vol. 60, no. 2, pp. 704–709, 2011.

[199] M. M. Wang, W. Xiao, and T. Brown, "Soft decision metric generation for QAM with channel estimation error," *IEEE Transactions on Communications*, vol. 50, no. 7, pp. 1058–1061, 2002.

[200] L. Cao and N. C. Beaulieu, "Exact error-rate analysis of diversity 16-QAM with channel estimation error," *IEEE Transactions on Communications*, vol. 52, no. 6, pp. 1019–1029, 2004.

[201] X. Cai and G. B. Giannakis, "Adaptive PSAM accounting for channel estimation and prediction errors," *IEEE Transactions on Wireless Communications*, vol. 4, no. 1, pp. 246–256, 2005.

[202] P. Tan and N. C. Beaulieu, "Bit error probability analysis of OFDM systems in the presence of channel estimation error over Rayleigh and Ricean fading channels," in *Proceedings of IEEE International Conference on Communications (ICC '06)*, vol. 11, pp. 5172–5179, 2006.

[203] P. Tan and N. C. Beaulieu, "Effect of channel estimation error on bit error probability in OFDM systems over Rayleigh and Ricean fading channels," *IEEE Transactions on Communications*, vol. 56, no. 4, pp. 675–685, 2008.

[204] Y.-H. You, H.-K. Jung, W.-G. Jeon, and H.-R. Cho, "Impact of imperfect channel estimation in OFDM-based spatial multiplexing systems," *Electronics Letters*, vol. 38, no. 24, pp. 1589–1591, 2002.

[205] G. Taricco and E. Biglieri, "Space-time decoding with imperfect channel estimation," in *Proceeding of the 3rd IEEE International Symposium on Signal Processing and Information Technology*, pp. 302–305, 2003.

[206] G. Taricco and E. Biglieri, "Decoding space-time codes with imperfect channel estimation," in *Proceedings of the IEEE International Conference on Communications*, vol. 5, pp. 2741–2745, 2004.

[207] G. Taricco and E. Biglieri, "Space-time decoding with imperfect channel estimation," *IEEE Transactions on Wireless Communications*, vol. 4, no. 4, pp. 1874–1888, 2005.

[208] Z. Ni, J. Wang, and D. Li, "Performance of space-time transmit diversity with imperfect channel estimation over correlated Nakagami fading channels," in *Proceedings of IEEE Global Telecommunications Conference (GLOBECOM '03)*, vol. 1, pp. 312–316, 2003.

[209] X. Wang and J. Wang, "Effect of imperfect channel estimation on transmit diversity in CDMA systems," *IEEE Transactions on Vehicular Technology*, vol. 53, no. 5, pp. 1400–1412, 2004.

[210] L. L. Chong and L. B. Milstein, "The effects of channel-estimation errors on a space-time spreading CDMA system with dual transmit and dual receive diversity," *IEEE Transactions on Communications*, vol. 52, no. 7, pp. 1145–1151, 2004.

[211] E. Baccarelli and M. Biagi, "Performance and optimized design of space-time codes for MIMO wireless systems with imperfect channel estimates," *IEEE Transactions on Signal Processing*, vol. 52, no. 10, pp. 2911–2923, 2004.

[212] L. Xiao and X. Dong, "Error performance of selection combining and switched combining systems in Rayleigh fading channels with imperfect channel estimation," *IEEE Transactions on Vehicular Technology*, vol. 54, no. 6, pp. 2054–2065, 2005.

[213] Y. Li and P. Y. Kam, "Space-time trellis codes over rapid Rayleigh fading channels with channel estimation—part i: Receiver design and performance analysis," *IEEE Transactions on Communications*, vol. 55, no. 8, pp. 1640–1644, 2007.

[214] Y. Li and P. Y. Kam, "Space-time trellis codes over rapid Rayleigh fading channels with channel estimation-part ii: performance analysis and code design for non-identical channels," *IEEE Transactions on Communications*, vol. 57, no. 2, pp. 343–347, 2009.

[215] H. K. Bizaki and A. Falahati, "Tomlinson-Harashima precoding with imperfect channel state information," *IET Communications*, vol. 2, no. 1, pp. 151–158, 2008.

[216] P. Amihood, E. Masry, L. B. Milstein, and J. G. Proakis, "The effects of channel estimation errors on a nonlinear precoder for multiple antenna downlink channels," *IEEE Transactions on Communications*, vol. 57, no. 11, pp. 3307–3315, 2009.

[217] M. Teimouri, N. Rezaee, and A. Hedayat, "Concatenated coded modulation techniques and orthogonal space-time block codes in the presence of fading channel estimation errors," *IET Communications*, vol. 4, no. 2, pp. 135–143, 2010.

[218] B. Gedik and M. Uysal, "Impact of imperfect channel estimation on the performance of amplify-and-forward relaying," *IEEE Transactions on Wireless Communications*, vol. 8, pp. 1468–1479, March 2009.

[219] L. Hanzo, C. H. Wong, and M. S. Yee, *Adaptive Wireless Transceivers: Turbo-Coded, Space-Time Coded TDMA, CDMA and OFDM Systems*. Wiley-IEEE Press, 2002.

[220] Y. Wu and M. Patzold, "Performance analysis of cooperative communication systems with imperfect channel estimation," in *Proceedings of IEEE International Conference on Communications (ICC '09)*, pp. 1–6, 2009.

[221] H. Muhaidat, M. Uysal, and R. Adve, "Pilot-symbol-assisted detection scheme for distributed orthogonal space-time block coding," *IEEE Transactions on Wireless Communications*, vol. 8, no. 3, pp. 1057–1061, 2009.

[222] S. Han, S. Ahn, E. Oh, and D. Hong, "Effect of channel-estimation error on BER performance in cooperative transmission," *IEEE Transactions on Vehicular Technology*, vol. 58, no. 4, pp. 2083–2088, 2009.

[223] S. Ikki, S. I. Al-Dharrab, and M. Uysal, "Exact closed-form error probability expression for cooperative diversity networks with channel estimation errors in time selective Rayleigh fading channels," in *Proceedings of IEEE International Conference on Communications (ICC'10), Cape Town, South Africa*, pp. 1–5, 2010.

[224] S. Ikki, A. Al-Dharrab, and M. Uysal, "Error probability of DF relaying with pilot-assisted channel estimation over time-varying fading channels," *IEEE Transactions on Vehicular Technology*, no. 99, 2011. Early Access.

[225] X. J. Zhang and Y. Gong, "On the diversity gain in dynamic decode-and-forward channels with imperfect CSIT," *IEEE Transactions on Communications*, vol. 59, no. 1, pp. 59–63, 2011.

[226] N. S. Ferdinand and N. Rajatheva, "Performance analysis of imperfect channel estimation in MIMO two hop fixed gain relay network with beamforming," *IEEE Communications Letters*, vol. 15, no. 2, pp. 208–210, 2011.

[227] S. Haykin, *Adaptive Filter Theory*. Prentice Hall, 4th ed., 2002.

[228] P. Y. Kam, "Optimal detection of digital data over the nonselective rayleigh fading channel with diversity reception," *IEEE Transactions on Communications*, vol. 39, pp. 214–219, Feb. 1991.

[229] Y. Zhu, P.-Y. Kam, and Y. Xin, "A decision-feedback channel estimation receiver for independent nonidentical Rayleigh fading channels," in *Proceedings of the IEEE Vehicular Technology Conference (VTC'08-Spring)*, pp. 376–379, may, 11–14 2008.

[230] L. Hanzo, S. X. Ng, T. Keller, and T. Webb, *Quadrature Amplitue Modulation: From Basics to Adaptive Trellis-Coded, Turbo-Equalized and Space-time Coded OFDM. CDMA and MC-CDMA Systems*. Wiley, 3 ed., Sept. 2004.

[231] J. Baltersee, G. Fock, and H. Meyr, "An information theoretic foundation of synchronized detection," *IEEE Transactions on Communications*, vol. 49, pp. 2115–2123, Dec. 2001.

[232] P. Tarasak, H. Minn, and V. K. Bhargava, "Differential modulation for two-user cooperative diversity systems," *IEEE Journal on Selected Areas in Communications*, vol. 23, no. 9, pp. 1891–1900, 2005.

[233] S. Yiu, R. Schober, and L. Lampe, "Differential distributed space-time block coding," in *Proceedings of IEEE Pacific Rim Conference on Communications, Computers and Signal Processing (PACRIM'05)*, pp. 53–56, 2005.

[234] Y. Jing and H. Jafarkhani, "Distributed differential space-time coding for wireless relay networks," *IEEE Transactions on Communications*, vol. 56, no. 7, pp. 1092–1100, 2008.

[235] Y. Jing and B. Hassibi, "Design of fully diverse multiple-antenna codes based on Sp(2)," *IEEE Transactions on Information Theory*, vol. 50, no. 11, pp. 2639–2656, 2004.

[236] D. Divsalar and M. K. Simon, "Multiple-symbol differential detection of MPSK," *IEEE Transactions on Communications*, vol. 38, pp. 300–308, March 1990.

[237] G. Farhadi and N. C. Beaulieu, "A low complexity receiver for noncoherent amplify-and-forward cooperative systems," *IEEE Transactions on Communications*, vol. 58, no. 9, pp. 2499–2504, 2010.

[238] T. Himsoon, W. Su, and K. J. R. Liu, "Differential transmission for amplify-and-forward cooperative communications," *IEEE Signal Processing Letters*, vol. 12, no. 9, pp. 597–600, 2005.

[239] R. Annavajjala, P. C. Cosman, and L. B. Milstein, "On the performance of optimum noncoherent amplify-and-forward reception for cooperative diversity," in *Proceedings of IEEE Military Communications Conference (MILCOM'05)*, pp. 3280–3288, 2005.

[240] G. Wang, Y. Zhang, and M. Amin, "Differential distributed space-time modulation for cooperative networks," *IEEE Transactions on Wireless Communications*, vol. 5, no. 11, pp. 3097–3108, 2006.

[241] F. Oggier and E. Lequeu, "Differential distributed Cayley space-time codes," *IEEE Transactions on Wireless Communications*, vol. 8, no. 7, pp. 3808–3814, 2009.

[242] P. Ho and D. Fung, "Error performance of multiple-symbol differential detection of PSK signals transmitted over correlated Rayleigh fading channels," *IEEE Transactions on Communications*, vol. 40, no. 10, pp. 1566–1569, 1992.

[243] D. Dereniowski and M. Kubale, "Cholesky factorization of matrices in parallel and ranking of graphs," in *Parallel Processing and Applied Mathematics* (R. Wyrzykowski, J. Dongarra, M. Paprzycki, and J. Wasniewski, eds.), vol. 3019, pp. 985–992, Springer - Berlin, Heidelberg, 2004.

[244] E. Agrell, T. Eriksson, A. Vardy, E. Vardy, and K. Zeger, "Closest point search in lattices," *IEEE Transaction on Information Theory*, vol. 48, pp. 2201–2214, 2002.

[245] Z. B. Krusevac, P. B. Rapajic, and R. A. Kennedy, "Mutual information performance of differential M-PSK detection over time-varying channels," in *Proceedings of IEEE International Symposium on Information Theory (ISIT)*, pp. 2752–2756, 2008.

[246] W. Stark, "Coding for frequency-hopped spread-spectrum communication with partial-band interference–part i: Capacity and cutoff rate," *IEEE Transactions on Communications*, vol. 33, no. 10, pp. 1036–1044, 1985.

[247] W. Stark, "Coding for frequency-hopped spread-spectrum communication with partial-band interference–part ii: Coded performance," *IEEE Transactions on Communications*, vol. 33, no. 10, pp. 1045–1057, 1985.

[248] M. Pursley and W. Stark, "Performance of Reed-Solomon coded frequency-hop spread-spectrum communications in partial-band interference," *IEEE Transactions on Communications*, vol. 33, no. 8, pp. 767–774, 1985.

[249] S. W. Kim and W. Stark, "Optimum rate Reed-Solomon codes for frequency-hopped spread-spectrum multiple-access communication systems," *IEEE Transactions on Communications*, vol. 37, no. 2, pp. 138–144, 1989.

[250] A. J. Viterbi, "A robust ratio-threshold technique to mitigate tone and partial band jamming in coded MFSK systems," in *IEEE Military Communications Conference - Progress in Spread Spectrum Communications, 1982. MILCOM 1982.*, vol. 1, pp. 22.4–1 –22.4–5, 17-20 1982.

[251] L.-L. Yang and L. Hanzo, "Low complexity erasure insertion in RS-coded SFH spread-spectrum communications with partial-band interference and Nakagami-m fading," *IEEE Transactions on Communications*, vol. 50, pp. 914 –925, June 2002.

[252] L. liang Yang and L. Hanzo, "Performance analysis of coded m-ary orthogonal signaling using errors-and-erasures decoding over frequency-selective fading channels," *IEEE Journal on Selected Areas in Communications*, vol. 19, pp. 211–221, 2001.

[253] S. Ahmed, L.-L. Yang, and L. Hanzo, "Erasure insertion in RS-Coded SFH MFSK subjected to tone jamming and Rayleigh fading," *IEEE Transactions on Vehicular Technology*, vol. 56, pp. 3563 –3571, Nov. 2007.

[254] C. W. Baum and M. Pursley, "Bayesian methods for erasure insertion in frequency-hop communication systems with partial-band interference," *IEEE Transactions on Communications*, vol. 40, pp. 1231 –1238, July 1992.

[255] P. Hahn, "Theoretical diversity improvement in multiple frequency shift keying," *IRE Transactions on Communications Systems*, vol. 10, pp. 177 –184, June 1962.

[256] L.-L. Yang, K. Yen, and L. Hanzo, "A Reed-Solomon coded DS-CDMA system using noncoherent M-ary orthogonal modulation over multipath fading channels," *IEEE Journal on Selected Areas in Communications*, vol. 18, pp. 2240 –2251, Nov. 2000.

[257] S. B. Wicker, "Reed-Solomon error control coding for Rayleigh fading channels with feedback," *IEEE Transactions on Vehicular Technology*, vol. 41, pp. 124–133, May 1992.

[258] L. Lampe, R. Schober, V. Pauli, and C. Windpassinger, "Multiple-symbol differential sphere decoding," in *Proceedings of IEEE International Conference on Communications (ICC'04)*, vol. 2, pp. 787–791, 2004.

[259] L. Lampe, R. Schober, V. Pauli, and C. Windpassinger, "Multiple-symbol differential sphere decoding," *IEEE Transactions on Communications*, vol. 53, no. 12, pp. 1981–1985, 2005.

[260] I. S. Gradshteyn, A. Jeffrey, and I. M. Ryzhik, *Table of integrals, series, and products*. New York, NY: Academic Press, 7th ed., 2007.

[261] G. Leus, W. Zhao, G. B. Giannakis, and H. Delic, "Space-time frequency-shift keying," *IEEE Transactions on Communications*, vol. 52, pp. 346 – 349, march 2004.

[262] S. X. Ng and L. Hanzo, "On the MIMO channel capacity of multi-dimensional signal sets," *IEEE Transactions on Vehicular Technology*, vol. 55, pp. 528–536, March 2006.

[263] M. Jiang and L. Hanzo, "Unitary linear dispersion code design and optimization for MIMO communication systems," *IEEE Signal Processing Letters*, vol. 17, no. 5, pp. 497–500, 2010.

[264] D. Liang, S. X. Ng, and L. Hanzo, "Soft-decision star-QAM aided BICM-ID," *IEEE Signal Processing Letters*, vol. 18, pp. 169–172, January 2011.

[265] N. Bonello, S. Chen, and L. Hanzo, "Pilot symbol assisted coding," *Electronics Letters*, vol. 45, no. 10, pp. 518–519, 2009.

[266] A. Tanenbaum, *Computer Networks*. Prentice Hall Professional Technical Reference, 4th ed., 2002.

[267] V. Kawadia and P. R. Kumar, "A cautionary perspective on cross-layer design," *IEEE Wireless Communications Magazine*, vol. 12, pp. 3 – 11, feb. 2005.

[268] M. van Der Schaar and N. S. Shankar, "Cross-layer wireless multimedia transmission: challenges, principles, and new paradigms," *IEEE Wireless Communications Magazine*, vol. 12, pp. 50 – 58, aug. 2005.

[269] X. Lin, N. B. Shroff, and R. Srikant, "A tutorial on cross-layer optimization in wireless networks," *IEEE Journal on Selected Areas in Communications*, vol. 24, pp. 1452 –1463, aug. 2006.

[270] T. E. Hunter and A. Nosratinia, "Distributed protocols for user cooperation in multi-user wireless networks," in *Proceedings of IEEE Global Telecommunications Conference, GLOBECOM'04*, vol. 6, pp. 3788–3792, 2004.

[271] S. Y. R. Li, R. W. Yeung, and N. Cai, "Linear network coding," *IEEE Transactions on Information Theory*, vol. 49, no. 2, pp. 371–381, 2003.

[272] R. Koetter and M. Medard, "An algebraic approach to network coding," *IEEE/ACM Transactions on Networking*, vol. 11, no. 5, pp. 782–795, 2003.

[273] C. Peng, Q. Zhang, M. Zhao, Y. Yao, and W. Jia, "On the performance analysis of network-coded cooperation in wireless networks," *IEEE Transactions on Wireless Communications*, vol. 7, no. 8, pp. 3090–3097, 2008.

[274] Z. Ding, K. K. Leung, D. L. Goeckel, and D. Towsley, "On the study of network coding with diversity," *IEEE Transactions on Wireless Communications*, vol. 8, no. 3, pp. 1247–1259, 2009.

[275] R. Thobaben, "Joint network/channel coding for bandwidth-efficient multi-user ARQ," in *Proceedings og the IEEE 10th Workshop on Signal Processing Advances in Wireless Communications (SPAWC'09)*, pp. 419–423, 2009.

[276] S. Shamai and B. M. Zaidel, "Enhancing the cellular downlink capacity via co-processing at the transmitting end," in *Proceedings of the IEEE 53rd Vehicular Technology Conference - Spring (VTC'01-Spring)*, vol. 3, pp. 1745–1749, 2001.

[277] A. Goldsmith, S. A. Jafar, N. Jindal, and S. Vishwanath, "Capacity limits of MIMO channels," *IEEE Journal on Selected Areas in Communications*, vol. 21, no. 5, pp. 684–702, 2003.

[278] H. Zhang and H. Dai, "Cochannel interference mitigation and cooperative processing in downlink multicell multiuser MIMO networks," *EURASIP Journal on Wireless Communication Network*, vol. 4, no. 2, pp. 222–235, 2004.

# Index

# Author Index

## D



## E



## F



## G

## H



## I



## J

## S



## T

## Z